

2011

Stoichiometric and catalytic reactivity of tris(oxazoliny)borate main group metal compounds

James Francis Dunne
Iowa State University

Follow this and additional works at: <https://lib.dr.iastate.edu/etd>

 Part of the [Chemistry Commons](#)

Recommended Citation

Dunne, James Francis, "Stoichiometric and catalytic reactivity of tris(oxazoliny)borate main group metal compounds" (2011).
Graduate Theses and Dissertations. 12237.
<https://lib.dr.iastate.edu/etd/12237>

This Dissertation is brought to you for free and open access by the Iowa State University Capstones, Theses and Dissertations at Iowa State University Digital Repository. It has been accepted for inclusion in Graduate Theses and Dissertations by an authorized administrator of Iowa State University Digital Repository. For more information, please contact digirep@iastate.edu.

**Stoichiometric and catalytic reactivity of tris(oxazoliny)borate main group metal
compounds**

by

James Francis Dunne

A dissertation submitted to the graduate faculty
in partial fulfillment of the requirements for the degree of

DOCTOR OF PHILOSOPHY

Major: Inorganic Chemistry

Program of Study Committee:
Aaron D. Sadow, Major Professor
Andreja Bakac
Keith Woo
Robert Houk
Javier Vela

Iowa State University

Ames, Iowa

2011

Copyright © James Francis Dunne, 2011. All rights reserved.

To my dad, James F. Dunne, Jr., and my friend, Ben Baird,
both of whom are always in my thoughts and prayers.

Table of Contents

Acknowledgements	v
Abstract	vii
Chapter 1 - Introduction	
General Introduction	1
Thesis Organization	4
References	5
Chapter 2 – A new scorpionate ligand: tris(4,4-dimethyl-2-oxazolinyl)borate and its zirconium(IV) complexes	
Abstract	8
Introduction	8
Results and Discussion	12
Conclusions	24
Experimental	24
References	30
Chapter 3 – Bis(oxazolinyl)phenylborane: A Lewis acid-containing ligand for methide abstraction-based coordination to aluminum(III)	
Abstract	35
Introduction	36
Results and Discussion	39
Conclusions	57
Experimental	59
References	67

**Chapter 4 – Concerted C–N and C–H bond formation in a
magnesium-catalyzed hydroamination**

Abstract	71
Introduction	71
Results and Discussion	75
Conclusions	100
Experimental	101
References	116

**Chapter 5 – Magnesium amide-catalyzed dehydrocoupling of
organosilanes with amines, hydrazines, and ammonia for
silicon-nitrogen bond formation**

Abstract	119
Introduction	119
Results and Discussion	123
Conclusions	136
Experimental	137
References	151

Chapter 6 - Conclusions

General Conclusions	155
Future Directions	156

Acknowledgments

These past years have been some of the shortest and longest of my life. I must truly have begun the descent into old age, as my time spent here at Iowa State University has begun to blur into one very long day (and night) in the lab. However, before consigning my years as a graduate student to the good old days, there are a number of people to whom I am deeply indebted and would like to thank.

First, my Ph.D. advisor Dr. Aaron Sadow, for giving me the opportunity to learn what real research is and to discover how much joy there can be in the making of molecules. Through his guidance, suggestions, and critiques I have learned to write, speak, and think like a scientist. Six years ago I thought I was taking a chance on him, when in fact it was the other way around.

Thank you to all of my POS committee members – Dr. Keith Woo, Dr. Andreja Bakac, Dr. Robert Houk, and Dr. Javier Vela – for their insight, comments, exceedingly valuable time, and willingness to go out of their way to meet with me when I would remember (at the last minute) that I needed to do so.

A very large thank you to the members of the Sadow research group (listed by when they joined the group) – Ben Baird, Jiachun Su, KaKing Yan, Hung-An Ho, Steven Neal, Ryang Kim, Dr. Andrew Pawlikowski, Stephanie Smith, Kuntal Manna, Debabrata Mukherjee, Songchen Xu, Dr. Barun Jana, Jing Zhu, Nicole Lampland, Naresh Eedugurala, and Aradhana Pindwal – who were forced to put up with my singing, shouting, complaining, and exaggerating. Without any one of them, my years here would have been greatly impoverished both intellectually and socially. We celebrated and mourned together, and did it all over a beer or three. Keep up the good work ... and do more reactions.

To the many undergraduates who have worked in our lab over the years – Dan, Patricia, David, Shawna, Marlie, Tristan, Jared, Kate, Jooyoung, Brianna, Rick, Josh, Marissa, Megan, and Yitzhak – thanks for all the laughs, the chance to teach, and the chance to learn how little I actually know. And I’m sorry for not inviting you to my wedding. Again.

Thanks to my close friends here in the land of Iowa – Misty and Jacob, Jeff and Lynnette, Gregg and Tiffany – for the support, advice, prayers, and fun that made the overnight kinetic runs palatable. Even when the chemistry was miserable there was always something to look forward to.

A deep debt of thanks to my family – Mom, Dad, Matt, Liz, Karen, Hobe, Jeremy, and Jonny – for the love, understanding, support, and for never asking when I was going to finish.

Lastly, from the depth of my heart, my thanks to my beautiful wife, Jennifer - for letting me work when I needed to, believing in me when I did not, and most importantly for all the love. I love you, too.

Abstract

Scorpionate ligands, exemplified by the tris(pyrazolyl)borate (Tp) ligand, have been widely used to form metal catalysts across the periodic table. This class of monoanionic ligands commonly binds in either a bi- or tridentate fashion, and is capable of donating up to six electrons to the metal center. However, the B–N bond is susceptible to isomerization resulting in a loss of steric protection around the metal center. We set out to address this problem by developing a new class of scorpionate ligands based on oxazoline rings in which the B–N bond is replaced by a more robust B–C bond.

The first example of this new oxazoline-based scorpionate ligand, tris(4,4-dimethyl-2-oxazoliny)phenyl borate, To^M , is prepared by reaction of 2-lithio-4,4-dimethyl-2-oxazolidine and 0.30 equiv of dichlorophenylborane. The resulting lithium salt is found to be competent as a transfer agent to Group IV transition metals via salt metathesis. Both the protonated form of To^M and the thallium salt, HTo^M and $TlTo^M$, are also successfully prepared, and are found to transfer To^M to transition metals in higher yield than the lithium analog. The steric bulk of this ligand is greater than that of tris(3,5-Me₂-pyrazolyl)borate (Tp^*), as quantified by solid angles of crystallographically characterized zirconium(IV) complexes.

The unique steric pocket created by the To^M ligand led us to examine the reactivity of To^M main group metal compounds. When reacted with $[AlMe_3]_2$, To^M binds in a bidentate fashion to give $\kappa^2-To^MAlMe_2$. The reactivity of this compound is explored and compared to the bis(oxazoliny)borate, $\{\kappa^2-PhMeB(Ox^{Me_2})\}AlMe_2$, which is synthesized *via* a methide abstraction/oxazoline coordination reaction of the parent borane $PhB(Ox^{Me_2})_2$ with $[AlMe_3]_2$. These compounds were found to be surprisingly robust, and were capable catalysts for the ring opening polymerization of lactide at high temperature.

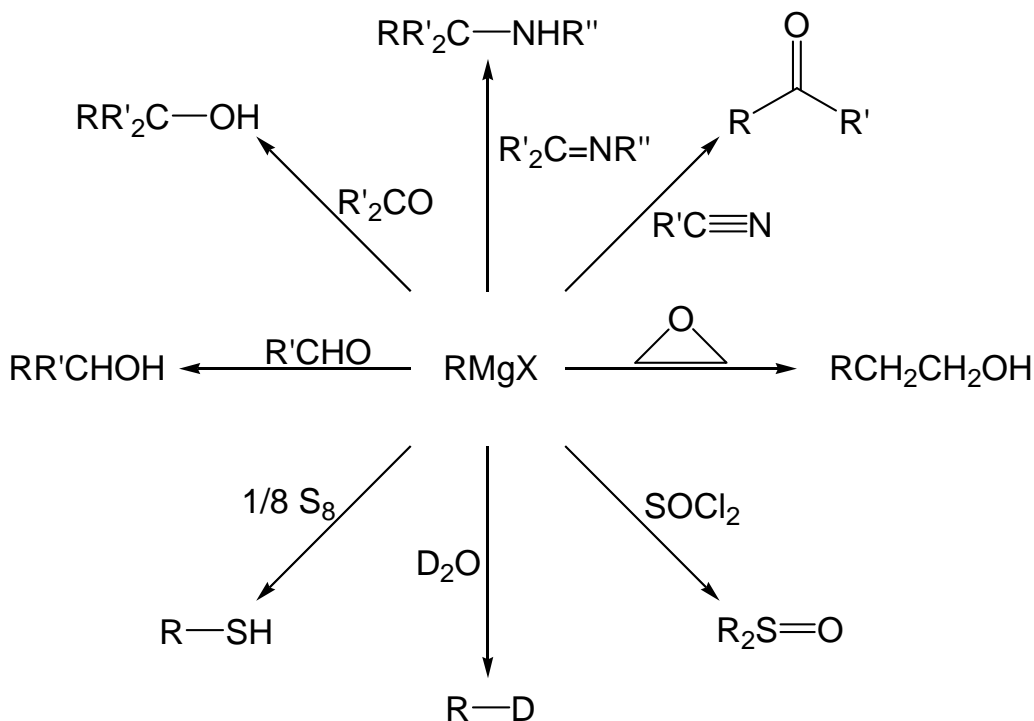
The aluminum metal center proved to be too small for tridentate coordination of To^M , and so we began investigating the reactivity of the larger metal, magnesium. $To^M MgMe$ is coordinatively saturated as the tridentate coordination of To^M prevents the binding of ethereal solvents to the magnesium center. The steric bulk of To^M results in a well-defined, monomeric species with no evidence of homoleptic species resulting from Schlenk equilibrium. $To^M MgMe$ is an active precatalyst for intramolecular hydroamination/cyclization at 50 °C. The catalytic system displays Michaelis-Menten-type kinetics which is consistent with a mechanism involving reversible catalyst-substrate association prior to cyclization. The isolated magnesium amidoalkene intermediate does not undergo cyclization, however addition of trace amounts of substrate allows cyclization to occur. Therefore, we propose a two-substrate, six-center transition state involving concerted C–N bond formation and N–H bond cleavage as the turnover limiting step of the catalytic cycle.

$To^M MgMe$ is also an effective pre-catalyst for the cross-dehydrocoupling of Si–H in organosilanes and N–H bonds in amines to give Si–N bonds and H_2 . Using this catalyst system, a range of silazanes can be prepared in high conversion and high yields. In reactions for which multiple dehydrocoupling steps could give mixtures and oligomers, carefully controlled ratios of silane to amine allow isolation of a single product. Interestingly, both hydrazine and ammonia can be functionalized via coupling with tertiary silanes to selectively give the corresponding aminosilanes $R_3SiNHNH_2$ and R_3SiNH_2 .

Chapter 1 - Introduction

General Introduction

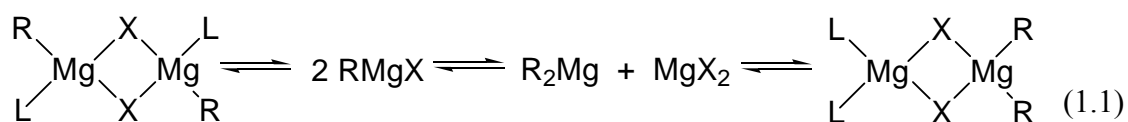
Organomagnesium reagents have found widespread applications since their discovery in 1900 by Grignard.^{1,2} The combination of both high reactivity and ease of access makes Grignards one of the most desirable reagents for the functionalization of organic molecules (Scheme 1.1).³ Additionally, the transmetalation of organic groups from magnesium to less reactive, but more chemoselective, organometallic species (*i.e.*, zinc, copper, titanium) allows for additional fine tuning of their already extensive reactivity.⁴



Scheme 1.1. Representative examples of applications of Grignard reagents. Products are shown after hydrolysis.

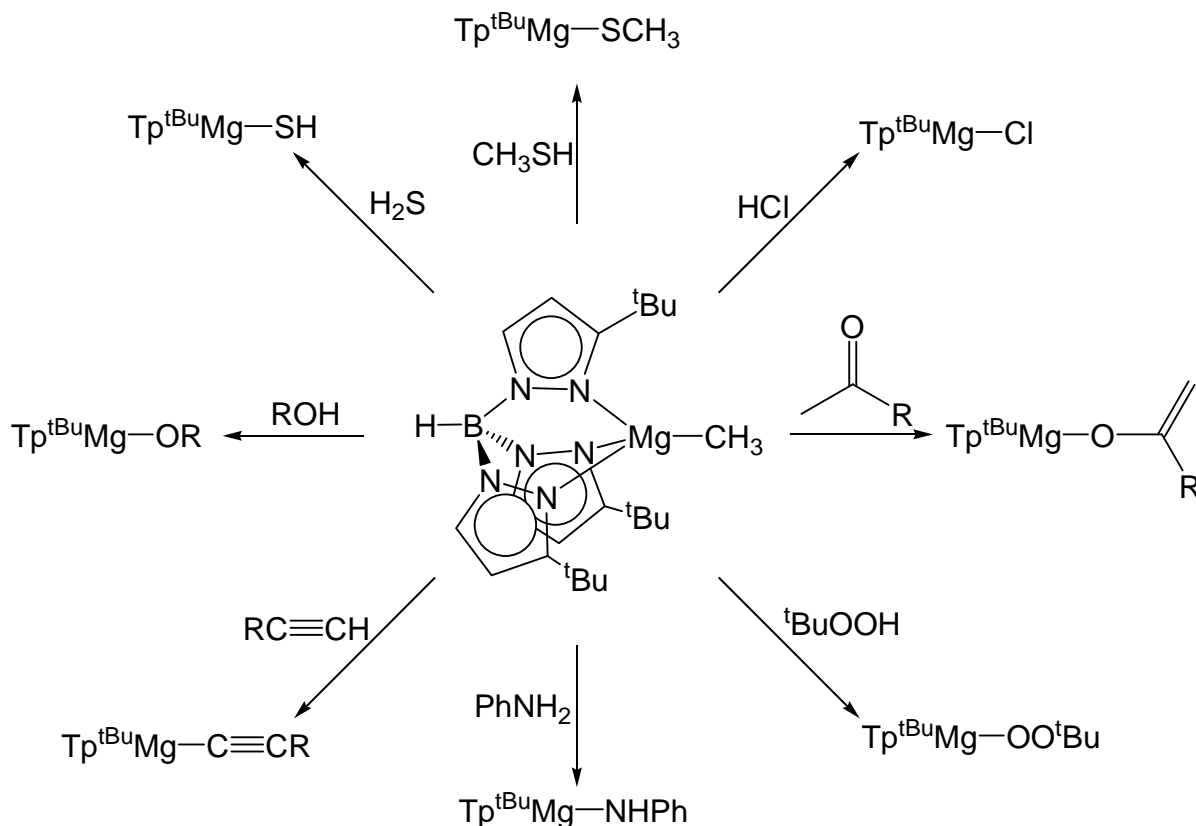
Recently, new innovations have focused on the development of “turbo-Grignards” of the general formula $RMgCl \cdot LiCl$.^{5,6} These compounds display enhanced kinetic basicity and

regioselectivity combined with greater functional group tolerance in comparison to traditional Grignards. However, the widespread use of organomagnesium compounds has largely been restricted to stoichiometric transformations, and the mechanistic details of these reactions are often not elucidated.⁷ This may in part be attributed to the poorly defined structures of Grignard reagents. While solid state structures have been reported for a variety of Grignards^{1,7}, structures in the solution state are far more complex. Generally, Grignard reagents exist as a complicated mixture of aggregated species which can interchange via the Schlenk equilibrium as seen in eq 1.1.^{7,8} The actual species present in solution are highly dependent on the nature of R, the nature of X, the properties of the coordinating solvent, concentration, and the temperature.^{1,2} The scarcity of organomagnesium compounds as homogeneous catalysts can be partly attributed to this lack of well-defined species in solution.



One method of addressing this is through the use of chelating ancillary ligands. Substitution of the halide of RMgX with a bulky, chelating ligand can disrupt aggregation and prevent the Schlenk equilibria from being established. This can result in the isolation of well-defined, monomeric magnesium species while retaining the high reactivity exhibited by traditional Grignards. This is best exemplified by the tris(pyrazolyl)borate magnesium alkyl compounds.⁹ The bulky tris(3-*tert*-butylpyrazolyl)borate (Tp^{tBu}) ligand binds to magnesium alkyls in a tridentate fashion, and the steric pocket created by the *tert*-butyl substituents

prevents ligand redistribution to give the homoleptic $\text{Tp}^{\text{tBu}}_2\text{Mg}$. The resulting monomeric $\text{Tp}^{\text{tBu}}\text{MgCH}_3$ can then be further substituted with range of organic functional groups making it an attractive pre-catalyst for a variety of transformations (Scheme 1.2). In light of this, it is surprising that magnesium scorpionates have only rarely been employed in catalytic



Scheme 1.2. Stoichiometric transformations of $\text{Tp}^{\text{tBu}}\text{MgCH}_3$

transformations.¹⁰ Other ligand systems, particularly β -diketonates,^{11,12} aminotroponates, and aminotroponiminates¹³ have been extensively explored, and display excellent catalytic activity in ring opening polymerization,¹¹ hydroamination,^{12,13} hydrosilylation,¹⁴ and hydrophosphination.¹⁵

The potential of magnesium scorpionates for use as catalysts in a range of transformations was the inspiration for the work described in this thesis. The need to easily tune the steric properties of the ancillary ligand led us to develop a new class of oxazoline-based scorpionate ligands, tris(oxazoliny)borates. The availability of an array of substituted oxazoline rings should allow for the facile synthesis of ligands with variable steric pockets. Additionally, the available enantiopure *2H*-oxazolines could lead to the generation of chiral directing ligands for enantioselective catalysis.¹⁶ The following chapters discuss the development of this new ligand class, as well as our initial exploration into the reactivity of both aluminum and magnesium complexes and their use in catalysis.

Thesis Organization

This thesis is composed mainly of published journal papers on the synthesis of the tris(4,4-dimethyl-2-oxazoliny)phenyl borate (To^M) ligand, and the subsequent synthesis and reactivity of To^M compounds of zirconium, aluminum, and magnesium. Chapters 2 through 4 contain material that has already been published, and Chapter 5 has been submitted for publication. Each of these chapters has been significantly modified from the published versions in order to give a more complete view of the research. As the thesis encompasses a diverse range of topics, relevant literature is reviewed in the introduction of each chapter to provide an adequate understanding of the background and significance of the results.

Chapter 2 discusses the synthesis of the To^M ligand which is the first example of a new class of oxazoline-based scorpionate ligands. The X-ray crystal structure of HTo^M was obtained by Jiachun Su, but all remaining work was performed by James Dunne. Chapter 3 studies the structure and reactivity of aluminum complexes formed by coordination of the

To^M ligand. The analogous bis(oxazolinyl)borate aluminum species, {κ²-PhMeB(Ox^{Me2})₂}AlMe₂, is also studied, and the reactivity of both species as catalysts for the ring opening polymerization of lactide is then examined. The contributions of the authors Kuntal Manna, Dr. Jerzy Wiench, and Dr. Marek Pruski to the published paper have been removed from this thesis chapter, and their work is included in the references at the end of the chapter.

In Chapter 4, the reactivity of To^MMgMe is investigated beginning with its potential as a catalyst for intramolecular hydroamination/cyclization of aminoalkenes. To^MMgMe is found to be coordinatively saturated, which enables isolation of the metal-amidoalkene intermediates in the catalytic cycle for the first time. All of the work contained in this chapter was performed by James Dunne, though the pulse program for the selective population inversion experiments was written by Dr. Bruce Fulton. Chapter 5 continues to explore the reactivity of To^MMgMe as a pre-catalyst for the dehydrogenative coupling of amines and silanes to selectively generate monomeric silazanes. DFT calculations were performed by Joshua Engelkemier and Dr. Theresa Windus, while all experimental work was done by James Dunne. In all chapters, X-ray crystal structures were solved by Dr. Arkady Ellern.

References

- 1) Jastrzebski, J.T.B.H.; Boersma, J.; Van Koten, G. *The Chemistry of Organomagnesium Compounds*; Rappoport, Z., Ed.; Wiley: Hoboken, 2008; Vol. 1, p. 2-4.
- 2) Hanusa, T.P. *Comprehensive Organometallic Chemistry III*; Crabtree, R.H.; Mingos, M.D.P., Ed.; Elsevier: Oxford, 2006; Vol. 2, p.66-152.

- 3) Elschenbroich, C.; Salzer, A. *Organometallics: A Concise Introduction*; VCH: Weinheim, 1992; p. 38-46.
- 4) Knochel, P.; Gavryushin, A.; Brade, K. *The Chemistry of Organomagnesium Compounds*; Rappoport, Z., Ed.; Wiley: Hoboken, 2008; Vol. 2, p. 511-512.
- 5) Armstrong, D.R.; Garcia-Alvarez, P.; Kennedy, A.R.; Mulvey, R.E.; Parkinson, J.A.; *Angew. Chem. Int. Ed.* **2010**, *49*, 3185-3188.
- 6) For representative examples, see: (a) Krasovskiy, A.; Knochel, P. *Angew. Chem. Int. Ed.* **2004**, *43*, 3333.; Krasovskiy, A.; Straub, B.F.; Knochel, P. *Angew. Chem. Int. Ed.* **2006**, *45*, 159.; (c) Krasovskiy, A.; Krasovskaya, V.; Knochel, P. *Angew. Chem. Int. Ed.* **2006**, *45*, 2958.; (d) Rohbogner, J.; Clososki, G.; Knochel, P. *Angew. Chem. Int. Ed.* **2008**, *47*, 1503.
- 7) Cotton, F.A.; Wilkinson, G. *Advanced Inorganic Chemistry*, 5th ed.; Wiley: New York, 1988; p. 158-161.
- 8) Schlenk, W.; Schlenk, Jr., W. *Chem Ber.* **1929**, *62*, 920.
- 9) Han, R. Parkin, G. *J. Am. Chem. Soc.* **1992**, *114*, 748-757.
- 10) (a) Chisholm, M.H.; Eilerts, N.W.; Huffman, J.C.; Iyer, S.S; Pacold, M.; Phomphrai, K. *J. Am. Chem. Soc.* **2000**, *122*, 11845-11854.; (b) Sánchez-Barba, L.F; Garcés, A.; Fajardo, M.; Alonso-Moreno, C.; Fernández-Baeza, J.; Otero, A.; Antinolo, A.; Tejeda, J.; Lara-Sánchez, A.; Lopez-Solera, M.I. *Organometallics* **2007**, *26*, 6403-6411.
- 11) (a) Chisholm, M.H.; Huffman, J.C.; Phomphrai, K. *J. Chem. Soc., Dalton Trans.* **2001**,

- 222-224.; (b) Chisholm, M.H.; Gallucci, J.; Phomphrai, K. *Inorg. Chem.* **2002**, *41*, 2785-2794.; (c) Chisholm, M.H.; Phomphrai, K. *Inorg. Chimica Acta* **2003**, *350*, 121-125.
- 12) (a) Crimmin, M.R.; Casely, I.J.; Hill, M.S. *J. Am. Chem. Soc.* **2005**, *127*, 2042-2043.; (b) Barrett, A.G.M.; Crimmin, M.R.; Hill, M.S.; Kociok-Kohn, G.; Lachs, J.R.; Procopiou, P.A. *Dalton Trans.* **2008**, 1292-1294.; (c) Crimmin, M.R.; Arrowsmith, M.; Barrett, A.G.M.; Casely, I.J.; Hill, M.S.; Procopiou, P.A. *J. Am. Chem. Soc.* **2009**, *131*, 9670-9685.
- 13) (a) Bailey, P.J.; Dick, C.M.E.; Fabre, S.; Parsons, S. *J. Chem. Soc., Dalton Trans.* 2000, 655-1661.; (b) Datta, S.; Roesky, P.W. *Organometallics* **2007**, *26*, 4392-4394.
- 14) (a) Buch, F.; Brettar, J.; Harder, S. *Angew. Chem. Int. Ed.* **2006**, *45*, 2741-2745.; (b) Buch, F.; Harder, S. *Z. Naturforsch* **2008**, *63b*, 169-177.
- 15) Crimmin, M.R.; Barrett, A.G.M.; Hill, M.S.; Hitchcock, P.B.; Procopiou, P.A. *Organometallics* **2007**, *26*, 2953-2956.
- 16) (a) Leonard, W.R.; Romine, J.L.; Meyers, A.I. *J. Org. Chem.* **1991**, *56*, 1961-1963. (b) Kamata, K.; Agata, I.; Meyers, A.I. *J. Org. Chem.* **1998**, *63*, 3113-3116.

Chapter 2: A new scorpionate ligand: tris(4,4-dimethyl-2-oxazolinyl)borate and its zirconium(IV) complexes

Modified from a paper published in *Organometallics*[‡]

James F. Dunne[†], Jiachun Su[§], Arkady Ellern, Aaron D. Sadow

Department of Chemistry, U.S. DOE Ames Laboratory, Iowa State University, Ames, IA

50011-3111

Abstract

The first example of a new class of oxazoline-based scorpionate ligand, tris(4,4-dimethyl-2-oxazolinyl)phenyl borate, To^M , is prepared by reaction of 2-lithio-4,4-dimethyl-2-oxazolidine and 0.30 equiv of dichlorophenylborane. The steric bulk of this ligand is greater than that of tris(3,5-Me₂-pyrazolyl)borate (Tp^*), as quantified by solid angles of crystallographically characterized zirconium(IV) complexes.

Introduction

Poly(pyrazolyl)borates have found a wide range of uses in coordination chemistry since their introduction by Trofimenko in 1967.¹ Both bidentate [$R_2B(pz)_2$] and tridentate [$RB(pz)_3$] analogs are readily available, and the ability of these ligands to donate 4 and 6 electrons, respectively, to metal centers has led to comparisons with β -diketonates and cyclopentadienyl ligands. Tris(pyrazolyl)borate (Tp) and its bulkier derivatives have proven to be excellent ancillary ligands, and scorpionate complexes of most of the metals in the

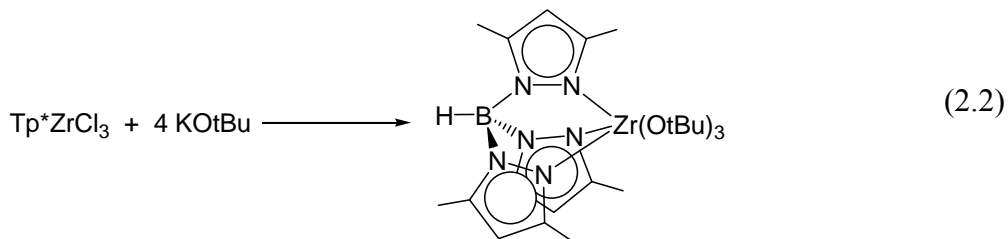
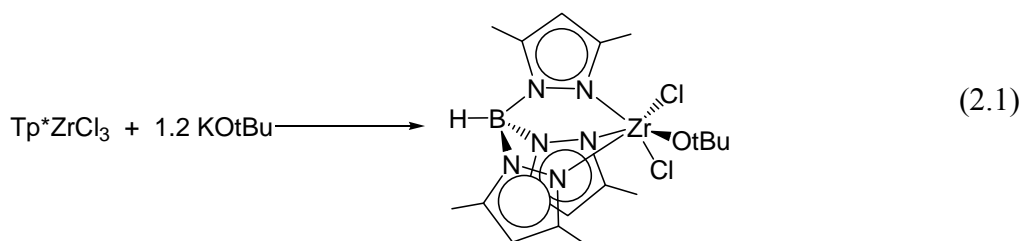
[‡]Parts of the paper are reprinted with permission of *Organometallics* **2008**, 27, 2399-2401.

[†]Primary researcher and author

[§]Contributed X-ray structure of HTo^M

periodic table have been prepared. For early transition metals, this is clearly illustrated by a variety of metal complexes displaying a wide array of interesting stoichiometric²⁻⁵ and catalytic chemistry.^{5a; 6-9}

Of particular interest is the chemistry of the Group IV tris(pyrazolyl)borate complexes. $TpMCl_3$ is generally synthesized via the salt metathesis reaction of MCl_4 and $M'Tp$ ($M = Ti, Zr, Hf$; $M' = Na, K, Tl$), and can be isolated in good yields. However, substitution of the halide ligands by salt metathesis pathways is limited to substitution with oxygen-based ligands. The ability to replace the chlorides with both phenoxide and alkoxide groups has been well documented.^{3,4} The substitution of all three chlorides was achieved easily with the use of sterically undemanding phenoxide derivatives.³ In contrast, the replacement of all three chlorides with alkoxide groups was found to be more difficult, requiring a substantial excess of alkoxide salt to substitute more than one halide ligand (eq 2.1 and 2.2).^{4b}



These successful replacements of the halide ligands can be attributed to the oxophilic nature of the zirconium center. However, upon substitution of one of the halides, a subsequent replacement of the two remaining halide ligands could be achieved. The

subsequent addition of either Grignard or alkyl lithium reagents to TpZr(OR)Cl_2 resulted in the loss of LiCl , and the formation of new Zr-C bonds.^{4c} These examples represent the extent of stoichiometric substitutions that can be achieved at TpMX_3 metal centers.

Despite the limited ability to vary the active sites of TpMX_3 compounds, there is a surprisingly rich array of catalytic olefin polymerization chemistry using these compounds as pre-catalysts. In the presence of either methylaluminoxane (MAO) or modified methylaluminoxane (MMAO), TpTiCl_3 and TpZrCl_3 are good catalysts for ethylene, propylene, and 1-hexene polymerizations, displaying activities similar to those of the corresponding Cp_2MCl_2 complex.^{6b, 7-9} Bulkier derivatives of the parent Tp ligand also display excellent activity as polymerization catalysts.⁶ $\text{Tp}^{\text{Ms}}\text{ZrCl}_3$ ($\text{Tp}^{\text{Ms}} = \text{HB}(3\text{-mesitylpyrazolyl})_3^-$) is an excellent catalyst for the copolymerization of ethylene and 1-hexene, producing ultrahigh-molecular weight polymers ($900\text{-}1500 \times 10^3$ Da) with substantial incorporation of hexene (up to 27%) and narrow molecular weight distributions ($M_w/M_n = 1.8 - 2.3$).^{6b} However, there are two drawbacks to these $\text{TpMCl}_3/\text{MAO}$ systems: 1) the identity of the active catalytic species is unknown due to the complex nature of MAO, and 2) low ratios ($\text{Al:Ti/Zr} = 200 - 1000$) of MAO to the active metal species tend to result in a broad molecular weight distribution due to a dominant chain transfer mechanism to the aluminum center. An additional problem, particularly in bulky Tp derivatives, is the isomerization of the ligand itself. Isomerization of Tp ligands via 1,2-sigmatropic shifts and B-N bond cleavage are common decomposition pathways for pyrazolylborate ligands in a wide array of transition metal complexes.^{1d,e,2,10} This isomerization is most often observed when extremely bulky substituents, such as mesityl groups, are located on the 3-position of the pyrazole ring. To relieve steric pressure around the metal center, one of the pyrazole

rings flips, placing the bulky substituent in the 5-position. The loss of steric pressure reduces the reactivity of the metal centers, hindering the utility of Tp complexes in catalysis.^{6c,d}

To avoid this decomposition pathway, we thought to prepare an oxazoline-based scorpionate ligand containing B–C linkages. As B–C bond cleavage would require a resonance structure involving the formation of a carbene, a scorpionate ligand based on this linkage should display a greater resistance to the cleavage and isomerization process.¹¹ Furthermore, oxazoline-based ligands have recently become widely used in a range of metal-catalyzed reactions (Figure 2.1).¹²⁻¹⁴

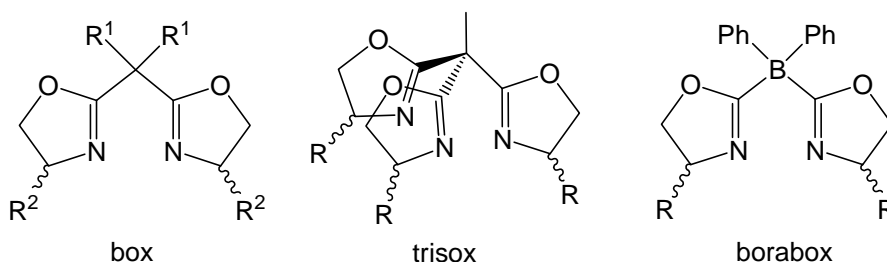
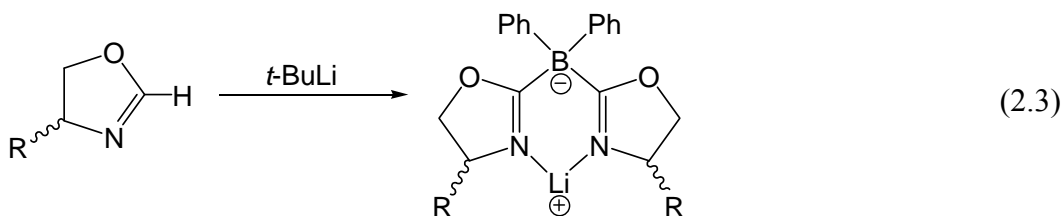


Figure 2.1. Examples of known oxazoline based ligands, box, trisox, and borabox

A neutral trisoxazoline ligand with a carbon backbone, trisox, has been reported in the literature.¹⁴ However, this neutral ligand was found to be weakly bound to metal centers, and is easily replaced by either halogenated or coordinating solvents.^{14c} Changing the neutral carbon to an anionic boron backbone would transform the ligand from an L_3 type to a zwitterionic L_2X type ligand¹⁵, allowing the ligand to bind strongly to the metal center and resulting in a more robust metal complex. A boron-bridged bisoxazoline, borabox, has also been reported (eq 2.3)¹³, inspiring us to develop the first example of a trisoxazoline analog of Tp. Herein, we describe the synthesis of tris(4,4-dimethyl-2-oxazolinyl)phenyl borate, To^M ,

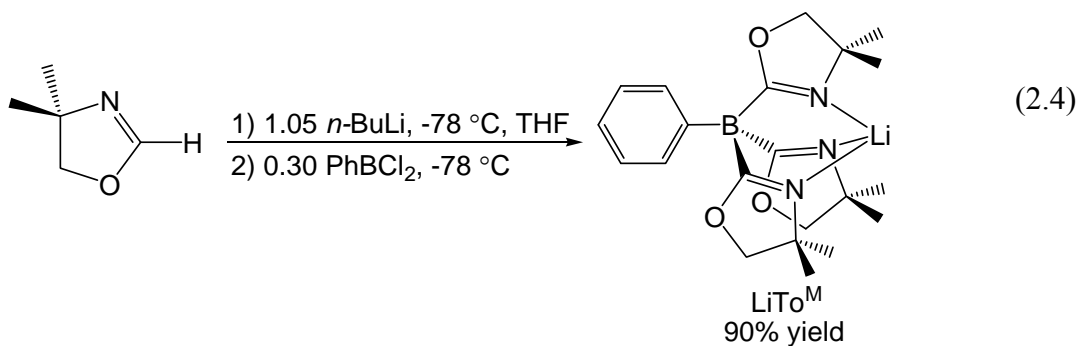


the first example of this new ligand class, as well as its coordination chemistry in new zirconium (IV) complexes. Appropriate transfer agents of the To^{M} ligand for the clean and facile binding of To^{M} to transition metal centers are investigated, as are the different binding modes of the To^{M} ligand to metal centers. Lastly, the ability of the To^{M} ligand to provide steric protection to highly reactive metal centers is explored using Zr(IV) complexes.

Results and Discussion

Synthesis of To^{M} and comparison of lithium, thallium, and protonated forms

Lithium tris(4,4-dimethyl-2-oxazolin-2-yl)phenyl borate (LiTo^{M}) is prepared by the deprotonation of 4,4-dimethyl-2-oxazoline using $n\text{-BuLi}$ followed by the addition of 0.30 equivalents of dichlorophenylborane (eq 2.4).

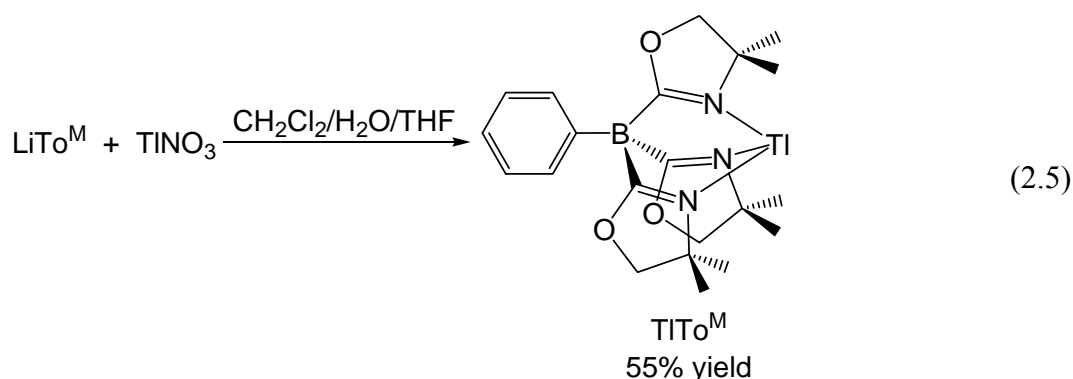


Quantitative deprotonation of the oxazoline was found to be necessary for clean product formation as the presence of $2H$ -oxazoline in the reaction resulted in the formation of several unidentifiable side products. Two of these products were observed to form in independent reactions of 4,4-dimethyl-2-oxazoline with PhBCl_2 , confirming the necessity of using a small

excess of *n*-BuLi to ensure complete deprotonation. Additionally, an excess of the 2-lithio-oxazolidine was needed, in conjunction with reaction times in excess of 24 h, for the clean formation of LiTo^{M} . Shorter reaction times or larger quantities of PhBCl_2 (> 0.30 equiv) resulted in inseparable mixtures of LiTo^{M} and the bisoxazoline product, bis(4,4-dimethyl-2-oxazolin-2-yl)phenylborane ($\text{PhB}(\text{Ox}^{\text{Me}_2})_2$). This species was assigned based on the integration of its ^1H NMR spectrum as well as its ^{11}B NMR chemical shift (-7.26 ppm). $\text{PhB}(\text{Ox}^{\text{Me}_2})_2$ has been independently synthesized and reported¹⁶, and will be discussed in greater detail in a later chapter (see Chapter 3).

In either benzene- d_6 , chloroform- d_1 , or methylene chloride- d_2 , the ^1H NMR spectrum of LiTo^{M} shows broad resonances for both the methylene and 4,4-dimethyl groups centered at 3.3 and 1.4 ppm, respectively. In contrast to this, sharp singlet resonances for these groups are observed in acetonitrile- d_3 (3.60 and 1.19 ppm). The formation of a borate center is supported by the integrated ratio of the oxazoline methyls to phenyl resonances (18:5 H), as well as the broad singlet in the ^{11}B NMR at -16.9 ppm.¹⁷ All three oxazoline rings are equivalent on the NMR time scale, indicating pseudo- C_{3v} symmetry in solution. This is confirmed in the solid state by the observation of only a single ν_{CN} stretch in the solid state IR (1607 cm^{-1} , KBr), suggesting that all three nitrogen atoms in the oxazoline rings are coordinated to lithium.

The thallium salt of To^{M} is synthesized by the reaction of LiTo^{M} and TlNO_3 (eq 2.5). As with LiTo^{M} , the ^1H NMR spectrum of TlTo^{M} shows a single set of oxazoline resonances suggesting pseudo- C_{3v} symmetry in the solution state. A ^1H - ^{15}N HMBC experiment, performed using the natural abundance of ^{15}N , displays crosspeaks between the oxazoline



nitrogens and the ring methyl and methylene groups. Coupling between the thallium and nitrogen centers was also observed with a $^1J_{\text{TIN}} = 795 \text{ Hz}$.¹⁸ As these are the only nitrogen resonances observed, this data supports the tridentate binding of all three oxazoline rings to the thallium center. Only a single ν_{CN} band at 1600 cm^{-1} was observed in the solid state IR, suggesting that all three oxazolines are bound to thallium in the solid state as well. An X-ray crystal structure confirms this coordination mode (Figure 2.2).

The X-ray structure of TITo^M additionally shows the effect that the phenyl ring has on the bond lengths and angles in coordination complexes of To^M. The T11–N1 and T11–N2 bond lengths are approximately 0.05 \AA longer than the T11–N3 bond. This may be attributed to the nearly perpendicular orientation of the phenyl ring to the N3-containing oxazoline (torsion angle $\text{C17–C16–B1–C11} = 91.72^\circ$; $\text{C21–C16–B1–C11} = 81.23^\circ$). The phenyl ring is also oriented such that it points towards the other two oxazoline rings ($\text{C17–C16–B1–C1} = 30.54^\circ$; $\text{C21–C16–B1–C6} = 38.42^\circ$). This results in longer T11–N1 and T11–N2 distances versus the T11–N3 distance, disrupting the C_{3v} symmetry in the crystalline solid.

The purpose behind the synthesis of this thallium To^M transfer agent lies in the utility of the thallium center. The improved solubility of the thallium salt combined with its reactivity with alkyl groups as well as halides makes TITo^M a more synthetically useful reagent than

the lithium version. Additionally, the partial solubility of LiCl in polar ethereal solvents can cause difficulty in the purification of reactions using LiTo^{M} as the transfer agent. The ease of removal of the thallium by-products, either as thallium metal or halide salts, makes TlTo^{M} a superior reagent.

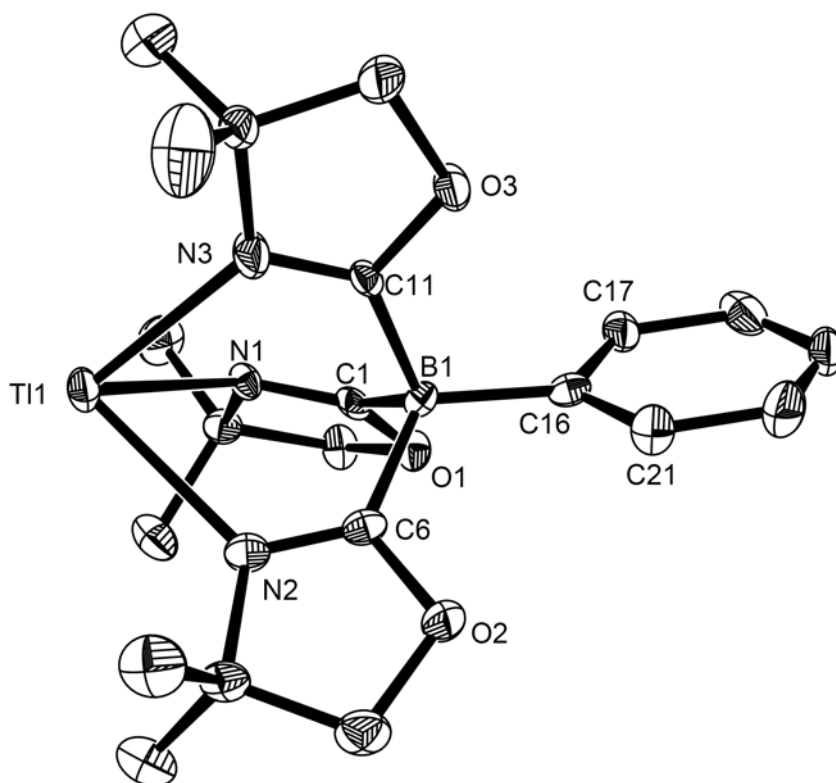
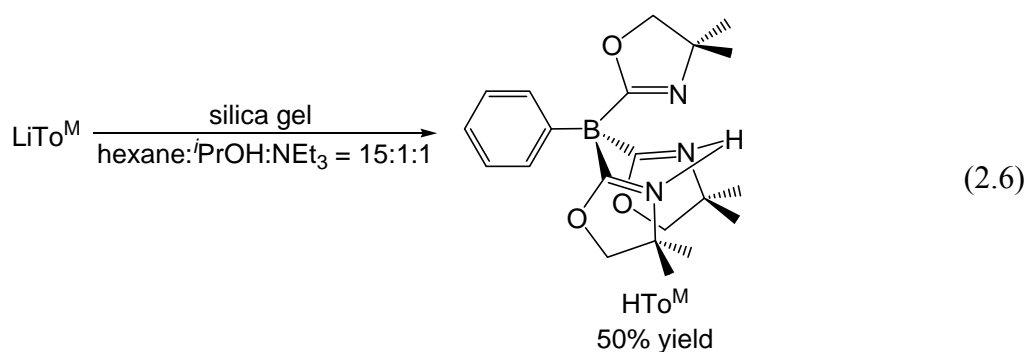


Figure 2.2. ORTEP diagram of TlTo^{M} at 50% probability. Hydrogen atoms are omitted for clarity. Relevant bond distances (Å): Tl1–N1, 2.550(4); Tl1–N2, 2.543(5); Tl1–N3, 2.498(5).

The protonated form of the ligand, HTo^{M} , was originally prepared by flash chromatography of LiTo^{M} on a silica gel column in $\text{C}_6\text{H}_{14}/i\text{-PrOH}/\text{NEt}_3$ (15:1:1). The product was isolated as an off-white solid in moderate yield (eq 2.6).



An alternative method for the preparation of this compound was later reported by Pawlikowski and Sadow.¹⁹ In this method, $[\text{HNEt}_3]\text{Cl}$ was used as the protonating agent in a stirred suspension of LiTo^{M} in methylene chloride. While the yields for both methods are equivalent, the advantage of the latter lies in the ability to synthesize HTo^{M} in the absence of water, giving an anhydrous product that can be used without further purification in the synthesis of extremely moisture sensitive early transition-metal and rare-earth compounds.

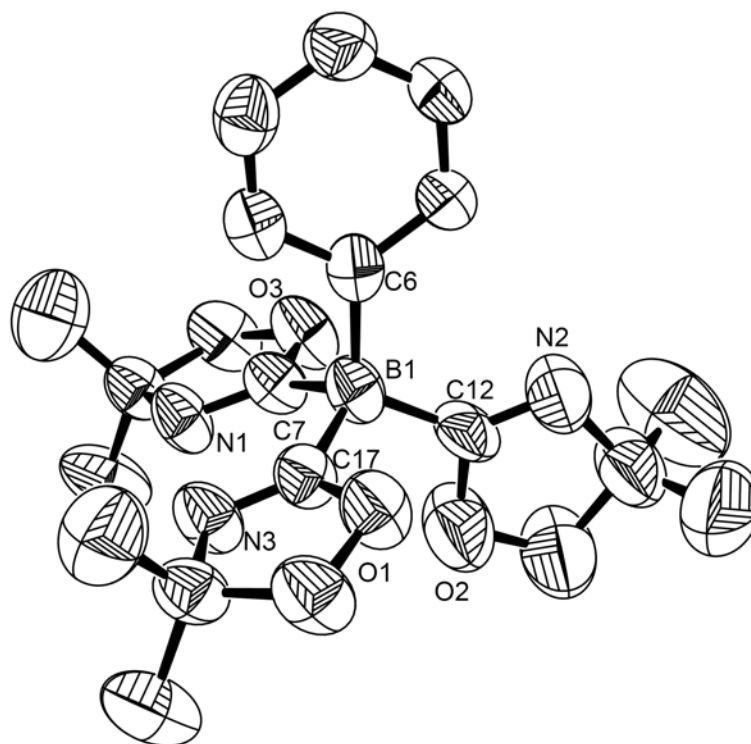
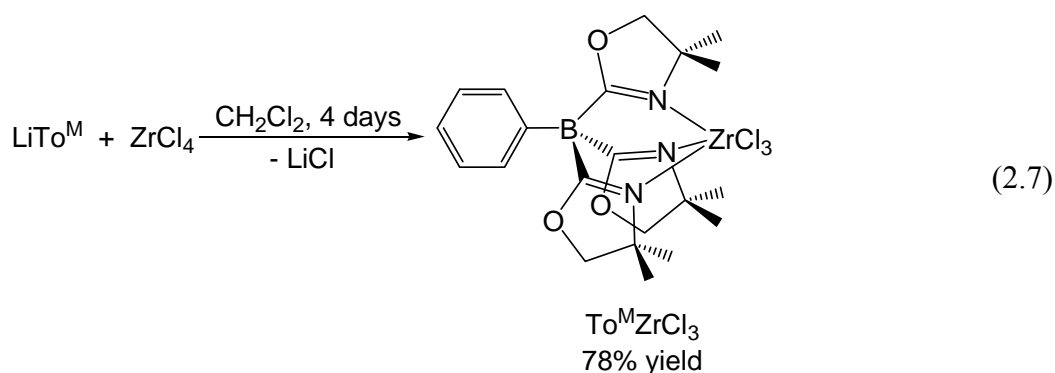


Figure 2.3. ORTEP diagram of HTo^{M} at 50% probability.²⁰ Hydrogen atoms are omitted for clarity.

In contrast to the broad resonances in the lithiated version, the ^1H NMR spectrum in benzene- d_6 contained sharp singlet resonances at 3.55 and 1.02 ppm for the methylene and methyl groups, respectively. In acetonitrile- d_3 , the oxazoline peaks are shifted downfield from LiTo^{M} (3.90 and 1.29 ppm), allowing for a clear distinction between the two compounds. Additionally, the acidic proton in HTo^{M} is observed at ~ 10 ppm. The solid state IR spectrum of HTo^{M} shows two distinct C=N bond stretches separated by 31 wavenumbers (1627 and 1594 cm^{-1}). This suggests a C_s symmetric structure in the solid state in which one of the oxazoline rings is inequivalent from the other two, as opposed to the NMR evidence in which all three rings are equivalent in solution. A single-crystal X-ray diffraction confirmed the solid state geometry, as two of the oxazoline rings' C=N are coplanar and oriented toward each other in a manner that forms a bidentate chelate. A mirror plane in the structure relates the two rings, and contains the third oxazoline as well as the phenyl ring on the tetrahedral borate center (Figure 2.3).

Synthesis and coordination chemistry of $\text{To}^{\text{M}}\text{ZrCl}_3$

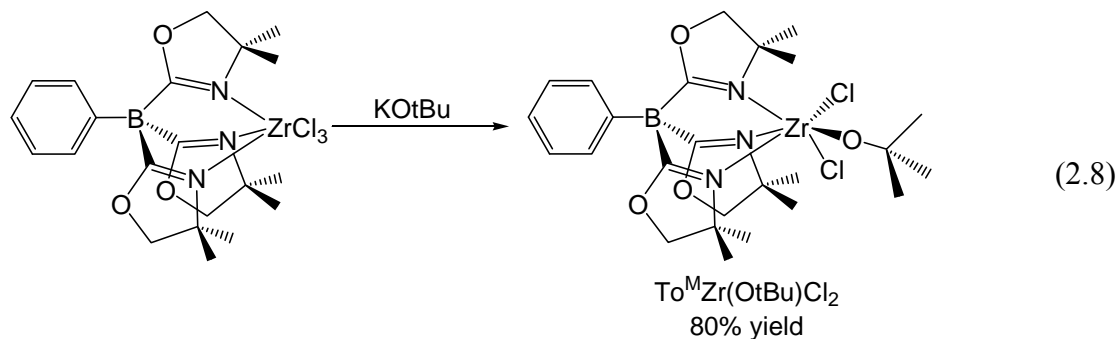
We began investigating the coordination chemistry of To^{M} with Zr(IV) to better understand the nature of the To^{M} ligand. $\text{To}^{\text{M}}\text{Zr(IV)}$ complexes were prepared both by salt elimination routes using LiTo^{M} and TITo^{M} as the transfer agents with ZrCl_4 , as well as by amine elimination with HTo^{M} and $\text{Zr(NMe}_2)_4$. The salt elimination reaction occurs when a suspension of LiTo^{M} and a small excess (1.05 equiv) of ZrCl_4 were stirred in methylene chloride for four days. The resulting yellow solution contained the product $\text{To}^{\text{M}}\text{ZrCl}_3$ and suspended lithium chloride (eq 2.7).



Re-dissolution of the product in either toluene or benzene typically resulted in the precipitation of a small quantity of white solid. This precipitate was identified as LiCl, which due to its sparingly soluble nature in methylene chloride, had been transferred in the initial filtration in addition to $\text{To}^{\text{M}}\text{ZrCl}_3$. Alternatively, $\text{To}^{\text{M}}\text{ZrCl}_3$ could be synthesized by the addition of one equivalent of ZrCl_4 to a methylene chloride solution of TlTo^{M} . Stirring the clear solution overnight resulted in the precipitation of TlCl , and gave the $\text{To}^{\text{M}}\text{ZrCl}_3$ product in a similar yield as the route using LiTo^{M} . The TlTo^{M} route reduces the time required to synthesize the zirconium complex by two days, after accounting for the time needed to first isolate TlTo^{M} itself. The reduced reaction time as well as the lack of retention of TlCl in the filtrate further emphasizes the utility of thallium salts as more effective ligand transfer agents than the analogous lithium salts.

$\text{To}^{\text{M}}\text{ZrCl}_3$ was found to be quite robust, as the isolated material displayed no decomposition after refluxing in a toluene solution for seven days. The compound displays C_{3v} symmetry in both the solution and solid state, as evidenced by a single set of resonances for the oxazoline methyl and methylene groups in the ^1H NMR spectrum at 1.36 and 3.28 ppm, respectively, and a single ν_{CN} stretching frequency in the IR spectrum which had been shifted to lower energy at 1545 cm^{-1} compared to LiTo^{M} .

To explore the viability of chloride substitution, a toluene solution of $\text{To}^{\text{M}}\text{ZrCl}_3$ and KOt-Bu was stirred overnight at room temperature to give $\text{To}^{\text{M}}\text{Zr}(\text{Ot-Bu})\text{Cl}_2$ (eq 2.8).



The ^1H NMR spectrum displays the C_s symmetry of the substituted product. A mirror plane contains the *tert*-butoxide oxygen, zirconium center, and *trans*-oxazoline ring resulting in equivalent methyl and methylene groups on the *trans* ring (1.52 and 3.38 ppm, respectively) (Figure 2.4). While the two other rings are related by the mirror plane, the methylene groups were either *endo* or *exo* to the *tert*-butoxide and were observed as two coupled doublets (3.38 and 3.25 ppm, $^2J_{\text{HH}} = 8.72$ Hz). Likewise, the methyl substituents of the oxazoline rings were also observed to be inequivalent resulting in two singlet resonances. These resonances, at 1.45 and 1.05 ppm, were assigned as *exo* and *endo*, respectively, through the use of a NOESY NMR experiment. These peaks were confirmed as being *cis* to the *tert*-butoxide in the ^1H - ^{15}N HMBC as they both correlate to a ^{15}N resonance at -142.9

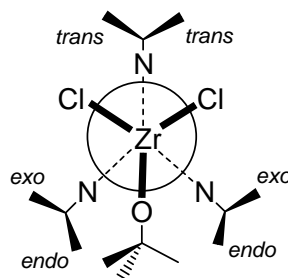


Figure 2.4. Newman projection illustrating the C_s -symmetry of $\text{To}^{\text{M}}\text{Zr}(\text{Ot-Bu})\text{Cl}_2$. The groups attached to N represent CH_2 and CMe_3 substituents on the oxazoline rings.

ppm, while the *trans* nitrogen was located at -140.9 ppm.

A solid state structure of the product confirmed the N,N,N- κ^3 coordination of the To^M ligand to zirconium, as well as the overall connectivity of the molecule (Figure 2.5). A distorted octahedral geometry is observed at the zirconium center, with a relatively short Zr – O bond ($1.891(3)$ Å) for a six-coordinate zirconium *tert*-butoxide. C_1 symmetry is observed for $To^M Zr(Or-Bu)Cl_2$ in the solid state due to inequivalent twist conformations of the three oxazoline rings. This results in the methyl groups on the 4-position being located either axially or equatorially (toward the zirconium center). Additionally, all of the distances from the zirconium center to the 4-methyl groups are inequivalent, and range from 3.76 to 4.23 Å. This creates an unusual steric pocket around the metal center, which can best be described by the solid angle for To^M .^{21,22} As the shape of the To^M ligand is far removed from that of a cone, a Tolman cone angle fails to provide an accurate measure of the steric size of the ligand. Solid angles give a more realistic representation of the steric bulk of To^M and similarly shaped scorpionates than the traditional cone angle. The solid angle of a ligand can be visualized by regarding the metal atom as a point source of light. Ligands bound to the metal center create shadows on a sphere centered at the light. Dividing the area of the shadow by the radius of the sphere gives the ligand's solid angle in units of steradians. Calculated from the crystallographic data, the solid angle was found to be 5.40 steradians, corresponding to 43% of the surface of a sphere. This shows To^M to be substantially larger than Tp^* , whose solid angle is calculated to be 3.62 steradians or 30% of a sphere's surface (determined for $Tp^* Zr(CH_2C_6H_5)_3$).^{6c}

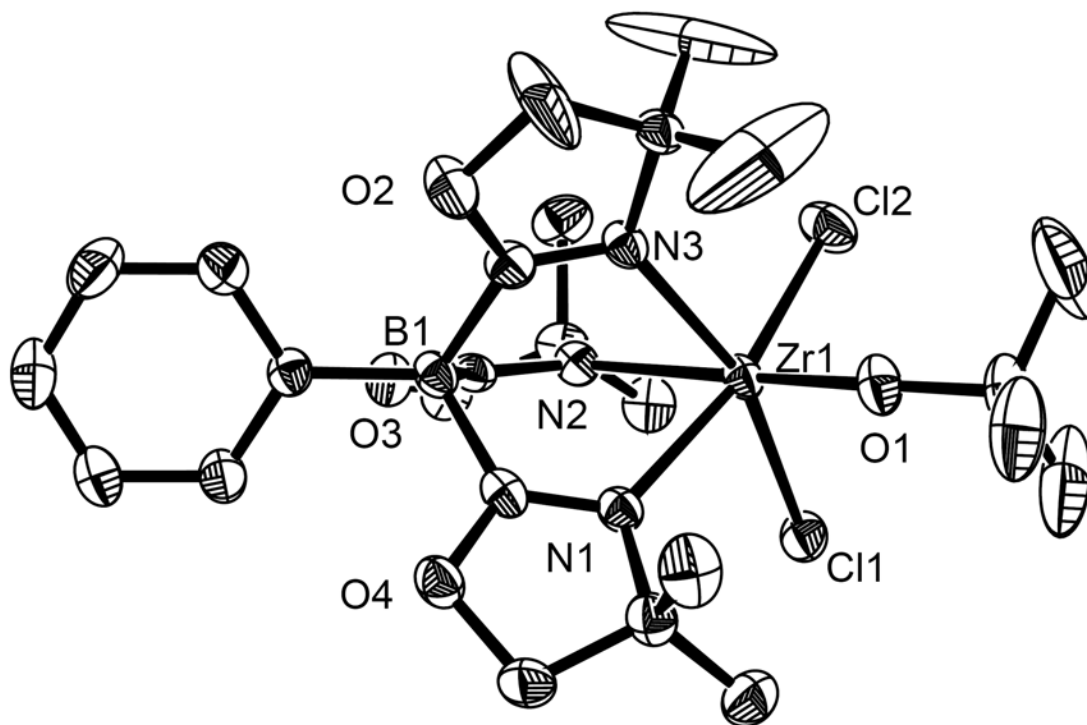
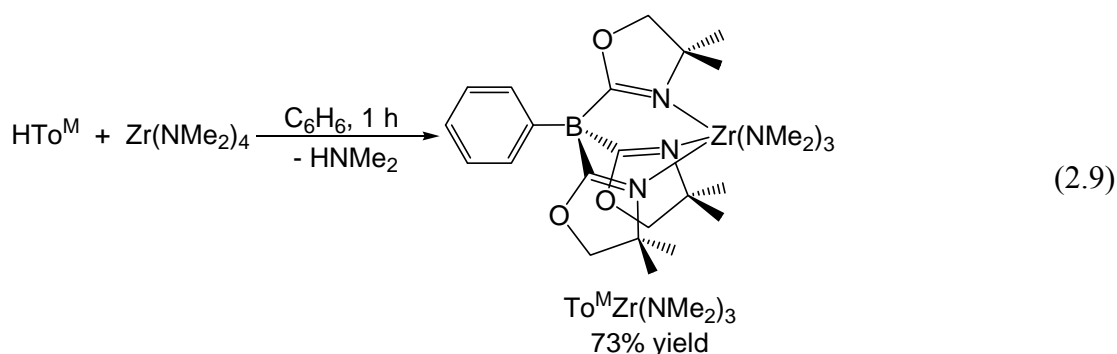


Figure 2.5. ORTEP diagram of $\text{To}^{\text{M}}\text{Zr}(\text{O}t\text{-Bu})\text{Cl}_2$ at 50% probability. Hydrogen atoms are omitted for clarity.

Amine elimination also proved to be a viable route for the preparation of $\text{To}^{\text{M}}\text{Zr}(\text{IV})$ compounds.²³ Reaction of HTo^{M} and $\text{Zr}(\text{NMe}_2)_4$ in benzene yielded $\text{To}^{\text{M}}\text{Zr}(\text{NMe}_2)_3$ as a white solid in good yield (73%, eq 2.9). Micromolar scale reactions monitored in situ by ^1H NMR revealed the rapid formation of 1 equivalent of HNMe_2 (< 10 min), as well as one set of oxazoline resonances (1.09 and 3.41 ppm) and a singlet corresponding to the equivalent NMe_2 groups at 3.15 ppm. In comparison to $\text{To}^{\text{M}}\text{ZrCl}_3$, $\text{To}^{\text{M}}\text{Zr}(\text{NMe}_2)_3$ proved to be thermally unstable in solution. Heating a benzene solution of $\text{To}^{\text{M}}\text{Zr}(\text{NMe}_2)_3$ at 60 °C for over one hour resulted in decomposition of the metal complex to unidentified products.

In contrast, the salt metathesis reaction of $\text{To}^{\text{M}}\text{ZrCl}_3$ and 3 equivalents of LiNMe_2 (benzene- d_6 , room temperature, 24 h) produced a C_s symmetric product with inequivalent



oxazoline resonances. The ^1H NMR spectrum of the reaction mixture showed a 1:1 ratio of To^{M} to NMe_2 groups, upon which the product was assigned as the mono-substituted $\text{To}^{\text{M}}\text{Zr}(\text{NMe}_2)\text{Cl}_2$. In an attempt to completely replace the Cl ligands, more forcing conditions were employed. In the presence of 6 equivalents of LiNMe_2 at elevated temperatures ($60\text{ }^\circ\text{C}$, 24 h), $\text{Zr}(\text{NMe}_2)_4$ and LiTo^{M} are observed to form in the reaction. A similar result was reported in the attempt to alkylate $\text{Tp}^*\text{ScCl}_2(\text{THF})_n$ with alkyl lithiums, resulting in mixtures of LiTp^* and the corresponding $\text{Tp}^*\text{ScR}_2(\text{THF})_n$ complexes.^{5b}

The transmetalation of To^{M} to Li in the presence of excess lithium salts suggested that the To^{M} ligand possesses a hard basic nature. To further test this, attempts were made at substituting the Cl ligands with a range of alkylating agents. The addition of alkyl lithium reagents (LiR , $\text{R} = \text{Me}$, CH_2CMe_3 , CH_2SiMe_3) to benzene solutions of $\text{To}^{\text{M}}\text{ZrCl}_3$ at room temperature resulted in the formation of LiTo^{M} and unidentified Zr salts. Similar results were observed when the reaction was performed at low temperature ($-78\text{ }^\circ\text{C}$), and when the solvent was varied to either toluene, CH_2Cl_2 , or THF. Reaction of $\text{To}^{\text{M}}\text{ZrCl}_3$ with Grignard reagents (RMgX ; $\text{R} = \text{Me}$, CH_2CMe_3 , Bn ; $\text{X} = \text{Cl}$, Br) at low ($-78\text{ }^\circ\text{C}$) or room temperature resulted in the decomposition of the starting materials in both polar (THF) and non-polar solvents (toluene, benzene). Transmetalation of To^{M} to aluminum was observed upon the addition of AlMe_3 to solutions of $\text{To}^{\text{M}}\text{ZrCl}_3$ ($-78\text{ }^\circ\text{C}$ to room temperature). A new To^{M}

product displaying C_s symmetry was observed in the ^1H NMR spectrum in addition to two singlet resonances corresponding to AlMe groups. The identity of the product was confirmed by the independent synthesis and isolation of $\text{To}^{\text{M}}\text{AlMe}_2$ (see Chapter 3). Softer alkylating reagents such as ZnMe_2 displayed no reactivity with $\text{To}^{\text{M}}\text{ZrCl}_3$ as the starting materials could be recovered even after heating a toluene solution to reflux for 18 hours. The inability to directly alkylate $\text{To}^{\text{M}}\text{ZrCl}_3$ is also observed for Tp or Tp^*ZrCl_3 .⁴ However, while $\text{Tp}^*\text{Zr}(\text{Ot-Bu})\text{Cl}_2$ could be alkylated upon the subsequent addition of alkyl lithium or Grignard reagents, similar attempts using $\text{To}^{\text{M}}\text{Zr}(\text{Ot-Bu})\text{Cl}_2$ as the metal precursor were also found to be unsuccessful. The addition of two equivalents of alkyl lithiums ($\text{R} = \text{Me}, \text{CH}_2\text{CMe}_3, \text{CH}_2\text{SiMe}_3$) to solutions of $\text{To}^{\text{M}}\text{Zr}(\text{Ot-Bu})\text{Cl}_2$ produced no observable reaction, while excess alkyl lithium resulted in the formation of LiTo^{M} . Solutions of $\text{To}^{\text{M}}\text{Zr}(\text{Ot-Bu})\text{Cl}_2$ and either Grignards or AlMe_3 resulted in recovery of the starting materials with no other products observed.

Because metathesis reactions did not prove to be a viable route to the formation of $\text{To}^{\text{M}}\text{Zr}$ alkyls, the protonation reaction between HTo^{M} and ZrR_4 ($\text{R} = \text{Bn}, \text{CH}_2\text{CMe}_3, \text{CH}_2\text{SiMe}_3$) was investigated. Decomposition was observed in the cases of ZrBn_4 and $\text{Zr}(\text{CH}_2\text{SiMe}_3)_4$, while no reaction was observed to take place between HTo^{M} and $\text{Zr}(\text{CH}_2\text{CMe}_3)_4$ even under elevated temperatures. Similar attempts at substituting the amide ligands on $\text{To}^{\text{M}}\text{Zr}(\text{NMe}_2)_3$ with primary amines also proved to be unsuccessful at room temperature, and decomposition was observed at higher temperatures (60 °C).

Conclusion

We have synthesized the first example of a trisoxazoline based scorpionate ligand, To^M . The facile synthesis of $LiTo^M$ should allow for a general synthetic route to a wide array of substituted trisoxazoline scorpionates. Combined with the availability of enantiopure *2H*-oxazolines²⁴, optically active C_3 -symmetric tris(oxazoliny)borates should be readily accessible for use as chiral directing ligands in enantioselective catalysis. A range of To^M transfer agents are easily accessible through either salt metathesis or protonation, allowing for selection of an appropriate transfer agent for a specific metal precursor. The robust nature of the To^MZrCl_3 demonstrates the improved binding of the zwitterionic To^M over the neutral trisox ligand, highlighting the significant electronic difference between these two species. The ability of To^M to more fully encompass the zirconium center than Tp^* suggests that To^M is better suited to providing steric protection to highly reactive metal centers, such as cationic zirconium alkyl and hydride complexes. Unfortunately, To^MZr alkyl complexes do not appear to be accessible as both salt metathesis and protonation pathways result in the decomposition of the zirconium complexes. We observed the facile transmetalation of the To^M ligand to main group metals such as aluminum and lithium. This prompted us to investigate the chemistry of main group To^M complexes, and explore their potential in catalysis.

Experimental

General. All manipulations were performed using either Schlenk techniques, or in a glovebox under an inert atmosphere of nitrogen unless otherwise indicated. Dry, oxygen-free solvents were used throughout. Benzene, toluene, methylene chloride, pentane, diethyl ether,

and tetrahydrofuran were degassed by sparging with nitrogen, filtered through activated alumina columns, and stored under N₂. Dichlorophenylborane was purchased from Aldrich and distilled prior to use. 4,4-dimethyl-2-oxazoline was purchased from Acros and used as received. ZrCl₄ was purchased from Strem and was purified by sublimation. ¹H, ¹³C{¹H}, and ¹¹B spectra were collected on a Bruker DRX-400 spectrometer, and ¹⁵N chemical shifts were determined by ¹H-¹⁵N HMBC experiments on a Bruker Avance II 700 spectrometer with a Bruker Z-gradient inverse TXI ¹H/¹³C/¹⁵N 5mm cryoprobe. These shifts were originally referenced to liquid NH₃ and recalculated to the CH₃NO₂ chemical shift scale by adding -381.9 ppm. Elemental analysis was performed using a Perkin-Elmer 2400 Series II CHN/S by the Iowa State Chemical Instrumentation Facility. X-ray diffraction data was collected on a Bruker-AXS SMART 1000 CCD diffractometer using Bruker-AXS SHELXTL software.

Lithium tris(4,4-dimethyl-2-oxazolin-2-yl)phenylborate LiTo^M. A 100 mL Schlenk flask was charged with 4,4-dimethyl-2-oxazoline (1.06 mL, 10.1 mmol), which was then degassed by three freeze-pump-thaw cycles. The degassed oxazoline was dissolved in 40 mL of THF and the flask was cooled to -78 °C. *n*-BuLi (4.24 mL, 10.6 mmol) was added to the cold solution via syringe, and the resulting solution stirred for 15 min at -78 °C. Dichlorophenylborane (0.397 mL, 3.03 mmol) was syringed slowly into the flask, which was allowed to gradually warm to room temperature. After stirring for 26 h, the solvent was removed under reduced pressure leaving a cream colored solid. The solid was extracted with methylene chloride (3 × 15 mL) and isolated *in vacuo*, and then re-extracted with toluene warmed to 80 °C (1 × 50 mL) to give the Li[To^M] (1.06 g, 2.73 mmol, 89.9%). ¹H NMR (acetonitrile-*d*₃, 400 MHz): δ 7.39 (br s, 2 H, *ortho*-C₆H₅), 7.07 (m, 2 H, *meta*-C₆H₅), 7.00

(m, 1 H, *para*-C₆H₅), 3.60 (s, 6 H, CNCMe₂CH₂O), 1.19 (s, 18 H, CNCMe₂CH₂O). ¹³C{¹H} NMR (acetonitrile-*d*₃, 400 MHz): δ 184.6 (br s, CNCMe₂CH₂O), 151.9 (br s, *ipso*-C₆H₅), 134.7 (s, *ortho*-C₆H₅), 127.7 (s, *meta*-C₆H₅), 125.6 (s, *para*-C₆H₅), 77.91 (s, CNCMe₂CH₂O), 67.65 (s, CNCMe₂CH₂O), 29.15 (s, CNCMe₂CH₂O). ¹¹B NMR (acetonitrile-*d*₃, 400 MHz): δ -16.99. IR (KBr, cm⁻¹): 3066 m, 3045 m, 2965 br s, 2930 s, 2872 s, 1607 s (ν_{CN}), 1586 s, 1463 s, 1365 s, 1260 s, 1194 s, 1112 br m, 1000 s, 970 s, 883 m, 734 m, 703 m. Anal. Calcd for C₂₁H₂₉BLiN₃O₃: C, 64.8; H, 7.46; N, 10.80. Found: C, 64.3; H, 7.61; N, 8.87. mp 202-4 °C.

Hydrogen tris(4,4-dimethyl-2-oxazolin-2-yl)phenylborate HTo^M. In air LiTo^M (2.00 g, 5.14 mmol) was dissolved in methylene chloride and filtered through a short silica gel plug in a solvent mixture of hexane:isopropanol:triethylamine (15:1:1). A single fraction was collected. The solvent was evaporated under reduced pressure yielding the off-white product in 50% yield (0.985 g, 2.57 mmol). The product was subsequently dried by stirring in neat chlorotrimethylsilane for 3 h, and then isolated by removal of the chlorotrimethylsilane *in vacuo* and stored under N₂. ¹H NMR (benzene-*d*₆, 400 MHz): δ 7.77 (br s, 2 H, *ortho*-C₆H₅), 7.38 (m, 2 H, *meta*-C₆H₅), 7.22 (m, 1 H, *para*-C₆H₅), 3.83 (s, 6 H, CNCMe₂CH₂O), 1.14 (s, 18 H, CNCMe₂CH₂O). ¹³C{¹H} NMR (benzene-*d*₆, 400 MHz): δ 187.1 (br s, CNCMe₂CH₂O), 142.6 (br s, *ipso*-C₆H₅), 134.0 (s, *ortho*-C₆H₅), *meta*-C₆H₅ obscured by benzene-*d*₆, 127.3 (s, *para*-C₆H₅), 81.48 (s, CNCMe₂CH₂O), 64.22 (s, CNCMe₂CH₂O), 27.50 (s, CNCMe₂CH₂O). ¹¹B NMR (acetonitrile-*d*₃, 400 MHz): δ -17.82. IR (KBr, cm⁻¹): 3067 m, 3049 m, 2966 br s, 2929 s, 2886 br s, 1669 w, 1627 s (ν_{CN}), 1594 s (ν_{CN}), 1461 s, 1425 s, 1387 m, 1361 m, 1317 s, 1189 s, 1149 m, 1114 m, 971 s, 930 m, 750 m, 709 s. Anal. Calcd

for $C_{21}H_{32}BO_4N_3$: C, 62.9; H, 7.98; N, 10.48. Found: C, 62.9; H, 7.90; N, 10.12. mp 104-106 °C.

Thallium tris(4,4-dimethyl-2-oxazolin-2-yl)phenylborate TITo^M. Thallium nitrate (4.50 g, 16.9 mmol) was placed in a 500 mL round bottom flask and dissolved in a water/methylene chloride mixture (1:1, 200 mL). In a separate flask, Li[To^M] (5.87 g, 15.1 mmol) was dissolved in a minimal amount of THF (70 mL). The Li[To^M] solution was added to the TINO₃ solution to produce a white precipitate. This mixture was vigorously stirred for 30 min, and then the precipitate was allowed to settle and the liquid separated into aqueous and organic layers. The aqueous layer was decanted, and the organic layer was washed with water (3 × 100 mL) to remove the precipitate. The volatiles from the organic layer were concentrated under reduced pressure to give a thick yellow solution. The resulting solution was triterated with pentane (5 × 40 mL) precipitating pure white product (5.47 g, 9.33 mmol, 61.7 %), which was used for further syntheses. Recrystallization from toluene at -35 °C gave analytically pure, white crystalline blocks (4.87 g, 8.32 mmol, 55.0%).

¹H NMR (benzene-*d*₆, 400 MHz): δ 8.36 (d, ³J_{HH} = 7.6 Hz, 2 H, *ortho*-C₆H₅), 7.58 (t, ³J_{HH} = 7.6 Hz, 2 H, *meta*-C₆H₅), 7.37 (t, ³J_{HH} = 7.6 Hz, 1 H, *para*-C₆H₅), 3.41 (s, 6 H, CNCMe₂CH₂O), 1.03 (s, 18 H, CNCMe₂CH₂O). ¹³C{¹H} NMR (benzene-*d*₆, 100 MHz): δ 190.5 (br, CNCMe₂CH₂O), 146.7 (br, *ipso*-C₆H₅), 136.59 (*ortho*-C₆H₅), 126.98 (*meta*-C₆H₅), 125.56 (*para*-C₆H₅), 79.83 (CNCMe₂CH₂O), 66.71 (CNCMe₂CH₂O), 28.84 (CNCMe₂CH₂O). ¹¹B NMR (benzene-*d*₆, 128 MHz): δ -16.0 (br s). ¹⁵N NMR (benzene-*d*₆, 71 MHz): δ -117.3 (¹J_{TIN} = 795 Hz). IR (KBr, cm⁻¹): 3071 m, 3039 m, 2963 s, 2928 s, 2889 s, 1600 s (ν_{CN}), 1460 s, 1430 m, 1381 m, 1363 s, 1348 m, 1258 s, 1187 s, 1133 s, 1014 w, 967

s, 926 w, 890 w, 809 w, 744 w, 706 s. Anal. Calc. for $C_{21}H_{29}BN_3O_3Ti$: C, 42.99; H, 4.98; N, 7.16. Found: C, 43.04; H, 4.63; N, 6.74. mp 218-220 °C.

To^MZrCl₃. A 200 mL Schlenk flask was charged with LiTo^M (2.00 g, 5.14 mmol) and ZrCl₄ (1.26 g, 5.40 mmol) in the glovebox. The solids were suspended in 120 mL of methylene chloride, and the mixture was stirred at room temperature for 4 days. The solution was filtered, and the filtrate was evaporated under reduced pressure yielding a crude pale yellow solid (2.32 g, 4.00 mmol, 77.8%). Analytically pure product was obtained by recrystallization from THF/hexane. ¹H NMR (benzene-*d*₆, 400 MHz): δ 8.15 (d, ³J_{HH} = 7.87 Hz, 2 H, *ortho*-C₆H₅), 7.52 (t, ³J_{HH} = 7.41 Hz, 2 H, *meta*-C₆H₅), 7.36 (t, ³J_{HH} = 7.29 Hz, 1 H, *para*-C₆H₅), 3.28 (s, 6 H, CNCMe₂CH₂O), 1.36 (s, 18 H, CNCMe₂CH₂O). ¹³C{¹H} NMR (dichloromethane-*d*₂, 400 MHz): δ 197.9 (br s, CNCMe₂CH₂O), 135.8 (s, *ortho*-C₆H₅), 127.1 (s, *meta*-C₆H₅), 126.7 (s, *para*-C₆H₅), 82.74 (s, CNCMe₂CH₂O), 70.50 (s, CNCMe₂CH₂O), 26.93 (s, CNCMe₂CH₂O). ¹¹B NMR (benzene-*d*₆, 400 MHz): δ -16.79. ¹⁵N NMR (benzene-*d*₆, 700 MHz): δ 141.4 (s, CNCMe₂CH₂O). IR (KBr, cm⁻¹): 3047 w, 2965 s, 2933 s, 2899 br s, 1545 s (ν_{CN}), 1461 s, 1373 s, 1358 m, 1295 s, 1199 s, 1156 m, 960 s, 931 m, 793 m, 705 m, 674 w. Anal. Calcd for C₂₅H₃₇BO₄N₃ZrCl₃: C, 46.0; H, 5.68; N, 6.45. Found: C, 45.8; H, 5.81; N, 6.20. mp 186-190 °C, dec.

To^MZr(O^tBu)Cl₂. In the glovebox To^MZrCl₃ (0.500 g, 0.863 mmol) and potassium *t*-butoxide (0.102 g, 0.906 mmol) were combined in a 100 mL Schlenk flask containing a magnetic stirring bar. Toluene (50 mL) was added to the flask, and the solution was allowed to stir for 18 h. The cloudy solution was filtered, and the solvent was removed from the filtrate under vacuum. The resulting white solid was washed with pentane to give the spectroscopically pure product (0.428 g, 0.694 mmol, 80.4%). X-ray quality crystals were

obtained by recrystallization in toluene at $-30\text{ }^{\circ}\text{C}$. ^1H NMR (benzene- d_6 , 400 MHz): δ 8.26 (d, $^3J_{\text{HH}} = 7.40$ Hz, 2 H, *ortho*- C_6H_5), 7.55 (t, $^3J_{\text{HH}} = 7.30$ Hz, 2 H, *meta*- C_6H_5), 7.37 (t, $^3J_{\text{HH}} = 7.46$ Hz, 1 H, *para*- C_6H_5), 3.38 (d, $^2J_{\text{HH}} = 8.72$ Hz, 2 H, *endo*- $\text{CNCMe}_2\text{CH}_2\text{O}$), 3.38 (s, 2 H, *trans*- $\text{CNCMe}_2\text{CH}_2\text{O}$), 3.25 (d, $^2J_{\text{HH}} = 8.72$ Hz, 2 H, *exo*- $\text{CNCMe}_2\text{CH}_2\text{O}$), 1.62 (s, 6 H, *trans*- $\text{CNCMe}_2\text{CH}_2\text{O}$), 1.59 (s, 9 H, CMe_3), 1.45 (s, 6 H, *exo*- $\text{CNCMe}_2\text{CH}_2\text{O}$), 1.05 (s, 6 H, *endo*- $\text{CNCMe}_2\text{CH}_2\text{O}$). $^{13}\text{C}\{^1\text{H}\}$ NMR (benzene- d_6 , 400 MHz): δ 197.7 (s, *cis*- $\text{CNCMe}_2\text{CH}_2\text{O}$), 192.4 (s, *trans*- $\text{CNCMe}_2\text{CH}_2\text{O}$), 141.9 (s, *ipso*- C_6H_5), 136.4 (s, *ortho*- C_6H_5), 127.4 (s, *meta*- C_6H_5), 126.6 (s, *para*- C_6H_5), 83.68 (s, $\text{CNCMe}_2\text{CH}_2\text{O}$), 81.43 (s, $\text{CNCMe}_2\text{CH}_2\text{O}$), 81.10 (s, $\text{CNCMe}_2\text{CH}_2\text{O}$), 70.41 (s, *trans*- $\text{CNCMe}_2\text{CH}_2\text{O}$), 68.50 (s, *cis*- $\text{CNCMe}_2\text{CH}_2\text{O}$), 31.73 (s, OCMe_3), 28.01 (s, *cis*- $\text{CNCMe}_2\text{CH}_2\text{O}$), 27.27 (s, *trans*- $\text{CNCMe}_2\text{CH}_2\text{O}$), 26.95 (s, *cis*- $\text{CNCMe}_2\text{CH}_2\text{O}$). ^{11}B NMR (benzene- d_6 , 400 MHz): δ -17.94. ^{15}N NMR (benzene- d_6 , 700 MHz): δ -140.9 (s, *trans*- $\text{CNCMe}_2\text{CH}_2\text{O}$), -142.9 (s, *cis*- $\text{CNCMe}_2\text{CH}_2\text{O}$). IR (KBr, cm^{-1}): 3044 w, 2973 s, 2931 s, 2896 s, 1561 s (ν_{CN}), 1463 s, 1391 w, 1370 s, 1287 s, 1251 w, 1236 w, 1198 s, 1176 s, 1028 w, 979 s, 961 s, 930 w, 887 w, 786 m, 705 m. Anal. Calcd for $\text{C}_{26}\text{H}_{41}\text{BO}_4\text{N}_3\text{ZrCl}_2$: C, 49.4; H, 6.49; N, 6.64. Found: C, 49.6; H, 6.49; N, 6.81. mp 168-170 $^{\circ}\text{C}$, dec.

To $^{\text{M}}\text{Zr}(\text{NMe}_2)_3$. In the glovebox HTo^{M} (0.50 g, 1.3 mmol) and $\text{Zr}(\text{NMe}_2)_4$ (0.35 g, 1.3 mmol) were placed into a 100 mL Schlenk flask. The solids were dissolved in 50 mL of benzene, and the solution was stirred for 1 h. Solvent was removed under reduced pressure, and the solid was washed with pentane giving a white product (0.58 g, 0.96 mmol, 73%). ^1H NMR (benzene- d_6 , 400 MHz): δ 8.27 (d, $^3J_{\text{HH}} = 6.91$ Hz, 2 H, *ortho*- C_6H_5), 7.56 (t, $^3J_{\text{HH}} = 7.37$, 2 H, *meta*- C_6H_5), 7.36 (t, $^3J_{\text{HH}} = 6.91$ Hz, 1 H, *para*- C_6H_5), 3.41 (s, 6 H, $\text{CNCMe}_2\text{CH}_2\text{O}$), 3.15 (s, 18 H, NMe_2), 1.09 (s, 18 H, $\text{CNCMe}_2\text{CH}_2\text{O}$). $^{13}\text{C}\{^1\text{H}\}$ NMR

(benzene-*d*₆, 400 MHz): δ 191.5 (br s, CNCMe₂CH₂O), 144.9 (br s, *ipso*-C₆H₅), 136.3 (s, *ortho*-C₆H₅), 127.2 (s, *meta*-C₆H₅), 125.9 (*para*-C₆H₅), 80.41 (s, CNCMe₂CH₂O), 69.32 (s, CNCMe₂CH₂O), 47.85 (s, NMe₂), 27.25 (s, CNCMe₂CH₂O). ¹¹B NMR (benzene-*d*₆, 400 MHz): δ -17.20. ¹⁵N NMR (benzene-*d*₆, 700 MHz): δ -141.9 (s, CNCMe₂CH₂O). IR (KBr, cm⁻¹): 3044 w, 2963 s, 2931 s, 2886 s, 2811 s, 2759 s, 1572 s (ν_{CN}), 1463 s, 1431 w, 1368 m, 1267 s, 1249 m, 1195 s, 1155 s, 992 s, 962 s, 943 s, 890 w, 839 w, 783 w, 745 m, 703 s, 680 w. Anal. Calcd for C₂₇H₄₇BN₆O₃Zr: C, 53.55; H, 7.77; N, 13.88. Found: C, 53.26; H, 8.12; N, 11.88. mp 120-122 °C, dec.

References:

- 1) (a) Trofimenko, S. *J. Am. Chem. Soc.* **1966**, 88, 1842-1844. (b) Calabrese, J. C.; Trofimenko, S.; Thompson, J.S. *J. Chem. Soc. Chem. Commun.* **1986**, 1122-1123. (c) Trofimenko, S.; Calabrese, J. C.; Thompson, J. S. *Inorg. Chem.* **1987**, 26, 1507-1514. (d) Trofimenko, S.; Calabrese, J. C.; Domaille, P. J.; Thompson, J. S. *Inorg. Chem.* **1989**, 28, 1091-1101. (e) Trofimenko, S. *Chem. Rev.* **1993**, 93, 943. (f) Trofimenko, S. *Scorpionates – The Coordination Chemistry of Polypyrazolylborate Ligands*; Imperial College Press: London, 1999.
- 2) (a) Hess, A.; Horz, M. R.; Liable-Sands, L. M.; Lindner, D. C.; Rheingold, A. L.; Theopold, K. H. *Angew. Chem. Int. Ed.* **1999**, 38, 166-168. (b) Qin, K.; Incarvito, C. D.; Rheingold, A. L.; Theopold, K. H. *Angew. Chem. Int. Ed.* **2002**, 41, 2333-2335. (c) Qin, K.; Incarvito, C. D.; Rheingold, A. L.; Theopold, K. H. *J. Am. Chem. Soc.* **2002**, 124, 14008-14009.
- 3) Kresinski, R. A.; Isam, L.; Hamor, T. A.; Jones, C. J.; McCleverty, J. A. *J. Chem. Soc.*,

- Dalton Trans.* **1991**, 1835-1842.
- 4) (a) Reger, D.L.; Tarquini, M.E. *Inorg. Chem.* **1982**, *21*, 840 – 842. (b) Reger, D.L.; Tarquini, M.E. *Inorg. Chem.* **1983**, *22*, 1064 – 1068. (c) Reger, D.L.; Tarquini, M.E.; Lebioda, L. *Organometallics* **1983**, *2*, 1763 – 1769.
- 5) (a) Long, D.P.; Bianconi, P.A. *J. Am. Chem. Soc.* **1996**, *118*, 12453 – 12454. (b) Blackwell, J.; Lehr, C.; Sun, Y.; Piers, W. E.; Pearce-Batchilder, S. D.; Zaworotko, M. J.; Young, V. G. *Can. J. Chem.* **1997**, *75*, 701 – 711. (c) Long, D. P.; Chandrasekaran, A.; Day, R. O.; Bianconi, P. A.; Rheingold, A. L. *Inorg. Chem.* **2000**, *39*, 4476 – 4487.
- 6) (a) Murtuza, S.; Casagrande, O. L.; Jordan, R. F. *Organometallics* **2002**, *21*, 1882 – 1890. (b) Michiue, K.; Jordan, R.F. *Organometallics* **2004**, *23*, 460 – 470. (c) Lee, H.; Jordan, R. F. *J. Am. Chem. Soc.* **2005**, *127*, 9384 – 9385. (d) Lee, H.; Nienkemper, K.; Jordan, R. F. *Organometallics* **2008**, *27*, 5075-5081. (e) Nienkemper, K.; Lee, H.; Jordan, R. F.; Ariaferd, A.; Dang, L.; Lin, Z. *Organometallics* **2008**, *27*, 5867-5875.
- 7) Nakazawa, H.; Ikai, S.; Imaoka, K.; Kai, Y.; Yano, T. *J. Mol. Cat. A.* **1998**, *132*, 33 – 41.
- 8) (a) Furlan, L. G.; Gil, M. P.; Casagrande, O. L. *Macromol. Rapid. Commun.* **2000**, *21*, 1054 – 1057. (b) Gil, M.P.; Casagrande Jr., O.L. *J. Organomet. Chem.* **2004**, *689*, 286 – 292.
- 9) Itagaki, K.; Kakinuki, K.; Katao, S.; Khamnaen, T.; Fujiki, M.; Nomura, K.; Hasumi, S. *Organometallics* **2009**, *28*, 1942-1949.
- 10) (a) Albinati, A.; Bovens, M.; Rügger, H.; Venanzi, L. M., *Inorg. Chem.* **1997**, *36*, 5991 – 5999. (b) Brunker, T. J.; Hascall, T.; Cowley, A. R.; Rees, L. H.; O'Hare, D., *Inorg. Chem.* **2001**, *40*, 3170 – 3176. (c) Küchkmann, T. I.; Abram, U. *Z. Anorg. Allg.*

- Chem.* **2004**, *630*, 783 – 785. (d) Biagini, P.; Calderazzo, F.; Marchetti, F.; Romano, A. M.; Spera, S. *J. Organomet. Chem.* **2006**, *691*, 4172 – 4180. (e) Zhao, N.; Van Stipdonk Michael, J.; Bauer, C.; Campana, C.; Eichhorn David, M., *Inorg. Chem.* **2007**, *46*, 8662 – 8667.
- 11) While B–C bond cleavage is less facile than B–N, metal-mediated examples are known. For representative examples, see: (a) Bianchini, C.; Meli, A.; Laschi, F.; Vizza, F.; Zanello, P. *Inorg. Chem.* **1989**, *28*, 227-233. (b) Konze, W.V.; Scott, B.L.; Kubas, G.J. *J. Chem. Soc., Chem. Commun.* **1999**, 1807-1808. (c) Strunkina, L.I.; Minacheva, M. Kh.; Lyssenko, K.A.; Petrovskii, P.V.; Burlakov, V.V.; Rosenthal, U.; Shur, V.B. *Russ. Chem. Bull., Int. Ed.* **2006**, *55*, 174-176. (d) Cho, J.; Yap, G.P.A.; Riordan, C.G. *Inorg. Chem.* **2007**, *36*, 11308-11315.
- 12) For reviews, see: (a) Ghosh, A.K.; Mathivanin, p.; Cappiello, J. *Tetrahedron: Asymmetr.* **1998**, *9*, 1-45. (b) McManus, H.A.; Guiry, P.J. *Chem. Rev.* **2004**, *104*, 4151-4202. For recent applications, see: (c) Gothelf, A.S.; Gothelf, K.V.; Hazell, R.G.; Jorgensen, K.A. *Angew. Chem. Int. Ed.* **2002**, *41*, 4236-4238. (d) Evans D.A.; Masse, C.E.; Wu, J. *Org. Lett.* **2002**, *4*, 3375-3378. (e) Evans, D.A.; Downey, C.W.; Hubbs, J.L. *J. Am. Chem. Soc.* **2003**, *125*, 8706-8707. (f) Sibi, M.P.; Itoh, K.; Jasperse, C.P. *J. Am. Chem. Soc.* **2004**, *126*, 5366-5367. (g) Palomo, C.; Oiarbide, M.; Kardak, B.G.; Garcia, J.M.; Linden, A. *J. Am. Chem. Soc.* **2005**, *127*, 4154-4155.
- 13) (a) Mazet, C.; Kohler, V.; Pfaltz, A. *Angew. Chem. Int. Ed.* **2005**, *44*, 4888 – 4891. (b) Mazet, C.; Roseblade, S.; Kohler, V.; Pfaltz, A., *Org. Lett.* **2006**, *8*, 1879 – 1882.
- 14) (a) Bellemin-Laponnaz, S.; Gade, L.H. *J. Chem. Soc., Chem. Commun.* **2002**, 1286 –

1287. (b) Bellemin-Lapponnaz, S.; Gade, L.H. *Angew. Chem. Int. Ed.* **2002**, *41*, 3473 – 3475. (c) Ward, B.D.; Bellemin-Lapponnaz, S.; Gade, L.H. *Angew. Chem. Int. Ed.* **2005**, *44*, 1668 – 1671. (d) Lukesova, L.; Ward, B. D.; Bellemin-Lapponnaz, S.; Wadepohl, H.; Gade, L. H., *J. Chem. Soc., Dalton Trans.* **2007**, 920 – 922.
- 15) Crabtree, R.H. *The Organometallic Chemistry of the Transition Metals*, 5th ed.; Wiley: Hoboken, 2009.
- 16) Dunne, J.F.; Manna, K.; Wiench, J.W.; Ellern, A.; Pruski, M.; Sadow, A.D. *Dalton Trans.* **2010**, *39*, 641-653.
- 17) Kidd, R.G. *NMR of Newly Accessible Nuclei*; Laszlo, P., Ed.; Academic Press: New York, **1983**; Vol. 2, pp 49 – 77.
- 18) For comparisons of ^{15}N - ^{205}Tl coupling constants reported for thallium scorpionates, see Claramunt, R.M.; Sanz, D.; Santa Maria, M.D.; Elguero, J.; Trofimenko, S. *J. Organomet. Chem.* **2004**, *689*, 463-470.
- 19) Pawlikowski, A.V.; Ellern, A.; Sadow, A.D. *Inorg. Chem.* **2009**, *48*, 8020-8029.
- 20) Dunne, J.F.; Su, J.; Ellern, A.; Sadow, A.D. *Organometallics* **2008**, *27*, 2399-2401.
- 21) (a) White, D.; Coville, N. *J. Adv. Organomet. Chem.* **1994**, *36*, 95-158. (b) Taverner, B. *C. J. Comp. Chem.* **1996**, *17*, 1612 – 1623. (c) The solid angles were calculated from X-ray coordinates of $\text{Tp}^*\text{Zr}(\text{CH}_2\text{C}_6\text{H}_5)_3$ and $\text{To}^{\text{M}}\text{Zr}(\text{Ot-Bu})\text{Cl}_2$ using the program *Steric* running the algorithms described in ref. 18a. (d) For comparison, the cone angles were also calculated using *Steric*: $[\text{To}^{\text{M}}]^-$, 242° ; $[\text{Tp}^*]^-$, 246° .
- 22) Taverner, B. C. *Steric* Version. 1.1., Structural Chemistry: University of the Witwatersrand, South Africa, 1995.
- 23) (a) Diamond, G.M.; Rodewald, S.; Jordan, R.F. *Organometallics* **1995**, *14*, 5 – 7. (b)

Diamond, G.M.; Jordan, R.F.; Petersen, J.L. *Organometallics* **1996**, *15*, 4030 – 4037.

24) (a) Leonard, W.R.; Romine, J.L.; Meyers, A.I. *J. Org. Chem.* **1991**, *56*, 1961-1963. (b)

Kamata, K.; Agata, I.; Meyers, A.I. *J. Org. Chem.* **1998**, *63*, 3113-3116.

Chapter 3: Bis(oxazoliny)phenylborane: A Lewis acid-containing ligand for methide abstraction-based coordination to aluminum(III)

Modified from a paper published in *Dalton Transactions*[‡]

James F. Dunne[†], Kuntal Manna[§], Jerzy W. Wiench^{*}, Arkady Ellern, Marek Pruski^{*}, and Aaron D. Sadow

Department of Chemistry and U.S. Department of Energy Ames Laboratory, Iowa State University, 1605 Gilman Hall, Ames, IA 50011-3111

Abstract

A compound that contains a Lewis acidic boron center and coordinating oxazoline groups, bis(4,4-dimethyl-2-oxazoliny)phenylborate $\text{PhB}(\text{Ox}^{\text{Me}_2})_2$, has been prepared and spectroscopically characterized. The bifunctional nature of $\text{PhB}(\text{Ox}^{\text{Me}_2})_2$ is demonstrated by its reaction with $[\text{AlMe}_3]_2$ which proceeds *via* methide abstraction by the boron and oxazoline coordination to aluminum to yield $\{\kappa^2\text{-PhMeB}(\text{Ox}^{\text{Me}_2})\}\text{AlMe}_2$. $\text{PhMeB}(\text{Ox}^{\text{Me}_2})\text{AlMe}_2$ contains a planar six-membered chelate ring in contrast to related bis(pyrazolyl) boratoaluminum compounds that are puckered. Additionally, $\text{PhMeB}(\text{Ox}^{\text{Me}_2})\text{AlMe}_2$ and related bidentate tris(oxazoliny)phenylborato dimethylaluminum are inert toward aluminum-methyl bond protonolysis with alcohols, water, and organic acids. This robust nature suggested the possibility of using these oxazolinyborato aluminum compounds in catalytic reactions, as is demonstrated by lactide ring opening polymerization.

‡Parts of this paper are reprinted with permission of *Dalton Trans.* **2008**, *39*, 641-653.

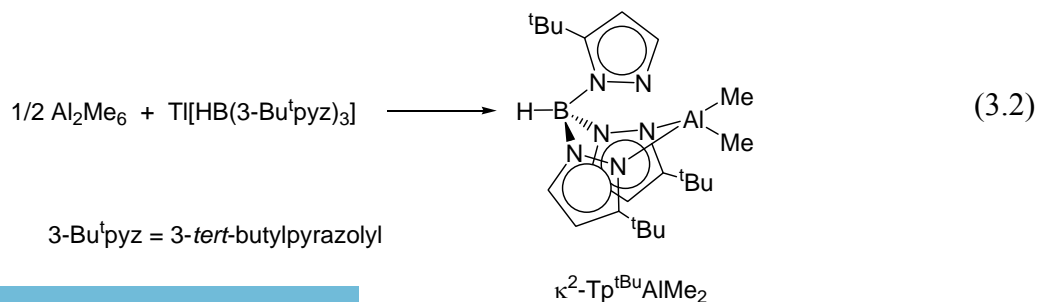
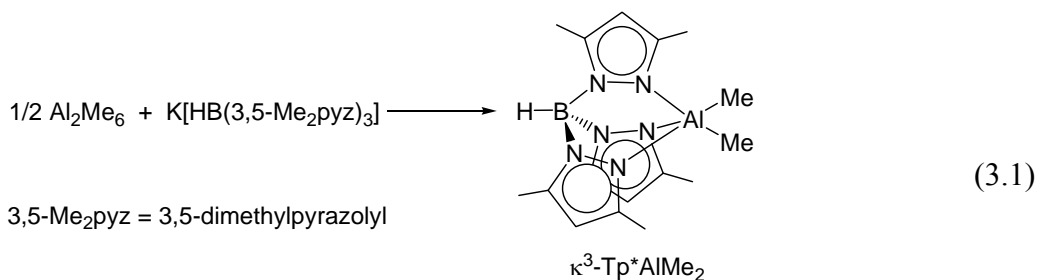
†Primary researcher and author

§Performed solution state NMR studies on $\text{PhB}(\text{Ox}^{\text{Me}_2})_2$.

*Performed solid state NMR experiments on $\text{PhB}(\text{Ox}^{\text{Me}_2})_2$.

Introduction

Organometallic compounds of *p*-block metals are extremely important reagents in synthetic chemistry¹, and as such significant efforts have been made to elucidate the mechanisms of their reactions.² Unfortunately, the exploration of main group metal reaction mechanisms is often hindered by the lack of well-defined organometallic species, and so single site metal complexes with well-defined structures are highly desirable.³ One of the most effective methods of accessing these structures is through the use of sterically demanding, multi-dentate ligands, which can create an environment in which ligand exchange and oligomerization of metal centers is significantly inhibited. Tris(pyrazolyl)borates are an attractive ligand set for this purpose, as the steric bulk on the pyrazolyl ring can be tuned by altering the substituents in the 3- and 5- positions. Increasing the bulk of the R groups at the 3-position of the ring can result in changing the coordination of the ligand between bi- and tridentate, which can alter the reactivity of the metal center.

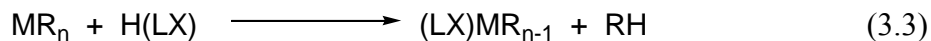


The change in the binding mode of the ligand is more pronounced in the cases of smaller metal centers, as exemplified by Tp^*AlMe_2 and $\text{Tp}^{\text{tBu}}\text{AlMe}_2$ (eq 3.1 and 3.2).⁴ Substitution of the methyl group in the 3-position on the pyrazolyl rings with a *tert*-butyl group changes the binding mode of the tris(pyrazolyl)borate from tridentate to bidentate, and concurrently changes the aluminum center from five-coordinate to four-coordinate.

Steric tuning is also possible with the tris(oxazolinyl)borate ligands as there exists a wide range of readily accessible amino acid starting materials. We had observed the unexpected formation of a $\text{To}^{\text{M}}\text{Al(III)}$ ($\text{To}^{\text{M}} = \text{tris(4,4-dimethyloxazolinyl)phenyl borate}$) species during the reaction of $(\text{AlMe}_3)_2$ and $\text{To}^{\text{M}}\text{ZrCl}_3$, and we were motivated to independently synthesize this species to determine the mode of coordination that To^{M} adopts on smaller metal centers. Additionally, while TpAl compounds have been known for some time, there are few investigations into the reactivity of these compounds.⁵

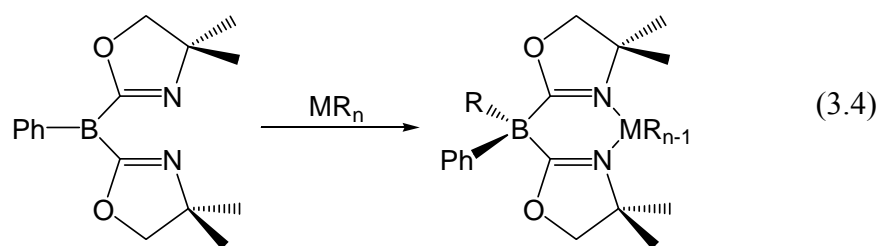
In addition to exploring the structure and reactivity of $\text{To}^{\text{M}}\text{Al}$ compounds, we were also interested in exploring new methods of introducing anionic ligands to metal centers. The salt metathesis reaction is a potent method of coordinating anionic ligands in inorganic synthesis. However, several problems can occur with this method including incomplete salt elimination, poor control of stoichiometry, and the potential for electron transfer reactions. One effective alternative to salt metathesis is the protonolytic elimination in which a Brønsted acidic proligand and a basic anionic group bound to a metal center react to formally open a coordination site at which the incoming ligand can bind (eq 3.3). The limitations of this method can be seen in the reaction of ZrR_4 ($\text{R} = \text{CH}_2\text{Ph}, \text{CH}_2\text{CMe}_3, \text{CH}_2\text{SiMe}_3$) with HTo^{M} (see Chapter 1) which result either in recovery of the starting materials, or decomposition to unidentified products. The limitations of these methods suggest that new

means of anionic ligand introduction would be valuable in synthetic chemistry.



Both the metathesis and protonolysis-based methods formally involve the abstraction of an anionic ligand from a metal center. A new synthetic method that continues to apply this general concept could involve the replacement of the Brønsted acid site (that mediates protonolysis) with a Lewis acidic center which could then act as an abstraction agent. Reaction of a Lewis acid-containing proligand with an organometallic precursor would then provide a direct, one-step route to zwitterionic metal compounds.⁶ In this manner, a variety of ambiphilic ligands utilizing phosphines as the Lewis basic coordinating group, and boranes⁷, alanes⁸, and gallanes⁹ as the Lewis acidic abstraction group have been reported and successfully transfer both alkyl and halide ligands from the metal center to the Lewis acidic center of the ambiphilic ligand.

The To^{M} ligand contains both a Lewis acidic boron center, as well as the Lewis basic coordinating groups of the oxazoline nitrogens. A bis(oxazoliny)borane analog of To^{M} could be capable of concurrent abstraction and coordination, resulting in an unsymmetrical bis(oxazoliny)phenylalkyl borate metal complex as shown in eq. 3.4. In the synthesis of LiTo^{M} , molar ratios of PhBCl_2 exceeding 0.30 equivalents relative to the starting $2H$ -oxazoline gave mixtures of LiTo^{M} and a species assigned as the borane product bis(oxazoliny)borane, $\text{PhB}(\text{Ox}^{\text{Me}_2})_2$ (see Chapter 2).

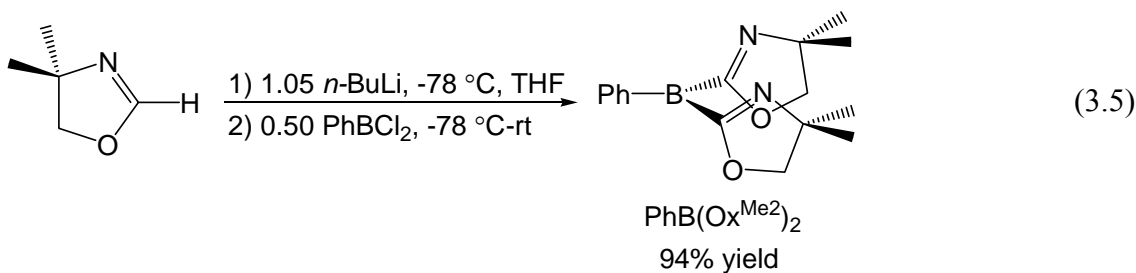


The accessibility of the bis(oxazoliny)borane led us to independently synthesize and isolate this species as well, and investigate the ability of this new borane in Lewis acid-mediated abstraction/ Lewis basic coordination to aluminum. The structure and reactivity of the tris(oxazoliny)borate aluminum compound, $\text{To}^{\text{M}}\text{AlMe}_2$, and the bis(oxazoliny)borate aluminum resulting from successful abstraction and coordination were compared, and found to be active catalysts for the ring opening polymerization of lactide.

Results and Discussion

Synthesis of $\text{PhB}(\text{Ox}^{\text{Me}_2})_2$

Reaction of 0.5 equivalents of PhBCl_2 with 2-lithio-4,4-dimethyl-2-oxazolidine, deprotonated in the same manner as described for the synthesis of LiTo^{M} , provides the desired bis(4,4-dimethyl-2-oxazoliny)phenylborane, $(\text{PhB}(\text{Ox}^{\text{Me}_2})_2)$, after 14 h in THF (eq. 3.5).



While bis(oxazoliny)borates have previously been reported¹⁰, $\text{PhB}(\text{Ox}^{\text{Me}_2})_2$ is the first neutral oxazoline substituted borane. Poly(pyrazolyl)boranes, which would be closely comparable to $\text{PhB}(\text{Ox}^{\text{Me}_2})_2$, are, to our knowledge, not reported. This may be related to the synthesis of poly(pyrazolyl)borates which are typically prepared through dehydrogenative condensation reactions of pyrazole rings and borohydride, and the corresponding boranes are not accessible through this route.

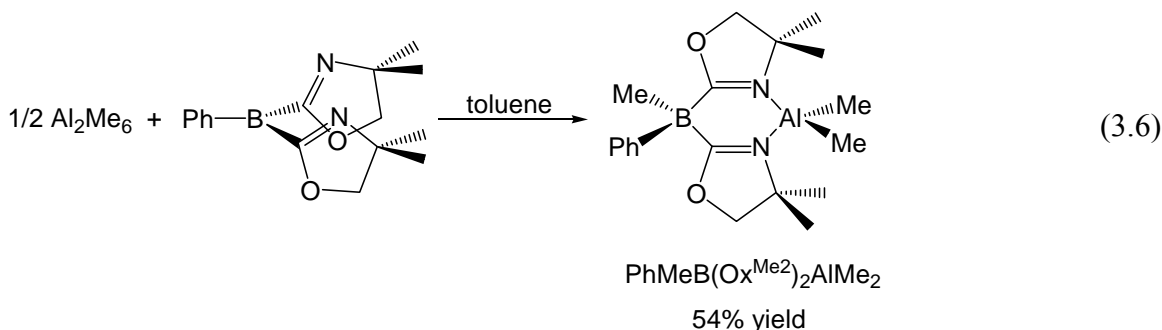
The ^1H , ^{11}B , and ^{15}N NMR spectroscopic properties of $\text{PhB}(\text{Ox}^{\text{Me}_2})_2$ are both solvent and temperature dependent, and a range of experiments have been conducted to determine the exact structure of the compound in both the solid and solution states.¹¹ The data reported is consistent with intermolecular oxazoline-boron interactions in both the solid and solution states, which results in the formation of a mixture of oligomers.

Synthesis of $\text{PhMeB}(\text{Ox}^{\text{Me}_2})_2\text{AlMe}_2$ and structural analysis

The bis(oxazoliny) borane $\text{PhB}(\text{Ox}^{\text{Me}_2})_2$ contains a Lewis acidic boron center as well as Lewis basic coordinating groups in both the O and N centers on the oxazoline rings. The combination of these structural features suggested that this compound would be appropriate for Lewis acid-mediated abstraction and Lewis base coordination to a metal center. As the intermolecular boron-oxazoline interactions that cause oligomers are labile, both the Lewis acid and base sites should be available to perform the abstraction/coordination reaction.

In a microliter scale experiment, addition of 0.5 equivalents of $(\text{AlMe}_3)_2$ to a benzene- d_6 solution of $\text{PhB}(\text{Ox}^{\text{Me}_2})_2$ results in a mixture of minor unidentified products and the desired compound $\text{PhMeB}(\text{Ox}^{\text{Me}_2})_2\text{AlMe}_2$. While the abstraction/coordination product is apparent in the ^1H NMR spectrum initially after mixing the reagents, the reaction proceeds slowly at room temperature over a 24 hour period to give $\text{PhMeB}(\text{Ox}^{\text{Me}_2})_2\text{AlMe}_2$ as the major

product. Trace amounts of the starting borane $\text{PhB}(\text{Ox}^{\text{Me}_2})_2$ are still present in the NMR spectra after the reaction has gone to completion.



On a larger scale, the zwitterionic product is isolated by crystallization from toluene as a pure, white solid (eq 3.6). Crystallization proved to be necessary to purify the product, as the remaining impurities are not removed either by extraction with benzene or column chromatography using silica gel or grade III alumina. As a consequence of the difficulty associated with isolation, the yield of $\text{PhMeB}(\text{Ox}^{\text{Me}_2})_2\text{AlMe}_2$ is a modest 54%. The ability of the boron center to mediate the Al-Me abstraction demonstrates the greater Lewis acidity of the borane than the aluminum(III) center in the parent $(\text{AlMe}_3)_2$.

The ^1H NMR spectrum of $\text{PhMe}(\text{Ox}^{\text{Me}_2})_2\text{AlMe}_2$ displays C_s symmetry, with two doublet resonances for the oxazoline methylene protons (3.23 and 3.12 ppm) and two singlets for the oxazoline methyls (0.93 and 0.92 ppm). Two upfield singlets (-0.27 and -0.33 ppm, 3 H each) were also observed and assigned as inequivalent aluminum methyl groups. The ^1H NMR spectrum also provided evidence for the abstraction of a methyl group from the aluminum center to boron by a broad resonance at 0.89 ppm (3 H). A ^1H - ^{11}B HMQC experiment confirmed the assignment of this peak as a B-CH₃ based on a crosspeak with the boron resonance at -16.7 ppm. The appearance of this resonance in the ^{11}B NMR spectrum

further confirmed the formation of a borate.^{11,12} The coordination of the oxazoline rings to aluminum through the nitrogen centers is indicated by the chemical shift of the oxazoline nitrogen in a ^1H - ^{15}N HMBC experiment. The resonance of the coordinated nitrogen centers is observed at -186.7 ppm, which is a difference of 59.2 ppm from the resonance of the nitrogen in free 2*H*-oxazoline (-127.5 ppm). A direct comparison of the nitrogen signals between $\text{PhB}(\text{Ox}^{\text{Me}_2})_2$ and $\text{PhMeB}(\text{Ox}^{\text{Me}_2})_2\text{AlMe}_2$ is not possible due to the lack of a nitrogen resonance for $\text{PhB}(\text{Ox}^{\text{Me}_2})_2$ in benzene-*d*₆. As both the O and N centers in the oxazoline rings are Lewis basic, coordination to the metal center could proceed through either donor. The bonding of the oxazolines to aluminum through nitrogen was confirmed by an ^1H - ^{15}N HMBC experiment, which contained crosspeaks between the AlMe and N-oxazoline resonances. The presence of these crosspeaks excludes the possibility of oxazoline coordination through the O centers. The observation of inter-ligand, through-bond ^{15}N -X coupling in nitrogen containing ligands at natural abundance is relatively rare, though some examples have been previously described.¹³ Additional crosspeaks to the expected ^1H - ^{15}N coupling within the oxazoline rings were also observed.

The solid state structure of $\text{PhMeB}(\text{Ox}^{\text{Me}_2})_2\text{AlMe}_2$ was determined from a single crystal X-ray diffraction study, and confirmed the identity of the product (Figure 3.1).

The solid state connectivity is consistent with the solution state data obtained from the NMR spectroscopic studies. The structure also provides support for the identity of $\text{PhB}(\text{Ox}^{\text{Me}_2})_2$, as it is a derivative of that compound. There are two notable structural features in $\text{PhMeB}(\text{Ox}^{\text{Me}_2})_2\text{AlMe}_2$: 1) the twisted oxazoline rings which result in a C_1 symmetric solid state structure, and 2) the planar six-membered $\text{BC}_2\text{N}_2\text{Al}$ chelate ring.

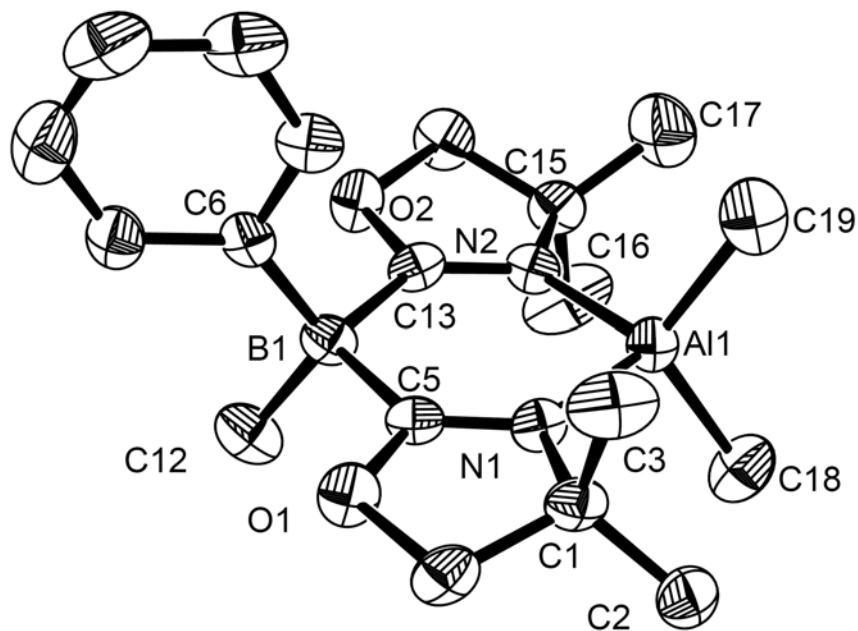


Figure 3.1. ORTEP diagram of $\text{PhMeB}(\text{Ox}^{\text{Me}_2})_2\text{AlMe}_2$ drawn at 50% probability. Hydrogen atoms are excluded for clarity.

In the solid state structure, the methyl groups on the oxazoline rings are positioned in either pseudo-axial (C3 and C16) or pseudo-equatorial (C2 and C17) positions. A twist in the oxazoline rings accounts for this positioning, with torsional angles between co-facial oxazoline C-CH₃ vectors on rings 1 and 2 (C2-C1-C15-C16; C3-C1-C15-C17) of 44.48° and 44.18°, respectively. The pseudo-axial groups (1.75 Å C3-plane distance, 1.83 Å C16-plane distance) are located much farther from the plane defined by Al1, C5, and C13 than the pseudo-equatorial groups (0.60 Å C2-plane, 0.44 Å C17-plane). Furthermore, the pseudo-axial groups are located on opposite faces of the plane in an *anti* fashion and contain a torsion angle of 161.37°. The twisted structure, which produces both the axial and equatorial

groups as well as overall C_1 symmetry, is not observed in the room temperature ^1H NMR spectra in which the *syn* methyl groups are equivalent.

A second interesting structural feature is the conformation of the six-membered chelate ring in $\text{PhMeB}(\text{Ox}^{\text{Me}_2})_2\text{AlMe}_2$. The conformation of this ring affects the position of the metal center relative to the oxazoline rings, and may provide insight into the nature of the bonding interaction of bis(oxazoliny)borate ligands to metals in comparison to pyrazolylborates and bis(oxazoline) ligands. The sum of the interior angles of the six-membered $\text{BC}_2\text{N}_2\text{Al}$ ring is $719.4(3)^\circ$, which indicates that the ring is planar as the sum of the interior angles of a perfect planar six-membered rings is 720° . The torsion angles C5-N1-N2-C13 and N1-C5-C13-N2 are 7.08 and 7.82° , respectively, indicating that the two $\text{C}=\text{N}$ are nearly co-planar. The boron center is also located (within error) in the plane described by the Al1 , C5 , and C13 atoms, and the two nitrogen atoms, N1 and N2 , are displaced slightly from the same plane by $+0.07$ and -0.11 \AA , respectively, but located on opposite sides. The aluminum methyl groups, C18 and C19 , are equidistant from this plane by 1.67 and 1.66 \AA , respectively.

A similarly planar six-membered $\text{C}_3\text{N}_2\text{Al}$ ring is found in the structure of $\{\text{BOX-Me}_2\}\text{AlCl}_2$ ($\text{BOX} = 1,1\text{-bis(oxazoliny)ethane}$), in which the delocalized π system is assumed to favor a planar conformation.¹⁴ However, in the case of $\text{PhMeB}(\text{Ox}^{\text{Me}_2})_2\text{AlMe}_2$, the tetrahedral borate center will disrupt the π -conjugation suggesting that another factor is responsible for the adoption of this conformation. A number of borabox metal complexes have been found to adopt similar planar structures.^{10,15} In the case of palladium(II) borabox complexes, a planar ring structure is adopted when smaller allyl ligands are bound to the Pd center, while a boat conformation is adopted when the larger 1,3-diphenylallyl ligand is

used.¹⁵ Boat conformations have also been observed for six-membered BC₂N₂Ir rings in κ^2 -To^MIrL₂ complexes.^{16,17} From these observations, we suggest that planar bis(oxazolinyl)borate chelate rings are formed in the absence of unfavorable interligand steric effects.

In contrast to PhMeB(Ox^{Me2})₂AlMe₂, related pyrazolylborate aluminum compounds form puckered six-membered rings upon chelation. The cause for this dissimilar conformation between oxazolinylborates versus pyrazolylborates is not immediately apparent. A number of κ^2 -pyrazolylborate aluminum(III) compounds have been crystallographically characterized, and the chelate rings are observed to adopt boat conformations.^{5b,c,18} The tendency of pyrazolylborates to adopt this puckered geometry

Table 3.1. Bond distances and angles from X-ray structures and DFT calculations.

	PhMeB(Ox ^{Me2}) ₂ AlMe ₂ (X-ray)	Me ₂ B(Ox ^{Me2}) ₂ AlMe ₂ (X; B3LYP)	Bp ^{tBu,Me} AlMe ₂ (X-ray) ^{Error!} Bookmark not defined.	H ₂ B(N ₂ C ₃ H ₂) ₂ AlMe ₂ (Z; B3LYP)
Al-N (Å)	1.918(5), 1.931(5)	1.951	2.0060(4), 1.9868(3)	1.968
N-Al-N (°)	98.4(2)	97.25	102.22	92.94
C-B or N-B (Å)	1.621(9), 1.621(8)	1.619	1.5536(2), 1.5499(2)	1.569
E-B-E (°)	109.5(5)	110.05	109.1	107.34

has been previously attributed to the constraints imposed on the chelate ring by the B–N and M–N bond lengths and angles.¹⁹ However, the Al–N and B–C bond lengths and angles between PhMeB(Ox^{Me2})₂AlMe₂ and the Al–N and B–N bond lengths and angles of

$\text{Bp}^{\text{tBu,Me}}\text{AlMe}_2$ ($\text{Bp}^{\text{tBu,Me}} = \text{H}_2\text{B}(3\text{-tBu-5-Me-N}_2\text{C}_3\text{H}_2)_2$)¹⁸ are reasonably similar (Table 3.1). The difference in these values is not sufficient to reasonably explain the conformational differences between the two compounds. Density functional theory (DFT) calculations support this conclusion as the planar and boat conformations of the bis(oxazoliny)borate- and bis(pyrazoly)borate-aluminum, respectively, are reproduced with similar B–C, B–N, and Al–N bond distances.

Another explanation for the difference in structures is unfavorable interligand steric interactions between the aluminum methyl groups, and the phenyl and methyl substituents on the boron center. There are several known dialuminum pyrazolyl compounds, such as $\text{tBu}_2\text{Al}(\mu\text{-N}_2\text{C}_3\text{H}_2)_2\text{Al}^{\text{tBu}}_2$ and $\text{Me}_2\text{Al}(\mu\text{-N}_2\text{C}_3\text{H}_2)\text{AlMe}_2$, that adopt geometries attributed to steric interactions from Al–R groups between metal centers.²⁰ However, for $\text{PhMeB}(\text{Ox}^{\text{Me}_2})_2\text{AlMe}_2$ the shortest C–C distance between the boron phenyl group and the aluminum methyl is long (C–C = 4.76 Å). Additionally, space-filling models show no close contacts between the substituents on the boron and aluminum centers. The solid angle of the $\text{PhMeB}(\text{Ox}^{\text{Me}_2})_2$ ligand was determined by using the program *Solid-G*²¹, and found to be 6.14 steradians (49% of the space surrounding the aluminum center) making unfavorable interligand steric interactions unlikely to occur in the complex.

DFT calculations of model complexes were employed to further investigate conformational dissimilarity between these oxazoline and pyrazole based compounds. $\text{Me}_2\text{B}(\text{Ox}^{\text{Me}_2})_2\text{AlMe}_2$ (**X**) was used as a model for $\text{PhMeB}(\text{Ox}^{\text{Me}_2})_2\text{AlMe}_2$, and $\text{H}_2\text{Bpz}_2\text{AlMe}_2$ (**Z**) was used in place of $\text{Bp}^{\text{tBu,Me}}\text{AlMe}_2$. Planar conformations were obtained in all geometry optimizations of the bis(oxazoliny)borate compound, while optimization of the bis(pyrazoly)borate complex resulted in the puckered boat conformation. Given the

unlikelihood of steric interactions being the cause of the adoption of a planar conformation in these systems, an electronic difference between oxazoline and pyrazole groups could reasonably account for two different configurations. An examination of the Kahn-Sham orbitals obtained from the DFT calculations supports this notion (Figure 3.2). The HOMO orbitals of both the model compounds primarily involve the aluminum-methyl bonding. The HOMO-2 orbitals of both **X** and **Z** are comprised primarily of p-orbitals with the important lobes located on the nitrogen centers bound to aluminum. While the lobes on the nitrogen of each ring are out of phase from each other, the nitrogen centers in both the oxazoline and pyrazole rings are sufficiently far apart (2.85 Å) that any interaction between them would be minimal in the absence of an extreme distortion of the ring. However, a substantial difference between **X** and **Z** is seen in the HOMO-1 orbital. While this orbital is located primarily on the B–C bond in the oxazoline model, the pyrazole containing model contains significant electron density on the nitrogens bound to the boron center as well as lobes corresponding to the B–H bonds. As the nitrogen p-orbitals and the B–H σ -bonds are out of phase, the interaction between the two results in an unfavorable interaction. This antibonding interaction is minimized by the adoption of a boat conformation by the pyrazolylborate model in which the boron center is displaced from the chelate ring.

Synthesis of $To^M AlMe_2$ and comparison of reactivity to $PhMeB(Ox^{Me_2})_2 AlMe_2$

In our attempts to alkylate the $To^M ZrCl_3$ complex, we had previously suspected that formation of a $To^M Al$ complex interfered with alkylation (see Chapter 2). Furthermore, the To^M ligand can bind either in a bi- or tridentate fashion to the aluminum center, and this

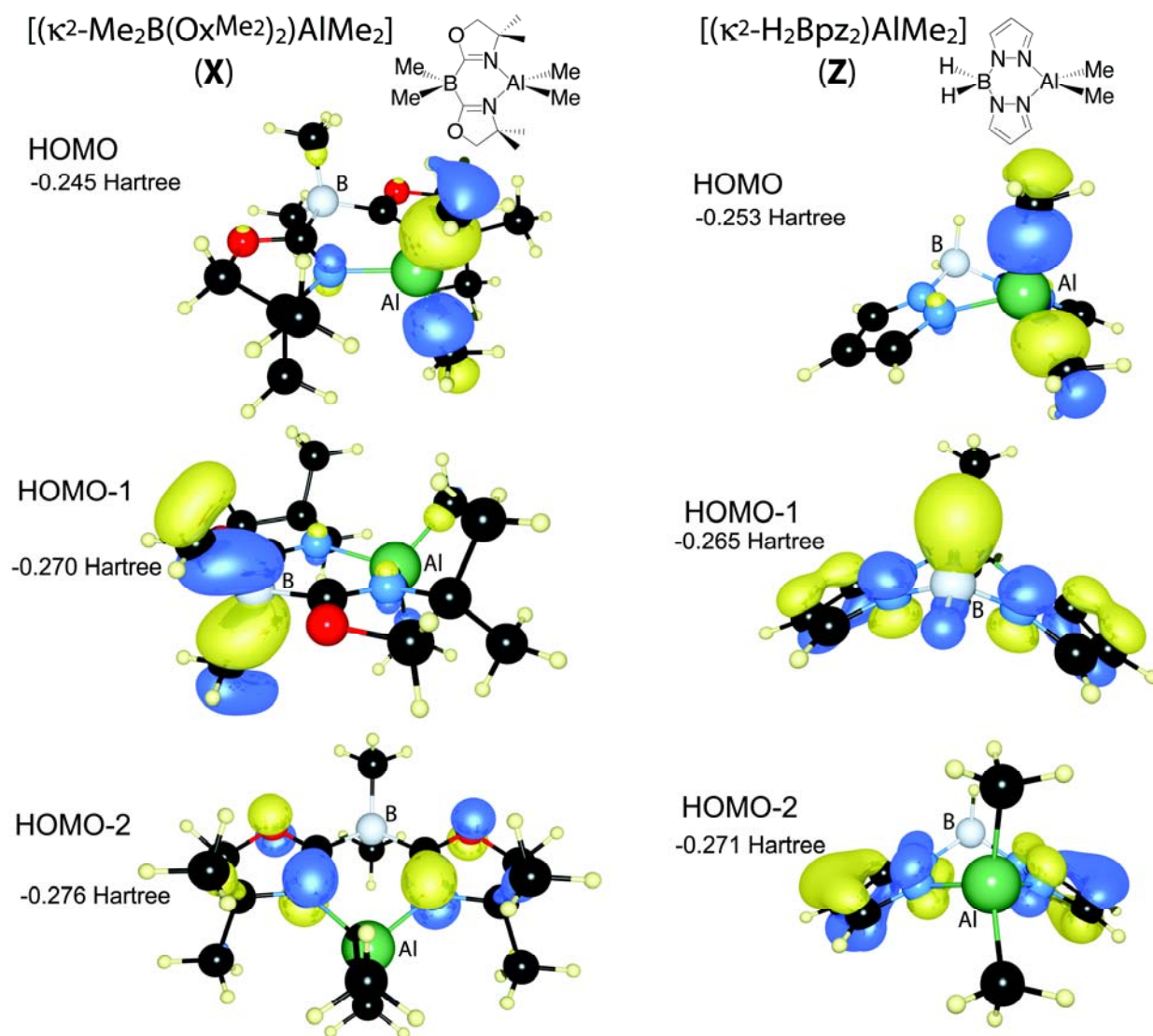
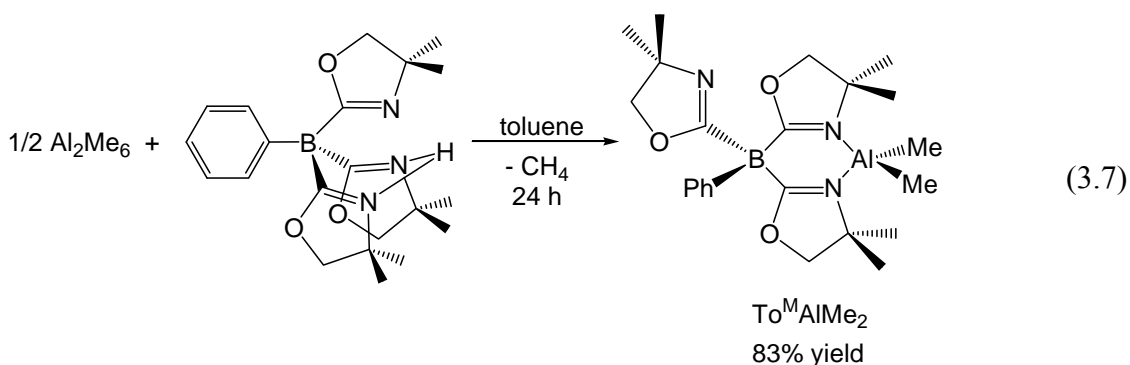


Figure 3.2. Kahn-Sham orbitals for $\text{Me}_2\text{B}(\text{Ox}^{\text{Me}_2})_2\text{AlMe}_2$ (X) and $\text{H}_2\text{Bpz}_2\text{AlMe}_2$ (Z) obtained from DFT calculations showing a) the HOMO, b) the HOMO-1, and c) the HOMO-2.

motivated us to compare the $\text{To}^{\text{M}}\text{Al}$ complex to the $\text{PhMeB}(\text{Ox}^{\text{Me}_2})_2\text{AlMe}_2$ obtained from the Lewis acid abstraction/Lewis base coordination. In benzene- d_6 , reaction of HTo^{M} with 0.5 equivalents of $(\text{AlMe}_3)_2$ generates the production of methane gas and the desired product $\text{To}^{\text{M}}\text{AlMe}_2$ (eq 3.7).



As previously observed, the ¹H NMR spectrum of the compound was consistent with a C_s symmetric complex. Three singlet resonances are observed for the oxazoline methyl groups, while the methylene protons appear as two diastereotopic doublets and a singlet. The aluminum methyl groups also appear as inequivalent singlet resonances. A ¹H-¹⁵N HMBC experiment confirmed the coordination of the To^M ligand to aluminum as bidentate (Figure 3.3) as seen by two separate ¹⁵N resonances at -184.2 and -120.2 ppm. The resonance at -184.2 ppm is close to that of the ¹⁵N signal for PhMeB(Ox^{Me2})₂AlMe₂, and displays crosspeaks to both the aluminum methyl groups and the diastereotopic doublets identifying it as the oxazoline nitrogens coordinated to aluminum. The signal at -120.2 ppm is close to that of the free 2H-oxazoline (-127.5 ppm), providing further evidence for its assignment as non-coordinated. The IR spectrum confirms the bidentate coordination mode in the solid state as two ν_{CN} stretches are observed at 1626 and 1565 cm⁻¹.

While To^M is bound to the aluminum center in a bidentate fashion, an EXSY experiment revealed crosspeaks between the coordinated and free oxazoline resonances

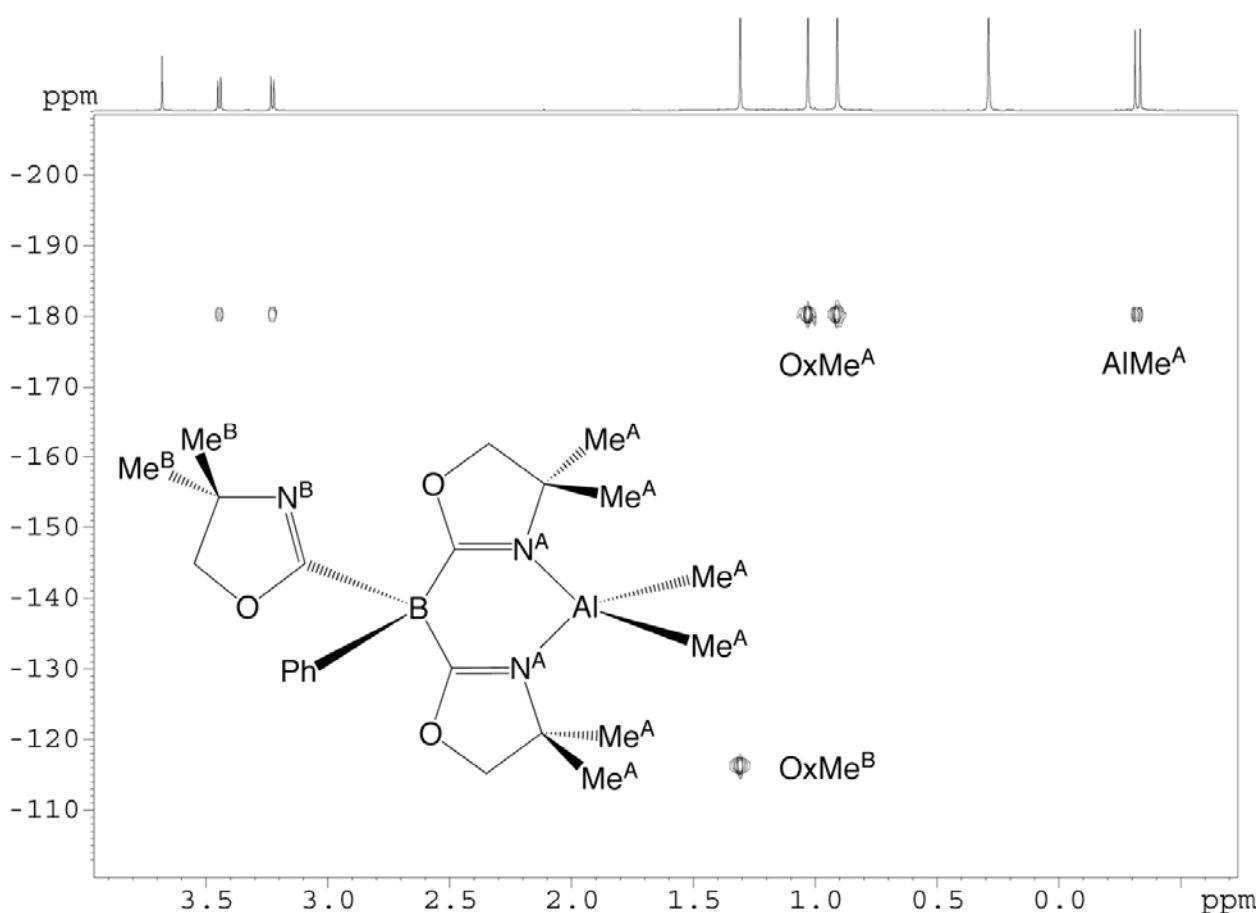
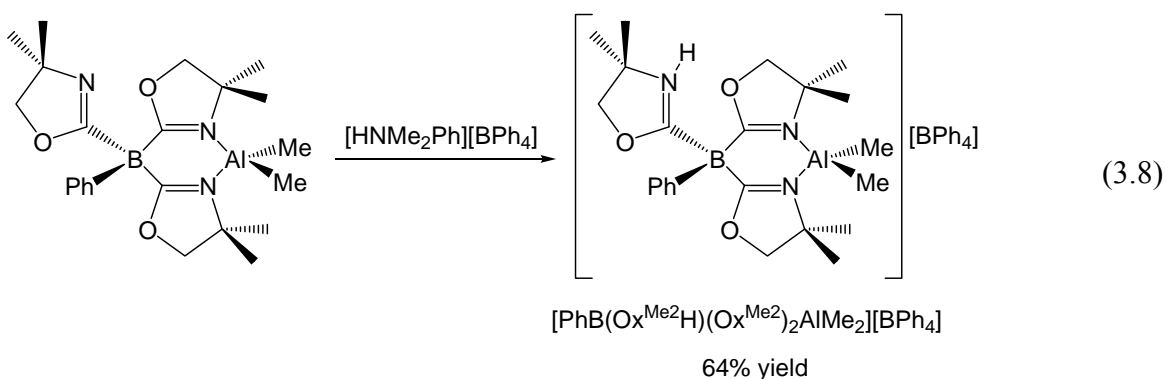


Figure 3.3. ^1H - ^{15}N HMBC experiment illustrating three bond coupling between the oxazoline nitrogen through aluminum to the methyl group in $\text{To}^{\text{M}}\text{AlMe}_2$.

indicating that the three oxazoline groups undergo slow exchange on the ^1H NMR timescale at room temperature. ^1H NMR spectra taken at elevated temperature in toluene- d_8 displayed broadened oxazoline resonances that had moved closer together, but coalescence was not observed up to 370 K.

In Tp^*AlMe_2 , the Tp^* ligand was found to bind in a tridentate fashion to the aluminum center.^{4,5a} However, attempts to coordinate the third oxazoline ligand by

protonolytic elimination of a methyl group were unsuccessful as the methyl groups were surprisingly inert to protonolysis. Addition of alcohols to solutions of $\text{To}^{\text{M}}\text{AlMe}_2$ resulted in the recovery of starting materials. Similar results were obtained by the addition of water to either benzene or THF solutions of $\text{To}^{\text{M}}\text{AlMe}_2$. Reaction of 1 equivalent of $[\text{HNMe}_2\text{Ph}][\text{BPh}_4]$ with $\text{To}^{\text{M}}\text{AlMe}_2$ in $\text{THF-}d_8$ at room temperature gives the cationic compound $[\text{PhB}(\text{Ox}^{\text{Me}_2}\text{H})(\text{Ox}^{\text{Me}_2})_2\text{AlMe}_2]$, in which the pendant oxazoline ring is protonated (eq 3.8) instead of the expected protonolytic elimination of methane.



Evidence for oxazoline protonation was provided by the ^1H NMR spectrum in which a downfield signal at 10.94 ppm is assigned as the NH of the protonated oxazoline. This assignment is confirmed by an ^1H - ^{15}N HMQC experiment which shows a crosspeak between this resonance and the new peak representing the oxazoline nitrogen at -202.8 ppm. This new peak is shifted by 82 ppm from the pendent oxazoline in $\text{To}^{\text{M}}\text{AlMe}_2$ (-120.2 ppm), however the ^{15}N NMR chemical shifts of the coordinated oxazoline nitrogens do not change significantly (-184.2 for $\text{To}^{\text{M}}\text{AlMe}_2$ vs -176.9 for $[\text{PhB}(\text{Ox}^{\text{Me}_2}\text{H})(\text{Ox}^{\text{Me}_2})_2\text{AlMe}_2]$). The addition of two equivalents of the anilinium salt results in the formation of the same protonated species with no evidence for the formation of a second product over a 48 hour period.

While the protonation of ligands in pyrazolylborates and oxazolylborates have been previously reported,²² the protonation site varies between ligand and metal center within isoelectronic and isostructural compounds. For example, protonation of $\text{Tp}^*\text{Ir}(\text{CO})_2$ gives the metal hydride $[\text{Tp}^*\text{IrH}(\text{CO})_2][\text{BF}_4]$, reaction of the rhodium analog gives the protonated pyrazole compound $[\text{HB}(\text{pz-H})(\text{pz})_2\text{Rh}(\text{CO})_2][\text{BF}_4]$.^{22a} For late transition metal tris(oxazolyl)-borates, reaction of $\text{To}^M\text{Ir}(\text{CO})_2$, $\text{To}^P\text{Ir}(\text{CO})_2$, or $\text{To}^P\text{Ir}(\eta^4\text{-C}_8\text{H}_{12})$ ($\text{To}^P = \text{tris}(4S\text{-isopropyl-2-oxazolyl})\text{phenyl borate}$) with strong acids (such as HOTf) afford oxazoline protonation over the formation of the metal hydride.^{16,17} However, the exclusive reaction of the pendant oxazoline with acid described here is unexpected given the strong nucleophilic and basic character of the aluminum methyl groups.

Furthermore, either intra- or intermolecular transfer of the proton to the aluminum center was expected to occur over time. The slow exchange of the oxazoline groups in To^MAlMe_2 indicates that the pendant oxazolinium must have access to the metal center. While coordination of three bulky, non-planar 4,4-dimethyl-2-oxazolyl groups on a small Al(III) center (4-coordinate radius = 0.39 Å)²³ is sterically disfavored, proton transfer to the methyl groups should be possible. However, over an extended period of time (1 month), $[\text{PhB}(\text{Ox}^{\text{Me}_2}\text{H})(\text{Ox}^{\text{Me}_2})_2\text{AlMe}_2][\text{BPh}_4]$ decomposes to form HTo^M . The decomposition process is accelerated thermally such that heating solutions of $[\text{PhB}(\text{Ox}^{\text{Me}_2}\text{H})(\text{Ox}^{\text{Me}_2})_2\text{AlMe}_2][\text{BPh}_4]$ at 100 °C gives HTo^M , methane, and unknown aluminum species after 48 hours.

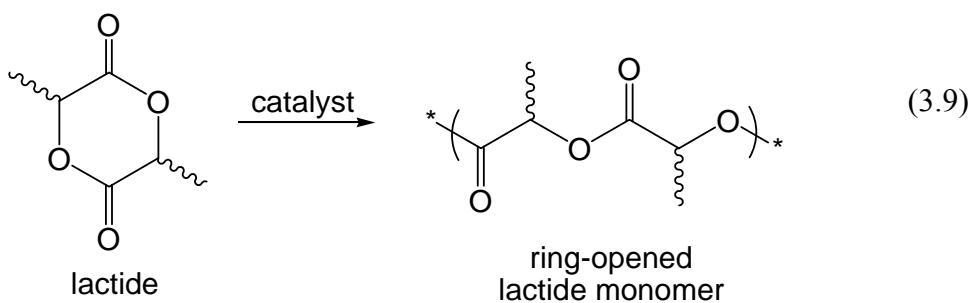
The inert nature of the aluminum methyl bonds in To^MAlMe_2 is not dependent on the presence of a pendant oxazoline group. $\text{PhMeB}(\text{Ox}^{\text{Me}_2})_2\text{AlMe}_2$ shows a similar resistance to protonolysis of the aluminum methyl groups. Only starting materials were observed in the

^1H NMR spectra of reactions of $\text{PhMeB}(\text{Ox}^{\text{Me}_2})_2\text{AlMe}_2$ and $[\text{HNMe}_2\text{Ph}][\text{BPh}_4]$ after 48 hours in $\text{THF-}d_8$. The difference in reactivity with acids between oxazolinyborate aluminum compounds and the carbon-bridged, π -delocalized $\{\text{BOX-Me}_2\}\text{AlMe}_2$ is quite remarkable. The latter compound is reported to react rapidly with $\text{B}(\text{C}_6\text{F}_5)_3$ to give the methyl abstracted product $[\{\text{BOX-Me}_2\}\text{AlMe}][\text{MeB}(\text{C}_6\text{F}_5)_3]$.¹⁵ In contrast, $\text{PhMeB}(\text{Ox}^{\text{Me}_2})_2\text{AlMe}_2$ reacts with $\text{B}(\text{C}_6\text{F}_5)_3$ giving complicated mixtures of products (in benzene- d_6 , bromobenzene- d_5 , and $\text{THF-}d_8$). A possible explanation for observed inability to form cationic compounds lies in the zwitterionic nature of the oxazolinyborate aluminum compounds. The formation of a cationic species would further exacerbate the separation of the charges. Indeed, this explanation is supported by the Mulliken charges calculated for the model compound **X**, giving boron a negative charge of -0.398, and aluminum a positive charge of +0.267.

Lactide ring opening polymerization

These oxazolinyborate aluminum compounds are thermally robust and resistant towards hydrolysis, suggesting that they may be useful in catalytic processes requiring relatively high temperatures. Because catalytic lactide ring-opening polymerization (ROP, eq 3.9) typically occurs in neat lactide at temperatures at or above 110 °C, this process is a good initial test reaction. Additionally, there have been a number of well-defined aluminum compounds reported as useful catalysts for lactide ROP.²⁴

$\text{To}^{\text{M}}\text{AlMe}_2$ was investigated as a potential catalyst for ROP of lactide. Initial NMR scale experiments in toluene- d_8 demonstrated that lactide is catalytically consumed at 110 °C



(5 mol% $\text{To}^{\text{M}}\text{AlMe}_2$). ^1H NMR spectrum resonances corresponding to lactide decreased in intensity over time, while broad resonances assigned to polylactic acid steadily emerged. Aluminum alkyl compounds that are active for ROP in the absence of a co-catalyst are rare in the literature²⁵, and so larger scale reactions were then investigated to determine the activity of $\text{To}^{\text{M}}\text{AlMe}_2$ in catalytic lactide ROP (Table 3.2). Generally, the catalyst was physically mixed with the lactide in an ampoule that was sealed under vacuum, and then heated from 110-130 °C. A 90% conversion (as determined by ^1H NMR spectroscopy) of monomer is observed after 24 hours at 130 °C (entry 8). Significantly lower conversion (46%) occurs at 110 °C during the same time frame (entry 5), but longer reaction times (48 and 72 h, entries 6 and 7) result in increased conversion. The improvement of monomer conversion over time suggests that the catalyst remains active over the entire course of the polymerization experiment. Gel permeation chromatography (GPC) of the isolated polymer reveals that the averaged molecular weights unexpectedly decrease with increasing conversion, while at the same time the polydispersity (PDI) narrows (entries 5-7). The polydispersity was additionally observed to increase with decreasing temperature.²⁶ The GPC trace indicates a monomodal polymer distribution suggesting that only a single active site is present in the compound, and that the pendant oxazoline and aluminum centers are not acting as independent catalysts. Higher catalyst loading results in greater monomer conversion over

equal time periods. While the polydispersity of the polymers generally improve with increasing conversion, this is accompanied by the generation of shorter polymer chain lengths as

Table 3.2. Polymerization of *rac*-lactide using $\text{To}^{\text{M}}\text{AlMe}_2^{\text{a}}$.

Entry	<i>rac</i> -LA:Al	Time (h)	Conversion (%) ^b	Yield (%) ^c	$M_{\text{n,th}}^{\text{d}}$	$M_{\text{n,exp}}$	M_{w}	PDI
1	100:1	24	80	39	11,500	28,200	44,300	1.57
2	100:1	48	100	85	14,400	26,600	45,000	1.69
3	200:1	24	60	38	17,300	33,500	56,900	1.70
4	200:1	48	88	62	25,300	44,400	68,900	1.55
5	500:1	24	46	34	33,100	39,500	68,400	1.73
6	500:1	48	61	53	43,900	31,400	51,100	1.63
7	500:1	72	90	64	64,800	27,600	40,000	1.45
8 ^e	500:1	24	90	87	64,800	26,200	41,300	1.57

^aStandard conditions: Lactide and $\text{To}^{\text{M}}\text{AlMe}_2$ are sealed in ampoules and heated at 110 °C. ^bConversion is determined by integration of the ¹H NMR spectrum of the crude reaction mixture. ^cYield is calculated as the ratio of the mass of isolated polymer versus the mass of the starting monomer. ^dTheoretical M_{n} calculated from molecular weight of lactide \times conv. \times [LA]/[Al]. ^ePolymerization experiment at 130 °C.

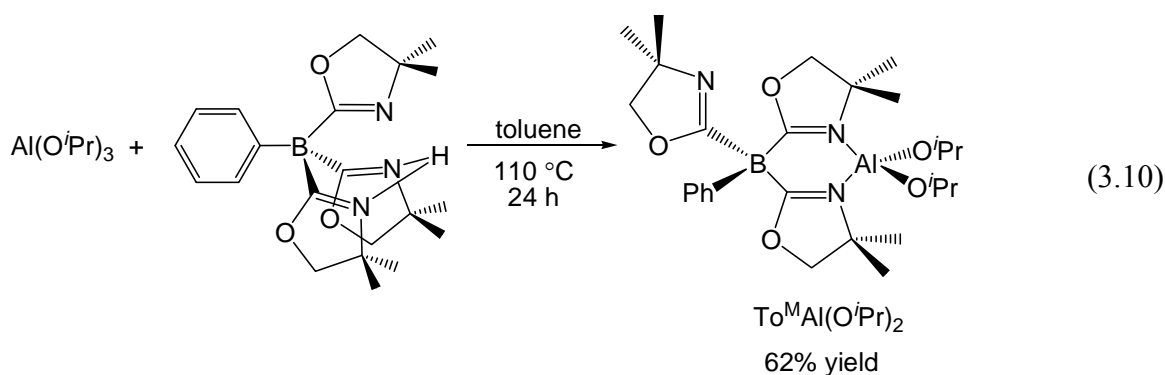
Table 3.3. Comparison of aluminum catalysts for *rac*-lactide polymerization^a.

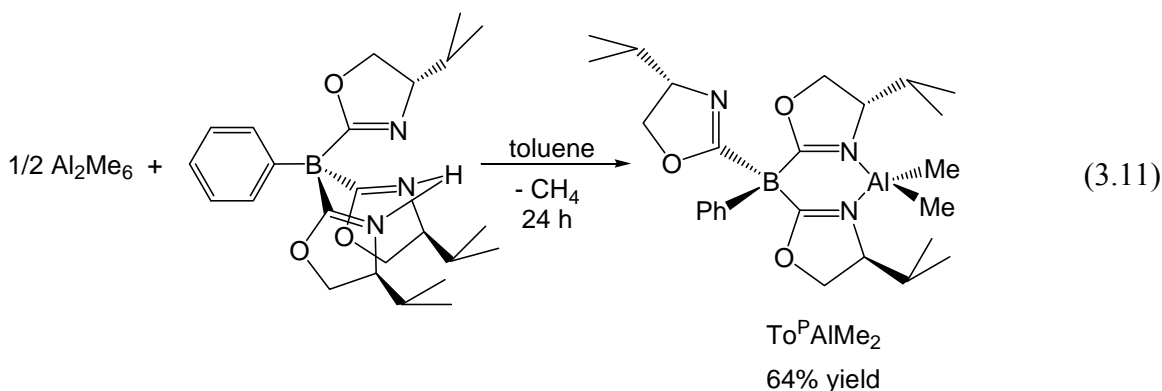
Entry	Catalyst	Conversion (%) ^b	Yield (%) ^c	$M_{\text{n,th}}^{\text{d}}$	$M_{\text{n,exp}}$	M_{w}	PDI
1	$\text{PhMeB}(\text{Ox}^{\text{Me}_2})_2\text{AlMe}_2$	82	42	59,000	10,300	13,900	1.34
2	$\text{To}^{\text{M}}\text{AlMe}_2$	90	87	64,800	26,200	41,300	1.57
3	$\text{To}^{\text{M}}\text{Al}(\text{O}^i\text{Pr})_2$	86	48	61,900	9,600	15,800	1.63
4	$\text{To}^{\text{P}}\text{AlMe}_2$	87	39	62,600	28,700	44,600	1.55

^aPolymerization experiments are performed in sealed ampoules in neat lactide at 500:1 lactide:catalyst for 24 h at 130 °C. ^bConversion is determined by integration of the ¹H NMR spectrum of the crude reaction mixture. ^cYield is calculated as the ratio of the mass of isolated polymer versus the mass of the starting monomer. ^dTheoretical M_{n} calculated from molecular weight of lactide \times conv. \times [LA]/[Al].

represented by the M_n and M_w values. The polydispersities obtained are also higher than those reported for other aluminum catalysts, though not by a significant amount.^{24b}

The success of $To^M AlMe_2$ as a catalyst for lactide ROP led us to investigate the utility of other oxazolinylborate aluminum compounds in lactide polymerization. In particular, $PhMeB(Ox^{Me_2})_2 AlMe_2$ was compared to $To^M AlMe_2$, and found to have a significantly different activity (Table 3.3). Approximately the same conversion of lactide occurs after 24 hours, however, the isolated polymer yield and resulting molecular weights are significantly lower for $PhMeB(Ox^{Me_2})_2 AlMe_2$ compared to $To^M AlMe_2$ (entries 1 and 2). That $PhMeB(Ox^{Me_2})_2 AlMe_2$ remains an active catalyst for lactide ROP without a pendant oxazoline further confirms that only the metal center is active for the catalysis. However, the significant difference in polymer yield and molecular weight suggests that the pendant oxazoline may play a role in the polymerization. As aluminum alkoxides are well-known initiators for lactide ROP, we synthesized the aluminum alkoxide compound $To^M Al(O^iPr)_2$ (eq 3.10). A comparison of lactide ROP activity of $To^M AlMe_2$ with $To^M Al(O^iPr)_2$ reveals that $To^M Al(O^iPr)_2$ produces polymers with substantially shorter chain lengths as well as broader molecular weight distributions (entries 2 and 3).





Additionally, we were interested in attempting stereo-controlled polymerization of lactide using the chiral analog $\text{To}^{\text{P}}\text{AlMe}_2$ (eq 3.11). $\text{To}^{\text{P}}\text{AlMe}_2$ is synthesized from the reaction of HTo^{P} and $(\text{AlMe}_3)_2$, and the ^1H NMR spectrum reveals its C_1 symmetric structure in solution by the six sets of isopropyl methyl resonances that are observed (all three oxazoline rings are inequivalent). In contrast to this, in the $^{13}\text{C}\{^1\text{H}\}$ NMR spectrum, four of the isopropyl methyl carbons are overlapping, and only two separate signals are observed. This is confirmed by a ^1H - ^{13}C HMQC experiment which allowed the assignment of these overlapping resonances. Polylactic acid polymers, produced by both the chiral $\text{To}^{\text{P}}\text{AlMe}_2$ and achiral $\text{To}^{\text{M}}\text{AlMe}_2$, have remarkably similar molecular weights and polydispersities (entries 2 and 4). Unfortunately, both catalysts produce polymers with atactic microstructures, as determined through examination of hexads by $^{13}\text{C}\{^1\text{H}\}$ NMR spectroscopy.²⁷

Conclusion

We have successfully synthesized the first bis(oxazolinyl)borane species, $\text{PhB}(\text{Ox}^{\text{Me}_2})_2$, which exists as a mixture of oligomers due to the presence of both Lewis acid and Lewis base centers in the compound.¹¹ Despite the intermolecular coordination of

oxazoline or solvent to the boron center, $\text{PhB}(\text{Ox}^{\text{Me}_2})_2$ is sufficiently accessible to abstract a methyl group from trimethylaluminum to give the zwitterionic complex $\text{PhMeB}(\text{Ox}^{\text{Me}_2})_2\text{AlMe}_2$. The strategy of concurrent abstraction/coordination is potentially valuable for the generation of new catalysts as the activation of metal centers often involves the formation of cationic species. In the solid state, this compound adopts a planar structure consisting of a six-membered $\text{BC}_2\text{N}_2\text{Al}$ chelate ring, which contrasts the puckered geometry that the analogous bis(pyrazolyl)borates adopt. The tris(oxazolinyl)borate derivative, $\text{To}^{\text{M}}\text{AlMe}_2$, is isolated via a protonolytic elimination and coordinates to the aluminum metal center in a bidentate fashion. All attempts at forcing the third oxazoline to coordinate to the aluminum center by removing an additional methyl group were unsuccessful, resulting either in the protonation of the pendent oxazoline nitrogen or decomposition to unidentified products. The inert nature of the Al-Me is also observed for the abstraction product $\text{PhMeB}(\text{Ox}^{\text{Me}_2})_2\text{AlMe}_2$, and the resistance to protonation displayed by both compounds is attributed to the difficulty in generating a charge separated species which would result from the formation of cationic metal center. Despite the unusually robust nature of the aluminum methyl groups, both the bis- and tris(oxazolinyl)borate aluminum compounds are active for the ring opening polymerization of lactide. While the one chiral tris(oxazolinyl)borate aluminum compound that was investigated for stereoselective lactide ROP produced only atactic polymer, modification of the oxazoline groups to other chiral substituents could result in a greater induction of chirality in the resulting polymer. Additionally, the induction of chirality at the metal center could be enhanced by the coordination of all three of the oxazoline rings to the metal. A larger metal center should allow the To^{M} ligand to bind η^3 without the need to generate a cationic species. As we were interested in further exploring

the catalytic reactivity of main group metals, we began to explore the reactivity of magnesium complexes chelated by the To^M ligand in Chapters 4 and 5.

Experimental

General. All manipulations were performed using either Schlenk techniques, or in a glovebox under an inert atmosphere of nitrogen unless otherwise indicated. Dry, oxygen-free solvents were used throughout. Benzene, toluene, methylene chloride, pentane, diethyl ether, and tetrahydrofuran were degassed by sparging with nitrogen, filtered through activated alumina columns, and stored under N_2 . Dichlorophenylborane was purchased from Aldrich and distilled prior to use. Trimethyl aluminum, aluminum isopropoxide, and 3,6-dimethyl-1,4-dioxane-2,5-dione were purchased from Aldrich and used as received. 4,4-dimethyl-2-oxazoline was purchased from Acros and used as received. Hydrogen tris(4,4-dimethyl-2-oxazoliny)phenylborate $(H[To^M])^{28}$ and hydrogen tris(4*S*-isopropyl-2-oxazoliny)phenylborate $(H[To^P])^{16}$ were prepared as previously reported. The anilinium salt $[HNMe_2Ph][BPh_4]$ was prepared via the reaction of *N,N*-dimethylaniline, sodium tetraphenylborate, and hydrochloric acid.

Solution 1H , $^{13}C\{^1H\}$, and ^{11}B NMR spectra were collected on a Bruker DRX-400 spectrometer, and ^{15}N chemical shifts were determined by 1H - ^{15}N HMBC experiments on a Bruker Avance II 700 spectrometer with a Bruker Z-gradient inverse TXI $^1H/^{13}C/^{15}N$ 5 mm cryoprobe. ^{15}N chemical shifts were originally referenced to liquid NH_3 and recalculated to the CH_3NO_2 chemical shift scale by adding -381.9 ppm. ^{11}B NMR spectra were referenced to an external sample of $BF_3 \cdot Et_2O$.

Elemental analysis was performed using a Perkin-Elmer 2400 Series II CHN/S by the Iowa State Chemical Instrumentation Facility. X-ray diffraction data was collected on a Bruker-AXS SMART 1000 CCD diffractometer using Bruker-AXS SHELXTL software. Gel permeation chromatography (GPC) measurements were performed on a Viscotek GPC Max 280 separation module equipped with three 5 μ m I-gel columns connected in series (guard, HMW, MMW and LMW) with a refractive index detector. Analyses were performed at 35 $^{\circ}$ C using THF as the eluent, and the flow rate was 1.0 mL/min. Calibration was based on polystyrene standards obtained from Viscotek.

[PhB(Ox^{Me2})₂]. A 100 mL Schlenk flask was charged with 4,4-dimethyl-2-oxazoline (1.0 mL, 9.48 mmol), which was then degassed by three freeze-pump-thaw cycles. The degassed oxazoline was dissolved in 50 mL of tetrahydrofuran and the flask was cooled to -78 $^{\circ}$ C. Using a syringe, *n*-BuLi (4.0 mL, 10.0 mmol) was added to the cold solution and the resultant solution was stirred for 45 min at -78 $^{\circ}$ C. Dichlorophenylborane (0.619 mL, 4.72 mmol) was added drop wise via syringe into the flask and the solution was stirred for 1 h at -78 $^{\circ}$ C. Then, the solution was allowed to gradually warm to room temperature. After stirring for 14 h at room temperature, the solvent was removed under reduced pressure to afford a light yellow solid. The resultant solid was extracted with benzene and pump off the solvent *in vacuo* to yield PhB(Ox^{Me2})₂ as a yellow solid (1.27 g, 4.47 mmol, 94.3%). ¹H NMR (acetonitrile-*d*₃, 400 MHz): δ 7.42 (d, ³*J* = 7.2 Hz, 2 H, *ortho*-C₆H₅), 7.13 (m, 2 H, *meta*-C₆H₅), 7.05 (m, 1 H, *para*-C₆H₅), 3.64 (d, 2 H, ²*J*_{HH} = 8.0 Hz, $\overline{\text{CNCMe}_2\text{CH}_2\text{O}}$), 3.57 (d, 2 H, ²*J*_{HH} = 8.0 Hz, $\overline{\text{CNCMe}_2\text{CH}_2\text{O}}$), 1.26 (s, 6 H, $\overline{\text{CNCMe}_2\text{CH}_2\text{O}}$), 1.17 (s, 6 H, $\overline{\text{CNCMe}_2\text{CH}_2\text{O}}$).

$\overline{\text{CNCMe}_2\text{CH}_2\text{O}}$). $^{13}\text{C}\{^1\text{H}\}$ NMR (acetonitrile- d_3 , 150 MHz): δ 183.00 (br, $\overline{\text{CNCMe}_2\text{CH}_2\text{O}}$), 132.86 (*ortho*- C_6H_5), 127.58 (*meta*- C_6H_5), 125.99 (*para*- C_6H_5), 77.79 ($\overline{\text{CNCMe}_2\text{CH}_2\text{O}}$), 67.44 ($\overline{\text{CNCMe}_2\text{CH}_2\text{O}}$), 28.71 ($\overline{\text{CNCMe}_2\text{CH}_2\text{O}}$). ^{11}B NMR (acetonitrile- d_3 , 128 MHz): δ -8.1. $^{15}\text{N}\{^1\text{H}\}$ NMR (acetonitrile- d_3 , 71 MHz): δ -147.0 ($\overline{\text{CNCMe}_2\text{CH}_2\text{O}}$). IR (KBr, cm^{-1}): 3069 w, 3046 w, 2964 s, 2930 s, 2872 m, 1621 s, 1601 s, 1462 s, 1432 s, 1384 m, 1346 w, 1260 s, 1194 s, 1126 m, 1083 w, 993 s, 970 s, 886 m, 703 s. Calcd for $\text{C}_{16}\text{H}_{21}\text{BN}_2\text{O}_2$: C, 67.63; H, 7.45; N, 9.86. Found: C, 64.69; H, 7.51; N, 8.26. mp 133–137 °C.

$[(\kappa^2\text{-PhMeB}(\text{Ox}^{\text{Me}_2})_2)\text{AlMe}_2]$. Solid $\text{PhB}(\text{Ox}^{\text{Me}_2})_2$ (1.00 g, 3.52 mmol) was placed in a 100 mL Schlenk flask in the glovebox. The solid was dissolved in 50 mL of toluene, and $[\text{AlMe}_3]_2$ (0.257 g, 1.78 mmol) was added via syringe to give a yellow solution. The resulting solution was stirred for 24 hours and then filtered to remove a white precipitate. The toluene filtrate was evaporated under reduced pressure to give a yellow solid. The crude solid was dissolved in toluene and cooled to -80 °C for 24 hours to give a pale yellow solid (0.674 g, 1.90 mmol, 54%) of suitable purity for further reactions. X-ray quality crystals were grown from a concentrated toluene solution after one week at -35 °C. ^1H NMR (benzene- d_6 , 400 MHz): δ 7.76 (d, $^3J_{\text{HH}} = 6.8$ Hz, 2 H, *ortho*- C_6H_5), 7.43 (vt, $^3J_{\text{HH}} = 7.6$ Hz, 2 H, *meta*- C_6H_5), 7.23 (t, $^3J_{\text{HH}} = 7.6$ Hz, 1 H, *para*- C_6H_5), 3.23 (d, $^3J_{\text{HH}} = 9.0$ Hz, 2 H, $\overline{\text{CNCMe}_2\text{CH}_2\text{O}}$), 3.12 (d, $^3J_{\text{HH}} = 9.0$ Hz, 2 H, $\overline{\text{CNCMe}_2\text{CH}_2\text{O}}$), 0.93 (s, 6 H, $\overline{\text{CNCMe}_2\text{CH}_2\text{O}}$), 0.92 (s, 6 H, $\overline{\text{CNCMe}_2\text{CH}_2\text{O}}$), 0.89 (s br, 3 H, *BMe*), -0.27 (s, 3 H, *AlMe*), -0.33 (s, 3 H, *AlMe*). $^{13}\text{C}\{^1\text{H}\}$ NMR (benzene- d_6 , 125 MHz): δ 180.5 (br, $\overline{\text{CNCMe}_2\text{CH}_2\text{O}}$), 135.6 (*ipso*- C_6H_5), 132.7 (*ortho*- C_6H_5), 128.3 (*meta*- C_6H_5), 126.3 (*para*- C_6H_5), 79.41 ($\overline{\text{CNCMe}_2\text{CH}_2\text{O}}$), 65.26

($\overline{\text{CNCMe}_2\text{CH}_2\text{O}}$), 27.17 ($\overline{\text{CNCMe}_2\text{CH}_2\text{O}}$), 26.96 ($\overline{\text{CNCMe}_2\text{CH}_2\text{O}}$), 4.76 (br, BCH_3), -5.53 (br, AlCH_3). ^{11}B NMR (benzene- d_6 , 128 MHz): δ -16.7. ^{15}N NMR (benzene- d_6 , 71 MHz): δ -186.7 ($\text{Al}(\overline{\text{NCMe}_2\text{CH}_2\text{OC}})_2\text{B}$). IR (KBr, cm^{-1}): 3042 w, 2981 s, 2931 s, 1551 sh s, 1465 s, 1431 m, 1372 s, 1293 s, 1256 m, 1201 s, 1163 m, 1017 m, 992 s, 828 w, 776 w, 703 s. Anal. Calcd for $\text{C}_{19}\text{H}_{30}\text{BAlN}_2\text{O}_2$: C, 64.06; H, 8.49; N, 7.86. Found: C, 63.88; H, 8.49; N, 7.74. mp 150-155 °C, dec.

$[(\kappa^2\text{-To}^{\text{M}})\text{AlMe}_2]$. $\text{H}[\text{To}^{\text{M}}]$ (1.00 g, 2.61 mmol) was dissolved in 50 mL of toluene, and $[\text{AlMe}_3]_2$ (0.19 g, 1.32 mmol) was added via syringe. The solution was stirred for 24 hours to give a pale yellow solution above a small amount of precipitate. The mixture was filtered and the filtrate was evaporated under reduced pressure to yield a crude white solid. Analytically pure $\text{To}^{\text{M}}\text{AlMe}_2$ (0.95 g, 2.17 mmol, 83%) was obtained by recrystallization from a toluene/pentane mixture. ^1H NMR (benzene- d_6 , 400 MHz): δ 7.98 (d, $^3J_{\text{HH}} = 7.5$ Hz, 2 H, *ortho*- C_6H_5), 7.43 (vt, $^3J_{\text{HH}} = 7.5$ Hz, 2 H, *meta*- C_6H_5), 7.22 (t, $^3J_{\text{HH}} = 7.5$ Hz, 1 H, *para*- C_6H_5), 3.69 (s, 2 H, $\overline{\text{CNCMe}_2\text{CH}_2\text{O}}$), 3.44 (d, $^3J_{\text{HH}} = 8.9$ Hz, 2 H, $\text{Al}(\overline{\text{NCMe}_2\text{CH}_2\text{OC}})_2\text{B}$), 3.21 (d, $^3J_{\text{HH}} = 8.9$ Hz, 2 H, $\text{Al}(\overline{\text{NCMe}_2\text{CH}_2\text{OC}})_2\text{B}$), 1.32 (s, 6 H, $\overline{\text{CNCMe}_2\text{CH}_2\text{O}}$), 1.02 (s, 6 H, $\text{Al}(\overline{\text{NCMe}_2\text{CH}_2\text{OC}})_2\text{B}$), 0.90 (s, 6 H, $\text{Al}(\overline{\text{NCMe}_2\text{CH}_2\text{OC}})_2\text{B}$), -0.30 (s, 3 H, AlMe), -0.32 (s, 3 H, AlMe). $^{13}\text{C}\{^1\text{H}\}$ NMR (benzene- d_6 , 125 MHz): δ 196.6 (br, $\overline{\text{CNCMe}_2\text{CH}_2\text{O}}$), 196.5 (br, $\overline{\text{CNCMe}_2\text{CH}_2\text{O}}$), 146.3 (br, *ipso*- C_6H_5), 134.16 (*ortho*- C_6H_5), 127.59 (*meta*- C_6H_5), 126.13 (*para*- C_6H_5), 79.83 ($\text{Al}(\overline{\text{NCMe}_2\text{CH}_2\text{OC}})_2\text{B}$), 77.25 ($\overline{\text{CNCMe}_2\text{CH}_2\text{O}}$), 68.04 ($\overline{\text{CNCMe}_2\text{CH}_2\text{O}}$), 65.46 ($\text{Al}(\overline{\text{NCMe}_2\text{CH}_2\text{OC}})_2\text{B}$), 29.00 ($\overline{\text{CNCMe}_2\text{CH}_2\text{O}}$), 27.07 ($\text{Al}(\overline{\text{NCMe}_2\text{CH}_2\text{OC}})_2\text{B}$), 26.78 ($\text{Al}(\overline{\text{NCMe}_2\text{CH}_2\text{OC}})_2\text{B}$), -5.88 (s, AlMe), -5.99 (s, AlMe).

^{11}B NMR (benzene- d_6 , 128 MHz): δ -16.5. $^{15}\text{N}\{^1\text{H}\}$ NMR (benzene- d_6 , 71 MHz): δ -120.2 ($\overline{\text{CNCMe}_2\text{CH}_2\text{O}}$), -184.2 ($\text{Al}(\overline{\text{NCMe}_2\text{CH}_2\text{OC}})_2\text{B}$). IR (KBr, cm^{-1}): 3053 m, 2968 s, 2930 s, 2889 s, 1626 s, 1565 s, 1462 s, 1433 m, 1373 s, 1360 s, 1294 s, 1252 m, 1200 s, 1160 s, 1100 s, 973 s, 887 m, 677 s. Anal. Calcd for $\text{C}_{23}\text{H}_{35}\text{BAlN}_3\text{O}_3$: C, 62.8; H, 8.03; N, 9.56. Found: C, 62.40; H, 8.15; N, 9.26. mp 155-161 °C.

[(PhB(Ox^{Me2}H)(Ox^{Me2})₂)AlMe₂][BPh₄]. A THF solution of $\text{To}^{\text{M}}\text{AlMe}_2$ (0.150 g, 0.342 mmol) was added to a vial containing $[\text{HNMe}_2\text{Ph}][\text{BPh}_4]$ (0.158 g, 0.359 mmol). The resulting colorless solution was stirred for 30 min, and then the solvent was removed under reduced pressure. The crude solid $[\text{PhB}(\text{Ox}^{\text{Me2}}\text{H})(\text{Ox}^{\text{Me2}})_2\text{AlMe}_2][\text{BPh}_4]$ was washed with pentane to remove dimethylaniline. Analytically pure off-white product (0.167 g, 0.220 mmol, 64%) was obtained by crystallization from a THF/pentane solution at -35 °C. ^1H NMR (THF- d_8 , 400 MHz): δ 10.94 (s, 1 H, NH), 7.26 (m, 8 H, *ortho*-Ph₄B), 7.25 (m, 2 H, *ortho*-C₆H₅), 6.83 (vt, $^3J_{\text{HH}} = 7.6$ Hz, 8 H, *meta*-Ph₄B), 6.83 (vt, $^3J_{\text{HH}} = 7.6$ Hz, 2 H, *meta*-C₆H₅), 6.69 (t, $^3J_{\text{HH}} = 7.1$ Hz, 4 H, *para*-Ph₄B), 6.65 (t, $^3J_{\text{HH}} = 7.1$ Hz, 1 H, *para*-C₆H₅B), 4.27 (s, 2 H, $\overline{\text{HNCMe}_2\text{CH}_2\text{OC}}$), 4.21 (d, 2 H, $^3J_{\text{HH}} = 8.8$ Hz, $\text{Al}(\overline{\text{NCMe}_2\text{CH}_2\text{OC}})_2\text{B}$), 4.09 (d, 2 H, $^3J_{\text{HH}} = 8.8$ Hz, $\text{Al}(\overline{\text{NCMe}_2\text{CH}_2\text{OC}})_2\text{B}$), 1.39 (s, 6 H, $\text{Al}(\overline{\text{NCMe}_2\text{CH}_2\text{OC}})_2\text{B}$), 1.37 (s, 6 H, $\text{Al}(\overline{\text{NCMe}_2\text{CH}_2\text{OC}})_2\text{B}$), 1.26 (s, 6 H, $\overline{\text{CNCMe}_2\text{CH}_2\text{O}}$), -0.52 (s, 3 H, AlMe), -0.92 (s, 3 H, AlMe). $^{13}\text{C}\{^1\text{H}\}$ NMR (THF- d_8 , 125 MHz): δ 190.02 (br, $\overline{\text{CNCMe}_2\text{CH}_2\text{O}}$), 165.20 (q, $^2J_{\text{B-C}} = 49.5$ Hz, *ipso*-Ph₄B), 137.19 (*ortho*-Ph₄B), 135.54 (*ortho*-C₆H₅), 125.90 (*meta*-C₆H₅), 125.81 (*meta*-Ph₄B), 121.91 (*para*-Ph₄B), 121.60 (*para*-C₆H₅), 84.09 ($\overline{\text{CNCH}_2\text{CH}_2\text{O}}$), 81.75 ($\text{Al}(\overline{\text{NCMe}_2\text{CH}_2\text{OC}})_2\text{B}$), 68.22 ($\overline{\text{CNCMe}_2\text{CH}_2\text{O}}$), 63.45

(Al($\overline{\text{NCMe}_2\text{CH}_2\text{OC}}$)₂B), 27.87 (Al($\overline{\text{NCMe}_2\text{CH}_2\text{OC}}$)₂B), 27.13 (Al($\overline{\text{NCMe}_2\text{CH}_2\text{OC}}$)₂B), 26.35 ($\overline{\text{CNCMe}_2\text{CH}_2\text{O}}$), -6.43 (AlMe₂), -6.92 (AlMe₂). ¹¹B NMR (THF-*d*₈, 128 MHz): δ -7.51 (BPh₄), -12.41 (PhB(Ox^{Me2}H)(Ox^{Me2})₂). ¹⁵N NMR (THF-*d*₈, 71 MHz): δ -202.8 ($\overline{\text{HNMe}_2\text{CH}_2\text{OC}}$), -176.9 (Al($\overline{\text{NCMe}_2\text{CH}_2\text{OC}}$)₂B). IR (KBr, cm⁻¹): 3361 br m, 3054 s, 2981 s, 2032 s, 1580 sh s, 1560 s, 1462 s, 1374 s, 1296 m, 1262 m, 1204 s, 1032 m, 969 s, 734 s, 705 sh s, 679 m. Anal. Calcd for C₄₇H₅₆B₂AlN₃O₃: C, 74.32; H, 7.43; N, 5.53. Found: C, 73.80; H, 7.48; N, 5.10. mp 144-148 °C.

[Al(κ^2 -To^M)(OⁱPr)₂]. A 100 mL Schlenk flask was charged with H[To^M] (0.400 g, 1.04 mmol) and [Al(OⁱPr)₃] (0.2134 g, 1.04 mmol). The solids were dissolved in 50 mL toluene, and the solution was heated to reflux under an inert atmosphere for 24 hours. The volatile materials were removed under reduced pressure leaving the product as a tan solid (0.34 g, 0.65 mmol, 62%). ¹H NMR (benzene-*d*₆, 400 MHz): δ 7.97 (d, ²J_{HH} = 7.1 Hz, 2 H, *ortho*-C₆H₅), 7.40 (vt, ²J_{HH} = 7.1 Hz, 2 H, *meta*-C₆H₅), 7.22 (t, ²J_{HH} = 7.1 Hz, 1 H, *para*-C₆H₅), 4.37 (septet, ²J_{HH} = 5.2 Hz, 2 H, OCHMe₂), 3.68 (s, 2 H, $\overline{\text{CNCMe}_2\text{CH}_2\text{O}}$), 3.45 (d, ²J_{HH} = 8.5 Hz, 2 H, Al($\overline{\text{NCMe}_2\text{CH}_2\text{OC}}$)₂B), 3.25 (d, ²J_{HH} = 8.5 Hz, 2 H, Al($\overline{\text{NCMe}_2\text{CH}_2\text{OC}}$)₂B), 1.37 (d, ²J_{HH} = 6.2 Hz, 6 H, CHMe₂), 1.34 (d, ²J_{HH} = 6.2 Hz, 6 H, CHMe₂), 1.31 (s, 6 H, $\overline{\text{CNCMe}_2\text{CH}_2\text{O}}$), 1.26 (s, 6 H, $\overline{\text{CNCMe}_2\text{CH}_2\text{O}}$), 1.16 (s, 6 H, $\overline{\text{CNCMe}_2\text{CH}_2\text{O}}$). ¹³C{¹H} NMR (benzene-*d*₆, 100 MHz): δ 145.3 (*ipso*-C₆H₅), 134.1 (*ortho*-C₆H₅), 127.8 (*meta*-C₆H₅), 126.1 (*para*-C₆H₅), 80.27 (Al($\overline{\text{NCMe}_2\text{CH}_2\text{OC}}$)₂B), 77.19 ($\overline{\text{CNCH}_2\text{CH}_2\text{O}}$), 67.74 ($\overline{\text{CNCMe}_2\text{CH}_2\text{O}}$), 65.7 (Al($\overline{\text{NCMe}_2\text{CH}_2\text{OC}}$)₂B), 64.02 (CHMe₂), 29.15 ($\overline{\text{CNCMe}_2\text{CH}_2\text{O}}$), 28.33 (CHMe₂), 27.04 (Al($\overline{\text{NCMe}_2\text{CH}_2\text{OC}}$)₂B), 26.80 (Al($\overline{\text{NCMe}_2\text{CH}_2\text{OC}}$)₂B). ¹¹B NMR

(benzene-*d*₆, 128 MHz): δ -16.6. IR (KBr, cm⁻¹): 3070 w, 3048 w, 2966 s, 2930 s, 2887 s, 2628 w, 1593 m, 1562 s sh, 1463 s, 1433 w, 1374 s, 1362 s, 1298 s, 1258 m, 1204 s, 1169 s, 1034 s br, 973 s, 850 w, 741 w, 710 s, 653 w. Anal. Calcd for C₂₇H₄₃BAIN₃O₅: C, 61.48; H, 8.22; N, 7.97. Found: C, 61.30; H, 8.15; N, 7.56. mp 140-145 °C.

[(κ^2 -To^P)AlMe₂]. A solution of H[To^P] (0.700 g, 1.65 mmol) in 50 mL of toluene was added to a 100 mL Schlenk flask. To this solution was added [AlMe₃]₂ (0.125 g, 1.73 mmol). Upon addition of the [AlMe₃]₂, methane production was observed as the solution bubbled vigorously for several minutes. The yellow solution was stirred for 24 hours under nitrogen. Volatiles were removed under dynamic vacuum to give the off-white product (0.503 g, 1.05 mmol, 63.6%). ¹H NMR (benzene-*d*₆, 400 MHz): δ 8.08 (d, ²J_{HH} = 7.6 Hz, 2 H, *ortho*-C₆H₅), 7.44 (vt, ²J_{HH} = 7.6 Hz, 2 H, *meta*-C₆H₅), 7.24 (t, ²J_{HH} = 7.6 Hz, 1 H, *para*-C₆H₅), 3.95 (m, 1 H, $\overline{\text{CNCH}(i\text{Pr})\text{CH}_2\text{O}}$), 3.68 (m, 6 H, overlapping Ox^{iPr}), 3.52 (m, 1 H, $\overline{\text{Al}(\text{NCH}(i\text{Pr})\text{CH}_2\text{OC})_2\text{B}}$), 3.36 (m, 1 H, $\overline{\text{Al}(\text{NCH}(i\text{Pr})\text{CH}_2\text{OC})_2\text{B}}$), 2.05 05 (septet, ²J_{HH} = 6.24 Hz, 1 H, $\overline{\text{Al}(\text{NCH}(\text{CHMe}_2)\text{CH}_2\text{OC})_2\text{B}}$), 1.97 (septet, ²J_{HH} = 6.24 Hz, 1 H, $\overline{\text{Al}(\text{NCH}(\text{CHMe}_2)\text{CH}_2\text{OC})_2\text{B}}$), 1.77 (septet, ²J_{HH} = 6.24 Hz, 1 H, $\overline{\text{CNCH}(\text{CHMe}_2)\text{CH}_2\text{O}}$), 1.03 (d, ²J_{HH} = 6.93 Hz, 3 H, $\overline{\text{CNCH}(\text{CHMe}_2)\text{CH}_2\text{O}}$), 0.93 (d, ²J_{HH} = 6.93 Hz, 3 H, $\overline{\text{CNCH}(\text{CHMe}_2)\text{CH}_2\text{O}}$), 0.84 (d, ²J_{HH} = 6.93 Hz, 3 H, $\overline{\text{Al}(\text{NCH}(\text{CHMe}_2)\text{CH}_2\text{OC})_2\text{B}}$), 0.53 (d, ²J_{HH} = 6.93 Hz, 3 H, $\overline{\text{Al}(\text{NCH}(\text{CHMe}_2)\text{CH}_2\text{OC})_2\text{B}}$), 0.38 (d, ²J_{HH} = 6.93 Hz, 3 H, $\overline{\text{Al}(\text{NCH}(\text{CHMe}_2)\text{CH}_2\text{OC})_2\text{B}}$), 0.27 (d, ²J_{HH} = 6.93 Hz, 3 H, $\overline{\text{Al}(\text{NCH}(\text{CHMe}_2)\text{CH}_2\text{OC})_2\text{B}}$), -0.29 (d, ²J_{HH} = 3.47 Hz, 6 H, AlMe₂). ¹³C {¹H} NMR (benzene-*d*₆, 100 MHz): δ 196.94 (br,), 196.04 (br,), 145.03 (br, *ipso*-C₆H₅), 134.35 (*ortho*-C₆H₅), 127.57 (*meta*-C₆H₅), 126.19

(*para*-C₆H₅), 73.90 ($\overline{\text{CNCH}(i\text{Pr})\text{CH}_2\text{O}}$), 68.04 ($\overline{\text{Al}(\text{NCH}(i\text{Pr})\text{CH}_2\text{OC})_2\text{B}}$), 67.97 ($\overline{\text{Al}(\text{NCH}(i\text{Pr})\text{CH}_2\text{OC})_2\text{B}}$), 67.71 ($\overline{\text{CNCH}(i\text{Pr})\text{CH}_2\text{O}}$), 66.95 ($\overline{\text{Al}(\text{NCH}(i\text{Pr})\text{CH}_2\text{OC})_2\text{B}}$), 66.79 ($\overline{\text{Al}(\text{NCH}(i\text{Pr})\text{CH}_2\text{OC})_2\text{B}}$), 33.37 ($\overline{\text{CNCH}(\text{CHMe}_2)\text{CH}_2\text{O}}$), 30.28 ($\overline{\text{Al}(\text{NCH}(\text{CHMe}_2)\text{CH}_2\text{OC})_2\text{B}}$), 29.87 ($\overline{\text{Al}(\text{NCH}(\text{CHMe}_2)\text{CH}_2\text{OC})_2\text{B}}$), 19.05 ($\overline{\text{CNCH}(\text{CHMe}_2)\text{CH}_2\text{O}}$), 13.92 ($\overline{\text{Al}(\text{NCH}(\text{CHMe}_2)\text{CH}_2\text{OC})_2\text{B}}$), -9.00 (AlMe), -9.30 (AlMe). ¹¹B NMR (benzene-*d*₆, 128 MHz): δ -16.4. IR (KBr, cm⁻¹): 3066 w, 3048 w, 2962 s, 2930 s, 2889 m, 1579 m, 1570 s sh, 1465 w, 1394 w, 1370 w, 1225 s, 1195 m, 990 m, 960 m, 735 w, 702 s, 680 s. Anal. Calcd for C₂₆H₄₁AlN₃O₃: C, 64.89; H, 8.53; N, 8.74. Found: C, 64.40; H, 8.18; N, 8.89. mp 110-114 °C, dec.

Representative aluminum-catalyzed polymerization to give poly(lactic acid).

Rac-3,6-dimethyl-1,4-dioxane-2,5-dione (*rac*-LA) (1.64 g, 11.4 mmol) and the catalyst To^MAlMe₂ (0.010 g, 0.023 mmol) were loaded into a glass ampoule inside of a glovebox. The ampoule was removed, sealed under vacuum, and immersed in an oil bath at 115 °C for 24 h. The ampoule was then removed from the bath and allowed to cool to room temperature. PLA was obtained by dissolving the crude product in acetone. A portion of the crude product was used to determine the monomer conversion *via* ¹H NMR. The polymer was then purified by precipitation from water, and was dried under vacuum for 24 h.

DFT Calculations. All calculations were performed with the NWChem software suite.²⁹ Density functional theory (DFT) was employed using the B3LYP hybrid functional³⁰ to obtain optimized geometries and frequencies (see supplementary material). Energies were

also calculated using DFT with the B3LYP functional and include the zero point energy correction. 6-311-(2d,2p) was used for aluminum and 6-311++G** basis set was used for all other atoms.³¹ All structures reported have positive second derivatives with respect to coordinates, indicating that they are all minima on the potential energy surface.

References

- 1) (a) Negishi, E. *Organometallics in Organic Synthesis*; Wiley: New York, 1980; Vol. 1.;
(b) Crabtree, R.H.; Mingos, M.P. *Comprehensive Organometallic Chemistry III*; Elsevier Ltd: Oxford, 2007; Vol. 3, p. 265.
- 2) Matteson, D.S. *Organometallic Reaction Mechanisms of the Non-transition Elements*; Academic Press: New York, 1974.
- 3) Dagorne, S.; Atwood, D.A. *Chem. Rev.* **2008**, *108*, 4037-4071.
- 4) Looney, A.; Parkin, G. *Polyhedron* **1990**, *9*, 265-276.
- 5) (a) Han, R.; Looney, A.; Parkin, G. *J. Am. Chem. Soc.* **1989**, *111*, 7276-7278.;
Chisholm, M.H.; Eilerts, N.W.; Huffman, J.C. *Inorg. Chem.* **1996**, *35*, 445-450.; (c)
Dias, H.V.R.; Jin, W. *Inorg. Chem.* **2003**, *42*, 5034-5036.
- 6) Fontaine, F.-G.; Boudreau, J.; Thibault, M.-H. *Eur. J. Inorg. Chem.* **2008**, 5439-5454.
- 7) Fischbach, A.; Bazinet, P.R.; Waterman, R.; Tilley, T.D. *Organometallics* **2008**, *27*, 1135-1139.
- 8) (a) Fontaine, F.-G.; Zargarian, D. *J. Am. Chem. Soc.* **2004**, *126*, 8786-8794.; (b) Thibault, M.-H.; Boudreau, J.; Mathiotte, S.; Drouin, F.; Sigouin, O.; Michaud, A.; Fontaine, F.-G. *Organometallics* **2007**, *26*, 3807-3815.; (c) Sircoglou, M.; Bouhadir, G.; Saffon, N.; Miqueu, K.; Bourissou, D. *Organometallics* **2008**, *27*, 1675-1678.

- 9) Sircoglou, M.; Mercy, M.; Saffon, N.; Coppel, Y.; Bouhadir, G.; Maron, L.; Bourissou, D. *Angew. Chem. Int. Ed.* **2009**, *48*, 3454-3457.
- 10) Mazet, C.; Kohler, V.; Pfaltz, A. *Angew. Chem. Int. Ed.* **2005**, *44*, 4888 – 4891.
- 11) Dunne, J.F.; Manna, K.; Wiench, J.W.; Ellern, A.; Pruski, M.; Sadow, A.D. *Dalton Trans.* **2010**, *39*, 641-653.
- 12) Kidd, R.G. *NMR of Newly Accessible Nuclei*; Laszlo, P., Ed.; Academic Press: New York, **1983**; Vol. 2, pp 49 – 77.
- 13) (a) Schenetti, L; Mucci, A.; Longato, A. *J. Chem. Soc., Dalton Trans.* **1996**, 299-303.;
(b) Gudat, D.; Dogan, A.; Kaim, W.; Klein, A. *Magn. Reson. Chem.* **2004**, *42*, 781-787.
- 14) Dagorne, S.; Bellemin-Laponnaz, S.; Welter, R. *Organometallics* **2004**, *23*, 3053-3061.
- 15) Kohler, V.; Mazet, C.; Toussaint, A.; Kulicke, K.; Haussinger, D.; Neuburger, M.; Schaffner, S.; Kaiser, S.; Pfaltz, A. *Chem.-Eur. J.* **2008**, *14*, 8530-8539.
- 16) Baird, B.; Pawlikowski, A.V.; Su, J.; Wiench, J.W.; Pruski, M.; Sadow, A.D. *Inorg. Chem.* **2008**, *47*, 10208-10210.
- 17) Pawlikowski, A.V.; Gray, T.S.; Schoendorff, G.; Baird, B.; Ellern, A.; Windus, T.L.; Sadow, A.D. *Inorg. Chim. Acta* **2009**, *362*, 4517-4525.
- 18) Dowling, C.M.; Parkin, G. *Polyhedron* **1999**, *18*, 3567-3571.
- 19) Trofimenko, S. *Acc. Chem. Res.*, **1971**, *4*, 17-22.
- 20) Lewinski, J.; Zachara, J.; Gos, P.; Grabska, E.; Kopec, T.; Madura, I.; Marciniak, W.; Prowotorow, I. *Chem.-Eur. J.* **2000**, *6*, 3215-3227.
- 21) Guzi, I.A.; Wendt, M. *Program Solid-G*. UW-Madison, WI, USA, 2004.
- 22) (a) Ball, R.G.; Ghosh, C.K.; Hoyano, J.K.; McMaster, A.D.; Graham, W.A.G. *J. Chem.*

- Soc., Chem. Commun.* **1989**, 341-342; (b) Bovens, M.; Gerfin, T.; Gramlich, V.; Petter, W.; Venanzi, L.M.; Haward, M.T.; Jackson, S.A.; Eisenstein, O. *New. J. Chem.* **1992**, *16*, 337-345.; (c) Cowley, R.E.; Bontchev, R.P.; Duesler, E.N.; Smith, J.M. *Inorg Chem.* **2006**, *45*, 9771-9779.
- 23) Shannon, R.D. *Acta Crystallogr., Sect. A.: Cryst. Phys., Diffr., Theor. Gen. Crystallogr.* **1976**, *32*, 751-767.
- 24) (a) Zhong, Z.; Dijkstra, P.J.; Feijen, J. *Angew. Chem. Int. Ed.* **2002**, *41*, 4510-4513.; (b) Dechy-Cabaret, O.; Martin-Vaca, B.; Bourissou, D. *Chem. Rev.* **2004**, *104*, 6147-6176.; (c) Tang, Z.; Yang, Y.; Pang, X.; Hu, J.; Chen, X.; Hu, N.; Jing, X. *J. Appl. Polym. Sci.* **2005**, *98*, 102-108.; (d) Nomura, N.; Ishii, R.; Yamamoto, Y.; Kondo, T. *Chem.-Eur. J.* **2007**, *13*, 4433-4451.; (e) Bouyahyi, M.; Grunova, E.; Marquet, N.; Kirillov, E.; Thomas, C.M.; Roisnel, T.; Carpentier, J.-F. *Organometallics* **2008**, *27*, 5815-5825.; (f) Alaaeddine, A.; Thomas, C.M.; Roisnel, T.; Carpentier, J.-F. *Organometallics* **2009**, *28*, 1469-1475.
- 25) Otero, A.; Lara-Sánchez, A.; Fernández-Baeza, J.; Alonso-Moreno, C.; Castro-Osma, J.A.; Márquez-Segovia, I.; Sánchez-Barba, L.F.; Rodríguez, A.M.; Garcia-Martinez, J.C. *Organometallics* **2011**, *30*, 1507-1522.
- 26) Li, H.; Wang, C.; Bai, F.; Yue, J.; Woo, H.-G. *Organometallics* **2004**, *23*, 1411-1415.
- 27) (a) Kasperczyk, J.E. *Macromolecules* **1995**, *28*, 3937-3939.; (b) Thakur, K.A.M.; Kean, R.T.; Hall, E.S.; Kolstad, J.J.; Lindgren, T.A.; Doscotch, M.A.; Siepmann, J.I.; Munson, E.J. *Macromolecules* **1997**, *30*, 2422-2428.
- 28) Dunne, J.F.; Su, J.C.; Ellern, A.; Sadow, A.D. *Organometallics* **2008**, *27*, 2399-2401.
- 29) (a) Kendall, R. A.; Apra, E.; Bernholdt, D. E.; Bylaska, E. J.; Dupuis, M.; Fann, G. I.;

- Harrison, R. J.; Ju, J.; Nichols, J. A.; Nieplocha, J.; Straatsma, T. P.; Windus, T. L.; Wong, A. T. *Computer Phys. Comm.* 2000, **128**, 260-283. (b) Bylaska, E. J.; Jong, W. A. d.; Govind, N.; Kowalski, K.; Straatsma, T. P.; Valiev, M.; Wang, D.; Apra, E.; Windus, T. L.; Hammond, J.; Nichols, P.; Hirata, S.; Hackler, M. T.; Zhao, Y.; Fan, P.-D.; Harrison, R. J.; Dupuis, M.; Smith, D. M. A.; Nieplocha, J.; Tipparaju, V.; Krishnan, M.; Wu, Q.; Voorhis, T. V.; Auer, A. A.; Nooijen, M.; Brown, E.; Cisneros, G.; Fann, G. I.; Fruchtl, H.; Garza, J.; Hirao, K.; Kendall, R.; Nichols, J. A.; Tsemekhman, K.; Wolinski, K.; Anchell, J.; Bernholdt, D.; Borowski, P.; Clark, T.; Clerc, D.; Dachsel, H.; Deegan, M.; Dyall, K.; Elwood, D.; Glendening, E.; Gutowski, M.; Hess, A.; Jaffe, J.; Johnson, B.; Ju, J.; Kobayashi, R.; Kutteh, R.; Lin, Z.; Littlefield, R.; Long, X.; Meng, B.; Nakajima, T.; Niu, S.; Pollack, L.; Rosing, M.; Sandrone, G.; Stave, M.; Taylor, H.; Thomas, G.; Lenthe, J. v.; Wong, A.; Zhang, Z. Pacific Northwest National Laboratory Richland, Washington 99352, USA, 2007.
- 30) (a) Becke, A.D. *J. Chem. Phys.* **1993**, 98, 5648-5652. (b) Lee, C.T.; Yang, W.T.; Parr, R.G. *Phys. Rev. B* **1988**, 37, 785-789.
- 31) Frisch, M.J.; Pople, J.A.; Binkley, J.S. *J. Chem. Phys.* **1984**, 80, 3265-3269.

Chapter 4: Concerted C–N and C–H bond formation in a magnesium-catalyzed hydroamination

Modified from a paper published in the *Journal of the American Chemical Society*[‡]

James F. Dunne[†], D. Bruce Fulton, Arkady Ellern, Aaron D. Sadow

Department of Chemistry and U.S. Department of Energy Ames Laboratory, Iowa State University, Ames, IA 50011, United States

Abstract

Coordinatively saturated $To^M MgMe$ [To^M = tris(4,4-dimethyl-2-oxazoliny)phenylborate] is an active precatalyst for intramolecular hydroamination/cyclization of aminoalkenes at 50 °C. The catalytic system displays Michaelis-Menten-type kinetics which are consistent with a mechanism involving reversible catalyst-substrate association prior to cyclization. The magnesium amidoalkene resting state of the catalyst, $To^M MgNHCH_2CR_2CH=CH_2$ [R = Ph, Me, $-(CH_2)_5-$], is isolable, but the isolated magnesium amidoalkene does not undergo cyclization at the catalytic temperature of 50 °C. However, addition of trace amounts of substrate allows cyclization to occur. Therefore, we propose a two-substrate, six-center transition state involving concerted C–N bond formation and N–H bond cleavage as the turnover limiting step of the catalytic cycle.

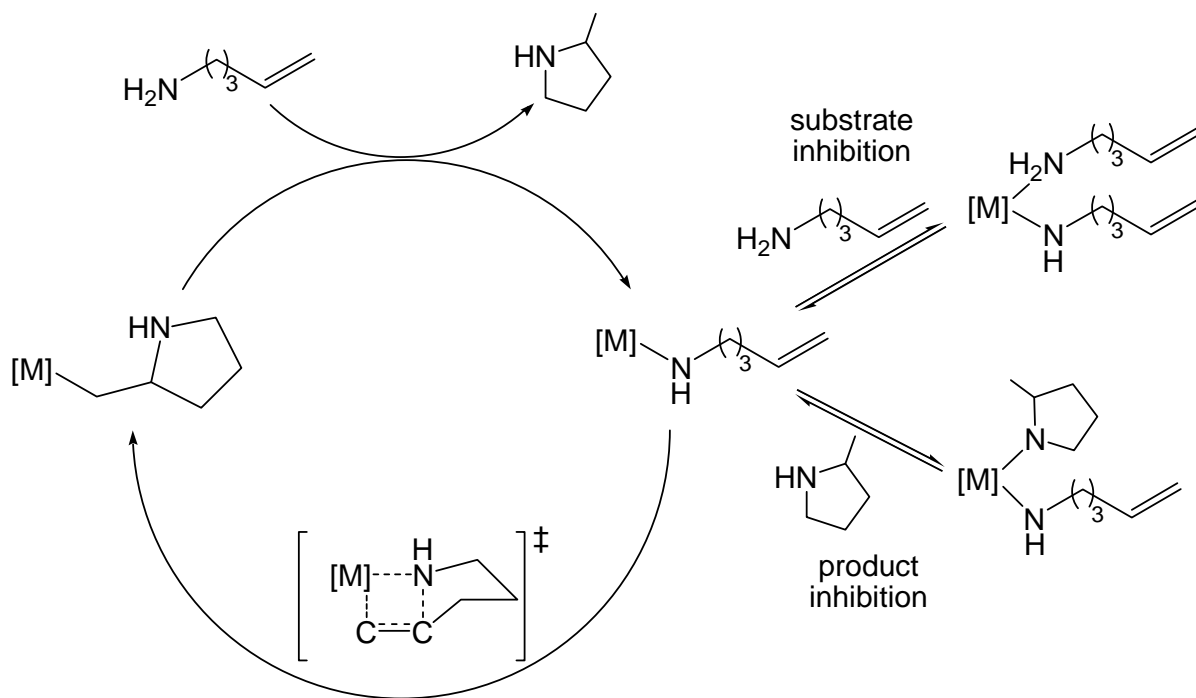
Introduction

The transition-metal-catalyzed addition of heteroatoms across C=C double bonds is one of the most common means of introducing new functional groups in organic molecules.

[‡]Parts of this paper reprinted with permission of the *Journal of the American Chemical Society* **2010**, *132*, 17680-17683.

[†]Primary researcher and author

This functionalization is exemplified by the insertion of olefins into M–N bonds in d^0 metal catalyzed intramolecular hydroamination/cyclization of aminoalkenes.¹ Based on mechanistic studies of these systems, the olefin of the amidoalkene is proposed to undergo turnover limiting insertion into the M–N bond to give the corresponding metal alkyl complex (Scheme 4.1).² The alkyl group is then rapidly replaced by a second substrate molecule to give the free pyrrolidine and regenerate the resting state of the catalyst.



Scheme 4.1. General proposed insertion mechanism for intramolecular hydroamination

However, kinetic studies of these systems only provide indirect access to the proposed insertion step. The typical empirical rate law is $-d[\text{substrate}]/dt = k_{\text{obs}}[\text{catalyst}]^1[\text{substrate}]^0$, and in most cases this simplifies the overall mechanism as k_{obs} is a combination of elementary rate and equilibrium constants. These rate constants often include

competitive association and/or substitution and inhibition by either product or substrate.³ The coordination of amine substrate may be mechanistically significant as in many systems an additional amine molecule is present in the catalyst resting state.^{1b} An additional problem with the insertion mechanism is the observation of significant primary isotope effects. Primary KIEs have been measured with k_H/k_D values ranging from 2 to 5 for H_2NR vs D_2NR substrates.^{3,4} These KIEs strongly suggest that N–H bond cleavage is involved in the rate-determining step, which is inconsistent with classical 1,2-insertion. Two possible explanations have been proposed in order to explain this: 1) proton transfer from a coordinated amine to the partially polarized olefinic carbon in a 4-membered insertion transition state, and 2) hydrogen bonding from the coordinated amine to the amido nitrogen followed by rapid proton migration to give the pyrrolidine product.³

Furthermore, examples of 1,2-insertion reactions of olefins into $M-NR_2$ bonds that yield isolable metal alkyls are rare in the literature. Examples with metals from group 4 are limited to alkyne insertions that yield vinyl amine products⁵, as is the only example involving a group 6 metal.⁶ Iridium(III) amido and platinum(II) amido compounds have been reported to react with activated olefins such as norbornylene and acrylonitrile, respectively.^{7,8} Palladium amido complexes have recently been shown to react through both intramolecular and intermolecular olefin insertion pathways.⁹ However, we are not aware of stoichiometric insertion reactions of d^0 metal amides and alkenes that yield isolable metal alkyls. Despite this, there is a wealth of data and computational models that support the general insertion mechanism for rare earth metal-catalyzed hydroamination.¹⁰

Recently, the first examples of alkaline earth metal compounds have been reported as active catalysts for hydroamination/cyclization (Figure 4.1).¹¹ Interest in these metals arose from the electronic similarities to the rare earth elements (d^0 with only one available

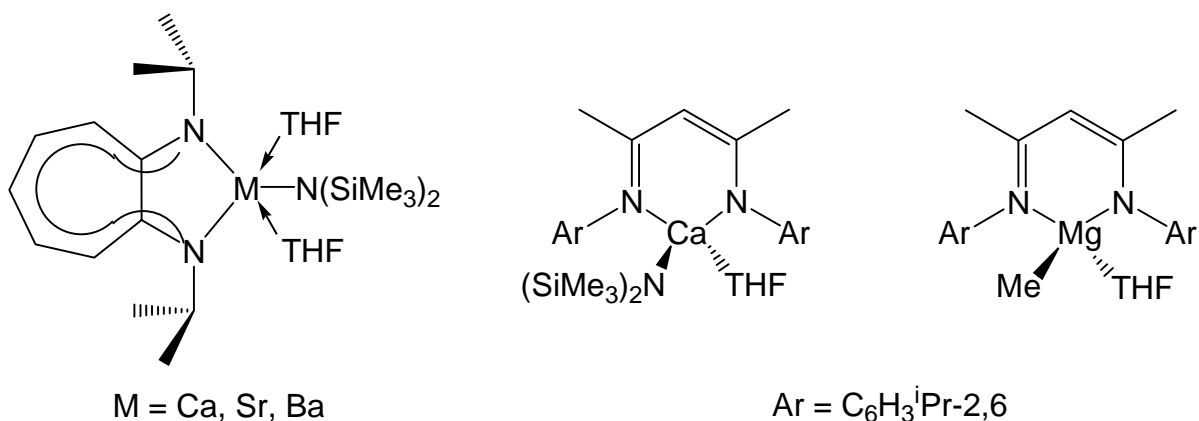


Figure 4.1. Examples of alkaline earth metal catalysts for hydroamination

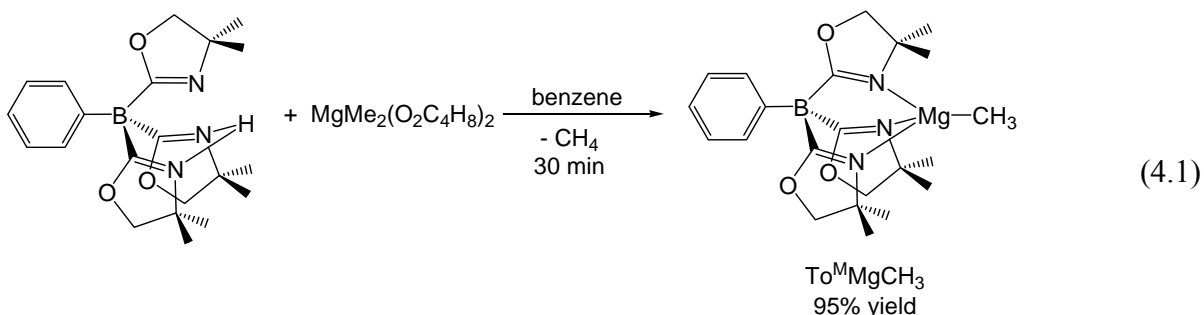
oxidation state), as well as their similar ionic radii.¹² While originally restricted to calcium complexes further investigations have expanded these systems to include the heavier alkaline earth metals of strontium and barium¹³, as well as the first examples of magnesium-catalyzed intramolecular hydroamination.¹⁴ The success of these catalysts led us to investigate $To^M Mg(II)$ compounds to explore the insertion step in hydroamination/cyclization. We hypothesized that the ability of To^M to coordinate in a tridentate manner could result in a metal center that is coordinatively saturated, and thus restrict the bonding of an additional substrate molecule to the metal center. By limiting the coordination sites at the metal, we planned to study the insertion reaction in the absence of a coordinated amine. We also thought that low-coordinate magnesium was needed for insertion to proceed, and hoped that low temperature reactions could allow isolation of the catalyst resting state and consequently allow for stoichiometric investigations into the insertion step. With these goals in mind, we

set about synthesizing $To^M MgR$, and exploring its reactivity in catalytic hydroamination /cyclization.

Results and Discussion

Synthesis of $To^M MgMe$ and $To^M_2 Mg$

$To^M MgMe$ is prepared by the reaction of equimolar amounts of HTo^M and $MgMe_2(O_2C_4H_8)_2$ (eq 4.1). The effervescence of methane gas is observed immediately upon the dissolution of the two solids in benzene, and the identity of the gas is confirmed by the observation of a methane peak in the 1H NMR spectrum in micromolar experiments.



$TITo^M$ may also be used in place of HTo^M to give the same product in equal yield (95%). Upon addition of $TITo^M$ to solutions of $MgMe_2(O_2C_4H_8)_2$, the solution immediately turns black as Tl metal precipitates, and small amounts of ethane gas are observed in the 1H NMR spectrum. The 1H NMR spectrum shows $To^M MgMe$ to be C_{3v} symmetric in the solution state, indicating that dioxane does not coordinate to the magnesium(II) center. Addition of excess (3 equivalents) THF to solutions of $To^M MgMe$ confirm coordinative saturation at magnesium as only the starting $To^M MgMe$ and free THF are observed. Fluxionality is ruled out by the observation of only one oxazoline ν_{CN} stretch in solution-state IR spectra of $To^M MgMe$ and dioxane. A 1H - ^{15}N HMBC experiment shows a crosspeak

between the oxazoline nitrogen and the methyl group bound to magnesium, indicating that the product is in fact the desired heteroleptic species and not simply a mixture of $\text{To}^{\text{M}}_2\text{Mg}$ and $\text{MgMe}_2(\text{O}_2\text{C}_4\text{H}_8)_2$ in solution. X-ray quality crystals were obtained from a diethyl ether solution cooled to $-30\text{ }^\circ\text{C}$, and confirmed the tridentate coordination of the To^{M} ligand in the solid state (Figure 4.2). Solid angles were calculated from the X-ray structure data and

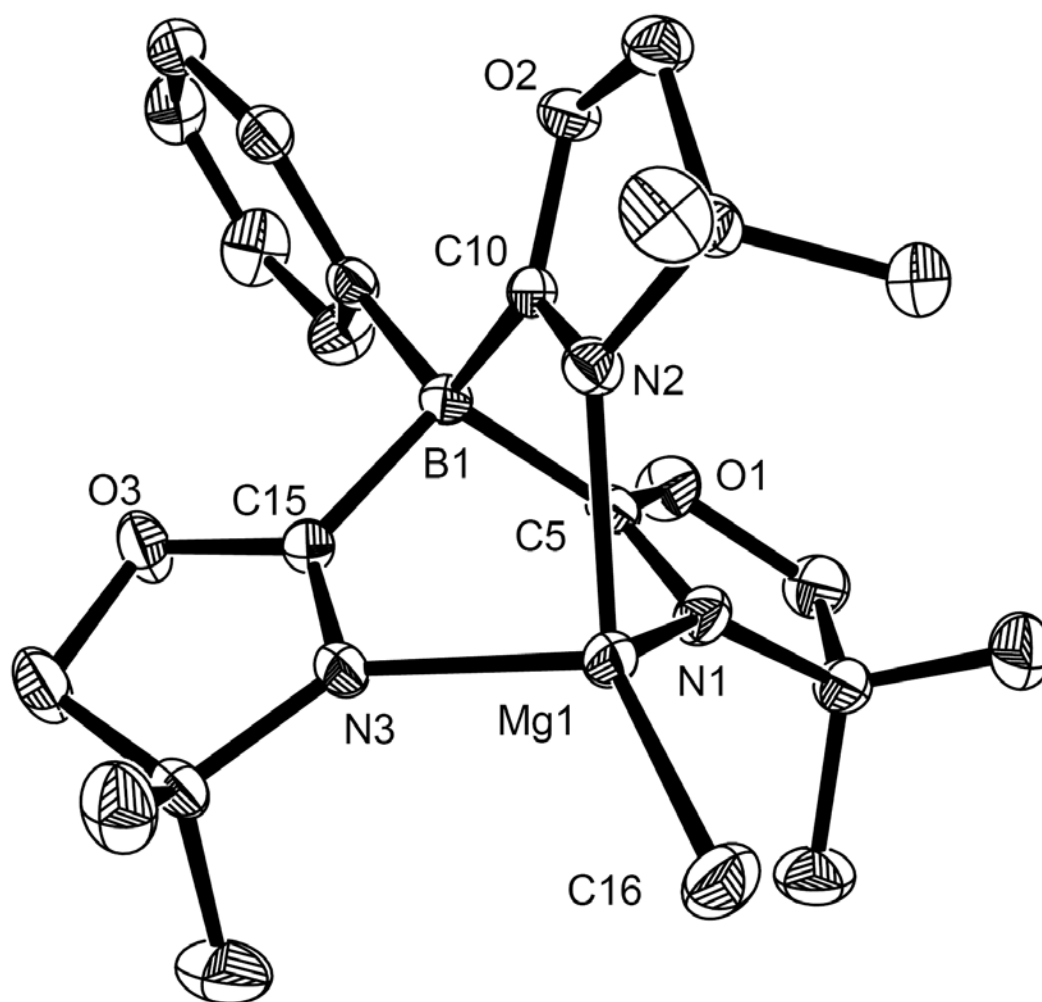
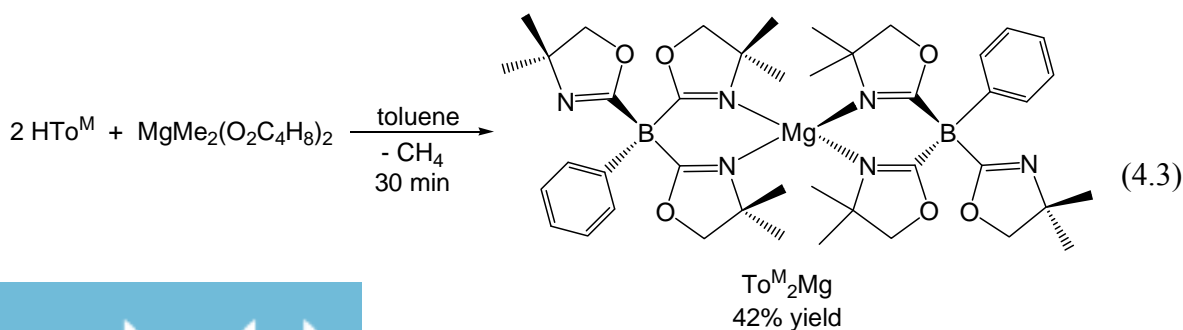


Figure 4.2. ORTEP diagram of $\text{To}^{\text{M}}\text{MgMe}$ drawn at 50% probability. Selected bond lengths (\AA): Mg1–N1, 2.122(1); Mg1–N2, 2.124(1); Mg1–N3, 2.090(1); Mg1–C16, 2.108(1).

showed that 75% of the space surrounding the magnesium center is occupied by the To^{M} (60%) and CH_3 (15%) ligands.¹⁵ Heteroleptic magnesium compounds are often susceptible to Schlenk-type equilibrium in which two molecules of the heteroleptic metal species disproportionate to give two different homoleptic molecules (eq 4.2).¹⁶ At room temperature there is no evidence of $\text{To}^{\text{M}}\text{MgMe}$ undergoing this Schlenk equilibrium. Thermolysis of a benzene- d_6 solution of $\text{To}^{\text{M}}\text{MgMe}$ in a sealed NMR tube shows no change in the ^1H NMR spectrum even up to 150 °C, indicating that the steric bulk of To^{M} is sufficient enough to prevent undesirable disproportionation reactions.



$\text{To}^{\text{M}}_2\text{Mg}$ was independently synthesized to ensure that none of this compound is formed during the thermolysis reaction. Reaction of two equivalents of HTo^{M} to $\text{MgMe}_2(\text{O}_2\text{C}_4\text{H}_8)_2$ in benzene gives the homoleptic $\text{To}^{\text{M}}_2\text{Mg}$ cleanly (eq 4.3). The molecule may also be obtained by the addition of one equivalent of HTo^{M} to a solution of $\text{To}^{\text{M}}\text{MgMe}$, demonstrating that the magnesium center in $\text{To}^{\text{M}}\text{MgMe}$ is still accessible for chemical reactions. Interestingly, when TITo^{M} is used in place of HTo^{M} no formation of $\text{To}^{\text{M}}_2\text{Mg}$ is observed. Reaction of two equivalents of TITo^{M} with $\text{MgMe}_2(\text{O}_2\text{C}_4\text{H}_8)_2$ shows only $\text{To}^{\text{M}}\text{MgMe}$ and unreacted TITo^{M} in the ^1H NMR spectrum.



An X-ray structure of $\text{To}^{\text{M}}_2\text{Mg}$ was obtained from crystals grown in a concentrated toluene solution at $-30\text{ }^\circ\text{C}$ (Figure 4.3). The structure shows each To^{M} ligand binding to the metal center in a bidentate fashion. The magnesium center is pseudo-tetrahedral with the two To^{M} ligands orthogonal to each other. The magnesium center is coordinatively saturated and

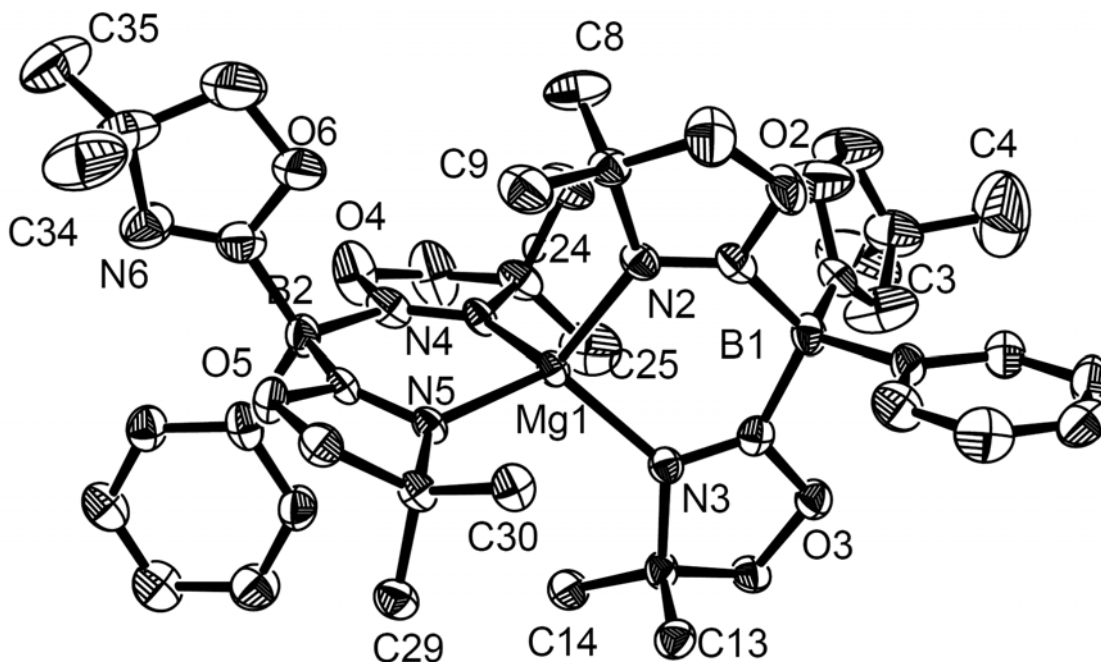


Figure 4.3. ORTEP diagram of $\text{To}^{\text{M}}_2\text{Mg}$ drawn at 50% probability. Selected bond lengths (\AA): Mg1–N2, 2.063(4); Mg1–N3, 2.046(5); Mg1–N4, 2.070(5); Mg1–N5, 2.065(4).

protected on all sides by the oxazoline methyl groups. In the solution state, $\text{To}^{\text{M}}_2\text{Mg}$ shows C_s symmetry as seen in the ^1H NMR spectrum. The two uncoordinated oxazoline rings are equivalent with singlet resonances for both the oxazoline methylene and methyl groups (3.69 and 1.31 ppm, respectively). Four singlet resonances are observed for the methyl groups on the oxazoline rings bound to the magnesium center. Two of these resonances correspond to

the pseudo-axial methyl groups on each To^{M} ligand, and two are the pseudo-equatorial methyl groups.

Catalytic hydroamination and empirical rate law

Having ascertained that $\text{To}^{\text{M}}\text{MgMe}$ does not undergo the Schlenk equilibrium, we began investigating whether $\text{To}^{\text{M}}\text{MgMe}$ is a viable catalyst for hydroamination/cyclization. Micromolar scale experiments of 1-amino-2,2-diphenyl-4-pentene and 10 mol% $\text{To}^{\text{M}}\text{MgMe}$ in benzene- d_6 were conducted and monitored via ^1H NMR spectroscopy. Upon mixing, methane is observed as a singlet resonance at 0.15 ppm in the ^1H NMR spectrum, and new To^{M} resonances appear suggesting that the magnesium methyl group is readily protonated to give the corresponding magnesium amide. However, at room temperature no hydroamination is observed over a 24 hour period. After warming the solution to 50 °C for one hour, new resonances began to appear in the ^1H NMR spectrum which were identified as the hydroamination/cyclization product 2-methyl-4,4-diphenylpyrrolidine. Quantitative conversion of the starting aminoalkene to the pyrrolidine product is achieved after 12 hours of heating at 50 °C.

Under these conditions (50 °C, benzene, 10 mol% catalyst), $\text{To}^{\text{M}}\text{MgMe}$ is a capable catalyst for the cyclization of primary 4-aminoalkenes, as well as one secondary aminoalkene affording the corresponding pyrrolidines (Table 4.1). 2,2-Disubstitution is required for cyclization to occur, and the unsubstituted parent substrate 4-pentene-1-amine is not cyclized by $\text{To}^{\text{M}}\text{MgMe}$ even when the temperature is increased up to 100 °C. Disubstitution at the 2 position of the aminoalkene substrate helps facilitate the amine and olefin into a favorable conformation for cyclization to occur via the Thorpe-Ingold effect, with bulkier substituents resulting in faster cyclization rates.¹⁷

Table 4.1. Hydroamination/cyclization of aminoalkenes catalyzed by $\text{To}^{\text{M}}\text{MgMe}^{\text{a}}$

Entry	Substrate	Product	Time (h)	Conversion (%) ^b
1			12	99
2			72	20
3			15	99
4			48	99 ^c

^aConditions: 10 mol % $\text{To}^{\text{M}}\text{MgMe}$, C_6D_6 , 50 °C. ^bConversion (%) was determined by ^1H NMR spectroscopy.

^c20 mol % $\text{To}^{\text{M}}\text{MgMe}$.

The lack of coordination of ethers to the metal center along with the calculated solid angles suggests that no open site exists for the olefin to coordinate to the metal center prior to insertion into the Mg–C bond. As this is uncommon in most catalytic hydroamination systems, we were motivated to further investigate the mechanism for cyclization. A series of experiments were carried out in which the concentration of the 1-amino-2,2-diphenylpentene substrate was monitored over the course of the reaction by ^1H NMR spectroscopy. Linear plots were obtained for graphs of $\ln[\text{substrate}]$ vs time through three half-lives giving a first-order dependence of the rate on substrate concentration (Figure 4.4). The concentration of the catalyst was varied from 14 mM to 38 mM in order to determine the order of reaction with respect to the catalyst. k_{obs} was measured over the catalyst concentration range and the

slopes of these curves were then plotted versus the concentration of $\text{To}^{\text{M}}\text{MgMe}$ giving a linear plot, and the empirical rate law: $-\text{d}[\text{substrate}]/\text{d}t = k'_{\text{obs}}[\text{To}^{\text{M}}\text{MgMe}]^1[\text{substrate}]^1$ ($k'^{(\text{H})}_{\text{obs}} = (6.9 \pm 1.1) \times 10^{-3} \text{ M}^{-1}\text{s}^{-1}$) (Figure 4.5). As a reminder the typical empirical rate law for hydroamination/cyclization is $-\text{d}[\text{substrate}]/\text{d}t = k_{\text{obs}}[\text{catalyst}]^1[\text{substrate}]^0$.

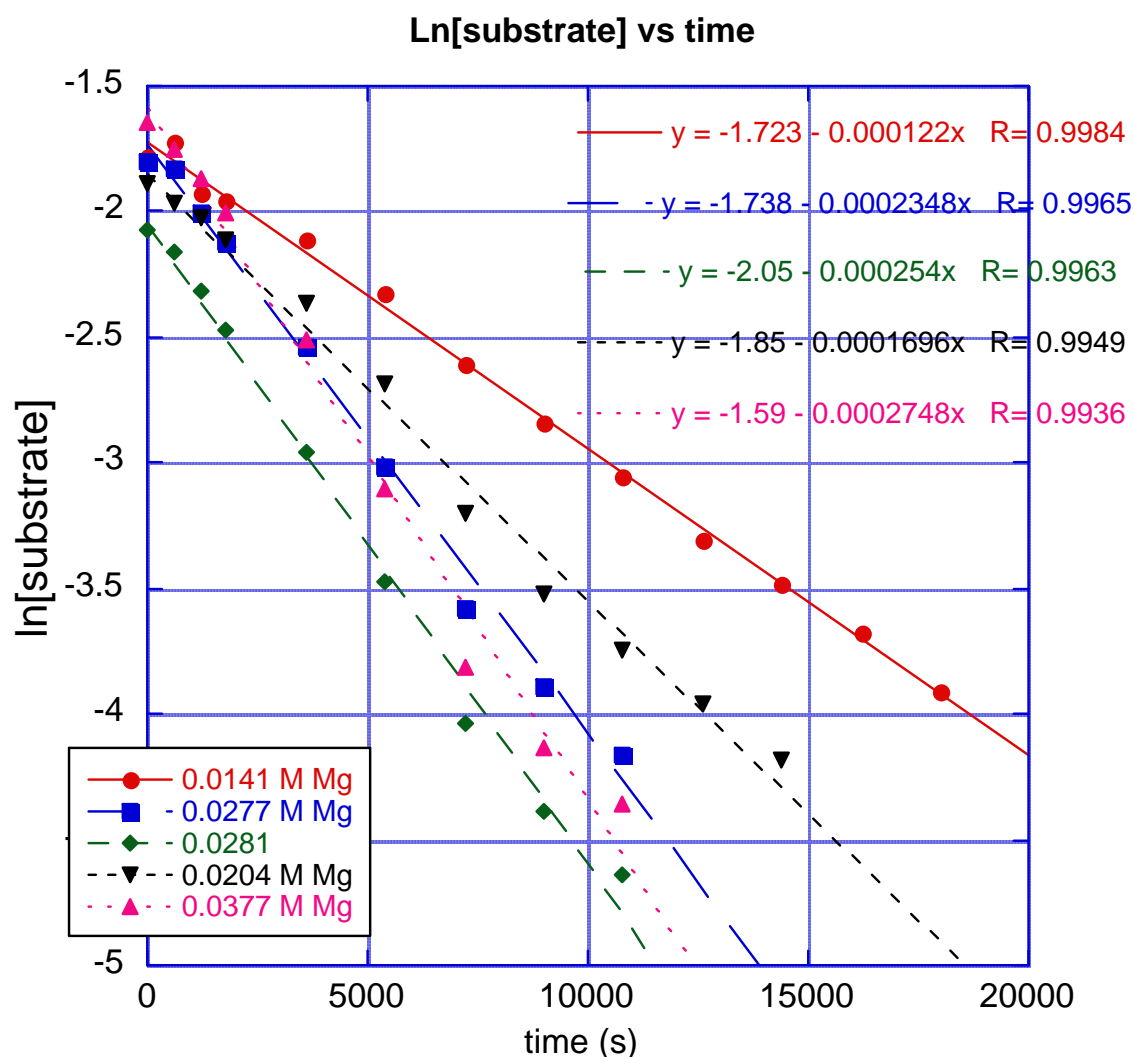


Figure 4.4. Plot of $\ln[1\text{-amino-2,2-diphenyl-4-pentene}]$ versus time at $50\text{ }^\circ\text{C}$ showing first order dependence on substrate concentration. Each data set represents a different concentration of precatalyst $[\text{To}^{\text{M}}\text{MgMe}]$, and the curves are linear least squares best fits of data to the equation $\ln[\text{substrate}] = C - mt$. The concentrations of $[\text{To}^{\text{M}}\text{MgMe}]$ are shown in the inset.

A plot of $k^{(D)}_{\text{obs}}$ for cyclization of 1-amino-2,2-diphenyl-4-pentene- d_2 versus $[\text{To}^{\text{M}}\text{MgMe}]$ gives the rate constant $k^{(D)}_{\text{obs}} = (1.5 \pm 0.3) \times 10^{-3} \text{ M}^{-1}\text{s}^{-1}$. The ratio of $k^{(H)}_{\text{obs}}/k^{(D)}_{\text{obs}}$ gives a primary isotope effect of 4.6 (Figure 4.5).

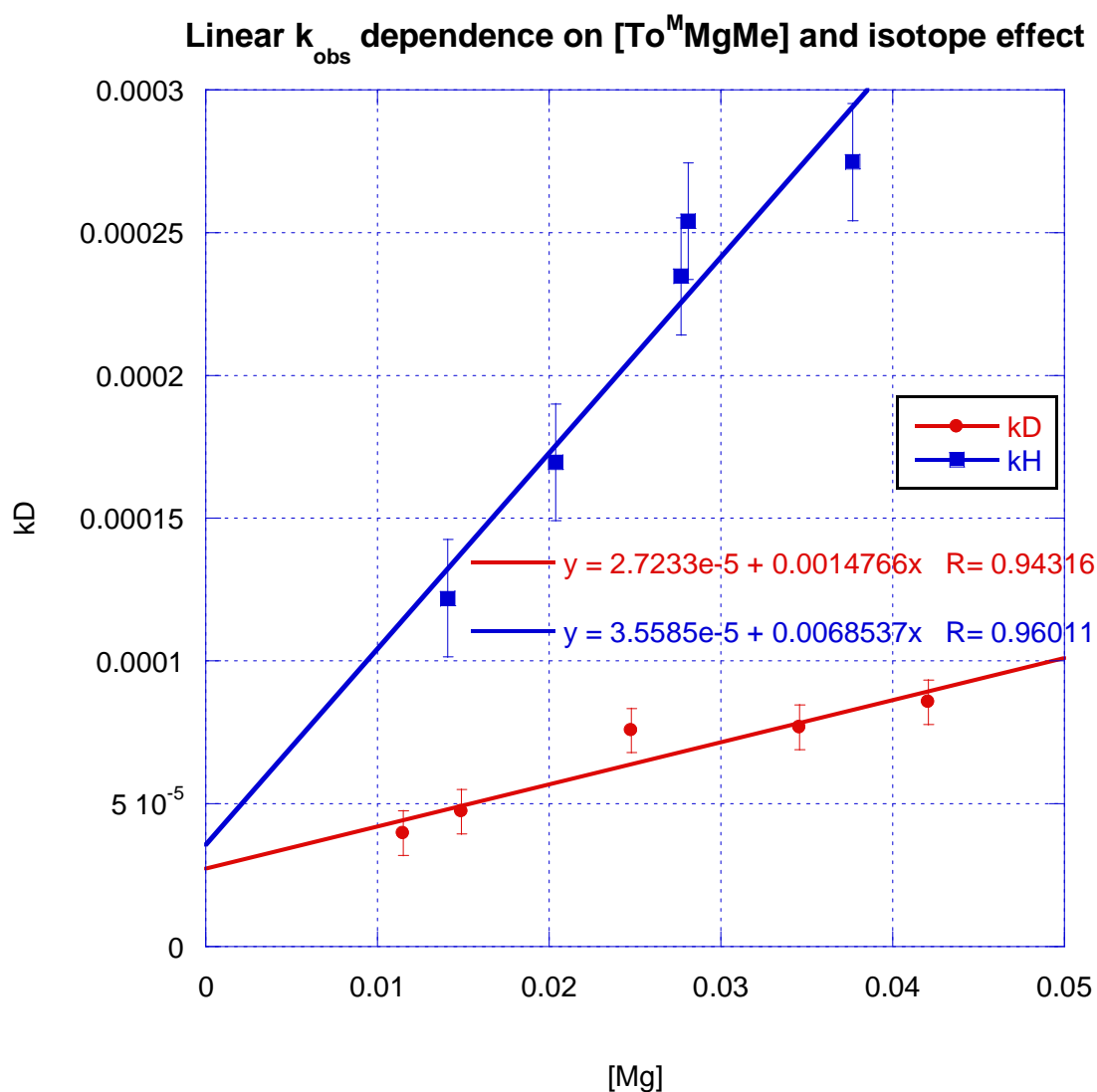
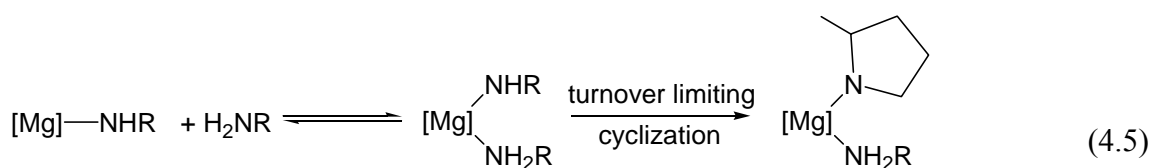
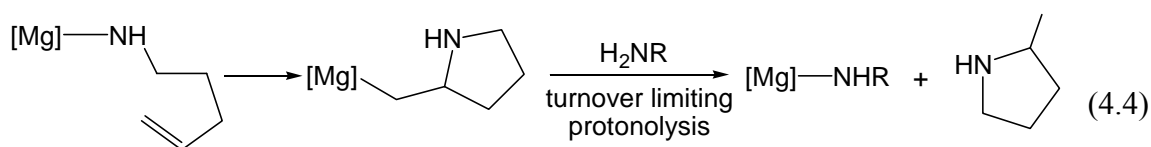


Figure 4.5. Plot establishing first-order dependence on concentration of catalyst $[\text{To}^{\text{M}}\text{MgMe}]$, and displaying isotope effect, $k_{\text{H}}/k_{\text{D}}$. All k_{obs} were measured at 50 °C.

The magnitude of this primary isotope effect is significant, and strongly suggests that the N–H bond is broken during the turnover-limiting step. While primary isotope effects of this magnitude are commonly observed in hydroamination/cyclization, the classical 1,2-insertion mechanism fails to adequately explain this observation, and suggests that C–N bond formation is more complicated than allowed for in the insertion mechanism.^{3,4} Additionally, second-order rate laws for aminoalkene hydroamination/cyclization are uncommon.¹⁸ The rate law and isotope effect are consistent with two possible mechanisms: 1) cyclization proceeding through insertion of the olefin into the Mg–N bond followed by turnover limiting intermolecular protonolysis of the resulting magnesium alkyl, and 2) a two step sequence in which the association of catalyst and substrate is reversible and precedes a unimolecular cyclization process (eq 4.4 and 4.5).



Synthesis of magnesium amidoalkenes and pyrrolides

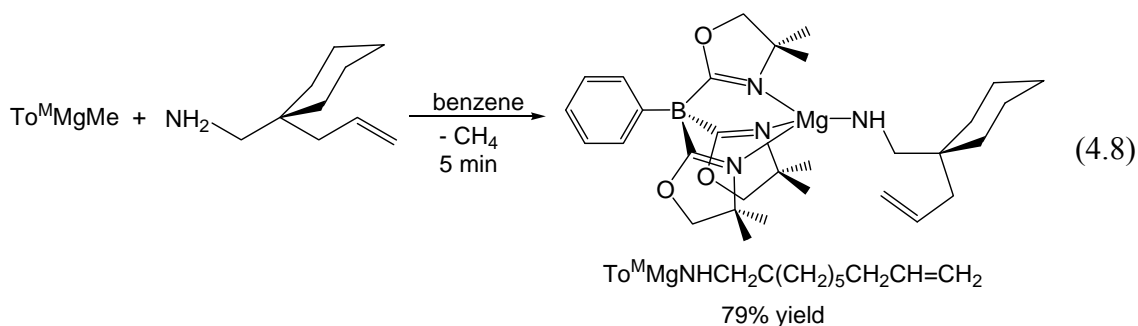
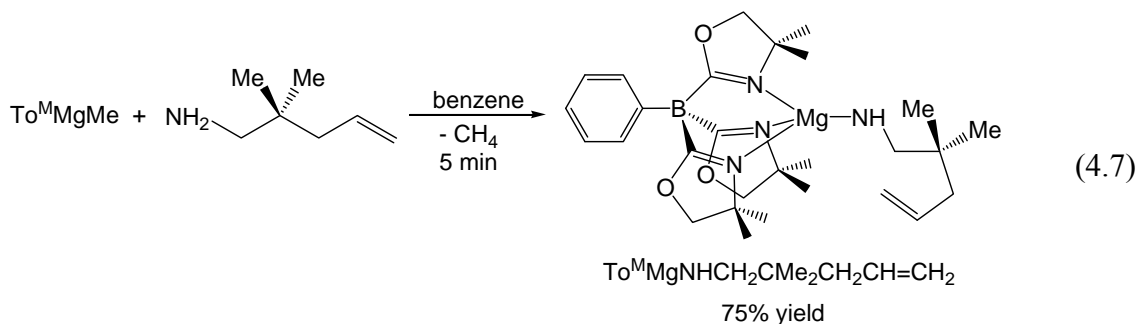
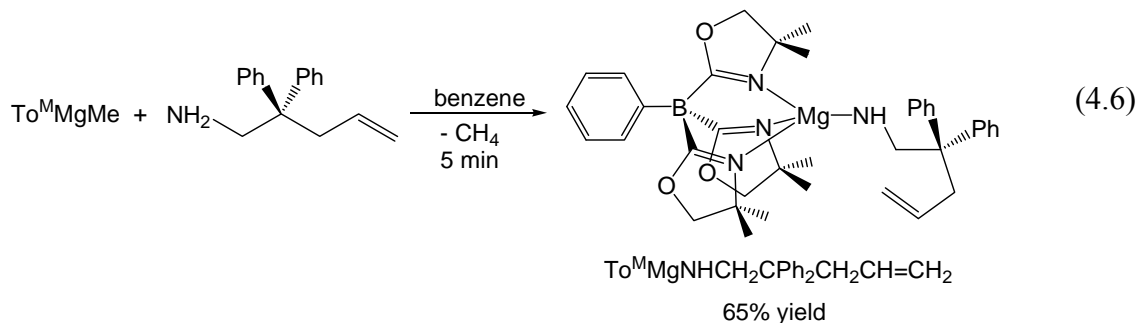
In order to explore the possibility of the first mechanism, we investigated the identities of the species present during catalysis. If protonolysis of the magnesium alkyl resulting from insertion and cyclization is turnover limiting, the magnesium alkyl species

should be the catalyst resting state and thus detectable via NMR spectroscopy. Inspection of the ^1H NMR spectra of catalytic reaction mixtures containing a 10:1 ratio of 1-amino-2,2-diphenyl-4-pentene substrate to $\text{To}^{\text{M}}\text{MgMe}$ reveals two new $\text{To}^{\text{M}}\text{Mg}$ species. The first compound is observed immediately upon dissolution of $\text{To}^{\text{M}}\text{MgMe}$ in the benzene solution of substrate and is accompanied by the rapid formation of methane gas. In the ^1H NMR spectrum, a new set of resonances corresponding to uncyclized substrate appear along with new To^{M} resonances, and based on this observation the magnesium species was assigned as the magnesium amide resulting from protonation of the methyl ligand, $\text{To}^{\text{M}}\text{MgNHCH}_2\text{-CPh}_2\text{CH}_2\text{CH}=\text{CH}_2$.

This magnesium amidoalkene was independently prepared and isolated from a stoichiometric reaction of $\text{To}^{\text{M}}\text{MgMe}$ with 1-amino-2,2-diphenyl-4-pentene, and the ^1H NMR spectrum of this authentic sample matched exactly with the species formed *in situ* during catalysis (eq 4.6). The related magnesium amidoalkenes, from treatment of $\text{To}^{\text{M}}\text{MgMe}$ with either 1-amino-2,2-dimethyl-4-pentene or (1-allylcyclohexyl)methylamine, were also isolated and fully characterized (eq 4.7 and 4.8). All three of these species display pseudo- C_{3v} symmetry, as indicated by ^1H and $^{13}\text{C}\{^1\text{H}\}$ NMR spectra. Additionally, only one ν_{CN} band is observed in both the solid state and solution IR spectra which support the structures assigned in equations 4.6-4.8. This is the first instance in which these metal amidoalkene intermediates have been isolated from compounds that are catalytically active. Previously, $\text{Cp}'_2\text{LaNHR}(\text{NH}_2\text{R})$ ($\text{R} = \text{CH}_2\text{CMe}_2\text{CH}_2\text{CH}=\text{CH}_2$) had been characterized by NMR at low temperatures, but could not be isolated as cyclization to form the pyrrolidine product occurs at temperatures around $-20\text{ }^\circ\text{C}$.^{3a}

The second magnesium species observed in the catalytic reactions appears in significant quantities when the reaction proceeds through approximately two half-lives.

The appearance of a new doublet resonance at 1.50 ppm and the absence of olefinic resonances in the ^1H NMR spectrum suggested the identity of this species to be the cyclized



product bound to the metal center either through the pyrrolidine nitrogen or methyl group.

The doublet resonance at 1.50 ppm was assigned as the methyl group on the pyrrolidine. The integration of the resonance for three protons indicates that the methyl is not bound to the magnesium center. Additionally, the resonance is shifted too far downfield to be bound to

the metal center. Based on these observations and the lack of a resonance for a proton bound to nitrogen, this second magnesium species was identified as the $\text{To}^{\text{M}}\text{Mg}(\text{NC}_4\text{H}_5\text{-2-Me-4,4-Ph}_2)$ and not the magnesium alkyl that would result from insertion.

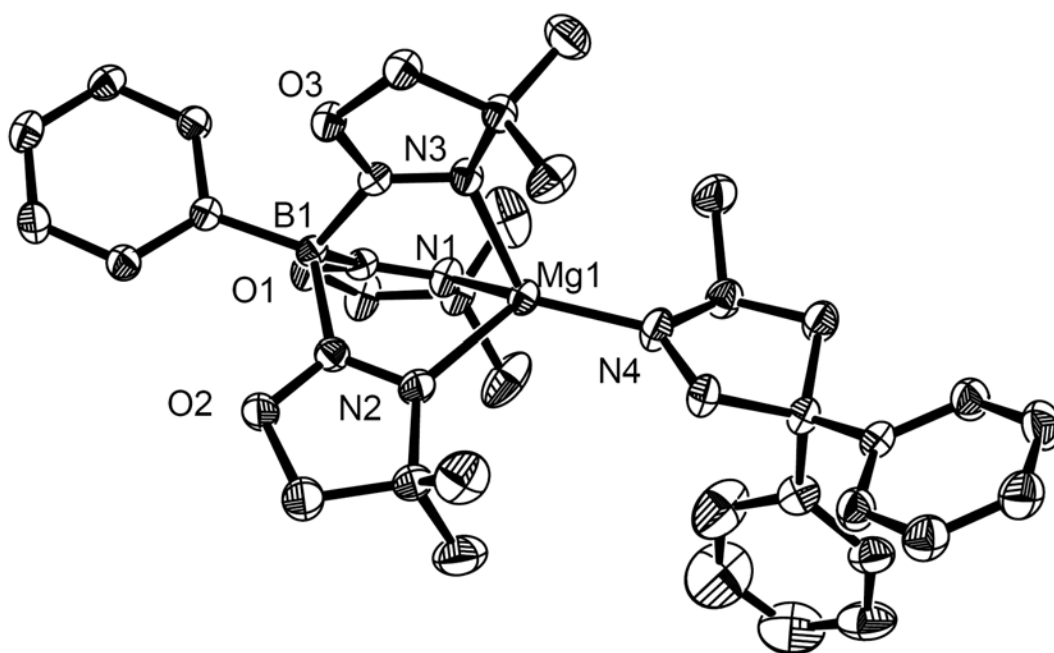
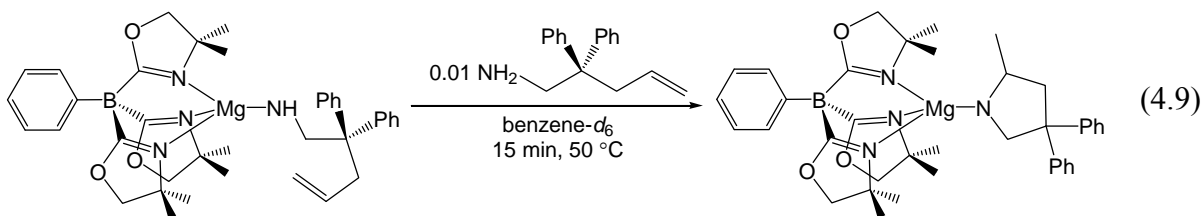


Figure 4.6. ORTEP diagram of $\text{To}^{\text{M}}\text{Mg}(\text{NC}_4\text{H}_5\text{-2-Me-4,4-Ph}_2)$ drawn at 50% probability.

The magnesium pyrrolide is prepared and isolated by reaction of $\text{To}^{\text{M}}\text{MgMe}$ and the diphenyl-pyrrolidine, and the NMR spectra match the species observed during catalysis (eq

4.9). X-ray crystals were obtained from a catalytic reaction mixture that was allowed to sit undisturbed for two weeks (Figure 4.6).

Formation of magnesium dimers and stoichiometric cyclization

As these are the only two magnesium species observed during catalysis, the sum of their concentrations in the catalytic reaction mixture should be equal to the initial concentration of To^{MgMe} . However, when these values are compared the concentrations of the magnesium amidoalkene and pyrrolide only add up to between 40-60% of the initial To^{MgMe} concentration. The remainder of this mass balance was accounted for in the formation of a white precipitate during catalysis. The precipitate was identified as a sparingly soluble dimer of the magnesium amidoalkene intermediate by crystals obtained from concentrated solutions of the isolated monomeric $\text{To}^{\text{Mg}}\text{NHCH}_2\text{C}(\text{CH}_2)_5\text{CH}_2\text{CH}=\text{CH}_2$ (Figure 4.7).

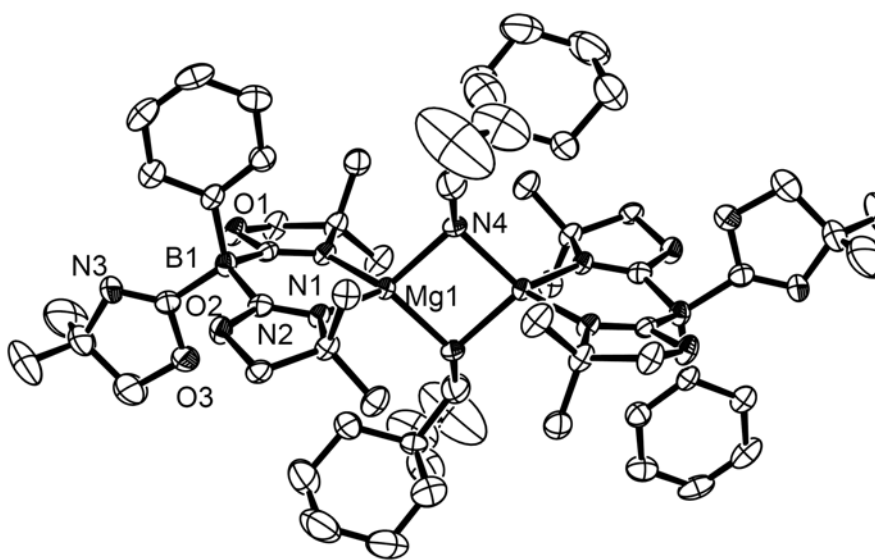
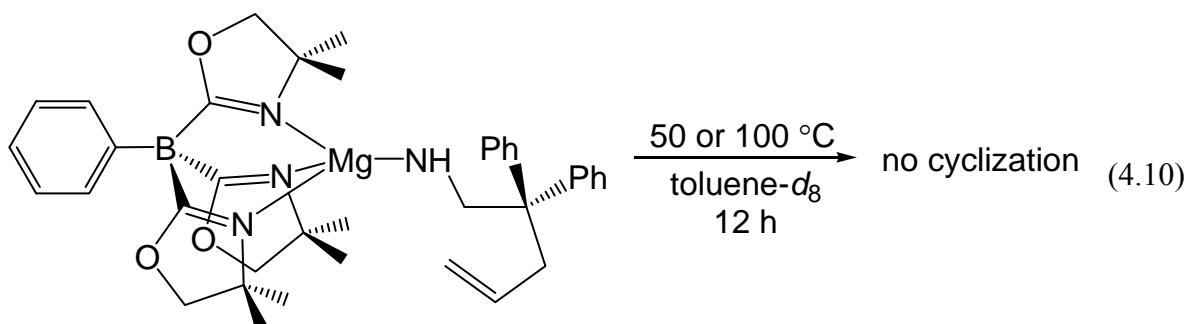


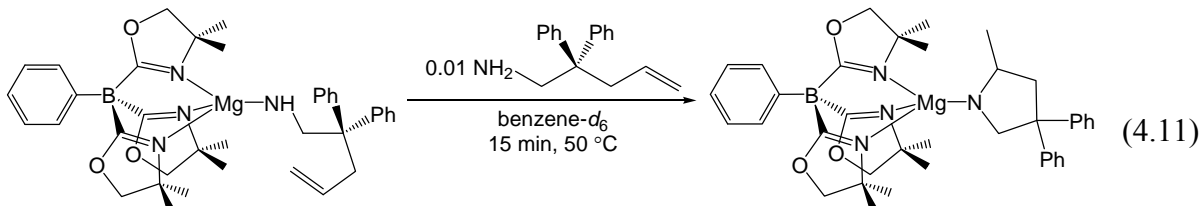
Figure 4.7. ORTEP diagram of $[\text{To}^{\text{Mg}}\text{NHCH}_2\text{C}(\text{CH}_2)_5\text{CH}_2\text{CH}=\text{CH}_2]_2$ drawn at 50% probability.

Similarly concentrated solutions of $\text{To}^{\text{M}}\text{MgNHCH}_2\text{CMe}_2\text{CH}_2\text{CH}=\text{CH}_2$ immediately produced microcrystals at room temperature which proved to be too small for single crystal diffraction, while $\text{To}^{\text{M}}\text{MgNHCH}_2\text{CPh}_2\text{CH}_2\text{CH}=\text{CH}_2$ resulted in the dimer compound powdering out of solution. Solid state IR spectra of these dimers show two distinct ν_{CN} bands for the oxazoline rings corresponding with the bidentate coordination of the To^{M} , and in contrast to the single ν_{CN} band observed for the monomers. Similar dimers of magnesium amides have been proposed as intermediates in hydroamination, in which the dimeric magnesium amide exists in rapid equilibrium with the reactive monomeric species.^{14a,19} However, in our case such an equilibrium is highly unlikely due to the insoluble nature of the dimeric species. While these dimers do account for the remaining mass balance of magnesium in catalysis, they do not play an active role in the reaction mechanism due to their poor solubility.

As only magnesium amides are observed under catalytic conditions, we attempted to generate the magnesium alkyl species by the stoichiometric cyclization of the isolated $\text{To}^{\text{M}}\text{MgNHCH}_2\text{CPh}_2\text{CH}_2\text{CH}=\text{CH}_2$. The reactivity of this species was tested by warming a benzene- d_6 solution of the isolated compound to 50 °C. Only starting materials are observed after two hours of heating, and so the temperature of the solution was increased to 100 °C for a 12 hour period. Surprisingly, the amidoalkene remains the only species observed under these conditions, and neither free pyrrolidine nor magnesium pyrrolide is formed (eq 4.10). The result of this stoichiometric reaction contrasts the catalytic cyclizations in which C–N bond formation readily occurs at 50 °C. Additionally, the lack of cyclization indicates that the intermediate $\text{To}^{\text{M}}\text{MgNHCH}_2\text{CPh}_2\text{CH}_2\text{CH}=\text{CH}_2$ is not kinetically competent to perform olefin insertion on its own.



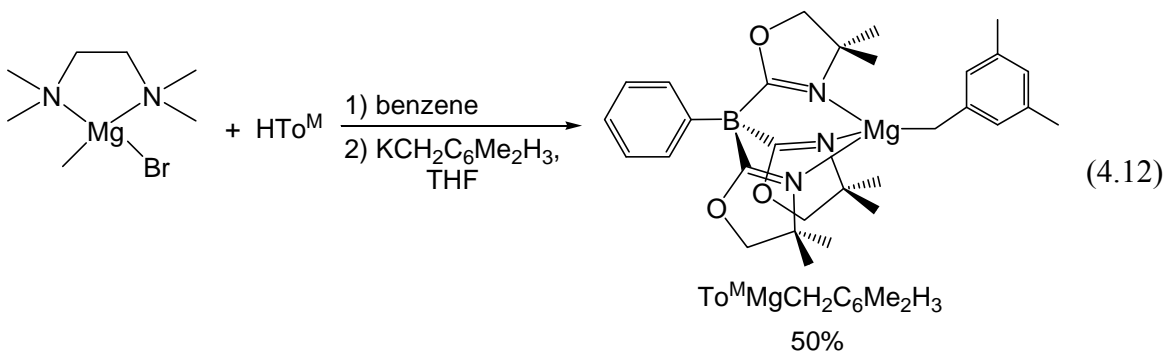
However, in the presence of a small excess (≥ 0.01 equiv) of substrate, the isolated magnesium amidoalkene is transformed to the magnesium pyrrolide after 15 minutes at 50 °C (eq 4.11). In fact, cyclization may be achieved by the addition of any primary amine to a solution of $\text{To}^{\text{M}}\text{MgNHCH}_2\text{CPh}_2\text{CH}_2\text{CH}=\text{CH}_2$. These stoichiometric reactions strongly suggest that C–N bond formation occurs from an amine adduct of the magnesium



amidoalkene (*i.e.*, $\text{To}^{\text{M}}\text{MgNHR}(\text{NH}_2\text{R})$) during catalysis. The existence of a magnesium amido•amine species would support the second possible mechanism in which there is a rapid reversible association of amine and magnesium amide prior to cyclization. In order to test our hypothesis and the importance of this pathway, the effect of aminoalkene concentration on the overall reaction was considered. If the reaction does follow this pathway, the rate could show saturation at high concentrations of aminoalkene.²⁰

Synthesis of $To^M MgCH_2C_6Me_2H_3$ and initial rates kinetic measurements

A new precatalyst $To^M MgCH_2C_6Me_2H_3$ to assay the $[Mg]$ for kinetic measurements. Protonation of this precatalyst by aminoalkene generates mesitylene which can be used as an internal standard to determine the number of active catalyst sites. In contrast, the methane gas generated from the reaction of $To^M MgMe$ with aminoalkene cannot be easily quantified in the 1H NMR spectrum, and so the assumption must be made that all magnesium sites are active in catalysis. Protonolysis of the methyl group of $(TMEDA)Mg(Br)CH_3$ (TMEDA = tetramethylethylenediamine) with HTo^M in benzene produces $To^M MgBr$ *in situ*. $To^M MgBr$ is then further reacted in THF with $KCH_2C_6Me_2H_3$ to give the desired precatalyst $To^M MgCH_2C_6Me_2H_3$ as an off-white solid (eq 4.12).



The active catalyst $To^M MgNHCH_2CPh_2CH_2CH=CH_2$ is preformed by reaction of $To^M MgCH_2C_6Me_2H_3$ and one equivalent of the diphenyl substrate prior to catalytic cyclization, and the concentration of the active catalyst equals the measured concentration of the mesitylene generated during protonolysis. This initial protonolysis of $To^M MgCH_2C_6Me_2H_3$ was extremely slow at room temperature, and the solution had to be warmed to $60\text{ }^\circ\text{C}$ for 10 minutes before all of the magnesium starting material was converted to the active catalytic species. This is in contrast to the rapid protonolysis of $To^M MgMe$, which is fully achieved in less than 10 minutes at room temperature.

The initial rates for the hydroamination of 1-amino-2,2-diphenyl-4-pentene were measured for several substrate concentrations at constant catalyst concentration (4.93 mM) at 60 °C.

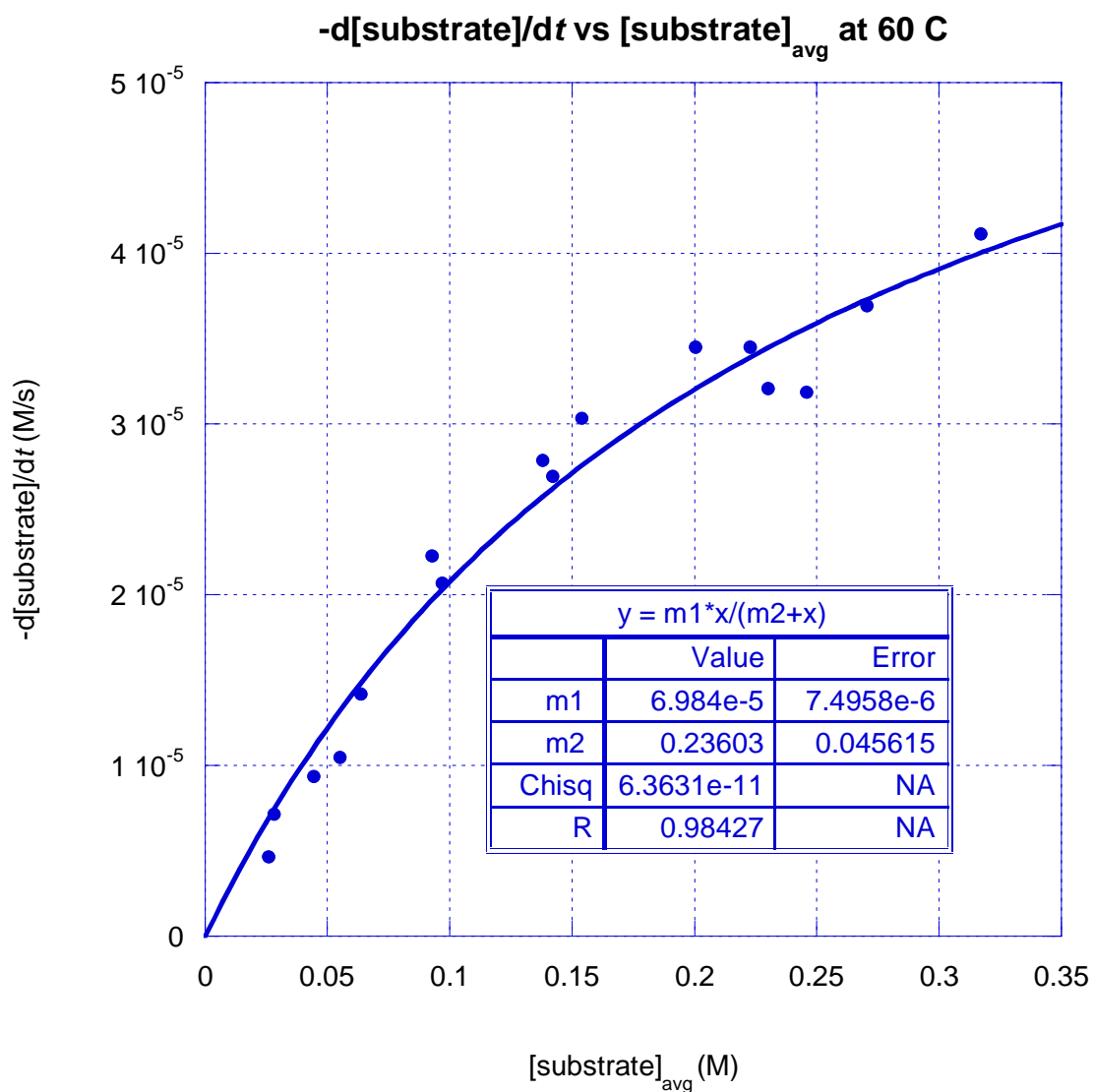
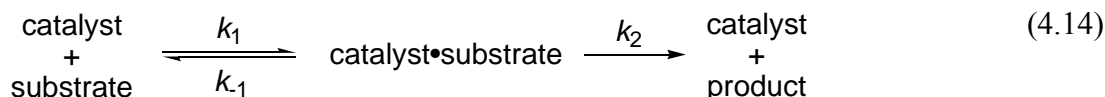


Figure 4.8. Plot of $\{-d[\text{substrate}]/dt\}_{\text{ini}}$ versus $[\text{substrate}]_{\text{ini}}$. The curve represents a non-linear least squares best fit to the data.

Linear regression fits for [substrate] versus time for the first 600 s of the reaction provided the initial rate $(-d[\text{substrate}]/dt)_{\text{ini}}$ for a particular initial substrate concentration (calculated as average substrate concentration over 600 s). A non-linear least squares regression analysis of $-d[\text{substrate}]/dt$ vs. $[\text{substrate}]_{\text{ini}}$ (Figure 4.8) showed good correlation to equation 4.13:²⁰

$$\frac{-d[\text{substrate}]}{dt} = \frac{k_2[\text{catalyst}][\text{substrate}]_{\text{ini}}}{K' + [\text{substrate}]_{\text{ini}}} \quad (4.13)$$

This corresponds to the general mechanism (eq 4.14) where $k_2 = (1.4 \pm 0.2) \times 10^{-2} \text{ s}^{-1}$ (cyclization) and $K' = (k_{-1} + k_2)/k_1 = 0.24 \pm 0.05 \text{ M}$ (Michaelis constant):

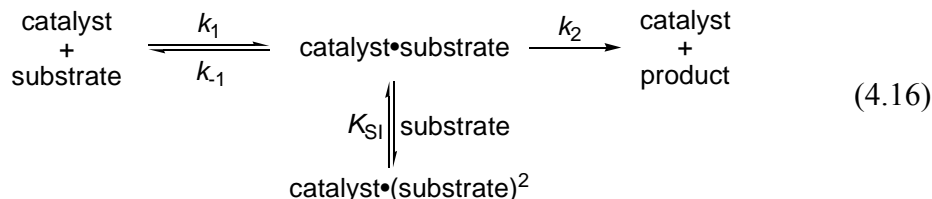


In contrast to this, turnover limiting metal-alkyl protonolysis would be expected to show linear dependence on substrate concentration over all concentrations.

At 50 °C, a competing equilibrium involving coordination of an additional substrate molecule to the catalyst becomes kinetically and mechanistically important, resulting in significant catalyst inhibition at high substrate concentrations (Figure 4.9), giving a qualitatively meaningful fit of equation 4.15:²¹

$$\frac{-d[\text{substrate}]}{dt} = \frac{k_2[\text{catalyst}][\text{substrate}]}{K' + [\text{substrate}] + \frac{[\text{substrate}]^2}{K_{SI}}} = \frac{k_2[\text{catalyst}][\text{sub-cat}]}{K' + [\text{sub-cat}] + \frac{[\text{sub-cat}]^2}{K_{SI}}} \quad (4.15)$$

which corresponds to the general mechanism in equation 4.16:



Because compound $\text{To}^{\text{M}}\text{MgCH}_2\text{C}_6\text{Me}_2\text{H}_3$ is not pre-activated in these experiments, the x-intercept is not zero in Figure 4.9 (*i.e.*, one equiv. of substrate is needed for catalyst initiation). This is treated by subtracting the precatalyst concentration from the substrate concentration in the rate expression.

As a result, a data treatment involving a three parameter fit is appropriate. Due to the dominating natures of the second equilibrium (K_{SI} , inhibition) and the k_2 value, our attempted fits do not converge (*i.e.* there are too many parameters). Therefore, we estimated the rate constant k_2 at low substrate concentration (Figure 4.10), giving a two parameter fit that converges. However, the resulting fit does not provide particularly meaningful numerical values for the dependent parameters.

Despite these problems, we have included these plots (Figures 4.9 and 4.10) because the data and (non-quantitative) conclusions importantly illustrate the need for two equivalents of substrate for cyclization to occur, the current temperature limitations of this system (for a multi-parameter kinetic analysis), and the additional substrate inhibition process that can be controlled by temperature due to its equilibrium nature.

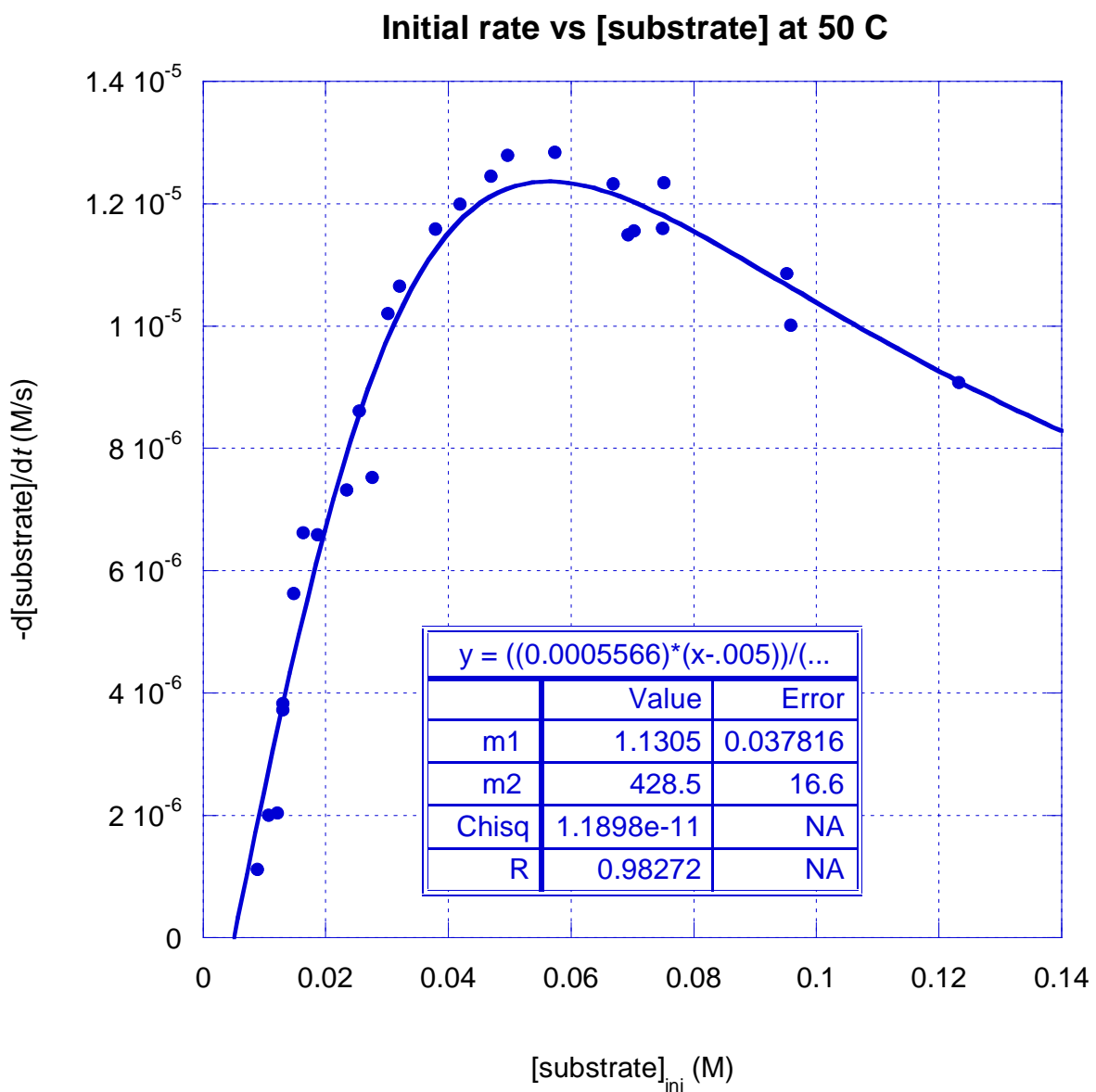


Figure 4.9. Plot of $-d[\text{substrate}]/dt$ versus $[\text{substrate}]$ at 50 °C. The curve represents a non-linear least squares best fit to the data.

Measurement of the rates of oxazoline exchange

These kinetic measurements strongly support the results of the stoichiometric reactions which argue for the formation of an amine adduct of $\text{To}^{\text{M}}\text{MgNHCH}_2\text{CR}_2\text{CH}_2\text{CH}$

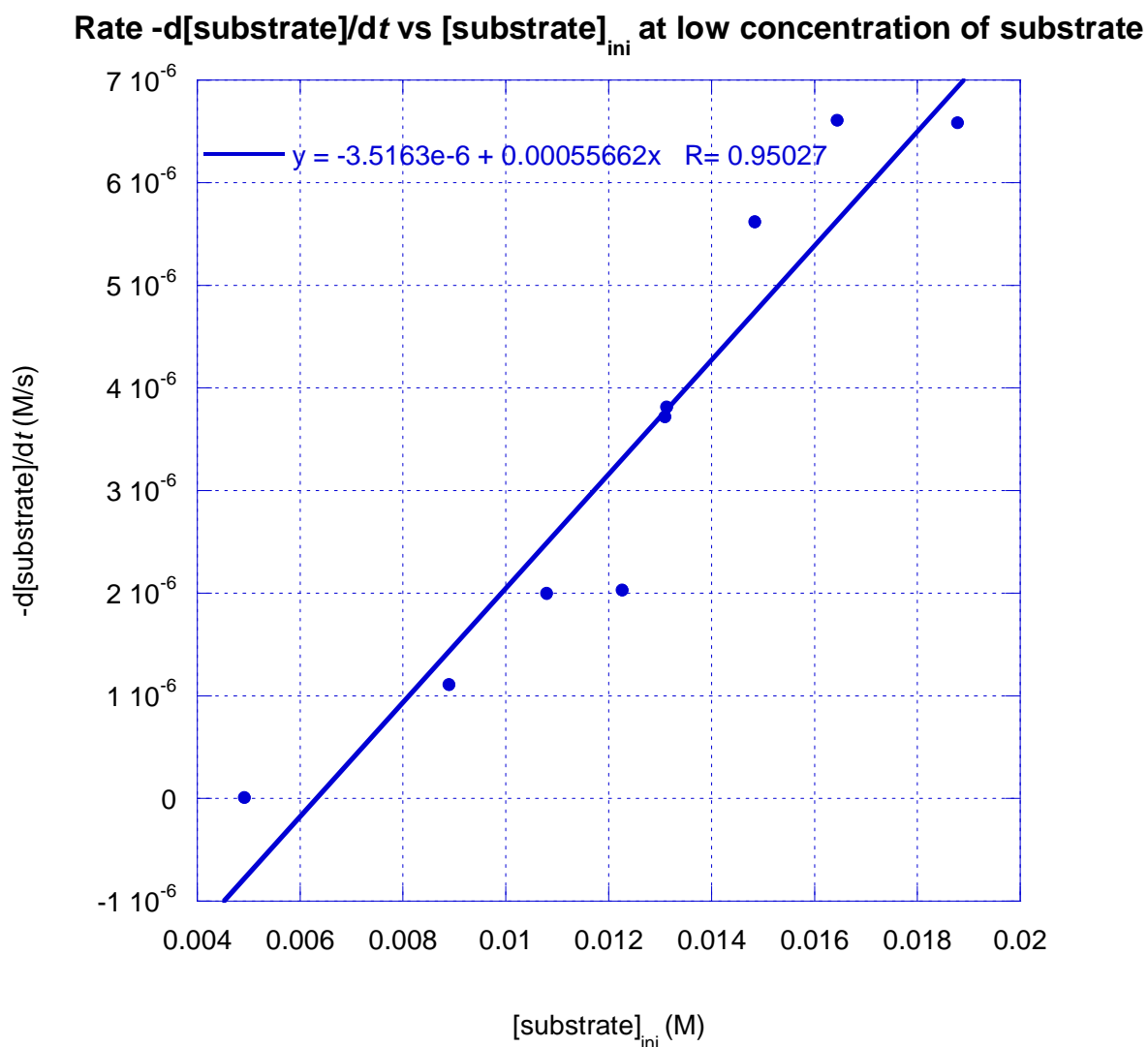


Figure 4.10. Plot of $-d[\text{substrate}]/dt$ for low concentrations of $[\text{substrate}]$ used to determine the rate constant k_2 at 50 °C for fit shown in Figure 9. Low initial concentrations were used to offset the effects of substrate saturation and substrate inhibition to measure k_2 . 1-amino-2,2-diphenyl-pent-4-ene was used as the substrate in these experiments.

$=\text{CH}_2$ during catalysis which allows C–N bond formation to occur. Indeed, an EXSY experiment conducted at 25 °C on a solution of the isolated magnesium amide and one

equivalent of substrate shows exchange between the coordinated amide ligand and free amine. As the magnesium amide catalyst is coordinatively saturated, the addition of an amine adduct might involve the dissociation of one oxazoline ring from the magnesium center. In order to assess this possibility, To^M_2Mg was used to determine the lability of the oxazoline rings on the magnesium center.

From the X-ray structure of To^M_2Mg , solid angles of each To^M ligand were calculated to be 5.70 and 5.77 steradians, encapsulating 45 and 46%, respectively, of the space around the metal center.¹⁵ As the magnesium center is well-protected on all sides by the dimethyl groups of the oxazoline rings (Figure 4.11), any exchange of the free and bound oxazoline rings is likely to proceed through a dissociative rather than associative process. An EXSY experiment conducted at 50 °C showed selective exchange between the methyl groups (C3, C9, and C13; C4, C8, and C14). The rates of oxazoline exchange (35-72 °C, benzene- d_6) were then measured using a selective population inversion experiment (SPI).²²

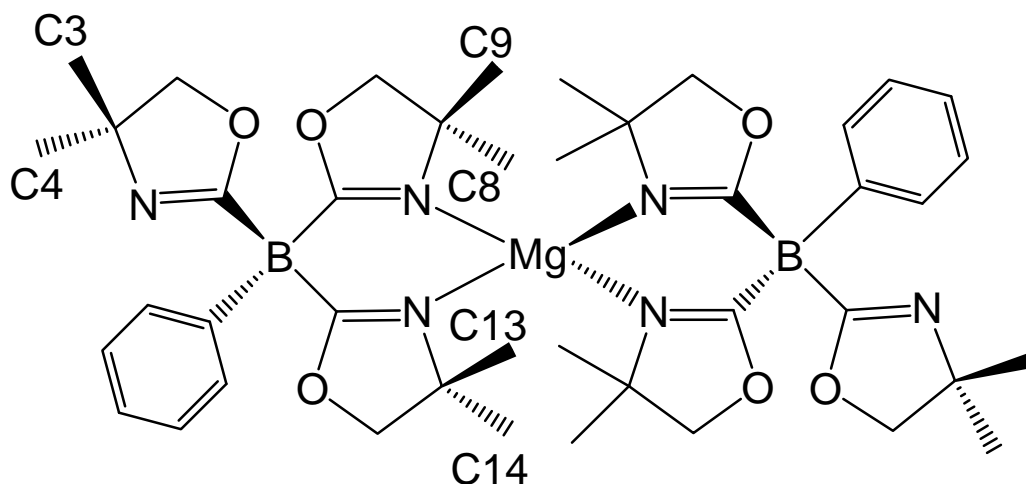


Figure 4.11. To^M_2Mg with exchanging methyl groups labeled.

At elevated temperatures, five separate resonances were observed for the methyl peaks on the oxazoline rings: four peaks for the methyl groups located on coordinated oxazoline rings, and one for the methyl groups on the uncoordinated oxazolines. The T_1 values for these peaks were initially measured using a standard inversion recovery experiment. One of the coordinated methyl resonances (*i.e.*, C9) is then selectively inverted, and the magnetization of this peak is measured via integration for a series of 15 experiments with increasing relaxation times. As the oxazoline rings exchange, the transfer of magnetization to the two corresponding methyl signals (C3 and C13) is observed and likewise measured (see Experimental section for a more detailed description). From the analysis of this data, the rate of dissociative exchange (k_{diss}) at 60 °C is calculated to be 0.20 s^{-1} , which is $\sim 14\times$ faster than k_2 (0.014 s^{-1}) calculated for cyclization. While $\text{To}^{\text{M}}\text{MgNHCH}_2\text{CR}_2\text{CH}_2\text{CH}=\text{CH}_2$ and $\text{To}^{\text{M}}_2\text{Mg}$ contain different steric environments, the longer Mg–N bond lengths and strain associated with κ^3 -coordination in the magnesium amide catalyst will likely result in an oxazoline dissociation rate constant equal to or greater than k_{diss} calculated for $\text{To}^{\text{M}}_2\text{Mg}$. Thus, the frequency of oxazoline dissociation is greater than the TOF for aminoalkene cyclization, and so while an amine ligand is necessary for cyclization to occur it is not required for oxazoline dissociation.

Mechanism for $\text{To}^{\text{M}}\text{Mg}$ mediated hydroamination/cyclization

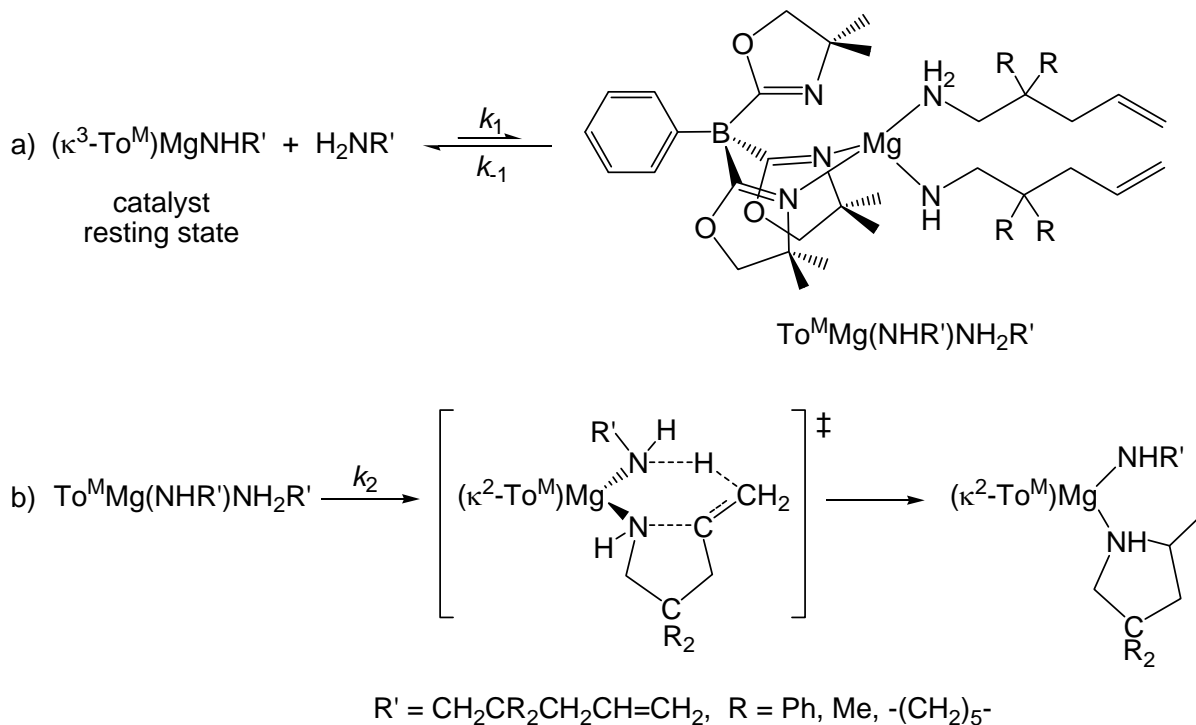
Amine interaction with the magnesium center further limits the availability of open coordination sites necessary for olefin insertion into the Mg–N bond. This limitation, taken together with the inability of the isolated magnesium amides to undergo cyclization in the absence of a second amine substrate molecule, rules out the possibility of C–N bond

formation occurring by the classical migratory insertion mechanism. The observation of the magnesium amidoalkene in catalytic reaction mixtures combined with the isolation of the compound from stoichiometric reactions demonstrates that $\text{To}^{\text{M}}\text{MgNHCH}_2\text{CR}_2\text{CH}_2\text{CH}=\text{CH}_2$ is the resting state of the catalyst.

EXSY experiments show that $\text{To}^{\text{M}}\text{MgCH}_2\text{CR}_2\text{CH}_2\text{CH}=\text{CH}_2$ and free aminoalkene substrate undergo exchange suggesting that the aminoalkene substrate interacts with the magnesium center. Because amine is needed for cyclization, we suggest that the first step of the catalytic cycle involves reversible coordination of $\text{To}^{\text{M}}\text{MgNHR}$ and H_2NR to give a magnesium amido•amine adduct. This rapid equilibrium heavily favors the magnesium amide catalyst and dissociated amine, and so the catalyst•substrate adduct is not detected on the NMR time scale. The presence of the equilibrium is confirmed by the Michaelis-Menten type kinetics displayed by the system. The reaction rate is first order dependent on [substrate] at low concentrations and gradually increases with increasing [substrate] until reaching a saturation level. The equilibrium process is extremely sensitive to temperature as at 50 °C saturation is quickly achieved at [substrate] = 0.06 M and followed by substrate inhibition. When the reaction is conducted at 60 °C, saturation is observed to begin at [substrate] = 0.25 M but is not completely reached even at [substrate] = 0.33 M. The metal center in the catalyst•substrate adduct may be either four or five coordinate depending on the binding mode of the To^{M} ligand (κ^2 versus κ^3), however a four coordinate magnesium is favored due to the ionic radius of magnesium (0.57 Å).

According to the general mechanism associated with the Michaelis-Menten equation, we propose that the rapid pre-equilibrium is followed by turnover limiting cyclization proceeding through a six-center transition state as seen in Scheme 4.2. In this transition state,

C–N bond formation to give the pyrrolidine product occurs concurrently with the transfer of a proton from the amine adduct to the resulting methyl group of the pyrrolidine. The cleavage of the N–H bond in the amine adduct accounts for the observed KIE, as well as why an additional amine molecule is necessary for cyclization to occur.



Scheme 4.2. Proposed mechanism for To^MMg -mediated intramolecular hydroamination

Related transition state structures have previously been proposed for the enolization of ketones by magnesium amides.²³ Additionally, zirconium(IV) catalysts for hydroamination/cyclization have been reported in which C–N bond formation involves proton transfer from an amido ligand to the olefinic carbon in a similar six-centered transition state.²⁴ The resting state of the catalyst is then regenerated by loss of the pyrrolidine, and the coordination of the pendent oxazoline to give $\kappa^3\text{-To}^M\text{MgNHR}$.

Conclusions

$\text{To}^{\text{M}}\text{MgMe}$ is a coordinatively saturated and robust magnesium complex. Spectroscopic studies of $\text{To}^{\text{M}}\text{MgMe}$ and $\text{To}^{\text{M}}\text{MgNHR}$ with possible ligands such as THF or dioxane show that the favored ground state is a four-coordinate magnesium center with the To^{M} ligand binding in a tridentate manner. Exchange of the oxazoline rings in $\text{To}^{\text{M}}_2\text{Mg}$ shows that a three-coordinate $\kappa^2\text{-To}^{\text{M}}\text{MgNHR}$ is likely accessible at room temperature, but again the four-coordinate structure $\kappa^3\text{-To}^{\text{M}}\text{MgNHR}$ is the favored ground state. Despite this exchange, no rearrangement of the compound by the Schlenk equilibrium to give two homoleptic species is observed in solution, even at temperatures up to 110 °C. $\text{To}^{\text{M}}\text{MgMe}$ is found to be an active pre-catalyst for hydroamination/cyclization of 2,2-disubstituted aminoalkenes at elevated temperatures. The coordinative saturation provided by the To^{M} ligand stabilizes the amine-free magnesium amido complex, and this affords a unique environment for mechanistic investigation in comparison to other coordinatively unsaturated hydroamination/cyclization catalysts.

The reactivity of the isolated magnesium amidoalkene and our kinetic studies provide unambiguous evidence that two substrate molecules are interacting with the magnesium center in the turnover limiting step of the catalytic cycle. For comparison, the resting states of many d^0 transition and lanthanide metal hydroamination catalysts are amido-amine complexes of the type $\{\text{L}_n\text{M}\}\text{NHR}(\text{NH}_2\text{R})_n$.^{3,11,14} The rate laws for these systems typically display a zero-order dependence on substrate, as well as operating at low catalyst loading (< 5 mol %). Under saturation conditions, the rate law for $\text{To}^{\text{M}}\text{MgMe}$ expressed in equation 4.13 reduces to the commonly observed rate law, providing a possible connection between the hydroaminations mediated by $\text{To}^{\text{M}}\text{MgMe}$ and other d^0 -metal based catalysts. However,

the importance of the proposed mechanism in Scheme 4.2 in relation to either the classical insertion or other mechanisms requires further investigation, particularly for catalysts with less demanding steric environments. Indeed, recent computational studies on Cp_2Sm systems for intramolecular hydroamination/cyclization suggest that differing spatial demands around the metal center dramatically affect the feasibility of both insertive and non-insertive mechanisms.²⁵ While these studies do not address the impact reaction conditions may have on observed rate laws (*i.e.*, rate saturation at high substrate concentrations), it does highlight the role that the steric environment surrounding the metal center has on the reaction pathway. As the steric demands of tris(oxazolinyl)borates can be tuned by altering the substituents on the oxazoline rings, these ligands may prove useful in controlling the pathways of catalytic reactions.

Experimental

General. All reactions were performed under a dry argon atmosphere using standard Schlenk techniques or under a nitrogen atmosphere in a glovebox, unless otherwise indicated. Water and oxygen were removed from benzene, toluene, pentane, diethyl ether, and tetrahydrofuran solvents using an IT PureSolv system. Benzene- d_6 and tetrahydrofuran- d_8 were heated to reflux over Na/K alloy and vacuum-transferred. HTo^{M} ,²⁶ TITo^{M} ,²⁷ $\text{Me}_2\text{Mg}(\text{O}_2\text{C}_4\text{H}_8)_2$,²⁸ 2,2-diphenyl-4-penten-1-amine,²⁹ 2,2-dimethyl-4-penten-1-amine, N-methyl-2,2-diphenyl-4-penten-1-amine⁴, and (1-allylcyclohexyl)methylamine³⁰ were prepared as previously reported. ^1H , $^{13}\text{C}\{^1\text{H}\}$, and ^{11}B NMR spectra were collected on a Bruker DRX400 spectrometer and referenced to tetramethylsilane. ^{11}B NMR spectra were referenced to an

external sample of $\text{BF}_3 \cdot \text{Et}_2\text{O}$. ^{15}N chemical shifts were determined by ^1H - ^{15}N HMBC experiments on a Bruker Avance II 700 spectrometer with a Bruker Z-gradient inverse TXI $^1\text{H}/^{13}\text{C}/^{15}\text{N}$ 5mm cryoprobe; ^{15}N chemical shifts were originally referenced to an external liquid NH_3 standard and recalculated to the CH_3NO_2 chemical shift scale by adding -381.9 ppm. Elemental analyses were performed using a Perkin-Elmer 2400 Series II CHN/S by the Iowa State Chemical Instrumentation Facility. X-ray diffraction data was collected on a Bruker APEX II as described below.

To^MMgMe. In the glovebox, $\text{H}[\text{To}^{\text{M}}]$ (2.32 g, 6.06 mmol) was dissolved in 100 mL of dry benzene. Solid $\text{MgMe}_2(\text{O}_2\text{C}_4\text{H}_8)_2$ (1.40 g, 6.06 mmol) was added to the solution, and immediately gas evolution was observed. The reaction mixture was stirred for 30 min. Evaporation of the solvent gave a white solid product of sufficient purity for further reactions (2.43 g, 5.77 mmol, 95.2%). Analytically pure product was obtained by recrystallization from diethyl ether at $-35\text{ }^\circ\text{C}$ (0.99 g, 2.4 mmol, 38%). ^1H NMR (benzene- d_6 , 400 MHz): δ 8.32 (d, $^3J_{\text{HH}} = 7.4$ Hz, 2 H, *ortho*- C_6H_5), 7.55 (t, $^3J_{\text{HH}} = 7.4$ Hz, 2 H, *meta*- C_6H_5), 7.37 (t, $^3J_{\text{HH}} = 7.4$ Hz, 1 H, *para*- C_6H_5), 3.40 (s, 6 H, $\text{CNCMe}_2\text{CH}_2\text{O}$), 1.01 (s, 18 H, $\text{CNCMe}_2\text{CH}_2\text{O}$), -0.65 (s, 3 H, MgCH_3). $^{13}\text{C}\{^1\text{H}\}$ NMR (benzene- d_6 , 100 MHz): δ 191.71 (br, $\text{CNCMe}_2\text{CH}_2\text{O}$), 142.19 (*ipso*- C_6H_5), 136.48 (*ortho*- C_6H_5), 127.22 (*meta*- C_6H_5), 126.25 (*para*- C_6H_5), 80.38 ($\text{CNCMe}_2\text{CH}_2\text{O}$), 65.60 ($\text{CNCMe}_2\text{CH}_2\text{O}$), 28.49 ($\text{CNCMe}_2\text{CH}_2\text{O}$), -18.29 (Mg-CH_3). ^{11}B NMR (benzene- d_6 , 128 MHz): δ -17.2 (br s). $^{15}\text{N}\{^1\text{H}\}$ NMR (benzene- d_6 , 71 MHz): δ -157.1. IR (KBr, cm^{-1}): 3075 m, 3046 m, 2965 s, 2929 s, 2894 s, 1592 s (ν_{CN}), 1461 s, 1386 m, 1366 s, 1351 m, 1269 s, 1251 m, 1192 s, 1158 s, 960 s, 709 s, 674 m. IR (C_6H_6 , cm^{-1}): 3090 m, 3071 m, 3036 s, 2964 m, 1592 s (ν_{CN}), 1479 s, 1317 m, 1260, 1191 m, 1035

s, 969 m, 673 s. Anal. Calc. for $C_{22}H_{32}BN_3O_3Mg$: C, 62.67; H, 7.65; N, 9.97. Found: C, 62.97; H, 7.60; N, 9.84. Mp 216-221 °C, dec.

(κ^2 -To^M)₂Mg. A vial was charged with H[To^M] (0.500 g, 1.19 mmol), toluene (15 mL), and a magnetic stir bar. $MgMe_2(O_2C_4H_8)_2$ (0.150 g, 0.653 mmol) was added to the solution and immediately vigorous bubbling was observed due to the formation of methane gas. Not all of the $MgMe_2(O_2C_4H_8)_2$ dissolved immediately, so the reaction was allowed to stir for 30 minutes to ensure complete formation of (To^M)₂Mg. The reaction mixture was then filtered, and the solution was concentrated and placed in a -30 °C freezer to give colorless crystals of (To^M)₂Mg (0.432 g, 0.549 mmol, 41.8%) after 2 days. ¹H NMR (benzene-*d*₆, 400 MHz): δ 8.11 (d, ³J_{HH} = 6.9 Hz, 4 H, *ortho*-C₆H₅), 7.45 (t, ³J_{HH} = 6.9 Hz, 4 H, *meta*-C₆H₅), 7.26 (t, ³J_{HH} = 6.9 Hz, 2 H, *para*-C₆H₅), 3.69 (s, 4 H, CNCMe₂CH₂O), 3.48 (d, ³J_{HH} = 8.5 Hz, 2 H, CN(Mg)CMe₂CH₂O), 3.29-3.36 (mult, 6 H, CN(Mg)CMe₂CH₂O), 1.31 (s, 18 H, CNCMe₂CH₂O), 1.23 (s, 6 H, CNCMe₂CH₂O), 1.11 (s, 6 H, CNCMe₂CH₂O), 0.94 (s, 6 H, CNCMe₂CH₂O). ¹³C{¹H} NMR (benzene-*d*₆, 100 MHz): δ 147.13 (*ipso*-C₆H₅), 134.09 (*ortho*-C₆H₅), 127.35 (*meta*-C₆H₅), 125.71 (*para*-C₆H₅), 78.60 (CN(Mg)CMe₂CH₂O), 78.06 (CN(Mg)CMe₂CH₂O), 76.89 (CNCMe₂CH₂O), 67.95 (CNCMe₂CH₂O), 66.45 (CN(Mg)CMe₂CH₂O), 65.75 (CN(Mg)CMe₂CH₂O), 29.15 (CNCMe₂CH₂O), 28.55 (CN(Mg)CMe₂CH₂O), 28.51 (CN(Mg)CMe₂CH₂O), 27.90 (CN(Mg)CMe₂CH₂O), 25.98 (CN(Mg)CMe₂CH₂O). ¹¹B NMR (benzene-*d*₆, 128 MHz): δ -16.8 (br, s). ¹⁵N{¹H} NMR (benzene-*d*₆, 71 MHz): δ -121.5 (CNCMe₂CH₂O), -171.8 (CN(Mg)CMe₂CH₂O). IR (KBr, cm⁻¹): 3069 m, 3044 m, 2965 s, 2929 s, 2880 s, 1602 m (ν_{CN}), 1555 s (ν_{CN}), 1490 w, 1464 m, 1432 w, 1370 m, 1360 w, 1276 m, 1250 w, 1196 m, 1150 m, 1026 w, 1002 s, 968 s, 892 w, 839 w, 742 w, 709 m; (C₆H₆, cm⁻¹) 3079 s, 3061 s, 3046 s, 3017 s, 2905 w, 2887 m, 1617 m

(ν_{CN}), 1587 s (ν_{CN}), 1488 s, 1392 s, 1310 m, 1249 m, 1176 s, 1042 m, 971 m, 850 m, 774 m, 707s. Anal. Calc. for $\text{C}_{42}\text{H}_{58}\text{B}_2\text{N}_6\text{O}_6\text{Mg}$: C, 63.95; H, 7.41; N, 10.65. Found: C, 63.74; H, 7.95; N, 10.88. Mp 138-142 °C.

To^MMgCH₂C₆H₃Me₂. A 100 mL Schlenk flask was charged with H[To^M] (2.00 g, 5.22 mmol) and (TMEDA)MgBrCH₃ (1.23 g, 5.22 mmol). The solids were dissolved in 50 mL of benzene and stirred for 1.5 h to ensure complete reaction. During the initial portion of the reaction, the solution was observed to vigorously bubble due to the rapid release of methane gas. The volatile materials were removed under vacuum to give an off-white crude solid of To^MMgBr. This material was washed once with pentane (35 mL) and then redissolved in THF. A solution of KCH₂C₆H₃Me₂ (0.750 g, 4.75 mmol) in THF (15 mL) was added in a dropwise fashion to a stirred solution of To^MMgBr, producing an opaque yellow solution. The reaction mixture was filtered, and the solvent removed in vacuo to give the glassy, yellow-orange product. The solid was extracted with benzene (3 × 20 mL), and the volatiles were removed to give the analytically pure compound as an off-white solid (1.25 g, 2.38 mmol, 50.1%). ¹H NMR (benzene-*d*₆, 400 MHz): δ 8.26 (d, ³J_{HH} = 7.6 Hz, 2 H, *ortho*-C₆H₅), 7.52 (t, ³J_{HH} = 7.6 Hz, 2 H, *meta*-C₆H₅), 7.35 (t, ³J_{HH} = 7.6 Hz, 1 H, *para*-C₆H₅), 6.97 (s, 2 H, *ortho*-CH₂C₆H₃Me₂), 6.49 (s, 1 H, *para*-CH₂C₆H₃Me₂), 3.37 (s, 6 H, CNCMe₂CH₂O), 2.31 (s, 6 H, C₆H₃Me₂), 1.99 (s, 2 H, CH₂C₆H₃Me₂), 0.94 (s, 18 H, CNCMe₂H₂O). ¹³C{¹H} NMR (benzene-*d*₆, 100 MHz): δ 137.43 (*ipso*-CH₂C₆H₃Me₂), 135.73 (*ortho*-C₆H₅), 127.70 (*meta*-C₆H₅), 126.06 (*para*-C₆H₅), 122.64 (*ortho*-CH₂C₆H₃Me₂), 121.04 (*meta*-CH₂C₆H₃Me₂), 119.52 (*para*-CH₂C₆H₃Me₂), 80.00 (CNCMe₂CH₂O), 65.60 (CNCMe₂CH₂O), 27.69 (CNCMe₂CH₂O), 21.85 (CH₂C₆H₃Me₂), 20.01 (CH₂C₆H₃Me₂). ¹¹B NMR (benzene-*d*₆, 128 MHz): δ -17.3 (br). ¹⁵N{¹H} NMR (benzene-*d*₆, 71 MHz): δ -158.3 (CNCMe₂CH₂O). IR

(KBr, cm^{-1}): 3044 m, 2970 s, 1587 s (ν_{CN}), 1462 s, 1434 m, 1367 s, 1272 s, 1158 s, 955 s, 840 m, 817 m, 737 m, 704 s, 660 s, 639 m. Anal. Calc. for $\text{C}_{30}\text{H}_{40}\text{N}_3\text{O}_3\text{BMg}$: C, 68.53; H, 7.67; N, 7.99. Found: C, 68.99; H, 7.44; N, 8.42. mp 170-178 °C, dec.

To^MMgNHCH₂CPh₂CH₂CH=CH₂. 1-Amino-2,2-diphenyl-4-pentene (0.0509 g, 0.215 mmol) was dissolved in toluene. A slight excess of To^MMgCH₃ (0.0913 g, 0.217 mmol) was dissolved in toluene and mixed with the solution of substrate. The solvent was evaporated affording a white solid. This crude material was washed with pentane and dried under vacuum to give the desired To^MMgNHCH₂CPh₂CH₂CH=CH₂ (0.0892 g, 0.139 mmol, 64.6%). ¹H NMR (benzene-*d*₆, 400 MHz): δ 8.27 (d, ³*J*_{HH} = 6.7 Hz, 2 H, *ortho*-C₆H₅), 7.53 (m, 6 H, *ortho*-NHCH₂CPh₂CH₂CH=CH₂ and *meta*-C₆H₅), 7.23 (vt, 5 H, *meta*-NHCH₂CPh₂CH₂CH=CH₂ and *para*-C₆H₅), 7.09 (vt, 2 H, *para*-NHCH₂CPh₂CH₂CH=CH₂), 5.94 (mult, 1 H, NHCH₂CPh₂CH₂CH=CH₂), 5.06 (mult, 2 H, NHCH₂CPh₂CH₂CH=CH₂), 4.20 (d, ³*J*_{HH} = 9.2 Hz, 2 H, NHCH₂CPh₂CH₂CH=CH₂), 3.38 (s, 6 H, CNCMe₂CH₂O), 3.37 (d, ³*J*_{HH} = 6.7 Hz, 2 H, NHCH₂CPh₂CH₂CH=CH₂), 1.00 (s, 18 H, CNCMe₂CH₂O), -0.98 (t, ³*J*_{HH} = 9.2 Hz, 1 H, NH). ¹³C{¹H} NMR (benzene-*d*₆, 100 MHz): δ 191.93 (br, CNCMe₂CH₂O), 149.63 (*ipso*-NHCH₂CPh₂CH₂CH=CH₂), 143.61 (br, *ipso*-C₆H₅), 137.73 (NHCH₂CPh₂CH₂CH=CH₂), 136.47 (*ortho*-C₆H₅), 136.44 (*ortho*-NHCH₂CPh₂CH₂CH=CH₂), 129.91 (*meta*-C₆H₅), 128.94 (*meta*-NHCH₂CPh₂CH₂CH=CH₂), 126.29 (*para*-C₆H₅), 125.86 (*para*-NHCH₂CPh₂CH₂CH=CH₂), 116.63 (NHCH₂CPh₂CH₂CH=CH₂), 80.39 (CNCMe₂CH₂O), 65.57 (CNCMe₂CH₂O), 57.87 (NHCH₂CPh₂CH₂CH=CH₂), 54.84 (NHCH₂CPh₂CH₂CH=CH₂), 42.16 (NHCH₂CPh₂CH₂CH=CH₂), 28.55 (CNCMe₂CH₂O). ¹¹B NMR (benzene-*d*₆, 128 MHz): δ -17.3 (br s). ¹⁵N{¹H} NMR (benzene-*d*₆, 71 MHz): δ -158.5 (CNCMe₂CH₂O), -174.5

(MgNH). IR (KBr, cm^{-1}): 3053 s, 2967 s, 2781 m, 1637 w, 1590 s (ν_{CN}), 1494 s, 1462 s, 1444 m, 1432 m, 1387 w, 1366 s, 1271 s, 1193 s, 1115 s, 1032 m, 963 s, 909 m, 841 w, 815 w, 756 m, 701 s, 682 m. IR (C_6H_6 , cm^{-1}): 3089 s, 3070 s, 3034 s, 1586 s (ν_{CN}), 1528 m, 1476 s, 1031 m, 703 s, 662 m, 633 w. Anal. Calc. for $\text{C}_{38}\text{H}_{47}\text{BN}_4\text{O}_3\text{Mg}$: C, 70.99; H, 7.37; N, 8.71. Found: C, 70.61; H, 7.36; N, 8.67. Mp 198-202 °C.

To^MMgNHCH₂CMe₂CH₂CH=CH₂. To^MMgCH₃ (0.037 g, 0.087 mmol) was dissolved in benzene (5 mL) and a benzene solution of 1-amino-2,2-dimethyl-pent-4-ene (0.0098 g, 0.087 mmol in 1 mL of benzene) was added. The solution was allowed to stir for 45 min, and then the volatiles were removed under reduced pressure to provide a white solid. This material was washed with pentane (3 × 1 mL) and dried under vacuum to give the desired magnesium amidoalkene (0.034 g, 0.066 mmol, 75.3%). ¹H NMR (benzene-*d*₆, 400 MHz): δ 8.27 (d, ³J_{HH} = 7.2 Hz, 2 H, *ortho*-C₆H₅), 7.52 (t, ³J_{HH} = 7.2 Hz, 2 H, *meta*-C₆H₅), 7.34 (t, ³J_{HH} = 7.2 Hz, 1 H, *para*-C₆H₅), 6.17 (mult, 1 H, NHCH₂CMe₂CH₂CH=CH₂), 5.17 (mult, 2 H, NHCH₂CMe₂CH₂CH=CH₂), 3.41 (s, 6 H, CNCMe₂CH₂O), 3.30 (d, ³J_{HH} = 10.4 Hz, 2 H, NHCH₂CMe₂CH₂CH=CH₂), 2.37 (d, ³J_{HH} = 7.2 Hz, 2 H, NHCH₂CMe₂CH₂CH=CH₂), 1.19 (s, 6 H, NHCH₂CMe₂CH₂CH=CH₂), 1.08 (s, 18 H, CNCMe₂CH₂O), -0.62 (br s, 1 H, NHCH₂CMe₂CH₂CH=CH₂). ¹³C{¹H} NMR (benzene-*d*₆, 100 MHz): δ 138.31 (NHCH₂CMe₂CH₂CH=CH₂), 136.45 (*ortho*-C₆H₅), 127.23 (*meta*-C₆H₅), 126.28 (*para*-C₆H₅), 116.18 (NHCH₂CMe₂CH₂CH=CH₂), 80.42 (CNCMe₂CH₂O), 65.65 (CNCMe₂CH₂O), 53.13 (NHCH₂CMe₂CH₂CH=CH₂), 45.41 (NHCH₂CMe₂CH₂CH=CH₂), 37.72 (NHCH₂CMe₂CH₂CH=CH₂), 29.60 (NHCH₂CMe₂CH₂CH=CH₂), 28.56 (CNCMe₂CH₂O). ¹¹B NMR (benzene-*d*₆, 128 MHz): δ -17.2. ¹⁵N{¹H} NMR (benzene-*d*₆, 71 MHz): δ -157.8 (CNCMe₂CH₂O), -174.0 (MgNH). IR (KBr, cm^{-1}): 3046 w, 2963 s, 2930 m, 2884 s, 1595 s

(ν_{CN}), 1465 w, 1365 m, 1350 w, 1268 s, 1197 s, 1153 s, 988 m, 967 s, 892 w, 810 w, 702 s, 658 s, 638 s. IR (C_6H_6 , cm^{-1}): 3448 w, 3091 s, 3071 s, 3036 s, 2905 w, 2887 m, 2818 w, 1589 s (ν_{CN}), 1521 m, 1479 s, 1393 m, 1249 w, 1176 m, 1036 s, 850 m, 774 m. Anal. Calc. for $\text{C}_{28}\text{H}_{43}\text{BN}_4\text{O}_3\text{Mg}$: C, 64.82; H, 8.35; N, 10.801. Found: C, 64.86; H, 8.44; N, 10.80. Mp 195-200 °C, dec.

To^MMgNHCH₂C(CH₂)₅CH₂CH=CH₂. To^MMgCH₃ (0.0845 g, 0.201 mmol) was dissolved in toluene (5 mL). A toluene solution of (1-allylcyclohexyl)methylamine (0.031 g, 0.20 mmol, 1 mL) was added to the To^MMgMe solution resulting in the vigorous release of methane. The solution was stirred for 15 min, and then the volatiles were removed under reduced pressure leaving a white solid. This solid was washed with pentane (3 × 1 mL) and dried under vacuum to give the desired To^MMgNHCH₂C(CH₂)₅CH₂CH=CH₂ product as a white solid (0.0883 g, 0.158 mmol, 78.8%). ¹H NMR (benzene-*d*₆, 400 MHz): δ 8.27 (d, ³J_{HH} = 7.3 Hz, 2 H, *ortho*-C₆H₅), 7.52 (t, ³J_{HH} = 7.3 Hz, 2 H, *meta*-C₆H₅), 7.34 (t, ³J_{HH} = 7.3 Hz, 1 H, *para*-C₆H₅), 6.20 (mult, 1 H, NHCH₂C(CH₂)₅CH₂CH=CH₂), 5.21 (mult, 2 H, NHCH₂C(CH₂)₅CH₂CH=CH₂), 3.40 (s, 6 H, CNCMe₂CH₂O), 3.36 (d, ³J_{HH} = 10.0 Hz, 2 H, NHCH₂C(CH₂)₅CH₂CH=CH₂), 2.49 (d, ³J_{HH} = 7.5 Hz, 2 H, NHCH₂C(CH₂)₅CH₂CH=CH₂), 1.65 (multiplet, 10 H, NHCH₂C(CH₂)₅CH₂CH=CH₂), 1.09 (s, CNCMe₂CH₂O), -0.75 (t, ³J_{HH} = 10.0 Hz, 1 H, NHCH₂C(CH₂)₅CH₂CH=CH₂). ¹³C{¹H} NMR (benzene-*d*₆, 100 MHz): δ 195.0 (br, CNCMe₂CH₂O), 137.99 (NHCH₂C(CH₂)₅CH₂CH=CH₂), 136.67 (*ortho*-C₆H₅), 127.05 (*meta*-C₆H₅), 126.04 (*para*-C₆H₅), 116.13 (NHCH₂C(CH₂)₅CH₂CH=CH₂), 80.91 (CNCMe₂CH₂O), 65.66 (CNCMe₂CH₂O), 57.48 (NHCH₂C(CH₂)₅CH₂CH=CH₂), 40.75 (NHCH₂C(CH₂)₅CH₂CH=CH₂), 34.34 (NHCH₂C(CH₂)₅CH₂CH=CH₂), 33.20 (NHCH₂C(CH₂)₅CH₂CH=CH₂), 28.27 (CNCMe₂CH₂O), 23.10

(NHCH₂C(CH₂)₅CH₂CH=CH₂). ¹¹B NMR (benzene-*d*₆, 128 MHz): δ -17.3. ¹⁵N{¹H} NMR (benzene-*d*₆, 71 MHz): δ -158.2 (CNCMe₂CH₂O), -178.1 (MgNH). IR (KBr, cm⁻¹): 3325 w, 3072 m, 3045 m, 2966 s, 2773 w, 1635 w, 1584 s (ν_{CN}), 1495 w, 1462 s, 1433 m, 1385 m, 1366 s, 1354 s, 1270 s, 1193 s, 1115 m, 1091 m, 954 s, 912 m, 815 m, 703 s, 639 s. IR (C₆H₆, cm⁻¹) 3481 w, 3072 s, 3036 s, 2967 s, 2926 s, 2887 s, 1617 w, 1590 s (ν_{CN}), 1528 m, 1478 s, 1392 s, 1366 m, 1350 m, 1269 m, 1250 m, 1177 m, 1090 w, 1036 m, 964 m, 907 w, 847 w, 774 w, 702 m, 672 s. Anal. Calc. for C₃₁H₄₇BN₃O₃Mg: C, 66.63; H, 8.48; N, 10.03. Found: C, 66.56; H, 8.17; N, 9.99. Mp 176-180 °C, dec.

To^MMg(NC₄H₅-2-Me-4,4-Ph₂). In the glovebox, a vial was charged with To^MMgMe (0.055 g, 0.13 mmol), benzene (2 mL), and a stir bar. 2-Methyl-4,4,-diphenylpyrrolidine (0.033 g, 0.14 mmol), dissolved in benzene (2 mL) was added to the solution of To^MMgMe. The reaction mixture was allowed to stir for 6 h at room temperature. The volatile materials were removed under vacuum, and excess pyrrolidine was removed by washing with pentane (3 × 1 mL). The solid was dried in vacuo to give pure product (0.073 g, 0.11 mmol, 87.0%) as a white solid. ¹H NMR (benzene-*d*₆, 400 MHz): δ 8.28 (d, ³J_{HH} = 7.7 Hz, 2 H, *ortho*-C₆H₅), 7.65 (d, ³J_{HH} = 7.7 Hz, 2 H, *ortho*-NC₄H₅-2-Me-4,4-Ph₂), 7.54 (multiplet, 4 H, *meta*-C₆H₅ and *ortho*-NC₄H₅-2-Me-4,4-Ph₂), 7.36 (t, ³J_{HH} = 7.7 Hz, 1 H, *para*-C₆H₅), 7.25-7.08 (multiplet, 6 H, *meta+para*-NC₄H₅-2-Me-4,4-Ph₂), 4.40 (dd, ³J_{HH} = 8.8 Hz, 2 H, MgNCHMeCH₂CPh₂CH₂), 4.19 (sextet, ³J_{HH} = 6.6 Hz, 1 H, MgNCHMeCH₂CPh₂CH₂), 3.40 (s, 6 H, CNCMe₂CH₂O), 2.78 (dd, ³J_{HH} = 6.6 Hz, 1 H, MgNCHMeCH₂CPh₂CH₂), 2.18 (dd, ³J_{HH} = 6.6 Hz, 1 H, MgNCHMeCH₂CPh₂CH₂), 1.50 (d, ³J_{HH} = 6.6 Hz, 3 H, MgNCHMeCH₂CPh₂CH₂), 1.03 (d, ⁴J_{HH} = 16.5 Hz, 18 H, CNCMe₂CH₂O). ¹³C{¹H} NMR (benzene-*d*₆, 100 MHz): δ 192.17 (br, CNCMe₂CH₂O), 151.95 (*ipso*-NC₄H₅-2-Me-4,4-Ph₂),

151.73 (*ipso*-NC₄H₅-2-Me-4,4-Ph₂), 142.92 (*ipso*-C₆H₅), 136.46 (*ortho*-C₆H₅), 128.85 (*ortho*-NC₄H₅-2-Me-4,4-Ph₂), 127.23 (*meta*-C₆H₅), 126.28 (*para*-C₆H₅), 125.96 (*para*-NC₄H₅-2-Me-4,4-Ph₂), 125.65 (*para*-NC₄H₅-2-Me-4,4-Ph₂), 80.52 (CNCMe₂CH₂O), 67.68 (MgNCHMeCH₂CPh₂CH₂), 65.87 (CNCMe₂CH₂O), 59.69 (MgNCHMeCH₂CPh₂CH₂), 59.00 (MgNCHMeCH₂CPh₂CH₂), 50.58 (MgNCHMeCH₂CPh₂CH₂), 28.82 (MgNCHMeCH₂CPh₂CH₂), 28.48 (CNCMe₂CH₂O), 28.45 (CNCMe₂CH₂O). ¹¹B NMR (benzene-*d*₆, 128 MHz): δ -17.3. ¹⁵N{¹H} NMR (benzene-*d*₆, 71 MHz): δ -132.3 (MgNCHMeCH₂CPh₂CH₂), -158.8 (CNCMe₂CH₂O). IR (KBr, cm⁻¹): 3045 m, 2965 s, 2740 m, 1584 s (ν_{CN}), 1492 m, 1462 m, 1385 w, 1366 m, 1354 m, 1272 s, 1194 s, 1031 m, 962 s, 933 m, 895 w, 841 w, 815 w, 748 m, 773 s, 638 s. Anal. Calc. for C₃₈H₄₇BN₄O₃Mg: C, 70.99; H, 7.37; N, 8.71. Found: C, 70.52; H, 7.24; N, 8.45. Mp 160-164 dec.

General procedure for catalytic hydroamination/cyclization. In a typical small scale experiment, 12 μmol of catalyst (To^MMgCH₃ or To^MMgCH₂C₆H₃Me₂) and 120 μmol of aminoalkene were dissolved in 0.7 mL benzene-*d*₆ and placed in a J. Young style NMR tube with a resealable Teflon valve. The tube was sealed, and placed into an oil bath that was preheated to 50 °C. The reaction was monitored at regular intervals by ¹H NMR spectroscopy.

Procedure for kinetic measurements. All kinetics measurements were conducted by monitoring the reaction with ¹H NMR spectroscopy using a Bruker DRX-400 spectrometer. The NMR probe was pre-warmed to 50 or 60 °C, and the temperature was calibrated using an 80% ethylene glycol sample in 20% DMSO-*d*₆. To ensure complete activation of the

catalyst, $\text{To}^{\text{M}}\text{MgCH}_2\text{C}_6\text{H}_3\text{Me}_2$ and one equivalent of substrate were dissolved in benzene- d_6 , and the resulting solution was heated for 10 minutes in a 60 °C oil bath. A ^1H NMR spectrum was acquired every two minutes to monitor the formation of mesitylene until no increase in the mesitylene concentration was observed. At that point, an excess amount of substrate was added to the activated catalyst solution. The conversion of substrate to product was monitored by taking a single scan ^1H NMR spectra at preset intervals. The concentration of substrate and product were determined by comparison of integrated resonance corresponding to substrate and product to a known concentration of tetrakis(trimethylsilyl) silane dissolved in benzene- d_6 . Kinetic isotope measurements were performed in the same manner using the N-deuterated substrate 2,2-diphenyl-4-penten-1-amine- d_2 .

Representative example. A 10 mL stock solution of benzene- d_6 containing a known concentration of the internal standard tetrakis(trimethylsilyl)silane and the pre-catalyst $\text{To}^{\text{M}}\text{MgCH}_2\text{C}_6\text{H}_3\text{Me}_2$ (4.93 mmol) was prepared using a 10 mL volumetric flask. The stock solution (0.7 mL) was added by glass syringe to a vial containing one equivalent of 1-amino-2,2-diphenylpent-4-ene substrate, and the solution was then transferred to a J. Young style NMR tube and activated as described above.

Exchange rate measurements. Measurements of the rate of oxazoline exchange were conducted on either a Bruker DRX-400 spectrometer or Bruker Avance 500 MHz spectrometer. Temperatures for Eyring analysis (Figure 4.15) were calibrated using an 80% ethylene glycol sample in 20% DMSO- d_6 . In a typical experiment, $\text{To}^{\text{M}}_2\text{Mg}$ was dissolved in a benzene- d_6 solution containing a known concentration of the internal standard

tetrakis(trimethylsilyl)silane. At elevated temperatures, five separate resonances were observed for the methyl peaks on the oxazoline rings: four peaks for the methyl groups located on coordinated oxazoline rings, and one for the methyl groups on the uncoordinated oxazoline (Figure 4.12). One of the coordinated oxazoline methyl peaks was inverted, and relaxation of both the corresponding coordinated peak and the uncoordinated peak was observed (Figures 4.13 and 4.14).

At each temperature, a ^1H NMR spectrum was acquired to determine the frequency offset of the peak to be inverted relative to the center of the spectral window. Using this value, a one-dimensional selective inversion experiment was then conducted to ensure that only the peak of interest was inverted. A typical non-selective inversion-recovery experiment was performed to measure the T_1 values of all peaks. Selective inversion experiments were then performed using a $180^\circ_{\text{selective}}-\tau-90^\circ_{\text{nonselective}}-\text{acquire}$ pulse sequence. A series of 15 experiments were performed with different mixing times (τ), and the peak intensities as a function of time were recorded. One scan was collected per experiment.

Data analysis was performed using the program CIFIT^{21,22} to give a nonlinear least-squares fit of the data collected. The T_1 values for both the inverted and non-inverted peaks were refined while fixing the values for the initial magnetizations for both peaks, infinity values of magnetization, and an initial guess of the rate constant, k . The refined T_1 values were then fixed, and the value of k and the initial magnetization of the inverted peak were refined. This process was repeated four times or until the values of T_1 and k remained constant.

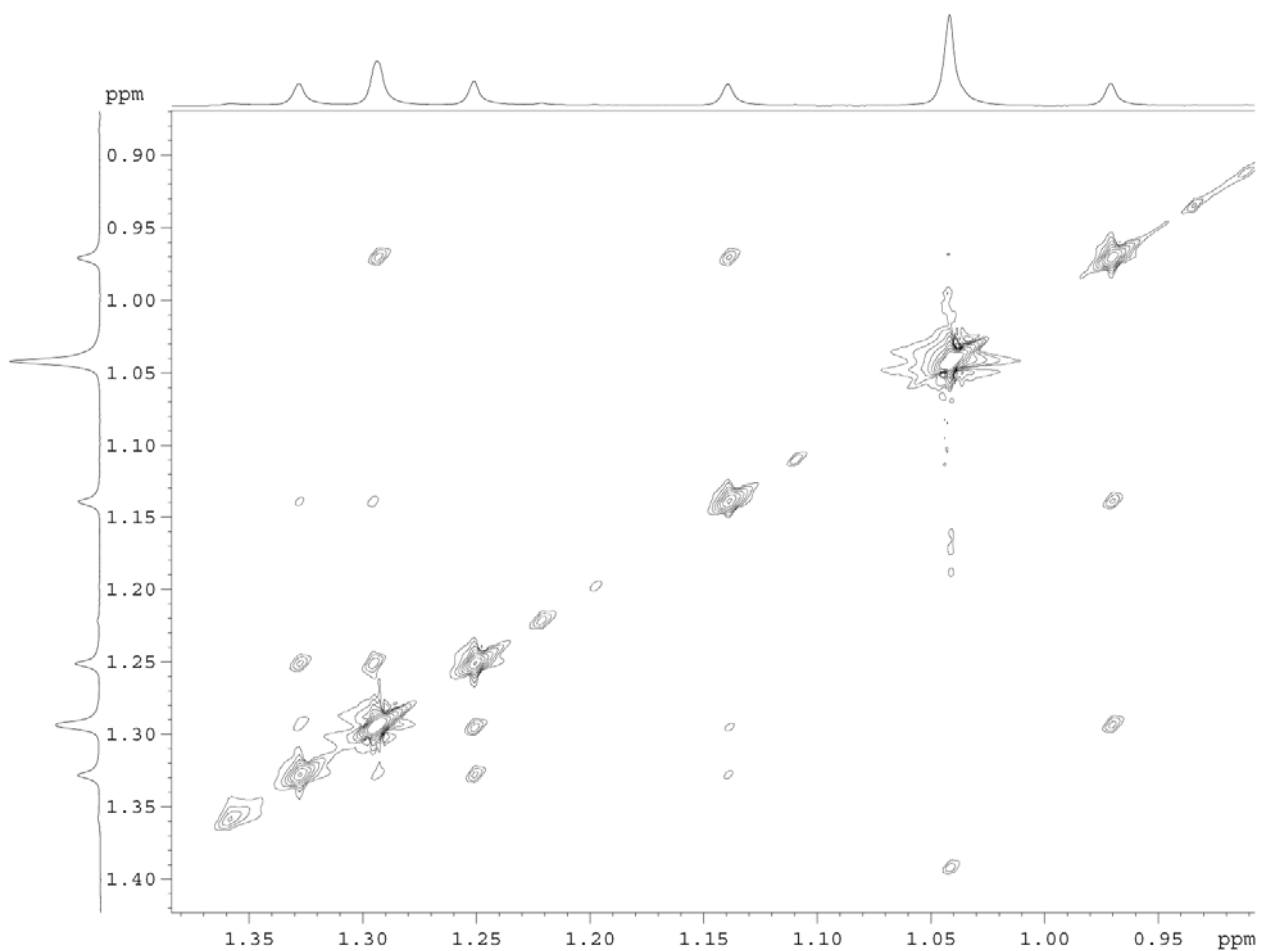


Figure 4.12. EXSY experiment of $\text{To}^{\text{M}}_2\text{Mg}$ showing selective exchange between methyl groups. The $\delta(\text{Me})$ for the non-coordinated 4,4-dimethyl-2-oxazoline group appears at 1.29. The resonance at 1.05 corresponds to an impurity of HTo^{M} in the sample. The rates of exchange were measured with analytically pure (HTo^{M} -free) samples.

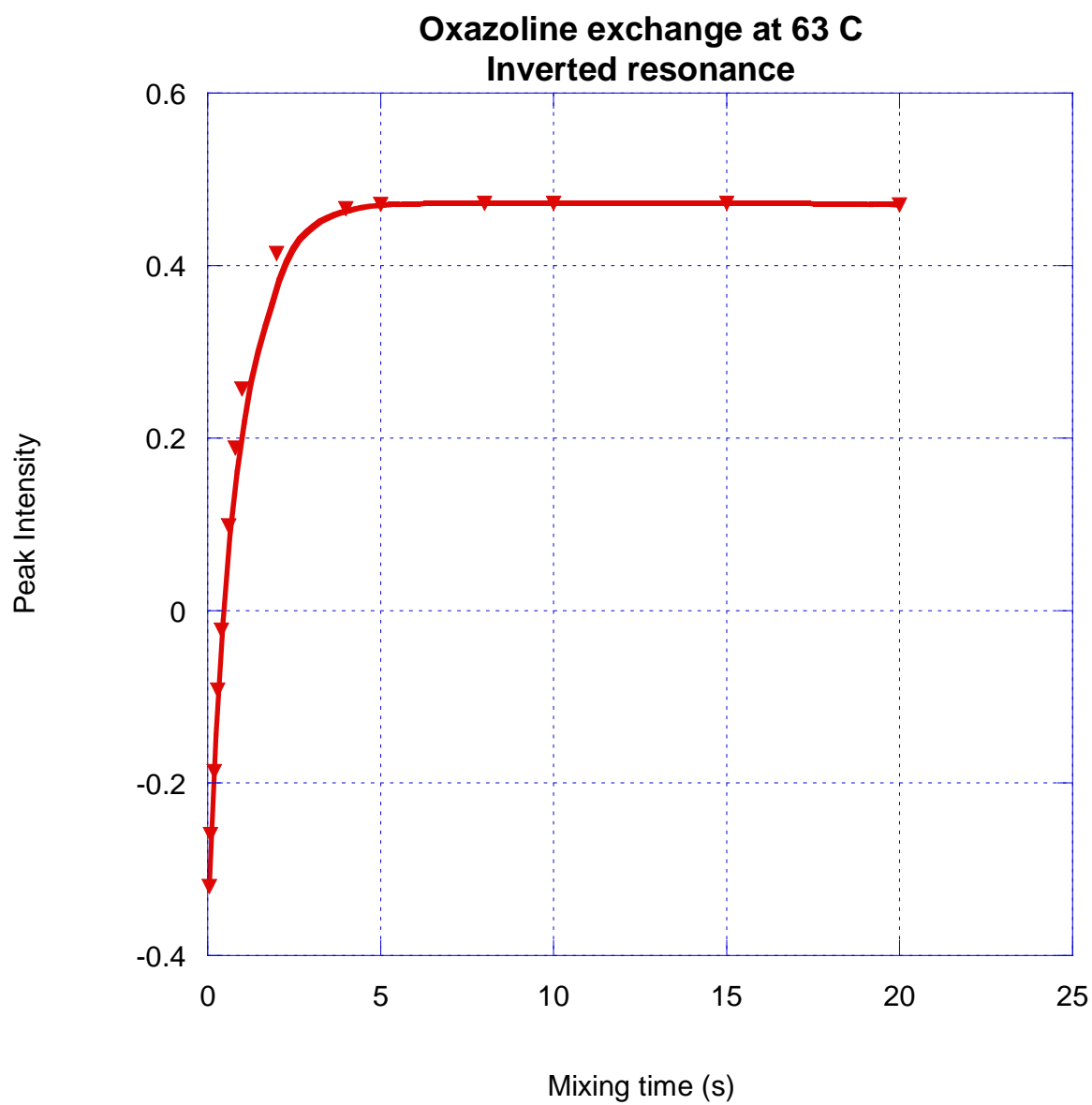


Figure 4.13. Plot of peak intensity versus mixing time for the inverted methyl resonance in $\text{To}^{\text{M}_2}\text{Mg}$.

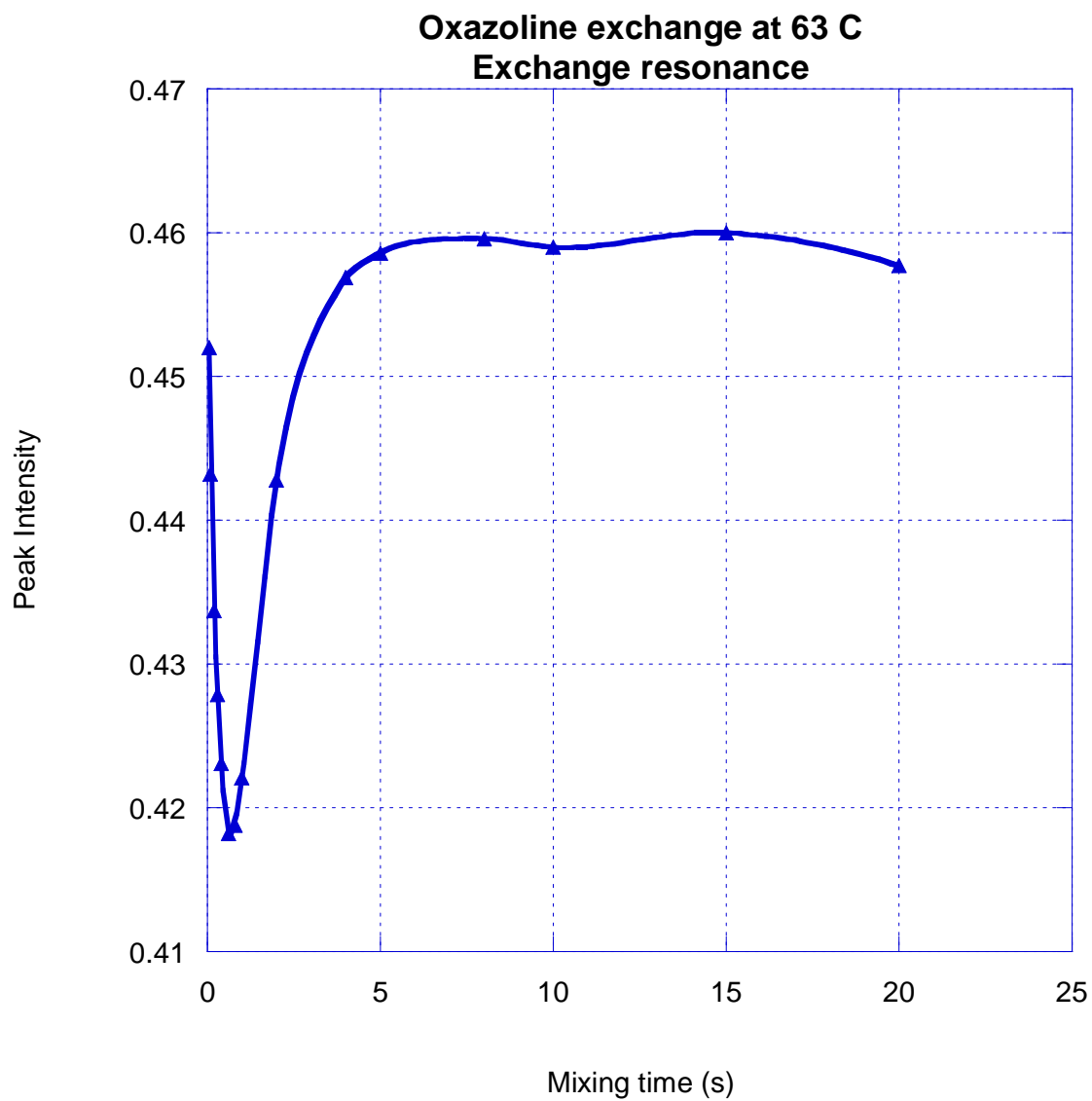


Figure 4.14. Plot of peak intensity versus mixing time for the non-inverted methyl resonance that is polarized via exchange in $\text{To}^{\text{M}}_2\text{Mg}$.

Eyring plot for oxazoline exchange in $\text{To}^{\text{M}}_2\text{Mg}$

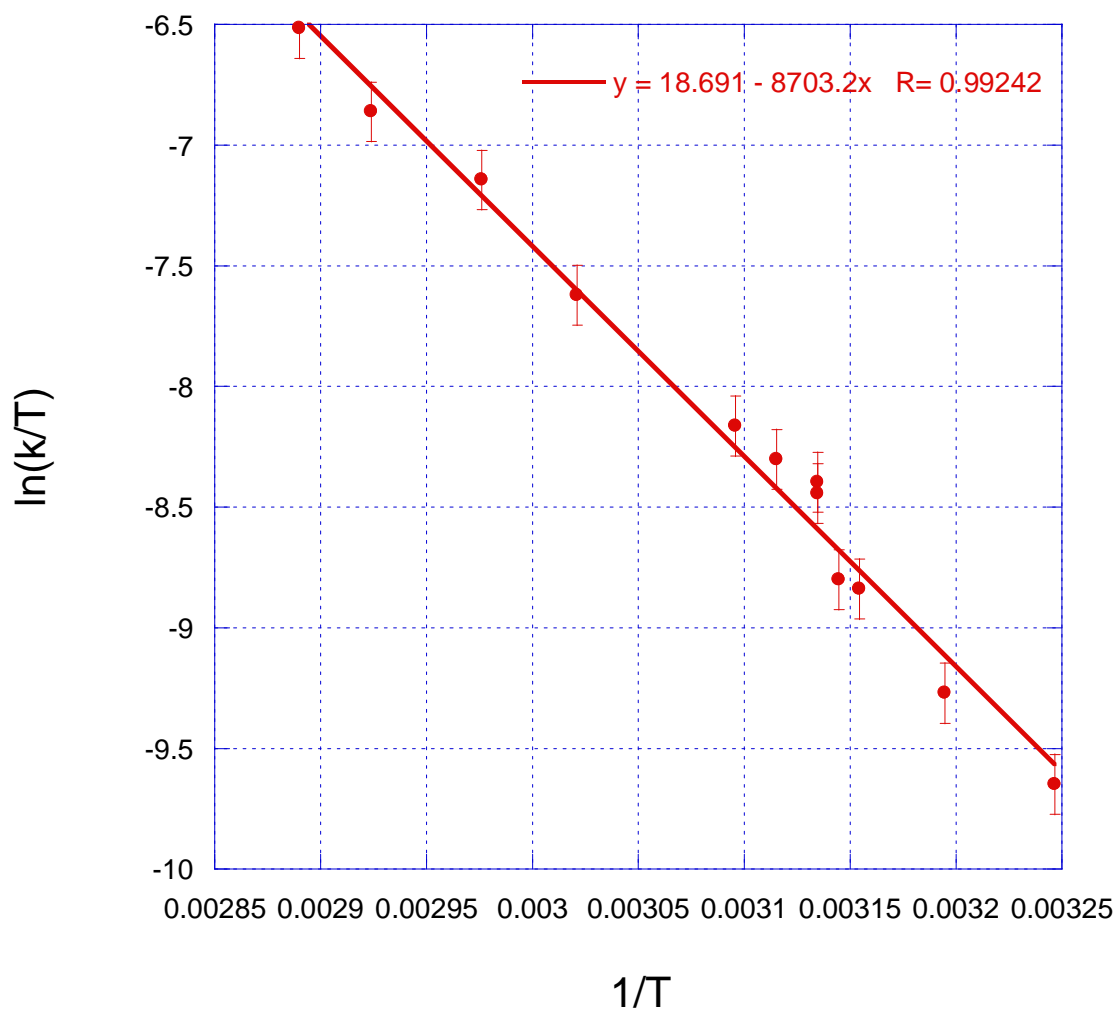


Figure 4.15. Plot of $\ln(k/T)$ vs $1/T$ where k = rate constant for oxazoline methyl exchange in $\text{To}^{\text{M}}_2\text{Mg}$ and T = temperature in K. Rate constants k are determined from analysis of selective population exchange (magnetization transfer) using the program CIFIT. From the plot, $\Delta S^\ddagger = -10 \pm 2$ eu and $\Delta H^\ddagger = 17.3 \pm 0.7$ kcal/mol. $\Delta G^\ddagger(298 \text{ K}) = 20 \pm 1$ kcal/mol; $\Delta G^\ddagger(333 \text{ K}) = 20 \pm 1$ kcal/mol; $k(333 \text{ K}) = v_{\text{exchange}} = 0.195 \text{ s}^{-1}$ ($k = v_{\text{exchange}}$ because exchange is unimolecular and therefore concentration independent).

References

- 1) (a) Hong, S.; Marks, T.J. *Acc. Chem. Res.* **2004**, *37*, 673-686.; (b) Muller, T.E.; Hultsch, K.C.; Yus, M.; Foubelo, F.; Tada, M. *Chem Rev.* **2008**, *108*, 3795-3892.
- 2) Gagne, M.R.; Marks, T.J. *J. Am. Chem. Soc.* **1989**, *111*, 4108-4109.
- 3) (a) Gagne, M.R.; Stern, C.L.; Marks, T.J. *J. Am. Chem. Soc.* **1992**, *114*, 275-294.; (b) Gribkov, D.V.; Hultsch, K.C.; Hampel, F. *J. Am. Chem. Soc.* **2006**, *128*, 3748-3759.
- 4) Stubbert, B.D.; Marks, T.J. *J. Am. Chem. Soc.* **2007**, *129*, 6149-6167.
- 5) (a) Walsh, P.J.; Hollander, F.J.; Bergman, R.G. *J. Am. Chem. Soc.* **1990**, *112*, 894-896.;
 b) Leitch, D.C.; Turner, C.S.; Schafer, L.L. *Angew. Chem. Int. Ed.* **2010**, *49*, 6382-6386.
- 6) Katayev, E.; Li, Y.; Odom, A.L. *Chem. Commun.* **2002**, 838-839.
- 7) (a) Cassalnuovo, A.L.; Calabrese, J.C.; Milstein, D. *J. Am. Chem. Soc.* **1988**, *110*, 6738-6744.; (b) Dorta, R.; Egli, P.; Zurcher, F.; Togni, A. *J. Am. Chem. Soc.* **1997**, *119*, 10857-10858.
- 8) (a) Cowan, R.L.; Trogler, W.C.; *Organometallics* **1987**, *6*, 2451-2453.; (b) Cowan, R.L.; Trogler, W.C. *J. Am. Chem. Soc.* **1989**, *111*, 4750-4761.; (c) Seligson, A.L.; Trogler, W.C. *Organometallics* **1993**, *12*, 744-751.
- 9) (a) Neukom, J.D.; Perch, N.S.; Wolfe, J.P. *J. Am. Chem. Soc.* **2010**, *132*, 6276-6277.; (b) Hanley, P.S.; Markovic, D.; Hartwig, J.F. *J. Am. Chem. Soc.* **2010**, *132*, 6302-6303.
- 10) Motta, A.; Lanza, G.; Fragala, I.L.; Marks, T.J. *Organometallics* **2004**, *23*, 4097-4104.
- 11) (a) Crimmin, M.R.; Casely, I.J.; Hill, M.S. *J. Am. Chem. Soc.* **2005**, *127*, 2042-2043.;

- (b) Datta, S.; Roesky, P.W.; Blechert, S. *Organometallics* **2007**, *26*, 4392-4394.; (c) Barrett, A.G.M.; Crimmin, M.R.; Hill, M.S.; Kociok-Kohn, G.; Lachs, J.R.; Procopiou, P.A. *Dalton Trans.* **2008**, 1292-1294.
- 12) Greenwood, N.N.; Earnshaw, A. *Chemistry of the Elements*; Pergamon Press: Oxford, 1984.
- 13) Datta, S.; Gamer, M.T.; Roesky, P.W. *Organometallics* **2008**, *27*, 1207-1213.
- 14) (a) Crimmin, M.R.; Arrowsmith, M.; Barrett, A.G.M.; Casely, I.J.; Hill, M.S.; Procopiou, P.A. *J. Am. Chem. Soc.* **2009**, *131*, 9670-9685.; (b) Horrillo-Martinez, P.; Hultzs, K.C. *Tetrahedron Lett.* **2009**, *50*, 2054-2056.; (c) Neal, S.R.; Ellern, A.; Sadow, A.D. *J. Organomet. Chem.* **2010**, *696*, 228-234.
- 15) Guzi, I.A.; Wendt, M. *Program Solid-G*. UW-Madison, WI, USA, 2004.
- 16) (a) Han, R.; Parkin, G. *Organometallics* **1991**, *10*, 1010-1020.; (b) Han, R. Parkin, G. *J. Am. Chem. Soc.* **1992**, *114*, 748-757.
- 17) (a) Beesley, R.M.; Ingold, C.K.; Thorpe, J.F. *J. Chem. Soc., Trans.* **1915**, *107*, 1080. (b) Ringer, A.L.; Magers, D.H. *J. Org. Chem.* **2007**, *72*, 2533-2537.; (c) Bachrach, S.M. *J. Org. Chem.* **2008**, *73*, 2466-2468.
- 18) (a) Hultzs, K.C.; Hampel, F.; Wagner, T. *Organometallics* **2004**, *23*, 2601-2612.; (b) Thomson, R.K.; Bexrud, J.A.; Schafer, L.L. *Organometallics* **2006**, *25*, 4069-4071.
- 19) Barrett, A.G.M.; Casely, I.J.; Crimmin, M.R.; Hill, M.S.; Lachs, J.R.; Mahon, M.F.; Procopiou, P.A. *Inorg. Chem.* **2009**, *48*, 4445-4453.
- 20) Espenson, J.H. *Chemical kinetics and reaction mechanisms*, 2nd ed.; McGraw-Hill: New York, 1995.

- 21) Cornish-Bowden, A. *Fundamentals of Enzyme Kinetics*, 3rd ed.; Portland Press, London, 2004, pp. 137-141.
- 22) (a) Bain, A.D.; Cramer, J.A. *J. Phys. Chem.* **1993**, *97*, 2884-2887.; (b) Bain, A.D. *CIFIT*; Chemistry Department, McMaster University, 2003.; (c) Kristian, K.E.; Iimura, M.; Cummings, S.A.; Norton, J.R.; Janak, K.E.; Pang, K. *Organometallics* **2009**, *28*, 493-498.
- 23) (a) Henderson, K.W.; Allan, J.F.; Kennedy, A.R. *Chem. Commun.* **1997**, 1149-1150.; (b) He, X.; Morris, J.J.; Noll, B.C.; Brown, S.N.; Henderson, K.W. *J. Am. Chem. Soc.* **2006**, *128*, 13599-13610.
- 24) Manna, K.; Xu, S.; Sadow, A.D. *Angew. Chem. Int. Ed.* **2011**, *50*, 1865-1868.
- 25) Tobisch, S. *Dalton. Trans.* **2011**, *40*, 249-261.
- 26) Dunne, J. F.; Su, J.; Ellern, A.; Sadow, A. D., *Organometallics* **2008**, *27*, 2399-2401.
- 27) Ho, H.-A.; Dunne, J.F.; Ellern, A.; Sadow, A.D. *Organometallics* **2010**, *29*, 4105-4114.
- 28) Tobia, D.; Baranski, J.; Rickborn, B. *J. Org. Chem.* **1989**, *54*, 4253.
- 29) Hong, S.; Tian, S.; Metz, M. V. ; Marks, T. J. *J. Am. Chem. Soc.*, **2003**, *125*, 14768.
- 30) Bender, C. F.; Widenhoefer, R. A. *J. Am. Chem. Soc.*, **2005**, *127*, 1070.

Chapter 5: Magnesium amide-catalyzed dehydrocoupling of organosilanes with amines, hydrazines, and ammonia for silicon-nitrogen bond formation

Modified from a paper to be submitted to *Organometallics*

James F. Dunne,[†] Joshua Engelkemier,[§] Arkady Ellern, Theresa L. Windus, and Aaron D. Sadow

Department of Chemistry and U.S. Department of Energy Ames Laboratory, Iowa State University, Ames, IA 50011, United States

Abstract

$\text{To}^{\text{M}}\text{MgMe}$ ($\text{To}^{\text{M}} = \text{tris}(4,4\text{-dimethyl-2-oxazolinyl})\text{phenylborate}$) is an effective pre-catalyst for the cross-dehydrocoupling of organosilanes and amines to form new Si–N bonds and generate H_2 gas. Using this catalyst system, a range of silazanes can be prepared in high yield from primary aliphatic amines, anilines, and primary or secondary silanes. In reactions where multiple Si–H and N–H groups are available for cross-coupling, carefully controlled ratios of silane and amine allow isolation of a single product. Polysilazane $-\text{[R}'\text{NSiR}_2\text{]}_n-$ and poly(aminosilane) $-\text{[SiR}(\text{NR}'_2)\text{]}_n-$ formation is not detected. This reaction can be extended to couple hydrazine and ammonia with tertiary silanes to give selectively the corresponding aminosilanes $\text{R}_3\text{SiNHNH}_2$ and R_3SiNH_2 .

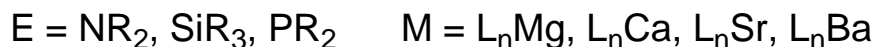
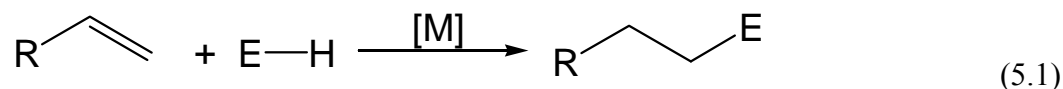
Introduction

The catalytic formation of new chemical bonds is one of the most important areas of research in organometallic chemistry. While transition metal compounds are most commonly used as the active catalyst in bond forming reactions, these compounds are

[†]Primary researcher and author

[§]Undergraduate student; performed DFT calculations

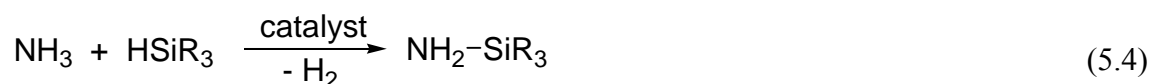
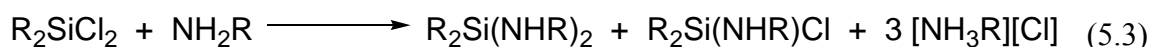
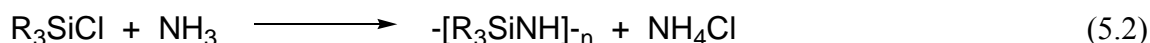
potentially environmentally harmful making catalyst toxicity an additional concern. Partly as a means of addressing this problem, main group metal complexes have begun to be explored as catalysts capable of replacing the transition metals.¹ The alkaline earth metals are an attractive choice for these new catalysts due to their non-toxic nature (except beryllium) and widespread natural abundance.² Recently, there have been a number of alkaline earth metal compounds reported as active catalysts for hydroamination,³⁻⁵ hydrosilylation,⁶ and hydrophosphination (eq 5.1).⁷ As several of these systems involve the catalytic formation of new C–N bonds,³⁻⁵ we were interested in expanding this reactivity to include the formation of Si–N bonds.



Silazanes are extensively used in synthetic organic chemistry as silyl transfer agents to a range of functional groups including alcohols, ketones, amines, amides, carboxylic acids, and thiols.⁸ Many of these functional groups display limited solubility in non-polar solvents, while the silylated analogs display greatly enhanced solubility in non-polar hydrocarbon solvents. Silazanes are also widely used as bases in organic chemistry,⁹ as well as ligands in organometallic compounds.¹⁰ The synthesis of silazanes molecules is of further importance due to the utility of tertiary silanes as protecting groups for amines.¹¹ The traditional synthetic route to silazanes proceeds through either ammonolysis (eq 5.2) or aminolysis (eq 5.3) of chlorosilanes.¹² However, this method generates equimolar quantities of ammonium halide by-products, and aminolysis requires chlorosilanes which are hydroscopically

sensitive and must be handled in the absence of both oxygen and water. Additionally, products are only controlled by the substituents on the chlorosilane and the amine partners, limiting control over selectivity.¹³

Catalytic dehydrocoupling of amines and organosilanes offers a complimentary synthetic method for the formation of Si–N bonds which can address some of these issues (eq 5.4). Organosilanes are robust starting materials in the presence of both air and moisture making handling and storage of the starting materials easier. Additionally, the only by-product of the reaction is hydrogen gas which can be easily separated from the desired products and collected as a useful chemical in and of itself.



Currently, only a few metal catalysts for the cross-couplings of silanes and amines have been described (Figure 5.1). Palladium on Al_2O_3 catalyzes the aminolysis of optically active tertiary naphthylphenylmethylsilane with inversion of the silicon stereocenter, while Pd/C gives racemic products.¹⁴ Reaction of $\text{HN}(\text{SiHMe}_2)_2$ with ammonia in the presence of $\text{Ru}_3(\text{CO})_{12}$ results in rapid oligomerization to give polysilazanes and H_2 ,¹⁵ while rhodium dimers give mixtures of oligosilazanes from amines and organosilanes.¹⁶ The chromium catalyst $(\eta^6\text{-C}_6\text{H}_6)\text{Cr}(\text{CO})_2(\eta^2\text{-HSiHPh}_2)$ provides $\text{Ph}_2\text{HSi-NHPh}$ from Ph_2SiH_2 and aniline.¹⁷

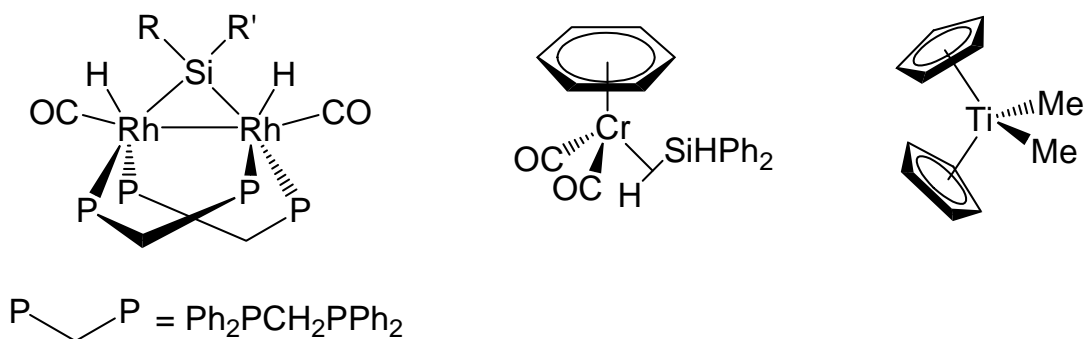
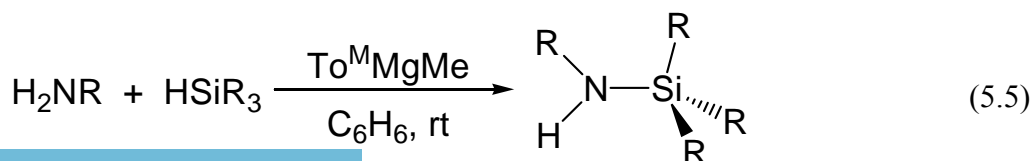


Figure 5.1. Examples of active catalysts for cross coupling of silanes and amines

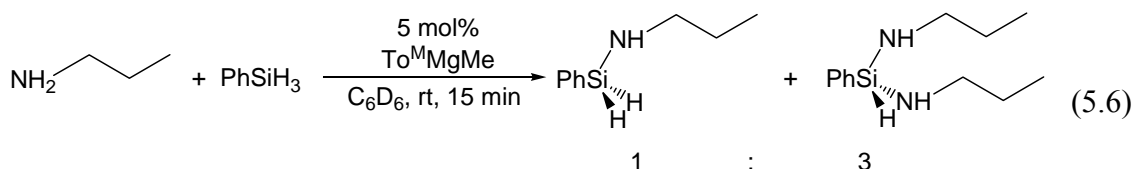
Dimethyltitanocene catalyzes the coupling of silanes with ammonia and hydrazine to give mixtures of polysilazanes as well as poly(aminosilanes).¹⁸ Finally, a number of silazanes are selectively prepared using $[\text{U}(\text{NMe}_2)_3][\text{BPh}_4]$ as a catalyst.¹⁹ However, there have been few opportunities to directly investigate the silicon-nitrogen bond forming steps of these reactions, and the general challenge of controlling the cross-coupling to generate a single product remains an important issue.

To address some of these issues, we explored the activity of $\text{To}^{\text{M}}\text{MgMe}$ ($\text{To}^{\text{M}} =$ tris(4,4-dimethyl-2-oxazoliny)phenyl borate) as a pre-catalyst for the cross-coupling of amines and organosilanes (eq 5.5). Herein, we report that $\text{To}^{\text{M}}\text{MgMe}$ catalyzes the dehydrocoupling of primary amines to silanes. Mono- and doubly-dehydrocoupled products can be selectively isolated by adjusting the ratio of the silane and amine starting materials. Additionally, both hydrazine and ammonia can be successfully transformed using tertiary silanes to give the corresponding aminosilanes as the sole product.



Results and Discussion

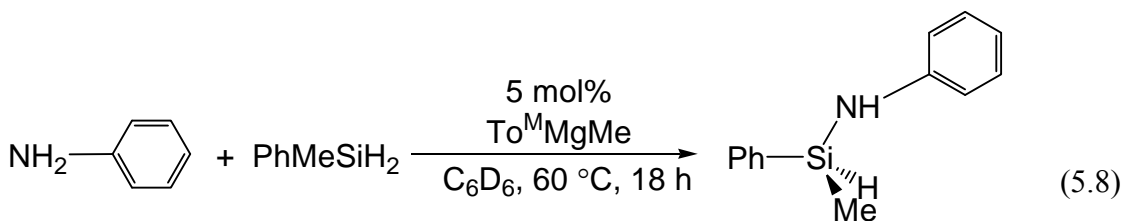
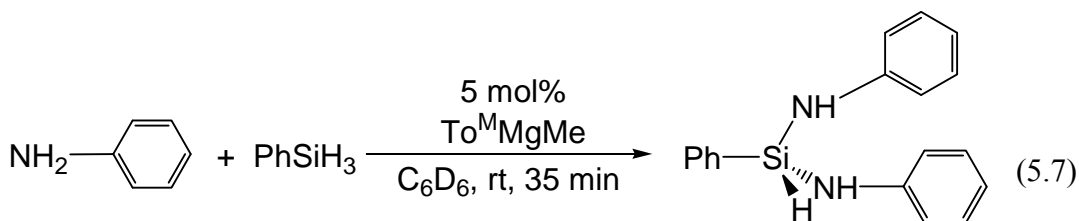
In micromolar scale experiments, the addition of *n*-propylamine to a benzene-*d*₆ solution of $\text{To}^{\text{M}}\text{MgMe}^{5\text{d}}$ immediately results in the formation of a new To^{M} species as observed by ¹H NMR spectroscopy. Subsequent addition of PhSiH_3 to the solution causes significant effervescence, and a small resonance at 4.47 ppm corresponding to dissolved H_2 gas appears in the ¹H NMR spectrum. Within 10 minutes, all of the amine starting materials are consumed and a mixture of silazane products can be observed along with unreacted PhSiH_3 (eq 5.6). The silazane products were identified by new Si–H resonances in the ¹H NMR spectrum, and the Si–H resonance was observed to shift further downfield as multiple amides were coupled to a single silicon center. The splitting pattern of the Si–H resonance resulting from ³*J*_{HH} coupling was used to distinguish between silicon centers with one and two amide groups. The fully substituted silazane, $\text{PhSi}(\text{NH}^n\text{Pr})_3$, is isolated by the addition of excess (3.5 equiv) *n*-propylamine relative to silane (Table 5.1, entry 1), and $\text{PhSi}(\text{NH}^n\text{Pr})_3$ was identified by the appearance of new amide resonances in the absence of a corresponding Si–H peak.



Si–N heterocoupling is primarily controlled by the steric demands of both substrates as well as the metal catalyst. Under identical catalytic conditions, the reaction of $\text{H}_2\text{N}^i\text{Pr}$ with PhSiH_3 proceeds less rapidly than is observed for $\text{H}_2\text{N}^n\text{Pr}$ and PhSiH_3 , requiring 45 and 15 minutes, respectively, for complete consumption of the amine starting materials.

Additionally, in the presence of excess (3.5 equiv) $\text{H}_2\text{N}^i\text{Pr}$ and one PhSiH_3 molecule and at elevated temperatures ($100\text{ }^\circ\text{C}$), $\text{PhHSi}(\text{NH}^i\text{Pr})_2$ is the sole product observed as the amine group is too sterically bulky for the formation of quaternary silyl centers to occur. Tert-butyl amine requires a substantially longer reaction time (24 h) in comparison to isopropyl amine for quantitative conversion of $\text{H}_2\text{N}^t\text{Bu}$ to the silazane product, $\text{PhH}_2\text{SiNH}^t\text{Bu}$. $\text{PhH}_2\text{SiNH}^t\text{Bu}$ is the sole product further demonstrating the important role of steric bulk in controlling the dehydrocoupling reaction.

Catalytic reactions of anilines and silanes are also affected by steric bulk. Aniline reacts rapidly with PhSiH_3 at room temperature to give the dianilido product $\text{PhHSi}(\text{NHPh})_2$ (eq 5.7), while the sterically encumbered 2,6-diisopropylaniline (H_2NDIPP) reacts slowly with PhSiH_3 to give a 1:1 mixture of $\text{PhH}_2\text{SiNHDIPP}$ and $\text{PhHSi}(\text{NHDIPP})_2$. In contrast to aliphatic amines, reaction of aniline with a secondary silane required warming of the solution to $60\text{ }^\circ\text{C}$ in order for catalysis to occur (eq 5.8, Table 4.1, entries 14 and 15).



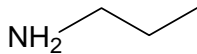
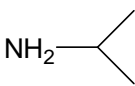
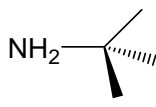
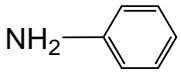
Warming a solution of H_2NDIPP and PhMeSiH_2 to $60\text{ }^\circ\text{C}$ for 24 h results in only 16% conversion to the silazane, PhMeHSiNHDIPP . Presumably, the *ortho*-substituents prevent the secondary silane from interacting with the magnesium amide. The reduced rate of reactivity of aromatic amines with secondary silanes suggests that electronic factors also play a substantial role in the rate-determining step of the reaction.

Secondary amines are less efficient as substrates for catalytic dehydrocoupling. For example, heating a solution of HNPh_2 and PhSiH_3 with 10 mol% $\text{To}^{\text{M}}\text{MgMe}$ at $110\text{ }^\circ\text{C}$ for 72 h results in one turnover to form the silazane product $\text{PhH}_2\text{SiNPh}_2$. Only starting materials are observed when the more sterically hindered secondary amine HN^iPr_2 and PhSiH_3 are heated for 5 days at $110\text{ }^\circ\text{C}$. Tertiary silanes BnMe_2SiH and Et_3SiH were likewise found to be unreactive with all primary amines even under elevated temperature ($110\text{ }^\circ\text{C}$) and extended reaction time (72 h).

Catalytic dehydrocoupling of hydrazine with organosilanes

Because $\text{To}^{\text{M}}\text{MgMe}$ -catalyzed dehydrocoupling reactions of small amines with organosilanes provide single products with high selectivity, we decided to test the ability of $\text{To}^{\text{M}}\text{MgMe}$ in the cross coupling reactions of hydrazine to silanes. Dimethyltitanocene dehydrocoupling of hydrazine with primary and secondary silanes gives mixtures of polymeric products.^{18b} The steric bulk of To^{M} combined with its tridentate binding mode leaves only one open reactive site on the metal which could result in the isolation of monomeric silazane products. Addition of excess hydrazine to a benzene solution of benzyldimethylsilane and 10 mol% $\text{To}^{\text{M}}\text{MgMe}$ resulted in the slow formation of the product $\text{NH}_2\text{NH-SiBnMe}_2$ ($\text{Bn} = \text{CH}_2\text{C}_6\text{H}_5$) (eq 5.9). The catalyst resting state $\text{To}^{\text{M}}\text{MgNHNH}_2$

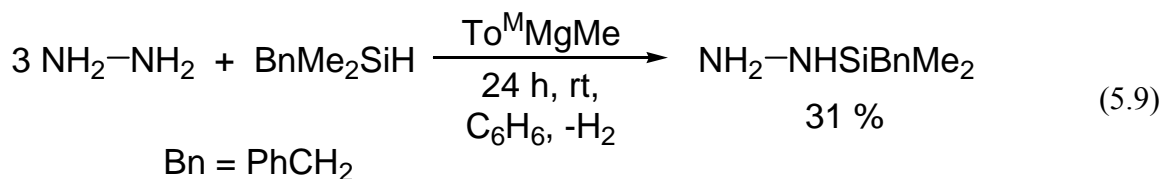
Table 5.1: Scope of isolated silazanes

Entry	Amine	Silane	Amine:silane	Product	NMR yield (isolated)
1		PhSiH ₃	3.5:1	PhSi(NH ⁿ Pr) ₃	99 (99)
2		PhMeSiH ₂	3:1	PhMeSi(NH ⁿ Pr) ₂	99 (92)
3		PhMeSiH ₂	1:2	PhMeHSiNH ⁿ Pr	99 (78)
4		Ph ₂ SiH ₂	3:1	Ph ₂ Si(NH ⁿ Pr) ₂	99 (99)
5		Ph ₂ SiH ₂	1:2	Ph ₂ HSiNH ⁿ Pr	99 (97)
6		PhSiH ₃	2.5:1	PhHSi(NH ⁱ Pr) ₂	99 (99)
7		PhSiH ₃	1:2	PhH ₂ SiNH ⁱ Pr	99 (45)
8		PhMeSiH ₂	2:1	PhMeHSi(NH ⁱ Pr)	89 (67)
9		Ph ₂ SiH ₂	2:1	Ph ₂ HSiNH ⁱ Pr	99 (97)
10		PhSiH ₃	2.5:1	PhH ₂ SiNH ^t Bu	99 (87)
11		PhMeSiH ₂	2:1	PhMeHSi(NH ^t Bu)	80 (60)
12		Ph ₂ SiH ₂	2:1	Ph ₂ HSiNH ^t Bu	99 (81)
13		PhSiH ₃	2.5:1	PhHSi(NHPh) ₂	99 (98)
14 ^b		PhMeSiH ₂	2:1	PhMeHSiNHPh	43 (19)
15 ^b		Ph ₂ SiH ₂	2:1	Ph ₂ HSiNHPh	53 (19)

^aConditions: 5 mol% To^MMgMe, C₆H₆, 24 h, rt. ^bSolution was warmed to 60 °C.

competitively disproportionates to give To^M₂Mg (as observed in the ¹H NMR spectrum), which was found to be inactive in Si–N cross coupling by an independent experiment. Consequently, the product is isolated only in low yields (31%). The other product from

disproportionation is presumed to be $\text{Mg}(\text{NHNH}_2)_2$, which is thought to decompose rapidly in solution as no evidence of the species is observed by NMR spectroscopy.



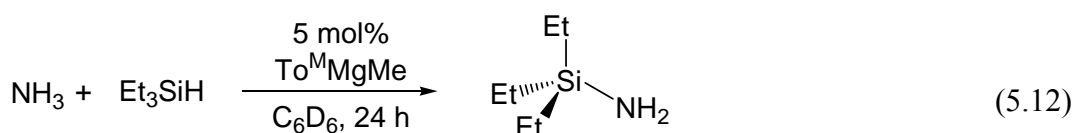
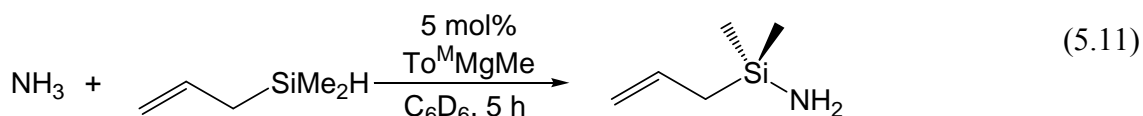
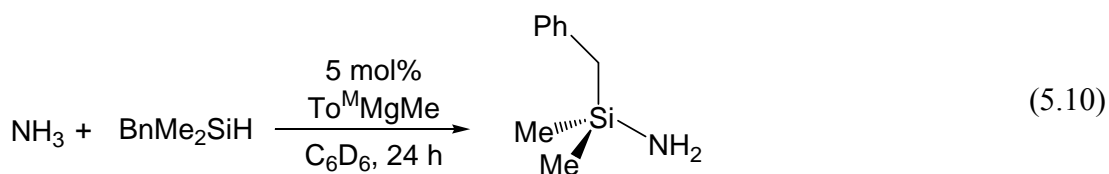
$\text{To}^{\text{M}}\text{MgMe}$ also catalyzes the dehydrocoupling of Et_3SiH and $(\text{C}_3\text{H}_5)\text{Me}_2\text{SiH}$ with hydrazine to give $\text{Et}_3\text{SiNHNH}_2$ and $(\text{C}_3\text{H}_5)\text{Me}_2\text{SiNHNH}_2$, respectively. Of the three silanes, $(\text{C}_3\text{H}_5)\text{Me}_2\text{SiH}$ reacts most rapidly and is quantitatively converted to the product after 7 hours. BnMe_2SiH and Et_3SiH proceeded only to 50% conversion after 12 hours, with no appreciable conversion observed after an additional 12 hours. Primary and secondary silanes react rapidly with hydrazine in the presence of $\text{To}^{\text{M}}\text{MgMe}$ to give mixtures of products, presumably resulting from multiple N–Si bond forming steps. The selectivity exhibited by $\text{To}^{\text{M}}\text{MgMe}$ for the monosilylation of hydrazine suggested that similar control might be accessible with NH_3 as a substrate for silane ammonolysis.

Catalytic dehydrocoupling of ammonia with organosilanes

The use of ammonia as a starting material for the generation of nitrogen-containing molecules is an important goal in synthetic chemistry.²⁰ However, the activation of ammonia by transition-metal centers remains a difficult transformation. This lack of reactivity can be attributed to several factors: 1) the deactivation of metal catalyst by the formation of stable Werner ammine complexes, 2) the strength of the N–H bond in ammonia (107 kcal/mol), and 3) the moderate basicity and low acidity of ammonia which disfavors proton exchange either

to or from ammonia.²⁰ The coordinative saturation of $\text{To}^{\text{M}}\text{MgMe}$ could address one of these issues in the prevention of the formation of a Werner complex. Additionally, the success observed for hydrazine and primary amines suggests that the magnesium center might be capable of activating the robust N–H bond.

The condensation of excess ammonia into a flask containing a benzene solution of BnMe_2SiH and $\text{To}^{\text{M}}\text{MgMe}$ (5 mol%, relative to silane) results in the slow formation of the silazane $\text{H}_2\text{N–SiMe}_2\text{Bn}$ over a 24 hour period (eq 5.10-5.12). After carefully release of the excess ammonia, the pure product could be isolated by Kugelrohr distillation (175 °C, 150 mmHg).



As in catalytic dehydrocoupling reactions with hydrazine, in the presence of $\text{To}^{\text{M}}\text{MgMe}$ $(\text{C}_3\text{H}_5)_2\text{SiH}$ reacts more rapidly with ammonia than either BnMe_2SiH or

Et₃SiH to give the corresponding silazane. Micromolar experiments (monitored by ¹H NMR spectroscopy) revealed quantitative conversion of (C₃H₅)Me₂SiH to NH₂-SiMe₂C₃H₅ after only 5 hours while BnMe₂SiH and Et₃SiH require 15 hours to give full conversion.

The monosilazanes are the only products detected by ¹H NMR spectroscopy, which further contrasts with the selectivity observed for reported titanium catalysts in which disilazanes are the sole product obtained by the coupling of ammonia with tertiary amines.^{18a} The reason for the selective formation of aminosilane may be attributed to the large steric bulk of the tertiary silane. After binding to magnesium, both ammonia and hydrazine are small enough to allow the tertiary silane to approach and interact with the metal center. However, upon coupling to one molecule of silane the resulting aminosilane can be considered analogous to a primary amine with a bulky R group (*i.e.*, H₂N^tBu). While this aminosilane can bind to the magnesium center, the steric bulk of the -SiR₃ group protects the nitrogen center from further reacting with a second equivalent of silane.

Kinetics/Mechanistic investigation for Si-N bond formation

¹H NMR spectra of mixtures of To^MMgMe and PhMeSiH₂, Ph₂SiH₂, or PhSiH₃ only contain resonances corresponding to magnesium and organosilane starting materials. In contrast, To^MMgMe reacts readily in the presence of primary amines (H₂NⁿPr, H₂NⁱPr, H₂N^tBu) to give the corresponding magnesium amides as seen by ¹H NMR spectroscopy. The magnesium amides could also be isolated in good yield, as seen in the case of To^MMgNH^tBu (see below). These observations suggest that the precatalyst To^MMgMe reacts with amine to produce the active catalyst To^MMgNHR. We then hypothesize that the magnesium amide subsequently reacts with silane to form the aminosilane product as well as

$\text{To}^{\text{M}}\text{MgH}$. The hydride species generated *in situ* undergoes protonolysis with a second equivalent of amine to generate H_2 gas and regenerate the active magnesium amide (Figure 5.2).

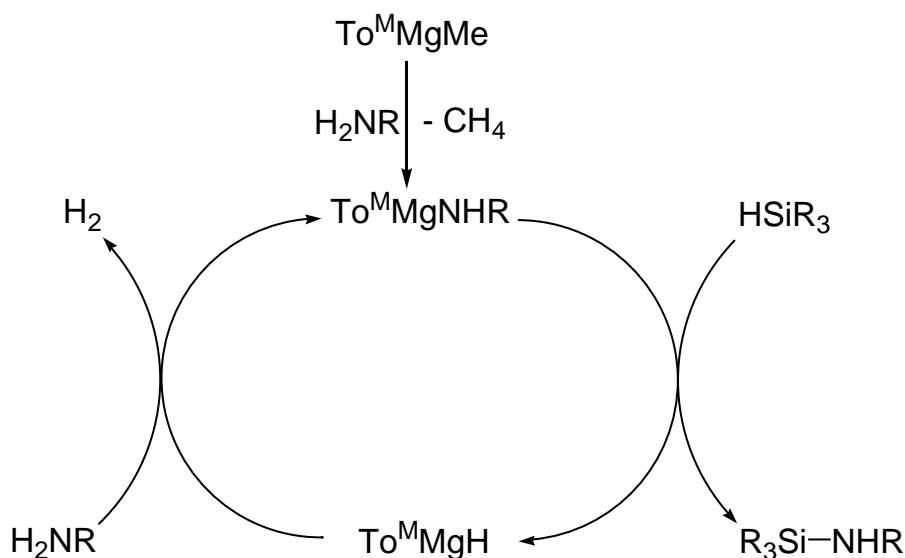
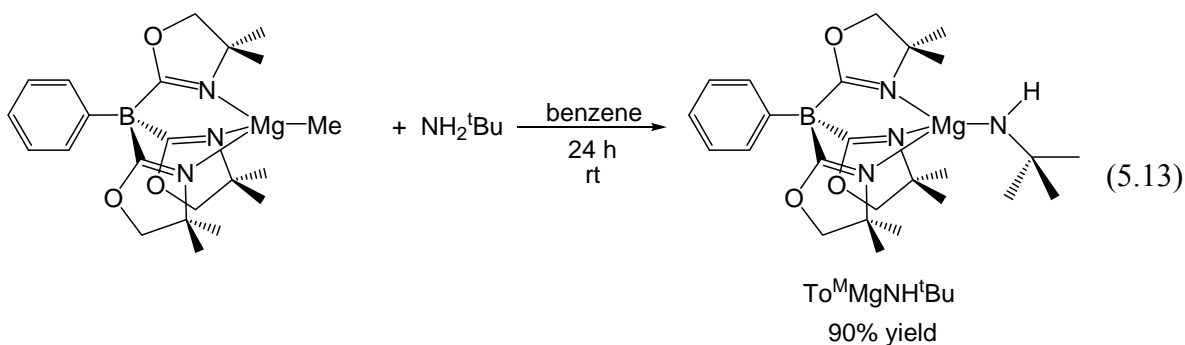


Figure 5.2. Proposed mechanism of magnesium catalyzed Si-N bond formation



To explore the proposed mechanism, $\text{To}^{\text{M}}\text{MgNH}^t\text{Bu}$ was isolated and fully characterized from the reaction of a small excess of $\text{H}_2\text{N}^t\text{Bu}$ (1.1 equiv) and $\text{To}^{\text{M}}\text{MgMe}$ (eq 5.13). X-ray quality crystals of $\text{To}^{\text{M}}\text{MgNH}^t\text{Bu}$ were obtained from toluene solutions cooled to $-30\text{ }^\circ\text{C}$ (Figure 5.3). In the solid state, the magnesium center is pseudo-tetrahedral with a slightly smaller Mg1–N4 bond length (1.92(8) Å) than Mg1–N1, Mg1–N2, and Mg1–N3

bond lengths (2.09(7), 2.10(4), and 2.11(2) Å, respectively). The nitrogen of the *tert*-butylamide ligand (N4) is observed to adopt a nearly planar geometry, which may be accounted for by Bent's rule.²¹

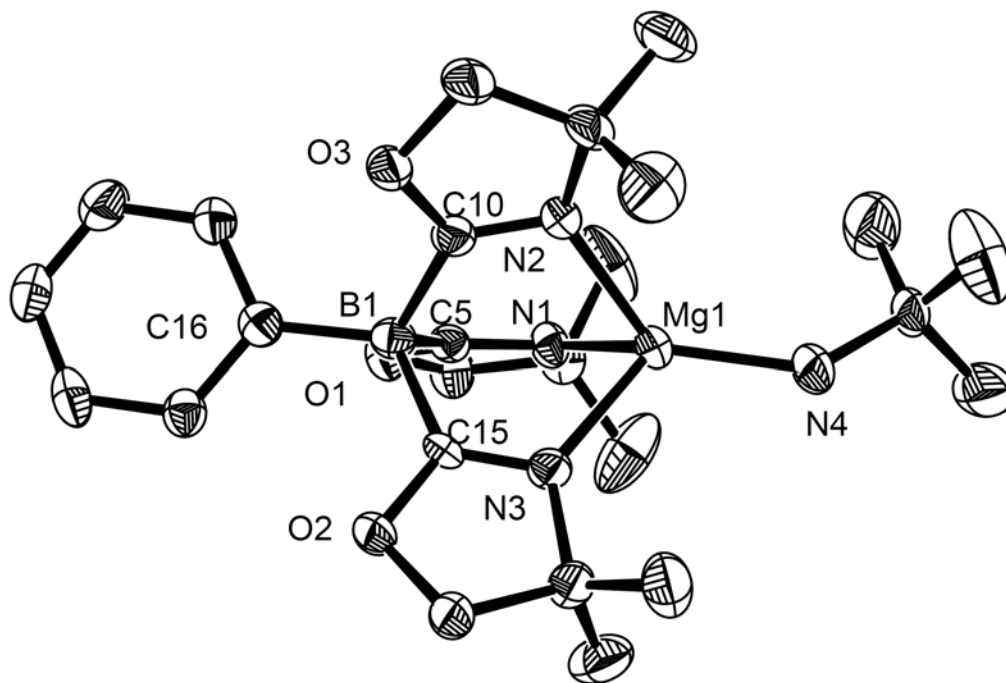


Figure 5.3. ORTEP of $\text{To}^{\text{Mg}}\text{NH}^t\text{Bu}$ drawn at 50% probability. Hydrogen atoms have been omitted for clarity.

This magnesium amide species reacts rapidly with both primary and secondary organosilanes to give the expected silazane products, and so the rate of Si–N bond formation could be directly examined. Addition of $\text{To}^{\text{Mg}}\text{NH}^t\text{Bu}$ to a toluene- d_8 solution of PhMeSiH_2 (1.4 equiv, $-20\text{ }^\circ\text{C}$ to $80\text{ }^\circ\text{C}$) reacts to give $\text{PhMeHSiNH}^t\text{Bu}$ quantitatively. A black precipitate is observed as the reaction proceeds and this was assigned as the decomposition product of $\text{To}^{\text{Mg}}\text{MgH}$. In an attempt to isolate the Mg–H intermediate, $\text{To}^{\text{Mg}}\text{MgMe}$ was mixed with a large excess of PhSiH_3 (100 equiv). Heating this solution to 80

°C over a period of 3 hours resulted in the generation of PhMeSiH_2 , as well as a new set of To^{M} resonances in the ^1H NMR spectrum. Additionally, a singlet resonance appeared at 6 ppm that integrated for one hydrogen relative to the unidentified To^{M} species and based on this, the new To^{M} species was tentatively assigned as $\text{To}^{\text{M}}\text{MgH}$. Unfortunately, we were unable to isolate the $\text{To}^{\text{M}}\text{MgH}$ as it rapidly decomposed in the absence of excess silane. Under catalytic conditions in which excess amine is present, only the $\text{To}^{\text{M}}\text{MgNHR}$ is observed in the ^1H NMR spectrum indicating that protonolysis by free amine to give the magnesium amide is rapid.

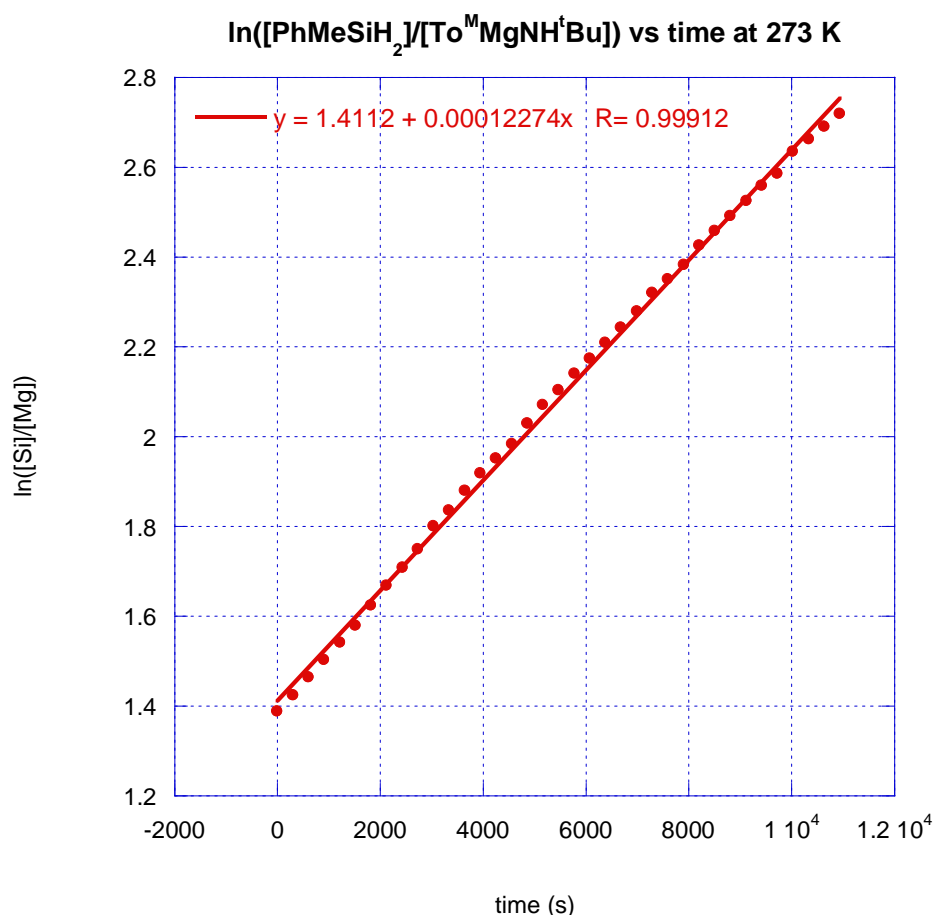
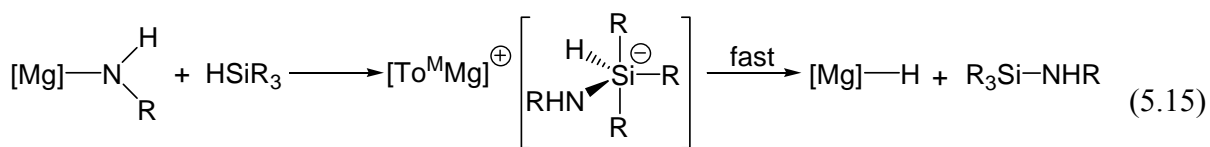
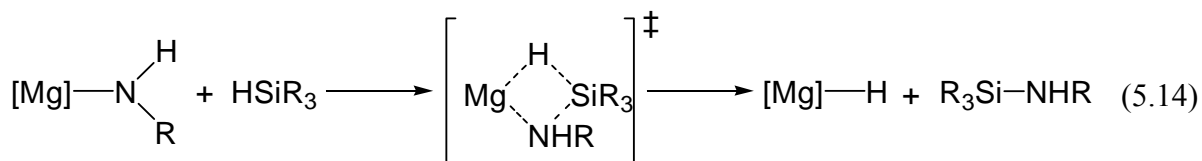


Figure 5.4. Plot of $\ln\{[\text{PhMeSiH}_2]/[\text{To}^{\text{M}}\text{MgNH}^t\text{Bu}]\}$ vs time at 0 °C for three half lives. $[\text{PhMeSiH}_2]_0 = 42$ mM, $[\text{To}^{\text{M}}\text{MgNH}^t\text{Bu}]_0 = 10.5$ mM.

Second order kinetic plots of $\ln\{[\text{PhMeSiH}_2]/[\text{To}^{\text{M}}\text{MgNH}^t\text{Bu}]\}$ vs time (Figure 5.4) are linear through three half-lives demonstrating that the reaction is first order both in silane and magnesium and gives an integrated rate law of $\text{rate} = k[\text{To}^{\text{M}}\text{MgNH}^t\text{Bu}]^1[\text{PhMeSiH}_2]^1$. The slope of the second-order plot was used to determine the second-order rate constant, $k = (3.906 \pm 0.003) \times 10^{-3} \text{ M}^{-1}\text{s}^{-1}$ at 0°C .²²

The activation parameters, calculated from plots of $\ln(k/T)$ vs $1/T$ over a temperature range of -20°C to 80°C , are $\Delta H^\ddagger = 5.9 \pm 0.1 \text{ kcal/mol}$ and $\Delta S^\ddagger = -46.5 \pm 0.5 \text{ e.u.}$ suggesting a highly ordered transition state (Figure 5.5).²² The transition state described above is consistent with two possible turnover limiting steps. The first is a four-centered, σ -bond metathesis pathway involving concerted Mg–H and Si–N bond formation as well as Mg–N and Si–H bond cleavage. The second possible pathway involves the nucleophilic attack of amide nitrogen on the silicon center, resulting in the formation of a five-coordinate silyl center. This charge separated species can then rapidly transfer a hydride from the silicon anion to the magnesium cation generating the product and $\text{To}^{\text{M}}\text{MgH}$ species (eqs 5.14 and 5.15).



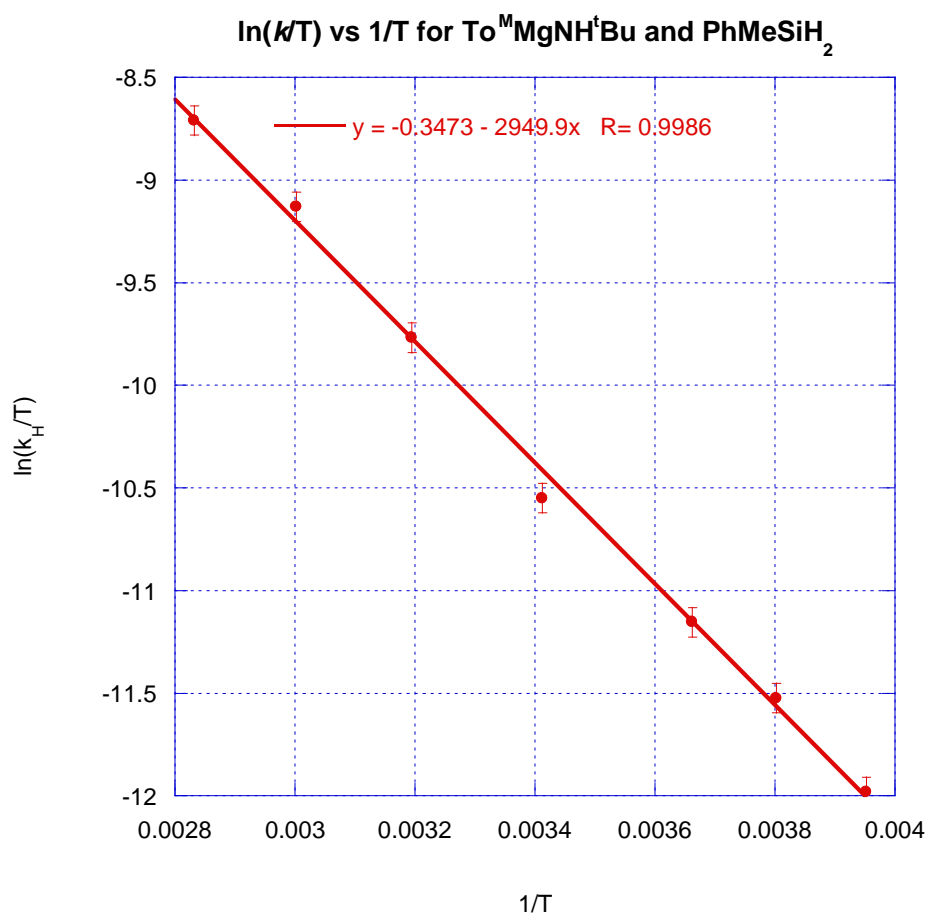


Figure 5.5. Eyring plot of $\ln(k/T)$ vs $1/T$ for reaction of $\text{To}^{\text{M}}\text{MgNH}^{\text{t}}\text{Bu} + \text{PhMeSiH}_2$ over the temperature range of -20 to 80 °C. $[\text{PhMeSiH}_2]_0 = 42$ mM, $[\text{To}^{\text{M}}\text{MgNH}^{\text{t}}\text{Bu}]_0 = 10.5$ mM.

As σ -bond metathesis involves the cleavage of a Si–H bond in the rate-determining step, a large primary isotope effect should be observable if the reaction proceeds through this pathway. To test this, the rate constant was measured for the reaction of $\text{To}^{\text{M}}\text{Mg}^{\text{t}}\text{Bu}$ with PhMeSiD_2 . A primary kinetic isotope effect of $k_{\text{H}}/k_{\text{D}} = 1.04$ at 0 °C was measured for the reaction, and was constant over the measured temperature range of -20 °C to 80 °C. This small isotope effect indicates that there is little to no Si–H bond cleavage during the

transition state, supporting the formation of a hyper-valent silyl center. However, an early σ -bond metathesis transition state with highly non-linear geometry would also exhibit a small KIE.²³ Additionally, a five-coordinate silyl center would result in significant charge build-up which is disfavored in non-polar solvents. As both the catalytic and stoichiometric reactions proceed readily in either benzene or toluene, it seems unlikely that a five-coordinate silyl center is formed.

Density functional theory (DFT) calculations were employed to more clearly distinguish between these two mechanistic pathways. ToMgNHMe (To = tris(2-oxazoliny)hydrido borate) was used as model for To^MMgNH^tBu, and SiH₄ was used in place of PhMeSiH₂. Optimized geometries containing zero imaginary frequencies were obtained for ToMgNHMe, SiH₄, ToMgH, and MeHNSiH₃, along with two interesting intermediate species (Figures 5.6 and 5.7). As the SiH₄ molecule approaches ToMgNHMe, the silicon center is observed to adopt a trigonal bipyramidal geometry with three equatorial hydrogens and one axial hydrogen (Figure 5.6). The axial Si–H bond length lengthens slightly from 1.48 Å to 1.52 Å, while the equatorial Si–H bonds remain at 1.49 Å. Additionally, the Mg–N bond is observed to lengthen from 1.93 Å (prior to SiH₄ approach) to 2.00 Å.

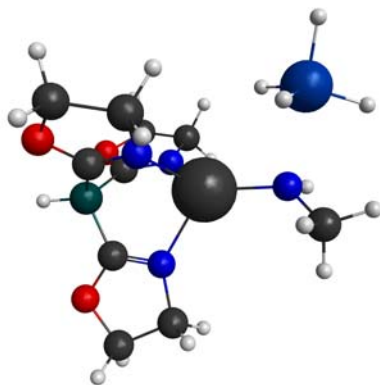


Figure 5.6. Calculated intermediate showing SiH₄ approach of ToMgNHMe.

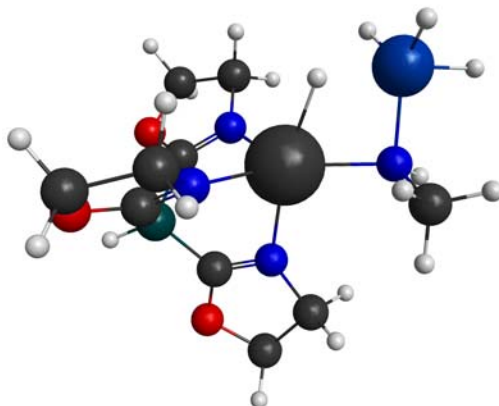


Figure 5.7. ToMgH•MeHNSiH₃ intermediate from DFT calculations.

After formation of the Si–N bond, a To^MMgH silazane adduct is observed (Figure 5.7). The ToMgH•NHMeSiH₃ intermediate displays a longer Mg–H bond than ToMgH (1.94 vs 1.74 Å), as well as a longer Mg–N bond than ToMgNHMe (2.12 vs 1.93 Å). Unfortunately, an optimized geometry for the transition state has not yet been obtained for the system and further calculations are currently underway to determine the exact pathway.

Conclusion

The monomeric magnesium alkyl To^MMgMe is a precatalyst for the coupling between the N–H bonds in amines and Si–H bonds in organosilanes to give Si–N bonds and H₂. Primary aliphatic amines and anilines react catalytically under ambient conditions to give silazanes. Primary and secondary silanes are effective coupling partners, while tertiary silanes are too sterically crowded to react in an appreciable amount. Using this catalyst system, a range of silazanes can be prepared in high yield with selective product formation. Notably, polysilazane formation is not observed, nor is the formation of polysilane. The

absence of these species is in contrast with reported early transition metal systems in which competitive Si–Si homocoupling is observed and polysilanes are formed in moderate to high yields.¹⁸ The isolable nature of the catalyst resting state, $To^M MgNHR$, allows for an in-depth investigation of the Si–N bond forming step. While the current kinetic and DFT studies do not provide conclusive evidence for the turnover limiting step of the catalytic cycle, nucleophilic attack of the nitrogen on silicon to form a zwitterionic transition state is favored. Further kinetic studies in which the substituents on both the amine and silane are individually varied may provide more conclusive evidence as to which reaction pathway is operative during catalysis. Since the formation of a five-coordinate silyl center will result in significant charge build-up, the generation of a Hammett plot may be useful in evaluating the likelihood of this reaction path. Additionally, structural changes on either the amine or silane could result in the observation of the $To^M MgH$ silazane adduct predicted by DFT. The ability of $To^M MgMe$ to selectively form monomeric silazanes illustrates the utility of alkaline earth metals in catalysis, and the facile functionalization of ammonia is indicative of the ways in which main group metal catalysts may be superior to the transition and rare earth metal analogs.

Experimental

General. All reactions were performed under a dry argon atmosphere using standard Schlenk techniques or under a nitrogen atmosphere in a glovebox unless otherwise indicated. Water and oxygen were removed from benzene, toluene, pentane, diethyl ether, and tetrahydrofuran solvents using an IT PureSolv system. Benzene- d_6 and tetrahydrofuran- d_8 were heated to reflux over Na/K alloy and vacuum-transferred. Prior to reactions, all glassware was

silylated by rinsing with a solution of 10% trimethylsilylchloride in chloroform in order to prevent disproportionation of the resulting silazane products. $\text{PhSi}(\text{NH}^n\text{Pr})_3$, $\text{PhMeHSi}(\text{NH}^n\text{Pr})$, $\text{PhMeSi}(\text{NH}^n\text{Pr})_2$, $\text{PhH}_2\text{Si}(\text{NH}^i\text{Pr})$, $\text{PhHSi}(\text{NH}^i\text{Pr})_2$, $\text{PhH}_2\text{Si}(\text{NH}^t\text{Bu})$ ¹⁹, $\text{Ph}_2\text{HSi}(\text{NHPh})$ ¹⁷, $\text{Ph}_2\text{Si}(\text{NH}^n\text{Pr})_2$ ²⁴, $\text{PhMeHSi}(\text{NHPh})$ ²⁵, and Et_3SiNH_2 ²⁶ have all been previously reported. ^1H and $^{13}\text{C}\{^1\text{H}\}$ NMR spectra were collected on a Bruker DRX400 spectrometer. ^{11}B NMR spectra were referenced to an external sample of $\text{BF}_3\cdot\text{Et}_2\text{O}$. ^{15}N chemical shifts were determined by ^1H - ^{15}N HMBC experiments on a Bruker Avance II 700 spectrometer with a Bruker Z-gradient inverse TXI $^1\text{H}/^{13}\text{C}/^{15}\text{N}$ 5mm cryoprobe; ^{15}N chemical shifts were originally referenced to liquid NH_3 and recalculated to the CH_3NO_2 chemical shift scale by adding -381.9 ppm. Elemental analyses were performed using a Perkin-Elmer 2400 Series II CHN/S by the Iowa State Chemical Instrumentation Facility. X-ray diffraction data was collected on a Bruker APEX II as described below.

To^MMgNH^tBu. A benzene solution of $\text{To}^{\text{M}}\text{MgMe}$ (1.50 g, 3.56 mmol, 60 mL) was placed in a 100 mL Teflon-resealable flask. *Tert*-butyl amine (0.41 mL, 3.9 mmol) was added, the flask was sealed, and the solution was heated at 75 °C for 18 h. The reaction mixture was allowed to cool to room temperature, and then the volatile materials were removed under vacuum. The resulting white solid $\text{To}^{\text{M}}\text{MgNH}^t\text{Bu}$ was obtained in sufficient purity for further reactions (1.53 g, 3.20 mmol, 89.9%). X-ray quality crystals were obtained from a concentrated toluene solution cooled to -30 °C. ^1H NMR (benzene-*d*₆, 400 MHz): δ 8.30 (d, $^3J_{\text{HH}} = 7.6$ Hz, 2 H, *ortho*-C₆H₅), 7.55 (t, $^3J_{\text{HH}} = 7.6$ Hz, 2 H, *meta*-C₆H₅), 7.36 (d, $^3J_{\text{HH}} = 7.6$ Hz, 1 H, *para*-C₆H₅), 3.93 (s, 6 H, $\text{CNCMe}_2\text{CH}_2\text{O}$), 1.63 (s, 9 H, NHCMe_3), 1.09 (s, 18 H, $\text{CNCMe}_2\text{CH}_2\text{O}$), -0.20 (s, 1 H, NHCMe_3).

$^{13}\text{C}\{^1\text{H}\}$ NMR (benzene- d_6 , 100 MHz): δ 191.11 (CNCMe $_2$ CH $_2$ O), 148.66 (*ipso*-C $_6$ H $_5$), 135.75 (*ortho*-C $_6$ H $_5$), 126.42 (*meta*-C $_6$ H $_5$), 125.45 (*para*-C $_6$ H $_5$), 79.74 (CNCMe $_2$ CH $_2$ O), 65.11 (CNCMe $_2$ CH $_2$ O), 38.21 (NHCMe $_3$), 28.78 (NHCMe $_3$), 27.91 (CNCMe $_2$ CH $_2$ O). ^{11}B NMR (benzene- d_6 , 128 MHz): δ -18.3. ^{15}N NMR (benzene- d_6 , 71 MHz): δ -158.4 (CNCMe $_2$ CH $_2$ O), -117.8 (NHCMe $_3$). IR (KBr, cm^{-1}): 3072 w, 3044 w, 2964 s, 2888 s, 2810 w, 1590 s (ν_{CN}), 1495 w, 1463 m, 1431 w, 1386 w, 1366 m, 1270 s, 1250 m, 1195 s, 1153 s, 1116 m, 989 m sh, 966 s, 894 w, 744 w, 704 s, 652 m. Anal. Calc. for C $_{25}$ H $_{39}$ O $_3$ N $_4$ BMg: C, 62.75; H, 8.16; N, 11.71. Found: C, 62.71; H, 8.24; N, 11.71. mp: 189-191 °C, dec.

Representative procedure for reactions of organosilanes and aliphatic amines.

PhSi(NH n Pr) $_3$. ToMMgMe (0.020 g, 0.048 mmol, 5 mol%) was dissolved in benzene (5 mL). The organosilane (PhSiH $_3$, 0.10 g, 0.95 mmol) was added to the solution, followed by the addition of amine (H $_2$ N n Pr, 0.20 g, 3.3 mmol). Immediately, the mixture was effervescent, the vial was quickly capped to prevent the solution from foaming out, and was stirred for 24 h. A brown precipitate was observed to form after 18 h as the catalyst decomposed due to the consumption of free amine. The solutions were filtered to remove magnesium salts and solvent was removed under vacuum. The remaining residue could then be purified by Kugelrohr distillation, if necessary. Yield: 0.263 g, 99%, ^1H NMR (benzene- d_6 , 400 MHz): δ 7.77 (mult, 2 H, *ortho*-C $_6$ H $_5$), 7.30 (mult, 3 H, *meta*- and *para*-C $_6$ H $_5$), 2.82 (q, $^3J_{\text{HH}} = 7.0$ Hz, 6 H, NHCH $_2$ CH $_2$ CH $_3$), 1.39 (sextet, $^3J_{\text{HH}} = 7.0$ Hz, 6 H., NHCH $_2$ CH $_2$ CH $_3$), 0.85 (t, $^3J_{\text{HH}} = 7.0$ Hz, 9 H, NHCH $_2$ CH $_2$ CH $_3$), 0.76 (br s, 3 H, NH)., $^{13}\text{C}\{^1\text{H}\}$ NMR (benzene- d_6 , 100 MHz): δ 139.57 (*ipso*-C $_6$ H $_5$), 135.00 (*ortho*-C $_6$ H $_5$), 129.61 (*meta*-C $_6$ H $_5$), 128.28 (*para*-C $_6$ H $_5$), 44.01 (NHCH $_2$ CH $_2$ CH $_3$), 28.53 (NHCH $_2$ CH $_2$ CH $_3$), 12.00 (NHCH $_2$ CH $_2$ CH $_3$),.

^{15}N NMR (benzene- d_6 , 41 MHz): δ -353.52 (d, $^2J_{\text{NH}} = 76$ Hz)., ^{29}Si NMR (benzene- d_6 , 79 MHz): δ -33.41., IR (neat, cm^{-1}): 3411 s (ν_{NH}), 3067 m, 2957 s, 2929 s, 2872 s, 2857, 1456 m, 1428 m, 1398 s, 1116 s, 1076 m, 1007 s, 839 m, 737 m, 701 m.

PhMeHSi(NHⁿPr). A procedure similar to that described for PhSi(NHⁿPr)₃ was followed, using PhMeSiH₂ (0.23 g, 1.9 mmol) as the silane and H₂NⁿPr (0.056 g, 0.95 mmol). Yield: 0.13 g, 78%. ^1H NMR (benzene- d_6 , 400 MHz): δ 7.65 (mult, 2 H, *ortho*-C₆H₅), 7.24 (mult, 3 H, *meta*- and *para*-C₆H₅), 5.15 (t, $^3J_{\text{HH}} = 2.6$ Hz, 1 H, SiH), 2.61 (q, $^3J_{\text{HH}} = 7.0$ Hz, 2 H, NHCH₂CH₂CH₃), 1.27 (sextet, $^3J_{\text{HH}} = 7.0$ Hz, 2 H, NHCH₂CH₂CH₃), 0.75 (t, $^3J_{\text{HH}} = 7.0$ Hz, 3 H, NHCH₂CH₂CH₃), 0.39 (br s, 1 H, NH), 0.30 (d, $^3J_{\text{HH}} = 3.0$ Hz, 3 H, SiMe). $^{13}\text{C}\{^1\text{H}\}$ NMR (benzene- d_6 , 100 MHz): δ 138.72 (*ipso*-C₆H₅), 134.79 (*ortho*-C₆H₅), 130.18 (*meta*-C₆H₅), 128.54 (*para*-C₆H₅), 45.31 (NHCH₂CH₂CH₃), 28.07 (NHCH₂CH₂CH₃), 11.77 (NHCH₂CH₂CH₃), -2.34 (SiMe). ^{15}N NMR (benzene- d_6 , 41 MHz): δ -351.72. ^{29}Si NMR (benzene- d_6 , 79 MHz): δ -14.23., IR (neat, cm^{-1}): 3372 br s (ν_{NH}), 3068 s, 2959 s, 2929 s, 2873 s, 2129 br s (ν_{SiH}), 1456 m, 1428 m, 1399 m, 1253 s, 1120 s, 871 m, 844 m, 699 m.

PhMeSi(NHⁿPr)₂. A procedure similar to that described for PhSi(NHⁿPr)₃ was followed, using PhMeSiH₂ (0.12 g, 0.95 mmol) as the silane and H₂NⁿPr (0.17 g, 2.9 mmol). Yield: 0.21 g, 92%. ^1H NMR (benzene- d_6 , 400 MHz): δ 7.72 (mult, 2 H, *ortho*-C₆H₅), 7.28 (mult, 3 H, *meta*- and *para*-C₆H₅), 2.75 (q, $^3J_{\text{HH}} = 7.2$ Hz, 4 H, NHCH₂CH₂CH₃), 1.35 (sextet, $^3J_{\text{HH}} = 7.2$ Hz, 4 H, NHCH₂CH₂CH₃), 0.83 (t, $^3J_{\text{HH}} = 7.2$ Hz, 6 H, NHCH₂CH₂CH₃), 0.65 (br s, 2 H, NH), 0.29 (s, 3 H, SiMe). $^{13}\text{C}\{^1\text{H}\}$ NMR (benzene- d_6 , 100 MHz): δ 140.36 (*ipso*-C₆H₅), 134.79 (*ortho*-C₆H₅), 129.72 (*meta*-C₆H₅), 128.34 (*para*-C₆H₅), 44.05 (NHCH₂CH₂CH₃), 28.46 (NHCH₂CH₂CH₃), 11.97 (NHCH₂CH₂CH₃), -1.86 (SiMe). ^{15}N NMR (benzene- d_6 , 41 MHz): δ -353.21 (d, $^2J_{\text{NH}} = 76$ Hz). ^{29}Si NMR (benzene- d_6 , 79 MHz): δ -17.32. IR (neat, cm^{-1}

¹): 3411 br s (ν_{NH}), 3067 s, 2958 s, 2929 s, 2873 s, 2857 s, 1457 m, 1428 m, 1398 m, 1252 s, 1232 m, 1115 s, 1007 m, 892 m, 848 m, 701 m.

Ph₂HSi(NHⁿPr). A procedure similar to that described for PhSi(NHⁿPr)₃ was followed, using Ph₂SiH₂ (0.35 g, 1.9 mmol) as the silane and H₂NⁿPr (0.056 g, 0.95 mmol). Yield: 0.22 g, 97%. ¹H NMR (benzene-*d*₆, 400 MHz): δ 7.71 (mult, 4 H, *ortho*-C₆H₅), 7.21 (mult, 6 H, *meta*- and *para*-C₆H₅), 5.61 (d, ³*J*_{HH} = 2.0 Hz, 1 H, SiH), 2.69 (q, ³*J*_{HH} = 7.0 Hz, 2 H, NHCH₂CH₂CH₃), 1.29 (sextet, ³*J*_{HH} = 7.0 Hz, 2 H, NHCH₂CH₂CH₃), 0.73 (t, ³*J*_{HH} = 7.0 Hz, 3 H, NHCH₂CH₂CH₃), 0.69 (br s, 1 H, NH). ¹³C{¹H} NMR (benzene-*d*₆, 100 MHz): δ 135.69 (*ipso*-C₆H₅), 134.91 (*ortho*-C₆H₅), 129.78 (*meta*-C₆H₅), 128.10 (*para*-C₆H₅), 44.73 (NHCH₂CH₂CH₃), 27.26 (NHCH₂CH₂CH₃), 11.04 (NHCH₂CH₂CH₃). ¹⁵N NMR (benzene-*d*₆, 41 MHz): δ -333.42. ²⁹Si NMR (benzene-*d*₆, 79 MHz): δ -17.29. IR (neat, cm⁻¹): 3404 br s (ν_{NH}), 3068 s, 3050 s, 3018 s, 3000 s, 2958 s, 2928 s, 2872 s, 2857 m, 2137 br s (ν_{SiH}), 1589 m, 1428 m, 1121 m, 1006 m, 937 m, 838 m, 734 m, 698 m. Anal. Calc. for C₁₅H₁₉NSi: C, 74.63; H, 7.93; N, 5.80. Found: C, 74.72; H, 7.88; N, 5.81.

Ph₂Si(NHⁿPr)₂. A procedure similar to that described for PhSi(NHⁿPr)₃ was followed, using Ph₂SiH₂ (0.18 g, 0.95 mmol) as the silane and H₂NⁿPr (0.17 g, 2.9 mmol). Yield: 0.28 g, 99%. ¹H NMR (benzene-*d*₆, 400 MHz): δ 7.74 (mult, 4 H, *ortho*-C₆H₅), 7.24 (mult, 6 H, *meta*- and *para*-C₆H₅), 2.84 (q, ³*J*_{HH} = 7.0 Hz, 4 H, NHCH₂CH₂CH₃), 1.38 (sextet, ³*J*_{HH} = 7.0 Hz, 4 H, NHCH₂CH₂CH₃), 1.03 (br s, 2 H, NH), 0.81 (t, ³*J*_{HH} = 7.0 Hz, 6 H, NHCH₂CH₂CH₃). ¹³C{¹H} NMR (benzene-*d*₆, 100 MHz): δ 138.31 (*ipso*-C₆H₅), 135.49 (*ortho*-C₆H₅), 129.94 (*meta*-C₆H₅), 128.40 (*para*-C₆H₅), 44.17 (NHCH₂CH₂CH₃), 28.31 (NHCH₂CH₂CH₃), 11.96 (NHCH₂CH₂CH₃). ¹⁵N NMR (benzene-*d*₆, 41 MHz): δ -354.88 (d, ²*J*_{NH} = 76 Hz). ²⁹Si NMR (benzene-*d*₆, 79 MHz): δ -25.55. IR (neat, cm⁻¹): 3409 br m (ν_{NH}),

3067 m, 3049 m, 2957 s, 2929 s, 2872 s, 2857 s, 1465 m, 1428 s, 1398 s, 1117 br s, 1007 s, 998 m, 840 m, 737 s, 701 s.

PhH₂Si(NHⁱPr). A procedure similar to that described for PhSi(NHⁿPr)₃ was followed, using PhSiH₃ (0.21 g, 1.9 mmol) as the silane and H₂NⁱPr (0.056 g, 0.95 mmol). Yield: 0.071 g, 45%. ¹H NMR (benzene-*d*₆, 400 MHz): δ 7.69 (mult, 2 H, *ortho*-C₆H₅), 7.21 (mult, 3 H, *meta*- and *para*-C₆H₅), 5.19 (d, ³J_{HH} = 2 Hz, 2 H, SiH), 3.08 (sextet, ³J_{HH} = 6.8 Hz, 1 H, NHCHMe₂), 1.06 (d, ³J_{HH} = 6.8 Hz, 6 H, NHCHMe₂), 0.61 (br s, 1 H, NH). ¹³C{¹H} NMR (benzene-*d*₆, 100 MHz): δ 135.53 (*ipso*-C₆H₅), 135.30 (*ortho*-C₆H₅), 130.17 (*meta*-C₆H₅), 128.54 (*para*-C₆H₅), 48.00 (NHCH₂Me₂), 24.76 (NHCH₂Me₂). ¹⁵N NMR (benzene-*d*₆, 41 MHz): δ -334.45. ²⁹Si NMR (benzene-*d*₆, 79 MHz): δ -38.22. IR (KBr, cm⁻¹): 3410 br s (ν_{NH}), 3068 s, 3044 s, 2928 s, 2869 s, 2131 br s (ν_{SiH}), 1570 m, 1461 s, 1365 s, 1267 s, 1116 s, 965 s, 858 m, 639 m.

PhHSi(NHⁱPr)₂. A procedure similar to that described for PhSi(NHⁿPr)₃ was followed, using PhSiH₃ (0.10 g, 0.95 mmol) as the silane and H₂NⁱPr (0.140 g, 2.38 mmol). Yield: 0.21 g, 99%. ¹H NMR (benzene-*d*₆, 400 MHz): δ 7.73 (mult, 2 H, *ortho*-C₆H₅), 7.27 (mult, 3 H, *meta*- and *para*-C₆H₅), 5.22 (s, 1 H, SiH), 3.22 (sextet, ³J_{HH} = 5.6 Hz, 2 H, NHCHMe₂), 1.03 (d, ³J_{HH} = 5.6 Hz, 12 H, NHCHMe₂), 0.91 (br s, 2 H, NH). ¹³C{¹H} NMR (benzene-*d*₆, 100 MHz): δ 136.79 (*ipso*-C₆H₅), 135.30 (*ortho*-C₆H₅), 130.25 (*meta*-C₆H₅), 128.93 (*para*-C₆H₅), 47.99 (NHCH₂Me₂), 24.71 (NHCH₂Me₂). ¹⁵N NMR (benzene-*d*₆, 41 MHz): δ -334.35. ²⁹Si NMR (benzene-*d*₆, 79 MHz): δ -37.96. IR (neat, cm⁻¹): 3583 br s (ν_{NH}), 3068 s, 3051 m, 2963 s, 2928 s, 2869 s, 2148 br s (ν_{SiH}), 1461 m, 1429 m, 1363 m, 1182 m, 1114 s, 990 s, 889 s, 699 s.

PhMeHSi(NHⁱPr). A procedure similar to that described for PhSi(NHⁿPr)₃ was followed, using PhMeSiH₂ (0.12 g, 0.95 mmol) as the silane and H₂NⁱPr (0.11 g, 1.9 mmol). Yield: 0.029 g, 67%. ¹H NMR (benzene-*d*₆, 400 MHz): δ 7.64 (mult, 2 H, *ortho*-C₆H₅), 7.24 (mult, 3 H, *meta*- and *para*-C₆H₅), 5.16 (t, ³J_{HH} = 3.2 Hz, 1 H, SiH), 2.99 (*pseudo*-sextet, ³J_{HH} = 6.4 Hz, 1 H, NHCHMe₂), 0.96 (d, ³J_{HH} = 6.4 Hz, 3 H, NHCHMe₂), 0.94 (d, ³J_{HH} = 6.4 Hz, 3 H, NHCHMe₂), 0.36 (br s, 1 H, NH), 0.29 (d, ³J_{HH} = 3.2 Hz, 3 H, SiMe). ¹³C{¹H} NMR (benzene-*d*₆, 100 MHz): δ 138.99 (*ipso*-C₆H₅), 134.78 (*ortho*-C₆H₅), 130.16 (*meta*-C₆H₅), 128.53 (*para*-C₆H₅), 44.57 (NHCH₂Me₂), 27.77 (NHCH₂Me₂), 27.70 (NHCH₂Me₂), -1.95 (SiMe). ¹⁵N NMR (benzene-*d*₆, 41 MHz): δ -340.53. ²⁹Si NMR (benzene-*d*₆, 79 MHz): δ -16.82. IR (neat, cm⁻¹): 3395 s (ν_{NH}), 3068 s, 3051 m, 2999 s, 2959 s, 2928 s, 2868 m, 2098 s (ν_{SiH}), 1428 s, 1399 m, 1250 s, 1115 s, 1014 s, 881 s, 724 s, 699. Anal. Calc. for C₁₀H₁₇NSi: C, 66.97; H, 9.55; N, 7.81. Found: C, 67.02; H, 9.49; N, 7.95.

Ph₂HSi(NHⁱPr). A procedure similar to that described for PhSi(NHⁿPr)₃ was followed, using Ph₂SiH₂ (0.18 g, 0.95 mmol) as the silane and H₂NⁱPr (0.11 g, 1.9 mmol). Yield: 0.22 g, 97%. ¹H NMR (benzene-*d*₆, 400 MHz): δ 7.72 (mult, 4 H, *ortho*-C₆H₅), 7.22 (mult, 6 H, *meta*- and *para*-C₆H₅), 5.63 (d, ³J_{HH} = 2 Hz, 1 H, SiH), 3.07 (sextet, ³J_{HH} = 6.2 Hz, 1 H, NHCHMe₂), 0.97 (d, ³J_{HH} = 6.2 Hz, 6 H, NHCHMe₂), 0.66 (br s, 1 H, NH). ¹³C{¹H} NMR (benzene-*d*₆, 100 MHz): δ 136.79 (*ipso*-C₆H₅), 135.59 (*ortho*-C₆H₅), 130.45 (*meta*-C₆H₅), 128.64 (*para*-C₆H₅), 44.77 (NHCH₂Me₂), 27.62 (NHCH₂Me₂). ¹⁵N NMR (benzene-*d*₆, 41 MHz): δ -341.62 (d, ²J_{NH} = 68 Hz). ²⁹Si NMR (benzene-*d*₆, 79 MHz): δ -20.18. IR (neat, cm⁻¹): 3392 br s (ν_{NH}), 3135 m, 3068 s, 3050 s, 2999 s, 2959 s, 2927 s, 2868 s, 2100 br s (ν_{SiH}), 1589 m, 1462 m, 1429 m, 1399 m, 1166 m, 1109 m, 1013 m, 805 m, 696 m. Anal. Calc. for C₁₅H₁₉NSi: C, 74.63; H, 7.93; N, 5.80. Found: C, 74.53; H, 7.87; N, 6.11.

PhH₂Si(NH^tBu). A procedure similar to that described for PhSi(NHⁿPr)₃ was followed, using PhSiH₃ (0.10 g, 0.95 mmol) as the silane and H₂N^tBu (0.174 g, 2.38 mmol). Yield: 0.15 g, 87%. ¹H NMR (benzene-*d*₆, 400 MHz): δ 7.68 (mult, 2 H, *ortho*-C₆H₅), 7.20 (mult, 3 H, *meta*- and *para*-C₆H₅), 5.12 (d, ³J_{HH} = 3.2 Hz, 2 H, SiH), 1.06 (s, 9 H, NHCMe₃), 0.67 (br s, 1 H, NH). ¹³C{¹H} NMR (benzene-*d*₆, 100 MHz): δ 136.85 (*ipso*-C₆H₅), 135.34 (*ortho*-C₆H₅), 130.40 (*meta*-C₆H₅), 128.64 (*para*-C₆H₅), 49.67 (NHCMe₃), 33.21 (NHCMe₃). ¹⁵N NMR (benzene-*d*₆, 41 MHz): δ -336.79. ²⁹Si NMR (benzene-*d*₆, 79 MHz): δ -37.36. IR (neat, cm⁻¹): 3389 br s (ν_{NH}), 3068 s, 3051 s, 3000 s, 2961 s, 2904 s, 2868 s, 2139 br s (ν_{SiH}), 1464 s, 1428 m, 1374 s, 1219 s, 1116 m, 1012 m, 742 m, 699 m.

PhMeHSi(NH^tBu). A procedure similar to that described for PhSi(NHⁿPr)₃ was followed, using PhMeSiH₂ (0.12 g, 0.95 mmol) as the silane and H₂N^tBu (0.14 g, 1.9 mmol). Yield: 0.11 g, 60%. ¹H NMR (benzene-*d*₆, 400 MHz): δ 7.67 (mult, 2 H, *ortho*-C₆H₅), 7.23 (mult, 3 H, *meta*- and *para*-C₆H₅), 5.23 (quintet, ³J_{HH} = 3.0 Hz, 1 H, SiH), 1.08 (s, 9 H, NHCMe₃), 0.64 (br s, 1 H, NH), 0.30 (d, ³J_{HH} = 3.0 Hz, 3 H, SiMe). ¹³C{¹H} NMR (benzene-*d*₆, 100 MHz): δ 140.02 (*ipso*-C₆H₅), 134.67 (*ortho*-C₆H₅), 130.00 (*meta*-C₆H₅), 128.52 (*para*-C₆H₅), 49.80 (NHCMe₃), 33.67 (NHCMe₃), -0.64 (PhMeSi). ¹⁵N NMR (benzene-*d*₆, 41 MHz): δ -329.65. ²⁹Si NMR (benzene-*d*₆, 79 MHz): δ -21.33. IR (KBr, cm⁻¹): 3506 br s (ν_{NH}), 3069 s, 2964 s, 2930 s, 2131 br s (ν_{SiH}), 1462 m, 1263 s, 1115 s, 887 m, 806 m, 703 m. Anal. Calc. for C₁₁H₁₉NSi: C, 68.33; H, 9.90; N, 7.24. Found: C, 68.29; H, 9.83; N, 7.25.

Ph₂HSi(NH^tBu). A procedure similar to that described for PhSi(NHⁿPr)₃ was followed, using Ph₂SiH₂ (0.18 g, 0.95 mmol) as the silane and H₂N^tBu (0.14 g, 1.9 mmol). Yield: 0.20 g, 81%. ¹H NMR (benzene-*d*₆, 400 MHz): δ 7.71 (mult, 4 H, *ortho*-C₆H₅), 7.20 (mult, 6 H, *meta*- and *para*-C₆H₅), 5.72 (d, ³J_{HH} = 3.2 Hz, 1 H, SiH), 1.11 (s, 9 H, NHCMe₃), 0.92 (br s,

1 H, NH). $^{13}\text{C}\{^1\text{H}\}$ NMR (benzene- d_6 , 100 MHz): δ 134.79 (*ipso*-C₆H₅), 131.33 (*ortho*-C₆H₅), 129.56 (*meta*-C₆H₅), 128.19 (*para*-C₆H₅), 32.90 (NHCM_e₃), 29.80 (NHCM_e₃). ^{15}N NMR (benzene- d_6 , 41 MHz): δ -329.66. ^{29}Si NMR (benzene- d_6 , 79 MHz): δ -18.71. IR (neat, cm⁻¹): 3384 br s (ν_{NH}), 3135 m, 3068 s, 3051 s, 3000 s, 2964 s, 2868 m, 2138 br s (ν_{SiH}), 1588 m, 1485 m, 1429 m, 1360 m, 1222 m, 1122 m, 936 m, 841 m, 697 m. Anal. Calc. for C₁₆H₂₁NSi: C, 75.23; H, 8.29; N, 5.48. Found: C, 75.40; H, 8.05; N, 5.51.

PhCH₂Me₂SiNHNH₂. A procedure similar to that described for PhSi(NHⁿPr)₃ was followed, using BnMe₂SiH (0.14 g, 0.95 mmol) as the silane and H₂NNH₂ (0.091 g, 2.85 mmol). Yield: 0.053 g, 31%. ^1H NMR (benzene- d_6 , 400 MHz): δ 7.19 (mult, 2 H, *ortho*-C₆H₅), 7.03 (mult, 3 H, *meta*- and *para*-C₆H₅), 2.35 (br s, 2 H, NH₂NHSi), 2.10 (s, 2 H, SiMe₂CH₂Ph), 2.07 (br s, 1 H, NH₂NHSi), 0.03 (s, 6 H, SiMe₂CH₂Ph). $^{13}\text{C}\{^1\text{H}\}$ NMR (benzene- d_6 , 100 MHz): δ 140.43 (*ipso*-C₆H₅), 129.04 (*ortho*-C₆H₅), 128.88 (*meta*-C₆H₅), 124.64 (*para*-C₆H₅), 26.52 (SiMe₂CH₂Ph), -2.90 (SiMe₂CH₂Ph). ^{15}N NMR (benzene- d_6 , 41 MHz): δ -335.06 (SiMHNH₂). ^{29}Si NMR (benzene- d_6 , 79 MHz): δ 2.51. IR (neat, cm⁻¹): 3421 sh (ν_{NH}), 3340 br s (ν_{NH}), 3081 m, 3060 s, 3023 s, 2962 s, 2927 s, 2884 m, 1598 m, 1493 m, 1451 m, 1364 m, 1251 s, 1153 s, 967 m, 836 m, 699 m. EA: Anal. Calc. for: C₉H₁₆N₂Si: C, 59.95; H, 8.94; N, 15.54. Found: C, 60.02; H, 9.01; N, 15.54.

Et₃SiNHNH₂. A procedure similar to that described for PhSi(NHⁿPr)₃ was followed, using Et₃SiH (0.11 g, 0.95 mmol) as the silane and H₂NNH₂ (0.091 g, 2.85 mmol). Yield: 0.079 g, 57%. ^1H NMR (benzene- d_6 , 400 MHz): δ 2.41 (br s, 2 H, NH₂), 2.14 (br s, 1 H, NHNH₂), 1.01 (t, $^3J_{\text{HH}} = 8.0$ Hz, 9 H, Si(CH₂CH₃)₃), 0.58 (d of q, $^3J_{\text{HH}} = 8.0$ Hz, $^4J_{\text{HH}} = 3.2$ Hz, 6 H, Si(CH₂CH₃)₃). $^{13}\text{C}\{^1\text{H}\}$ NMR (benzene- d_6 , 100 MHz): δ 8.76 (Si(CH₂CH₃)₃), -2.81 (Si(CH₂CH₃)₃). ^{15}N NMR (benzene- d_6 , 41 MHz): δ -332.63 (SiMHNH₂). ^{29}Si NMR (benzene-

d_6 , 79 MHz): δ -0.38. IR (neat, cm^{-1}): 3336 br s (ν_{NH}), 3289 br s (ν_{NH}), 2960 s, 2926 s, 2882 m, 1254 s, 1154 s, 1068 s, 835 m. Anal. Calc. for $\text{C}_6\text{H}_{18}\text{N}_2\text{Si}$: C, 49.26; H, 12.40; N, 19.15. Found: C, 49.13; H, 12.29; N, 19.10.

$\text{CH}_2=\text{CHCH}_2\text{Me}_2\text{SiNHNH}_2$. A procedure similar to that described for $\text{PhSi}(\text{NH}^i\text{Pr})_3$ was followed, using $\text{CH}_2\text{CHCH}_2\text{Me}_2\text{SiH}$ (0.095 g, 0.95 mmol) as the silane and H_2NNH_2 (0.091 g, 2.85 mmol). Yield: 0.082 g, 66%. ^1H NMR (benzene- d_6 , 400 MHz): δ 5.84 (mult, 1 H, $\text{CH}_2=\text{CHCH}_2\text{SiMe}_2$), 4.92 (mult, 2 H, $\text{CH}_2=\text{CHCH}_2\text{SiMe}_2$), 2.40 (br s, 2 H, NH_2NHSi), 2.14 (br s, 1 H, NH_2NHSi), 1.60 (d, $^3J_{\text{HH}} = 8.0$ Hz, 2 H, $\text{CH}_2=\text{CHCH}_2\text{SiMe}_2$), 0.06 (s, 6 H, $\text{CH}_2=\text{CHCH}_2\text{SiMe}_2$). $^{13}\text{C}\{^1\text{H}\}$ NMR (benzene- d_6 , 100 MHz): δ 135.92 ($\text{SiMe}_2\text{CH}_2\text{CH}=\text{CH}_2$), 113.27 ($\text{SiMe}_2\text{CH}_2\text{CH}=\text{CH}_2$), 24.35 ($\text{SiMe}_2\text{CH}_2\text{CH}=\text{CH}_2$), -2.96 ($\text{SiMe}_2\text{CH}_2\text{CH}=\text{CH}_2$). ^{15}N NMR (benzene- d_6 , 41 MHz): δ -329.25 (SiMHNH_2). ^{29}Si NMR (benzene- d_6 , 79 MHz): δ -2.25. IR (neat, cm^{-1}): 3334 br s (ν_{NH}), 3287 br s (ν_{NH}), 3077 s, 2960 s, 2925 s, 2883 m, 1457 m, 1254 s, 1155 s, 1067 s, 836 m, 667 m. Anal. Calc. for $\text{C}_5\text{H}_{14}\text{N}_2\text{Si}$: C, 46.10; H, 10.83; N, 21.51. Found: C, 45.96; H, 10.73; N, 21.46.

$\text{PhHSi}(\text{NHPH})_2$. A procedure similar to that described for $\text{PhSi}(\text{NH}^i\text{Pr})_3$ was followed, using PhSiH_3 (0.10 g, 0.95 mmol) as the silane and H_2NPh (0.221 g, 2.38 mmol). Yield: 0.27 g, 98%. ^1H NMR (benzene- d_6 , 400 MHz): δ 7.60 (d, $^3J_{\text{HH}} = 7.6$ Hz, 2 H, *ortho-PhSi*), 7.14 (mult, 3 H, *meta-* and *para-PhSi*), 7.04 (t, $^3J_{\text{HH}} = 7.6$ Hz, 4 H, *meta-NHPh*), 6.73 (t, $^3J_{\text{HH}} = 7.6$ Hz, 2 H, *para-NHPh*), 6.67 (d, $^3J_{\text{HH}} = 7.6$ Hz, 4 H, *ortho-NHPh*), 5.61 (s, 1 H, *SiH*), 3.45 (s, 2 H, *NHPh*). $^{13}\text{C}\{^1\text{H}\}$ NMR (benzene- d_6 , 100 MHz): δ 146.50 (*ipso-NHPh*), 135.15 (*ortho-PhSi*), 133.80 (*ipso-PhSi*), 131.37 (*meta-PhSi*), 129.99 (*meta-NHPh*), 128.93 (*para-PhSi*), 119.87 (*para-NHPh*), 117.47 (*ortho-NHPh*). ^{15}N NMR (benzene- d_6 , 41 MHz): δ -319.63. ^{29}Si NMR (benzene- d_6 , 79 MHz): δ -35.09. IR (neat, cm^{-1}): 3374 br s (ν_{NH}), 3069 s,

3040 s, 3011 m, 2148 br s (ν_{SiH}), 1498 m, 1474 m, 1429 m, 1287 m, 1116 m, 910 m, 829 m, 691 m. Anal. Calc. for $\text{C}_{18}\text{H}_{18}\text{N}_2\text{Si}$: C, 74.44; H, 6.25; N, 9.65. Found: C, 74.19; H, 6.19; N, 9.62.

PhMeHSi(NHPh). A procedure similar to that described for $\text{PhSi}(\text{NH}^n\text{Pr})_3$ was followed, using PhMeSiH_2 (0.12 g, 0.95 mmol) as the silane and H_2NPh (0.18 g, 1.9 mmol). The reaction mixture is heated to 60 °C while open to a nitrogen purge and the product is isolated by distilling off the solvent. Yield: 0.039 g, 19%. ^1H NMR (benzene- d_6 , 400 MHz): δ 7.55 (d, $^3J_{\text{HH}} = 7.6$ Hz, 2 H, *ortho-PhSi*), 7.15 (mult, 3 H, *meta-* and *para-PhSi*), 7.05 (t, $^3J_{\text{HH}} = 7.6$ Hz, 2 H, *meta-NHPh*), 6.72 (t, $^3J_{\text{HH}} = 7.6$ Hz, 1 H, *para-NHPh*), 6.61 (d, $^3J_{\text{HH}} = 7.6$ Hz, 2 H, *ortho-NHPh*), 5.24 (t, $^3J_{\text{HH}} = 3.2$ Hz, 1 H, *SiH*), 3.19 (br s, 1 H, *NHPh*), 0.27 (d, $^3J_{\text{HH}} = 3.2$ Hz, 3 H, *SiMe*). $^{13}\text{C}\{^1\text{H}\}$ NMR (benzene- d_6 , 100 MHz): δ 147.48 (*ipso-NHPh*), 136.11 (*ipso-PhSi*), 134.71 (*ortho-PhSi*), 130.64 (*meta-PhSi*), 129.92 (*meta-NHPh*), 128.79 (*para-PhSi*), 119.14 (*para-NHPh*), 117.04 (*ortho-NHPh*), -3.13 (*SiMe*). ^{15}N NMR (benzene- d_6 , 41 MHz): δ -318.60. ^{29}Si NMR (benzene- d_6 , 79 MHz): δ -19.98. IR (neat, cm^{-1}): 3378 br s (ν_{NH}), 3087 m, 3069 m, 3039 s, 3011 m, 2964 s, 2127 (ν_{SiH}), 1428 m, 1290 s, 900 s, 848 s, 752 s, 692 s.

Ph₂HSi(NHPh). A procedure similar to that described for $\text{PhSi}(\text{NH}^n\text{Pr})_3$ was followed, using Ph_2SiH_2 (0.18 g, 0.95 mmol) as the silane and H_2NPh (0.18 g, 1.9 mmol). The reaction mixture is heated to 60 °C while open to a nitrogen purge, and the product is isolated by distilling off the solvent. Yield: 0.050 g, 19%. ^1H NMR (benzene- d_6 , 400 MHz): δ 7.61 (d, $^3J_{\text{HH}} = 7.6$ Hz, 4 H, *ortho-Ph₂Si*), 7.14 (mult, 6 H, *meta-* and *para-Ph₂Si*), 7.11 (t, $^3J_{\text{HH}} = 7.6$ Hz, 2 H, *meta-NHPh*), 6.72 (t, $^3J_{\text{HH}} = 7.6$ Hz, 1 H, *para-NHPh*), 6.64 (d, $^3J_{\text{HH}} = 7.6$ Hz, 2 H, *ortho-NHPh*), 5.77 (d, $^3J_{\text{HH}} = 3.2$ Hz, 1 H, *SiH*), 3.48 (br s, 1 H, *NHPh*). $^{13}\text{C}\{^1\text{H}\}$ NMR

(benzene- d_6 , 100 MHz): δ 147.28 (*ipso*-NHP*h*), 135.68 (*ortho*-PhSi), 134.04 (*ipso*-PhSi), 130.96 (*meta*-PhSi), 129.90 (*meta*-NHP*h*), 128.88 (*para*-PhSi), 119.44 (*para*-NHP*h*), 117.25 (*ortho*-NHP*h*). ^{15}N NMR (benzene- d_6 , 41 MHz): δ -327.57. ^{29}Si NMR (benzene- d_6 , 79 MHz): δ -23.78. IR (neat, cm^{-1}): 3383 br s (ν_{NH}), 3087 m, 3068 s, 3044 s, 3010 s, 2965 m, 2130 (ν_{SiH}), 1428 s, 1289 s, 898 s, 830 s, 731 s, 698 s.

Representative procedure for reaction of organosilanes and ammonia.

PhCH₂Me₂SiNH₂. 20 mg To^MMgMe (0.048 mmol) was dissolved in benzene (2.5 mL) and transferred to a 50 mL flask with a Teflon valve. PhCH₂Me₂SiH (0.179 g, 1.19 mmol) in benzene (2.5 mL) was added to the flask and the combined solution was degassed via three freeze-pump-thaw cycles. The solution was then immersed in a liquid nitrogen bath and the flask was back-filled with anhydrous ammonia. Ammonia was allowed to condense in the flask until a volume of approximately 2-3 mL had been added. The flask was then closed, allowed to warm to room temperature, and stirred overnight. After 24 hours, the solution was cooled to -78 °C, and the flask was opened to nitrogen and allowed to slowly warm to room temperature to remove excess ammonia. The remaining solution was cannula transferred to a 50 mL Schlenk flask and the benzene was removed via distillation under nitrogen. The remaining product residue was purified by Kugelrohr distillation to give the analytically pure silazanes. Yield: 0.061 g, 31%. ^1H NMR (benzene- d_6 , 400 MHz): δ 7.18 (t, $^3J_{\text{HH}} = 8.0$ Hz, 4 H, *ortho*-C₆H₅), 7.02 (mult, 6 H, *meta*- and *para*-C₆H₅), 1.96 (s, 4 H, SiMe₂CH₂Ph), -0.00 (br s, 1 H, NH), -0.02 (s, 12 H, SiMe₂CH₂Ph). $^{13}\text{C}\{^1\text{H}\}$ NMR (benzene- d_6 , 100 MHz): δ 140.90 (*ipso*-C₆H₅), 128.93 (*ortho*-C₆H₅), 128.86 (*meta*-C₆H₅), 124.69 (*para*-C₆H₅), 29.42 (SiMe₂CH₂Ph), -0.25 (SiMe₂CH₂Ph). ^{15}N NMR (benzene- d_6 , 41 MHz): δ

-372.70. ^{29}Si NMR (benzene- d_6 , 79 MHz): δ 1.30. IR (neat, cm^{-1}): 3355 br s (ν_{NH}), 3060 s, 3024 s, 2957 s, 2890 m, 1493 s, 1252 s, 1207 m, 1155 s, 1056 m, 1028 m, 835 m, 698 m. Anal. Calc. for $\text{C}_9\text{H}_{15}\text{NSi}$: C, 65.39; H, 9.15; N, 8.47. Found: C, 64.90; H, 8.73; N, 8.50.

Et_3SiNH_2 . A procedure similar that described for $\text{PhCH}_2\text{Me}_2\text{SiNH}_2$ was followed, using Et_3SiH (0.138 g, 1.19 mmol). Due to the slow reaction of Et_3SiH with the catalyst, 10 mol% (50 mg, 0.12 mmol) of $\text{To}^{\text{M}}\text{MgMe}$ was used. Yield: 0.055 g, 35%. ^1H NMR (benzene- d_6 , 400 MHz): δ 0.97 (t, $^3J_{\text{HH}} = 8.0$ Hz, 9 H, $\text{Si}(\text{CH}_2\text{CH}_3)_3$), 0.54 (d of q, $^3J_{\text{HH}} = 8.0$ Hz, $^4J_{\text{HH}} = 3.2$ Hz, 6 H, $\text{Si}(\text{CH}_2\text{CH}_3)_3$), -0.12 (br s, 2 H, NH). $^{13}\text{C}\{^1\text{H}\}$ NMR (benzene- d_6 , 100 MHz): δ 8.75 ($\text{Si}(\text{CH}_2\text{CH}_3)_3$), 3.15 ($\text{Si}(\text{CH}_2\text{CH}_3)_3$). ^{15}N NMR (benzene- d_6 , 41 MHz): δ -370.60. ^{29}Si NMR (benzene- d_6 , 79 MHz): δ 0.08. IR (neat, cm^{-1}): 3235 br s (ν_{NH}), 2956 s, 2874 m, 1456 s.

$\text{C}_3\text{H}_5\text{Me}_2\text{SiNH}_2$. A procedure similar that described for $\text{PhCH}_2\text{Me}_2\text{SiNH}_2$ was followed, using $\text{C}_3\text{H}_5\text{Me}_2\text{SiNH}_2$ (0.119 g, 1.19 mmol). Toluene was used as the solvent in place of benzene due to the similar boiling points of solvent and product. Yield: 0.075 g, 55%. ^1H NMR (benzene- d_6 , 400 MHz): δ 5.82 (mult, 1 H, $\text{CH}_2=\text{CHCH}_2\text{Si}$), 4.93 (mult, 2 H, $\text{CH}_2=\text{CHCH}_2\text{Si}$), 1.46 (d, $^3J_{\text{HH}} = 6.8$ Hz, 2 H, $\text{CH}_2=\text{CHCH}_2\text{Si}$), -0.01 (s, 6 H, $\text{SiMe}_2\text{CH}_2\text{CH}=\text{CH}_2$), -0.06 (br s, 1 H, NH). $^{13}\text{C}\{^1\text{H}\}$ NMR (benzene- d_6 , 100 MHz): δ 135.79 ($\text{SiMe}_2\text{CH}_2\text{CH}=\text{CH}_2$), 113.27 ($\text{SiMe}_2\text{CH}_2\text{CH}=\text{CH}_2$), 27.13 ($\text{SiMe}_2\text{CH}_2\text{CH}=\text{CH}_2$), -0.22 ($\text{SiMe}_2\text{CH}_2\text{CH}=\text{CH}_2$). ^{15}N NMR (benzene- d_6 , 41 MHz): δ -373.95. ^{29}Si NMR (benzene- d_6 , 79 MHz): δ 1.02. IR (neat, cm^{-1}): 3336 br s (ν_{NH}), 2963 s, 2925 m, 1456 s.

Procedure for kinetic measurements.

All kinetics measurements were conducted by monitoring the reaction with ^1H NMR spectroscopy using a Bruker DRX-400 MHz spectrometer. A stock solution of toluene- d_8 was made containing the 1,3,5-trimethoxybenzene standard (10 mM), and PhMeSiH_2 (42.6 mM). In a typical experiment, 21 μmol of $\text{To}^{\text{M}}\text{MgNH}^t\text{Bu}$ was dissolved in 0.7 mL of the stock solution, and placed in a J. Young style NMR tube with resealable Teflon valve. The solution was frozen in liquid nitrogen, and was only thawed immediately prior to being inserted into the NMR probe. The reaction was monitored by taking a single ^1H NMR scan at regular preset intervals. The concentration of the reactants was determined by comparison of the integrated resonance corresponding to each reactant to the known concentration of the internal standard, 1,3,5-trimethoxybenzene. For the Eyring analysis, temperatures were calibrated using an 80% ethylene glycol sample in 20% $\text{DMSO-}d_6$. Kinetic isotope measurements were performed in the same manner using the deuterated silane PhMeSiD_2 . The rate constants at each temperature were calculated from the slope of the plot of $\ln([\text{PhMeSiD}_2]/[\text{To}^{\text{M}}\text{MgNH}^t\text{Bu}])$ vs time, and then compared with the proteo rate constants at each specific temperature.

DFT calculations. All calculations were performed with the NWChem software suite.²⁷ Density functional theory (DFT) was employed using the B3LYP hybrid functional to obtain optimized geometries, frequencies, and energies, including zero point energy correction.²⁸ The recently revised, uncontracted effective core potential (LANL08) developed at Los Alamos National Lab was used for magnesium, and the 6-311++G** basis set was used for all other heavy atoms.²⁹ The basis used for hydrogen was 6-311+G*. Initial geometries were found with a 6-31+G* basis set for all atoms before being refined with the

larger basis set. The software package MacMolPlt was used for viewing optimized geometries.³⁰

References

- 1) Kobayashi, S.; Yamashita, Y. *Acc. Chem. Res.* **2011**, *44*, 58-71.
- 2) Housecroft, C.E.; Sharpe, A.G. *Inorganic Chemistry*, 3rd ed.; Prentice Hall: New York, 2008, p.305-306.
- 3) For calcium, see: (a) Crimmin, M.R.; Casely, I.J.; Hill, M.S. *J. Am. Chem. Soc.* **2005**, *127*, 2042-2043.; (b) Datta, S.; Roesky, P.W. *Organometallics* **2007**, *26*, 4392-4394.; (c) Barrett, A.G.M.; Crimmin, M.R.; Hill, M.S.; Kociok-Kohn, G.; Lachs, J.R.; Procopiou, P.A. *Dalton Trans.* **2008**, 1292-1294.
- 4) For strontium and barium see: (a) Datta, S.; Gamer, M.T.; Roesky, P.W. *Organometallics* **2008**, *27*, 1207-1213.; (b) Barrett, A.G.M.; Brinkmann, C.; Crimmin, M.R.; Hill, M.S.; Hunt, P.; Procopiou, P.A. *J. Am. Chem. Soc.* **2009**, *131*, 12906-12907.
- 5) For magnesium see: (a) Crimmin, M.R.; Arrowsmith, M.; Barrett, A.G.M.; Casely, I.J.; Hill, M.S.; Procopiou, P.A. *J. Am. Chem. Soc.* **2009**, *131*, 9670-9685.; (b) Horrillo-Martinez, P.; Hultzsch, K.C. *Tetrahedron Lett.* **2009**, *50*, 2054-2056.; (c) Neal, S.R.; Ellern, A.; Sadow, A.D. *J. Organomet. Chem.* **2010**, *696*, 228-234.; (d) Dunne, J.F.; Fulton, D.B.; Ellern, A.; Sadow, A.D. *J. Am. Chem. Soc.* **2010**, *132*, 17680-17683.
- 6) (a) Buch, F.; Brettar, J.; Harder, S. *Angew. Chem. Int. Ed.* **2006**, *45*, 2741-2745.; (b) Buch, F.; Harder, S. *Z. Naturforsch* **2008**, *63b*, 169-177.
- 7) Crimmin, M.R.; Barrett, A.G.M.; Hill, M.S.; Hitchcock, P.B.; Procopiou, P.A. *Organometallics* **2007**, *26*, 2953-2956.

- 8) (a) Roth, C.A. *Ind. Eng. Chem. Prod. Res. Develop.* **1972**, *11*, 134-139. (b) Tanabe, Y.; Murakami, M.; Kitaichi, K.; Yoshida, Y. *Tetrahedron Lett.* **1994**, *35*, 8409-8412.; (c) Tanabe, Y.; Misaki, T.; Kurihara, M.; Iida, A.; Nishii, Y. *Chem. Commun.* **2002**, 1628-1629. (d) Iida, A.; Horii, A.; Misaki, T.; Tanabe, Y. *Synthesis* **2005**, *16*, 2677-2682.
- 9) Fieser, L.F.; Fieser, M. *Reagents in Organic Chemistry*; Wiley: New York, 1967.
- 10) For representative examples, see: (a) Deschner, T.; Lonstad, B.-T.; Widenmeyer, M.; Anwander, R. *J. Mat. Chem.* **2011**, *21*, 5620-5628.; (b) Le Roux, E.; Liang, Y.; Storz, M.P.; Anwander, R. *J. Am. Chem. Soc.* **2010**, *132*, 16368-16371.; (c) Schaedle, C.; Meermann, C.; Toernroos, K.W.; Anwander, R. *Eur. J. Inorg. Chem.* **2010**, *18*, 2841-2852.; (d) Meermann, C.; Ohno, K.; Tornroos, K.W.; Mashima, K.; Anwander, R. *Eur. J. Inorg. Chem.* **2009**, *1*, 76-85.
- 11) Wuts, P.G.M.; Greene, T.W. *Protecting Groups in Organic Synthesis*, 4th ed.; Wiley: New York, 2006.
- 12) Eaborn, C. *Organosilicon Compounds*; Butterworths: London, 1960; p.333.; (b) Fessenden, R.; Fessenden, J.S. *Chem Rev.* **1960**, *61*, 361.
- 13) Passarelli, V.; Carta, G.; Rossetto, G.; Zanella, P. *Dalton Trans.* **2003**, 413-419.
- 14) Sommer, L. H.; Citron, J. D. *J. Org. Chem.* **1967**, *32*, 2470-2742.
- 15) Blum, Y.; Laine, R. M. *Organometallics* **1986**, *5*, 2081-2086.
- 16) Wang, W. D.; Eisenberg, R. *Organometallics* **1991**, *10*, 2222-2227.
- 17) Matarasso-Tchiroukhine, E. *J. Chem. Soc., Chem. Commun.* **1990**, 681.
- 18) (a) Liu, H. Q.; Harrod, J. F. *Organometallics* **1992**, *11*, 822-827.; (b) He, J. L.; Liu, H. Q.; Harrod, J. F.; Hynes, R. *Organometallics* **1994**, *13*, 336-343.

- 19) Wang, J. X.; Dash, A. K.; Berthet, J. C.; Ephritikhine, M.; Eisen, M. S. *J. Organomet. Chem.* **2000**, *610*, 49-57.
- 20) Klinkenberg, J.L.; Hartwig, J.F. *Angew. Chem. Int. Ed.* **2011**, *50*, 86-95. and the references therein.
- 21) Bent, H.A. *Chem. Rev.* **1961**, *61*, 275-311.
- 22) Espenson, J.H. *Chemical kinetics and reaction mechanisms*, 2nd ed.; McGraw-Hill: New York, 1995.
- 23) Sadow, A.D.; Tilley, T.D. *J. Am. Chem. Soc.* **2005**, *127*, 643-656.
- 24) Larsson, E.; Bjellerup, L. *J. Am. Chem. Soc.* **1953**, *75*, 995-997.
- 25) Dzheliya, M. I.; Baramidze, L. V.; Kiladze, S. Kh. *Soobshcheniya Akademii Nauk Gruzinskoi SSR* **1987**, *126*, 557-559.
- 26) Sauer, Robert O.; Hasek, R. H. *J. Am. Chem. Soc.* **1946**, *68*, 241-244.
- 27) (a) Kendall, R. A.; Apra, E.; Bernholdt, D. E.; Bylaska, E. J.; Dupuis, M.; Fann, G. I.; Harrison, R. J.; Ju, J.; Nichols, J. A.; Nieplocha, J.; Straatsma, T. P.; Windus, T. L.; Wong, A. T. *Computer Phys. Comm.* 2000, **128**, 260-283. (b) Bylaska, E. J.; Jong, W. A. d.; Govind, N.; Kowalski, K.; Straatsma, T. P.; Valiev, M.; Wang, D.; Apra, E.; Windus, T. L.; Hammond, J.; Nichols, P.; Hirata, S.; Hackler, M. T.; Zhao, Y.; Fan, P.-D.; Harrison, R. J.; Dupuis, M.; Smith, D. M. A.; Nieplocha, J.; Tipparaju, V.; Krishnan, M.; Wu, Q.; Voorhis, T. V.; Auer, A. A.; Nooijen, M.; Brown, E.; Cisneros, G.; Fann, G. I.; Fruchtl, H.; Garza, J.; Hirao, K.; Kendall, R.; Nichols, J. A.; Tsemekhman, K.; Wolinski, K.; Anchell, J.; Bernholdt, D.; Borowski, P.; Clark, T.; Clerc, D.; Dachsel, H.; Deegan, M.; Dyall, K.; Elwood, D.; Glendening, E.; Gutowski, M.; Hess, A.; Jaffe, J.; Johnson, B.; Ju, J.; Kobayashi, R.; Kutteh, R.; Lin,

- Z.; Littlefield, R.; Long, X.; Meng, B.; Nakajima, T.; Niu, S.; Pollack, L.; Rosing, M.; Sandrone, G.; Stave, M.; Taylor, H.; Thomas, G.; Lenthe, J. v.; Wong, A.; Zhang, Z. Pacific Northwest National Laboratory Richland, Washington 99352, USA, 2007.
- 28) (a) Becke, A.D. *J. Chem. Phys.* **1993**, *98*, 5648-5652. (b) Lee, C.T.; Yang, W.T.; Parr, R.G. *Phys. Rev. B* **1988**, *37*, 785-789.
- 29) Frisch, M.J.; Pople, J.A.; Binkley, J.S. *J. Chem. Phys.* **1984**, *80*, 3265-3269.
- 30) Bode, B. M. and Gordon, M. S. *J. Mol. Graphics Mod.*, *16*, **1998**, 133-138.

Chapter 6 - Conclusion

General Conclusions

The development of main group metal catalysts remains an important area of research within the field of organometallic chemistry. The non-toxic nature of the alkaline earth metals makes them ideal replacements for more harmful metals from a safety and environment standpoint. Moreover, the abundance of these elements makes the use of alkaline earth metals in place of rare metals highly desirable as the exhaustion of these rare metals may become a serious problem. The work described in this thesis highlights several roles that the main group metals aluminum and magnesium can perform in the catalytic formation of new and useful chemicals.

The selection and design of ancillary ligands is essential to the successful development of useful main group metal catalysts. We have shown that tris(oxazolinyl)borate ligands provide unique steric pockets for the protection of highly reactive metal centers such as aluminum and magnesium. In the case of aluminum, the steric and electronic environments provided by the ligand resulted in an unexpectedly inert compound. The Al–C and Al–N bonds were found to be quite robust, and were shown to react only under high temperatures (150 °C). These results stand in stark contrast to analogous aluminum compounds in which pyrazole rings are used instead of oxazolines, and this further highlights the importance that careful ligand selection plays in catalyst development.

In contrast to aluminum, tris(oxazolinyl)borate magnesium compounds display a variety of useful catalytic transformations under mild reaction conditions. Magnesium amide complexes were shown to be capable of the catalytic formation of new C–N bonds as well as

new Si–N bonds. For the cross coupling reactions of silanes and amines, excellent control of product formation was observed, as demonstrated by the selective formation of monomeric silazanes in the dehydrocoupling of hydrazine or ammonia with tertiary silanes.

The steric bulk provided by tris(oxazolanyl)borate ligands was also found to be useful in the mechanistic explorations. Catalytic intermediates in intramolecular hydroamination/cyclization were isolated for the first time, and allowed for the study stoichiometric cyclization in the absence of complicating equilibria. These studies led to the proposal of a new mechanism for hydroamination which more adequately accounted for the previously observed kinetic isotope effects.

Future directions

In light of these advances, a number of future directions are possible for this research. As tris(oxazolanyl)borate magnesium compounds have been found to be active catalysts for the cross coupling of silanes and amines, an appropriate chiral analog of the To^M ligand could be developed for the enantioselective synthesis of silazanes with chiral silicon centers. Chiral silazanes would be extremely useful as simple chiral ligands in organometallic compounds. Additionally, the ability to easily transfer the chiral silyl center to other organic functional groups could result in the generation of a wide range of organic starting materials. The high degree of control exhibited in silazane formation by $To^M MgMe$ indicates limited access for substrate molecules to interact with the metal center. This could easily be capitalized on by a chirality-inducing ligand to give the desired enantiopure products.

Secondly, the ability of magnesium amides to catalyze dehydrocoupling reactions with silicon could be expanded to include elements. The formation and cleavage of B–N

bonds is currently a hot topic in hydrogen fuel cell research as this is a primary method of storing and releasing hydrogen gas. A magnesium compound capable of catalytically releasing H₂ gas via the dehydrocoupling of boranes and amines under mild conditions would be an inexpensive alternative to the known fuel cell catalysts.

Lastly, given the remarkable synergistic effect displayed by LiCl on Grignard reagents, studies should be carried out to determine if a similar effect can be induced in catalytic systems. The ability to enhance catalytic reactivity by the addition of simple inorganic salts would be an inexpensive and easy method of improving the scope of catalytic reactions, and would further the usefulness of the alkaline earth metals in homogeneous catalysis.